Mitteilungen aus dem Institut für Mechanik

Kianoush Molla-Abbasi

A Consistent Anisotropic Brittle Damage Model Based on the Concept of Growing Elliptical Cracks

Heft Nr. 146

RUHR-UNIVERSITÄT BOCHUM

A Consistent Anisotropic Brittle Damage Model Based on the Concept of Growing Elliptical Cracks

Dissertation
zur
Erlangung des akademischen Grades
Doktor-Ingenieur

der
Fakultät für Maschinenbau
der Ruhr-Universität Bochum

von
Kianoush Molla-Abbasi

aus
Mashad (Iran)

Bochum 2007

Herausgeber:

Institut für Mechanik
— Schriftenreihe —
Ruhr-Universität Bochum
D-44780 Bochum

ISBN 978-3-935892-23-0

Summary

It is known from experiments that all materials and in more special case, brittle materials develop anisotropic damage under general loading conditions. A micromechanical based continuum damage model based on the reduction of stiffness due to kinking elliptical microcracks is proposed to show the anisotropic irreversible process of damage accumulation due to microcrack kinking and growth in brittle and quasi-brittle materials. The model is formulated consistently in a fully analytical way based on the concept of linear elastic fracture mechanics. The degradation of the elastic properties is associated with the irreversible process of crack kinking and growth. In order to make the formulation of the model mathematically traceable, the concept of an equivalent elliptical crack is proposed. The geometry and the orientation of the equivalent crack are resulting from the postulates of equivalent dissipation and equivalent damage induced anisotropy. The evolution of the cracks is governed by the criterion of maximum driving force coupled with a fatigue crack evolution law. The proposed formulation yields a consistent damage model which considers the kinking and growth of microcracks, and accounts for the type of damage induced anisotropy in a local sense. The proposed model is appropriate to show the evolution of damage in brittle and quasi-brittle materials under fatigue conditions.

Zusammenfassung

Es ist aus Experimenten bekannt, dass alle Materialien und insbesondere spröde Materialien unter allgemeine Belastungen anisotrope Schädigung entwickeln. In der vorliegende Arbeit wird ein Kontinuumsschädigungsmodell basierend auf wachsenden elliptischen Mikrorissen vorgeschlagen, mit dem der anisotrope irreversible Prozess der Schädigungsakkumulation basierend auf Mikrorissen die sich ausbreiten und hierbei abknicken modelliert werden kann. Das Modell wird in einer völlig analytischen Weise basierend auf dem Konzept der linear elastischen Bruchmechanik formuliert. Der Abbau der elastischen Eigenschaften ist mit dem irreversiblen Prozess der Mikrorissausbreitung verbunden. Ein Konzept äquivalenter elliptischer Risse wird vorgeschlagen um die Formulierung mathematisch nachvollziehbar herleiten zu können. Die Geometrie und die Orientierung des äquivalenten Risses resultieren aus den Postulaten der Äquivalenz der Dissipation und der Äquivalenz der schädigungsinduzierten Anisotropie. Die Ausbreitung der Risse wird durch das Kriterium der maximalen treibenden Kraft verbunden mit einem Ermüdungs-Riss-Ausbreitungs-Gesetz bestimmt. Die vorgeschlagene Formulierung liefert ein konsistentes Schädigungsmodell, unter Berücksichtigung des Wachstums von Mikrorissen und der schädigungsinduzierten Anisotropie in einem lokalen Sinne. Das vorgeschlagene Modell ist geeignet, um die Schädigungsakkumulation der spröden und quasi-spröden Materialien unter zyklische Belastungen zu betrachten.

Acknowledgment

This thesis is the account of three years of work on the project SFB398-C10, at the Chair of Technical Mechanics, Institute of Mechanics, Ruhr-University Bochum, and was financed by the Deutsche Forschungsgemeinschaft (DFG). This work would not have been possible without the help of many.

A few lines are too short to express my complete account of gratitude to my advisor, Professor Henning Schütte. I wish to thank him first for his constant support, encouragement, trust and all the fruitful discussions. I wish to thank him for his unique understanding and being such an attainable and likable teacher. I want to extend my appreciation to him for providing me the opportunity to follow and perform my ideas, and the nice working environment throughout the last three years. His understanding and account of life outside work, his friendship and his efforts in understanding a student's personality made the last three years very pleasant for me. It has been a distinct privilege for me to work with Professor Henning Schütte.

I would like to express my sincere gratitude to Professor Otto Timme Bruhns for accepting me so readily as a new member of his team at the Chair of Technical Mechanics, supporting me constantly throughout this work and his helpful comments and discussions.

I had the chance to work in a very nice working environment at the Institute of Mechanics among many good scientists and colleagues. I thank all of my colleagues, especially my colleagues and friends at the Chair of Technical Mechanics for their support.

The last but not the least, I wish to thank my family for their unconditional love, support and encouragement, especially my brother, Amir, for his constant support.

Bochum, October 2007 Kianoush Molla-Abbasi

References:

1. Prof. Dr.-Ing. Henning Schütte
2. Prof. Dr.-Ing. Otto Timme Bruhns

Date of submission: October 15, 2007

Date of oral exam: December 20, 2007

Contents

Nomenclature

The choice of notation is tried to be as classical as possible, but using the same letter for different meanings cannot be avoided. The general symbols which are used throughout the thesis are given below and if there is a different meaning for a symbol, it is given subsequently. In general scalars are denoted by lightface symbols, and vectors and tensors by boldface symbols.

Symbol	Notation
a	crack size
$\mathrm{am}(u_1)$	Jacobi amplitude
$A_{\mathcal{F}}, A_{\mathcal{H}}, A_{\mathcal{L}}$	unknown functions
$B_{\mathcal{F}}, B_{\mathcal{H}}$	functions of the given form in the thesis
B_α	coefficients in the stress expansion formula
C, η	material parameters in the considered crack evolution law
$C_{\lambda\mu}$	components of the curvature tensor
$\mathbf{C}$	curvature tensor
$da/dN, \dot{a}, \dot{s}$	fatigue crack growth rate
$dl, d\Gamma$	length increment along the considered path
dr	length increment in the radial direction
ds	length increment in the direction of kink
dA	area increment
dV	volume increment
$\mathbb{D}_{ijmn}$	components of the damage tensor
$\mathcal{D}$	damage variable
e	dilatation
$\mathbf{e_i}$	local orthogonal basis
$\mathbf{e_n}, \mathbf{e_r}$	unit vectors in the normal and radial directions to the circumference of an ellipse
E	Young's modulus
$E(k_1)$	complete elliptical integral of the second kind

$E(\phi\|k_1)$	elliptical integral of the second kind
$\mathcal{F}$	material force
$F(\phi\|k_1)$	elliptical integral of the first kind
f_{ij}^{α}, g_{ij}^{α}, h_{ij}^{α}, l_{ij}^{α}, $m_{ij}^{\alpha\lambda\mu}$, n_{ij}^{α}, ν_i	universal functions in terms of θ
$\mathcal{F}$, $\mathcal{G}$, $\mathcal{H}$, $\mathcal{L}$	ellipsoidal harmonic potential functions
$\mathcal{F}_{ORT}$, $\mathcal{F}_1$, $\mathcal{F}_2$	target functions of the form defined in the thesis
G	energy release rate
G_{ij}, R_{ij}	functions of the given form in the thesis
G_{max}, G_{min}	maximum and minimum value for G in a load cycle
G_o, G_o^*	threshold value for G and G*, respectively
$G(\epsilon)$	energy release rate for the kinked crack with an extension length of ϵ
G^*	strain energy release rate for the kinked crack with $\epsilon \rightarrow 0$
J_1, J_2, J_3	components of the path independent J-integral
$J_2(\sigma)$	von Mises yield function
J_c	threshold value for J-integral
J_{max}, J_{min}	maximum and minimum value for J-integral in a load cycle
k_1, k_2, k_3	functions of the aspect ration β/α
K_{Ic}, G_{Ic}	fracture toughness
K_{max}, K_{min}	maximum and minimum value for stress intensity factors in a load cycle
K'_{α}	derivatives of the stress intensity factors along the crack front
K_{α}	stress intensity factors
$K_{\alpha}(\epsilon)$	stress intensity factors for the kinked crack with an extension length of ϵ
K^*_{α}	stress intensity factors for the kinked crack with $\epsilon \rightarrow 0$
$K(k_1)$	complete elliptical integral of the first kind
$M_{\alpha\beta}$	coefficient matrix of the given form in the thesis
$\mathbb{M}_{ijmn}$	components of the tensor valued function in terms of the damage variables
$\mathcal{M}_i(\varphi)$	functions of the given form in the thesis, where $i = 1..4$
$\mathbf{n}$	normal vector to the considered path
(n, t, z)	local trihedral at the crack front
N	number of load cycles
$N^{(k)}$	eigenvectors of the stiffness tensor
$ORT(\bullet)$	an operator that nulls out the non-orthotropic components of a given tensor deviating from zero

p_{ij}	projections of the remote loading into the plane of the crack
p_{II}	second invariant of the deviatoric stress tensor
p^{∞}	remote tensile loading
q	shear stress
$Q(s)$	function of the form given in the thesis
r, θ	local polar coordinates at the crack tip
R	stress ratio of the load cycle
$\mathbf{R}$	orthogonal transformation
$\mathbf{R}^{ORT}$	orthogonal transformation corresponding to the best approximate orthotropic representation
$\mathbb{S}_{ijmn}$, $\mathbb{C}_{ijmn}$	components of the compliance and stiffness tensors, respectively
$\widetilde{\mathbb{S}}$	effective compliance tensor
$\mathbb{S}^{Matrix}$	compliance tensor of the undamaged matrix
$\widetilde{\mathbb{S}}_{ijmn}$, $\widetilde{\mathbb{C}}_{ijmn}$	components of the compliance/stiffness tensors modified by damage
$\mathbb{S}^{Kink}_{ijmn}$	components of the tensor for the rate of the change of compliance due to crack kinking
T_{α}	non-singular constant terms in the stress expansion formula (T-stresses)
$\mathbf{u}$	displacement vector
u_i	components of the displacement vector
W^e	strain energy density
(x_1, x_2, x_3)	
(x, y, z)	Cartesian coordinates
(x_1', x_2', x_3')	
(x', y', z')	rotated and shifted Cartesian coordinates at the new crack tip
$(\bullet)_{\alpha}$ and $(\bullet)^{\alpha}$	mode of crack deformation
α, β	semi-major and semi-minor axes of the ellipse, respectively
δA	total area element
$\delta \widetilde{A}$	remaining area element
$\delta A_{\mathcal{D}}$	damaged area elements
$\Delta\mathbb{S}^{Crack}$	compliance tensor corresponding to the considered crack
$\Delta\mathbb{S}^{Kink}$	compliance tensor corresponding to crack kinking
$\Delta\mathbb{S}_C$	tensor of the change of compliance corresponding to crack growth

$\Delta\widehat{\mathbb{S}}_C^{ORT}$	best approximate orthotropic representation of the compliance tensor
ϵ	crack extension length
ε_{ij}	components of the strain tensor in the corresponding coordinate system
$\widetilde{\varepsilon}$	effective strain
$\gamma_x, \gamma_y, \gamma_z$	rotation angles of the crack (Euler angles)
Γ	curvature of the projected crack front to the tangent plane
λ_1, λ_2	mode-mixities
λ_n, ξ_n	eigenvalues for symmetric and antisymmetric loading
Λ_k	eigenvalues of the stiffness tensor
μ	shear modulus
$\boldsymbol{\mu}$	Eshelby's stress tensor
∇^2	Laplacian operator
∇	Del operator
ν	Poisson's ratio
ω	angle between the shear load and the x-axis
ω	continuity parameter
ϕ_{max}	kinking angle
Φ	Airy stress function
ψ^*	energy dissipation corresponding to self-similar crack growth
ψ^{**}	energy dissipation corresponding to crack kinking
σ_{ij}	components of the stress tensor in the corresponding coordinate system
$\boldsymbol{\sigma}$	stress tensor
$\boldsymbol{\sigma}'$	deviatoric part of the stress tensor $\boldsymbol{\sigma}$
σ_{yield}	tensile yield strength
$\widetilde{\sigma}$	effective stress
ϑ_n	angle between the normal vector to the ellipse and the x-axis
(ξ, η, ζ)	ellipsoidal coordinates

Introduction

"everything should be made as simple as possible, but not simpler."

Albert Einstein

Since people started to design and make components, most of their effort have been spent trying to detect and avoid damage and failure. Many failure criteria have been proposed so far, and the pioneering works in this field go back to TRESCA (1872), MOHR (1900),VON MISES (1913), DRUCKER & PRAGER (1952). Their theories were based on a combination of the stress or the strain components, given in the form of a function. In designing parts to resist failure, the critical value of this function is to be lower than a material parameter, e.g. the yield strength for ductile materials or ultimate strength for brittle materials. These are *yes or no* criteria, but in practice it was observed that many components designed using these criteria failed as well. This is because these theories were based on static loading, while real structures and components are experiencing variable loadings. The concept of Wöhler diagram, also known as S-N diagram, proposed by WÖHLER (1860) was a great step to solve the problem of time varying loads. Using this concept, the strength of materials is determined under the action of cyclic loads, but it was observed that the S-N diagrams for two different specimens, but made of the same material, showed a significant difference. The diagrams also showed load dependency, i.e. depending on whether the load nature was cyclic with a constant amplitude or with a fluctuating amplitude, different curves were resulting. These and other observations suggested that for each individual component a unique S-N diagram should be measured.

Using the concept of S-N diagram, it is possible to characterize the evolution of damage in materials under cyclic loading. Damage is the deterioration which occurs in materials prior to failure. For centuries fracture has been studied as a *yes or no* process related to a critical value of load, stress, strain and time or number of load cycles. PALMGREEN (1924), MINER (1945) and ROBINSON (1952) pioneered the concept of the variables related to the progressive deterioration prior to failure. 1958 is the year to be considered as the starting point of continuum damage mechanics, when KACHANOV (1958) published the first paper on a field variable ω called *continuity*. About fifteen years later $\mathcal{D} = 1 - \omega$ received the status of a state variable in the thermodynamical sense, where $0 \leq \mathcal{D} \leq 1$ (0 for the undamaged state and 1 for failure). During these fifteen years, this concept did not improve noticeably, and only one important result appeared in 1968, introducing the concept of effective stress by RABOTNOV (1968). The basic development of damage mechanics occurred during the 1970s, at least ten years af-

ter the tremendous development of the field fracture mechanics. In the 1980s, the theory was set up on a more rigorous basis using thermodynamics and micromechanics, and applications to engineering problems began and accelerated as many more people involved themselves in this discipline.

Since the pioneering work of KACHANOV (1958) and RABOTNOV (1969), continuum damage mechanics is a successfully developing branch of solid mechanics, fracture mechanics, material science, physics of solids, etc. Surprisingly, rapid development in this field in the last decades has shown how important the problem is and how difficult is the proper irreversible thermodynamics based modeling of the material damage response. The ability to characterize and predict the mechanical failure modes, damage evolution and the remaining operational life of a mechanical system are the main concerns of this field. For example, in the field of damage mechanics based on fracture mechanics and crack growth, much material failure prediction has been accomplished using the Paris' law and the Forman's law for cyclic loading. There is no unique method for the prediction of damage evolution and material failure and, furthermore, one model may not be easily related to other models.

The larger portion of the literature on continuum damage mechanics is probably devoted to the development of damage variables and constitutive equations rather than to the development of damage evolution equations. Since damage is assumed to degrade, at least locally, the elastic properties of a material, modeling its response must address the formulation of constitutive properties. A task which may be approached using micromechanical or phenomenological approaches. An extensive review of such approaches can be found in (KRAJCINOVIC 1996). The micromechanical modeling process leads to a one to one correspondence between a discontinuous field on an inhomogeneous mesoscale and an effective continuous field on the homogenous macroscale. The homogenization (averaging) of the meso-structural field of defects within a representative volume element (RVE) into a macrofield of the effective continuum corresponds to micromechanical modeling. In contrast to micromechanical models, phenomenological models do not consider the micro-details of the material response, but describe damage indirectly by introducing internal (or hidden) variables. This has caused some confusion and spawned more extensive, substantially different, models of the same phenomena. Since the selection of the damage variables is perhaps the most important step, irreversible thermodynamics has been used to provide a scientific basis for theories of continuum damage mechanics (KESTIN & BATAILLE 1977), (MURAKAMI & OHNO 1981), (KRAJCINOVIC & FONSEKA 1981), (ZIEGLER 1983), (KRAJCINOVIC 1983A), (KRAJCINOVIC 1983B), (KRAJCINOVIC 1985), (LEMAITRE 1985).

All materials, and in more special case brittle materials, under general loading conditions develop anisotropic damage. For a given stress state, materials damaged by microcracks in general accumulate additional damage through the kinking and growth of these microcracks. Five decades of research on the identification of different damage mechanisms have provided this field with a wealth of damage models and variety of different

concepts to study the evolution of damage and failure analysis of materials and structures. However, there is still a need for new material models and ideas covering the natural aspects of the irreversible damage process. In the present work a micromechanics based continuum damage model for brittle materials is proposed, which is based on the reduction of stiffness due to the kinking and growth of elliptical microcracks. The proposed model captures the local damage induced anisotropy due to the kinking and growth of microcracks in a thermodynamically consistent manner, without considering any ad hoc assumption. The model is formulated consistently in a fully analytical way. In order to make the formulation of the model mathematically traceable, the concept of an equivalent elliptical crack is proposed. The geometry and the orientation of the equivalent crack are resulting from the postulates of equivalent dissipation and equivalent damage induced anisotropy in a local sense. Considering the kinking and growth of microcracks in the formulation of the proposed damage model makes it suitable for loadings with changing direction and amplitude (non-proportional loading). In such cases, the assumption of self-similar growth of microcracks is not sufficient to show the irreversible thermodynamic process of material degradation due to the kinking and growth of microcracks to other planes and shapes, and it may underestimate the accumulated damage.

This thesis is structured into six chapters. Subsequent to this preface, the principles of the fracture mechanics are addressed in chapter 1. A short and brief history review on the fracture mechanics is given first. This chapter covers the fundamentals and main principles of this field, including the physical irreversible process of fracture and crack growth, theory of the linear elastostatic fracture mechanics, the concepts of material forces and path independent integrals in linear elasticity, and the mechanism of fatigue crack growth.

Besides the stress intensity factors and the well known J-integral concept, the non-singular constant terms in the stress expansion formula have proven to play an important role in fracture mechanics and plasticity (LARSSON & CARLSSON 1973), (RICE 1974), (AYATOLLAHI, PAVIER & SMITH 1998), (SCHÜTTE & MOLLA-ABBASI 2007B), (MOLLA-ABBASI & SCHÜTTE 2008). The 2nd chapter is devoted to give the full set of the T-stresses for elliptical and circular cracks embedded in a homogenous isotropic infinite solid. Using the potential method and a transformation technique, the asymptotic solutions for the stress components are derived, from which the T-stress terms for elliptical and circular cracks in infinite isotropic linear elastic solids are resulting.

The prediction of crack paths under general mixed-mode loading conditions, using the theory of linear elastic fracture mechanics, has been the subject of many investigations, both in the two- and three-dimensions. These include both the theoretical works devoted to infinitesimal crack extension from a given geometry, and numerical studies simulating the propagation of cracks. The 3rd chapter deals with the theory, mechanism and simulation of crack growth phenomena. The maximum driving force fracture criterion, resulting from the variational principle of a cracked body in equilibrium, along with a modified Paris' law is considered further in the simulation of the quasi-static crack prop-

agation in linear elastic isotropic and homogenous solids. The model provides a general framework for mixed-mode linear elastic fracture mechanics under small strain assumptions, and gives the evolution of the stress intensity factors and the T-stresses by crack growth. A variety of numerical examples is presented, including central straight cracks in two-dimensional case, and internal circular and elliptical cracks in three-dimensions with different mode-mixities in linearly elastic, homogeneous and isotropic solids, with or without inclusions.

The 4th chapter is concerned with the numerical analysis of the evolution of the anisotropic damage due to a single growing mixed-mode internal elliptical or circular crack in a unit cell. This provides a better insight into the irreversible process of damage on the macroscale from the microscale level. For this, the concept of the unit cell damaged by a single growing mixed-mode crack is considered, and based on the results given in chapter 3, the type of the anisotropy induced by the damage due to the growth of the elliptical and circular microcracks are determined. To identify the type of material symmetry, the approach proposed by COWIN & MEHRABADI (1987) is applied, which is based on the characteristics of the eigenvalues and eigenvectors of the elasticity tensor. The results are then verified with the help of an optimization procedure.

The fundamentals of continuum damage mechanics are reviewed in chapter 5. With the help of the approach of micromechanics, the effective continuum elastic properties of isotropic linear elastic solids damaged respectively by an internal elliptical crack and a kinking elliptical crack are presented, from which the results corresponding to the initiation and the kinking of a single internal circular crack are resulting. Within the approach of micromechanics, the effective elastic properties of a solid damaged by a planar elliptical crack are derived from the contribution to the complementary strain energy corresponding to the quasi-static, selfsimilar growth of the crack. For this, the stress intensity factors suffice to give the energy released during the quasi-static, selfsimilar growth of the crack. However, for the formulation of the complementary strain energy corresponding to the kinking of a crack, the analytical expressions for the so called T-stresses are required as well. Based on the damage induced anisotropy due to a growing elliptical crack, in a local sense, a thermodynamically consistent continuum damage model for brittle materials is proposed, which is based on the reduction of stiffness due to the kinking and growth of elliptical microcracks. The model is formulated consistently in a fully analytical way and degradation of the elastic properties is associated with the irreversible process of crack kinking and growth. Combining the local damage due to the kinking of microcracks, with a power law model for fatigue crack growth in fracture mechanics and an appropriate fracture criterion yields a consistent damage evolution model for predicting the failure of structures and mechanical components subjected to fatigue conditions, independent of the type of loading. A variety of numerical examples is presented to illustrate the proposed damage model in more details, and to show its applicability to real mechanical components subjected to sequential loads.

Finally, the thesis is summarized and concluded in chapter 6. Some remarks concerning

the implementation of the proposed continuum damage model in an incremental scheme are given, and the report is closed with introducing the possible extensions of the model and some modifications to account for other dissipative mechanisms, such as friction.

1 Principles of Fracture Mechanics

Contents

19th March 1830, Great Britain; about 700 persons assembled on the Montrose suspension bridge to witness a boat race, when one of the main chains broke and caused considerable loss of life.

This is one of the earliest recorded brittle fractures in a major structure. Since then, there have been a number of catastrophic bridge failures, including the cases of the Husselt Bridge over the Albert Canal in Belgium (1938), King's Bridge in Melbourne, Australia (1962) and Point Pleasant Bridge in West Virginia (1967). Through the 19th century, railway accidents due to fracture in axles, rails and wheels were relatively common. During the decade 1860-1870, the number of people who died in railway accidents in Great Britain alone was in the order of two hundred per year. Among typical storage tank failures, one may mention the molasses tank accident in Boston. On January 19 1919, without an instant warning the top of the tank was blown into the air and the sides were burst apart, collapsing a number of buildings and part of the elevated railway structure and causing 12 deaths and forty injuries. Another typical pressure boundary failure has been the fracture propagation in natural gas transmission lines.

The structural failures that attracted the attention of mechanics and materials communities most were two systematic events in the 1940s and 1950s, namely the failures of welded ships and commercial jet airplanes. Starting in 1943, over 4000 Liberty type cargo ships and 530 T2 type tankers were built in various shipyards in the United States and Canada. Among these, over 1200 experienced brittle fracture of the hull, 233 of which were catastrophic and lead to loss of service and 16 broke in half. Subsequent research performed in the United States and Great Britain, mostly by the materials community,

identified notch brittleness as one of the major causes of these fractures. The concept of notch brittleness was, of course, not new and was known since 1885. What came out of these studies was, however, the concept of brittle-ductile transition temperature. Because of the presence of cyclic loading combined with occasional peak loads, low temperatures and a highly corrosive environment, marine vessels are particularly prone to brittle fracture and catastrophic failures continue to occur. Another case happened on January 16 1998 as a freighter, on its way from Rotterdam to Montreal, broke in half for unknown reasons and sank near the south coast of Newfoundland.

The second important incident was the loss of the Comet I airplanes. On January 10 1954, the world's first jet-propelled passenger aircraft entering the passenger service disintegrated in the air at approximately 30,000 feet and crashed into the Mediterranean Sea after 1286 pressurized flights. On January 11 1954, the Comets were removed from service and, after some modifications, they resumed to service on March 23 1954. Shortly after, on April 8 1954, another Comet disintegrated in the air at 35,000 feet and crashed into the Mediterranean near Naples. On April 12 1954, the certificate of airworthiness for the Comets was withdrawn. To determine the cause of the accidents, an aircraft which had accumulated 1230 flights was subjected to cyclic loading under water simulating pressurized flights and to 33% overload at approximately 1000 cycle intervals. It was under one of these proof tests, after 1830 further pressurization in the test facility, that the cabin failed. The fracture initiated at the corner of a passenger window. Examination of the failure indicated evidence of fatigue. Further investigation of the first failed aircraft recovered near Elba confirmed that the primary cause of the accident was pressure cabin failure due to fatigue.

In all these accidents resulting from brittle fracture, it appears that in each case the then existing design rules were fully followed and yet catastrophic failures continued to occur. It was, therefore, becoming very difficult to attribute the causes of the failures to material defects only, as was routinely done prior to the 1940s. Thus, the large scale ship failures during the 1940s and the failures in a highly critical industry of jet transportation in the 1950s were responsible not only for the recognition of brittle fracture as a serious problem but, to a great extent, for the extensive research that followed to find its causes and to develop methods for its control.

In designing structural or machine components, an important step is the identification of the most likely mode of failure and the application of a suitable failure criterion. Fracture characterized as the formation of new surfaces in the material is one such mode of mechanical failure. At the most basic level the essential feature of the process is breaking of interatomic bonds in the solid. From a macroscopic standpoint, however, fracture may be viewed as the rupture separation of the structural component into two or more pieces due to the propagation of cracks. In between the process involves the nucleation, growth and coalescence of microvoids and cracks in the material. Thus, in studying the fracture and damage of solids ideally one would have to consider such widely diverse factors as the microscopic phenomena taking place at various length scales, and the macroscopic aspects

regarding the loading, environmental conditions, and the geometry of the medium. Due to this highly complex nature of the phenomenon, at the present time there seems to be no single theory dealing satisfactorily with all its relevant aspects. Quite naturally, then, the theories developed to study the fracture of solids tend to treat the subject generally from one of the three major points of view, namely microscopic or atomic, micro-structural, and macroscopic or continuum mechanics.

From the standpoint of engineering applications, it has been the macroscopic theories based on the notions of continuum solid mechanics and classical thermodynamics that have provided the quantitative working tools in dealing with the fracture of structural materials. In the macroscopic approach to fracture, it is generally assumed that the material contains some flaws which may act as fracture nuclei and that the medium is a homogeneous continuum in the sense that the size of a dominant flaw is large in comparison with the characteristic micro-structural dimension of the material. The problem is, then, to study the influence of the applied loads, the flaw geometry, environmental conditions and material behavior on the fracture process in the solid, a subject which has come to be known as fracture mechanics.

The phenomenon of damage also represents surface discontinuities in the form of microcracks and volume discontinuities in the form of microvoids and microcavities, which at the mesoscale level the coalescence of these microdefects initiate one or more cracks. At the macroscale level, damage is concerned with the growth of cracks and defects. The first two stages of damage may be studied by means of damage variables of the mechanics of continuous media defined at the mesoscale level. The third stage is usually studied using fracture mechanics with variables defined at the macroscale level.

Fracture is only one way by which damage accumulation and mechanical failure can occur. Other types of processes leading to failure of structures are corrosion, wear and plastic collapse, which do not belong to the scope of this thesis. Closely related to fracture mechanics, however, is the plastic collapse. Fracture mechanics is rather a young discipline. Even though the interest in fracture prediction goes back to stone age, the systematic approach to tackle problems concerning cracks and crack growth and coalescence and the corresponding damage is typically the concept of the recent half century's research. Over the past few decades, the field of fracture mechanics has undoubtedly prevented a substantial number of structural failures.

1.1 History of the field

The early strength theories of solids were based on the maximum stress. However, it appears that the so called size effect, which plays a rather important role in fracture, was known before the introduction of the concept of stress to study the strength of solids. In one of his sketch books, Leonardo da Vinci describes his experiments on breaking iron wires and how the weight required to break the wire increases as its length is cut

in half in successive tests (TIMOSHENKO 1953). The trend was substantially verified later by Griffith's experiments on glass fibers (GRIFFITH 1921). Early studies showed that the strength was also dependent on surface quality and, particularly, on surface notches. This was observed by WÖHLER (1860) in his fatigue studies and later on by KOMMERS (1912). These and similar investigations showed that surface polishing could increase the strength of the machined specimens by as much as 20 to 50 percent.

It appears that the first elasticity solution in which the existence of stress singularity was recognized is due to WIEGHARDT (1907). In a remarkable, but little known, article, he essentially provided the solution for a linear elastic wedge subjected to an arbitrary concentrated force applied to one of the wedge boundaries. The solution includes the analysis of the asymptotic behavior of the stress state near the wedge apex and the special case of the crack problem in considerable detail. Its correct form of $r^{-\lambda}$ was obtained (r being the distance from the wedge apex and λ is the so called degree of singularity), and the dependence of λ on the wedge angle and on the symmetry of loading was demonstrated. However, since he did not question the validity of the maximum stress criterion for fracture, he was faced with a paradox. At the crack tip, where the stress becomes infinite for any arbitrarily small force and yet the experience shows that the material fractures only if the applied force is raised to a critical value.

To study the difference between the theoretical strength and the bulk strength of solids, Griffith simulated the defects with an elliptical hole, the solution for which was previously given by INGLIS (1913). The results showed that the calculated maximum stress is independent of the absolute size of the flaw and depends only on the ratio of the semi-axes of the ellipse. These findings were in apparent conflict with the test results and led Griffith to conclude that the maximum stress may not be an appropriate strength criterion and an alternative theory was needed (GRIFFITH 1921), (GRIFFITH 1924). The basic concept underlying Griffith's new theory was that, similar to liquids, solids possess surface energy and, in order to propagate a crack (or increase its surface area), the corresponding surface energy must be compensated through the externally added or internally released energy. For a linear elastic solid, this input energy which is needed to extend the crack may be calculated from the solution of the corresponding crack problem. Using the solution of INGLIS (1913) for a uniformly loaded plate with an elliptical hole, Griffith calculated the increase in strain energy and, from the energy balance, obtained the stress corresponding to fracture. Griffith's major contributions, regarding the fracture of brittle solids, were that he was able to resolve the infinite stress paradox recognized earlier by WIEGHARDT (1907) and to show that the fracture stress is dependent on the flaw size. He also verified his hypothesis by performing some carefully designed experiments on pressurized glass tubes and spherical bulbs containing cracks of various sizes. However, Griffith's work was largely ignored by the engineering community until the early 1950s.

In the early 1950s, the energy balance theory was also reconsidered by researchers who were primarily interested in catastrophic failure of large scale metallic structures. The X-ray studies conducted earlier by OROWAN (1948) showed that even in materials

fracturing in a purely brittle manner, there was evidence of extensive plastic deformation on the crack surfaces. This led IRWIN (1948) and OROWAN (1948) independently to conclude that the plastic work at the crack front must also be considered as dissipative energy in the surface energy model proposed by GRIFFITH (1921).

Irwin's second important contribution was the development of a universal method for calculating the rate of the energy available to fracture a solid. For this, the continuum elasticity solution for each crack geometry and loading condition is needed. Griffith's work showed only too well how difficult this task could be. During this period, the timely analytical results appear to be the work of SNEDDON (1946) on plane and axisymmetric crack problems. By using the solution proposed by WESTERGAARD (1939) for plane problems and by solving the circular crack problem, Sneddon obtained the correct asymptotic behavior of the stress field near the crack tip and showed that the results for the two cases differ only by a numerical factor of $2/\pi$. For the circular crack, he also obtained the correct expression of Griffith's energy balance equation. However, Sneddon seemed to have failed to recognize the universal nature of the crack tip stress field by stating (incorrectly) that the tangential stress component which appears in the axisymmetric problem has no analog in the plane problem. As later pointed out by IRWIN (1957), asymptotically, the stress state around the border of circular crack is one of plane strain and the identification of the numerical factor observed by SNEDDON (1946) is a key factor in generalizing the results. One of Irwin's major contributions, thus, was his recognition of the universal nature of asymptotic stress and displacement fields around the crack front in a linear elastic solid. He observed that the symmetric crack solutions given by SNEDDON (1946) and WESTERGAARD (1939) may be generalized to include the asymptotic expressions for all crack problems and, for a small distance r from the crack tip, the stresses may be expressed as $\sigma_{ij} \sim K_\alpha/\sqrt{2\pi r}\, f_{ij}^\alpha$, where f_{ij}^α are the functions previously obtained by WIEGHARDT (1907), WESTERGAARD (1939) and SNEDDON (1946) for specific crack geometries and loading conditions. Irwin called the coefficient of the singular stress term (K_α) the stress intensity factor.

To calculate the energy available for fracture, IRWIN (1957) then interpreted the fixed-grip strain energy release rate involving the entire solid in terms of the rate of crack closure energy, which can be calculated by using the local asymptotic expressions for the crack surface displacement and the corresponding cleavage stress only. For the symmetric loading of a planar crack, he then evaluated the energy release rate as $K^2/\bar{E}$ and designated it by G, where $\bar{E} = E/(1-\nu^2)$ in case of plane strain condition. Subsequently, by using Westergaard's solution he showed that the stresses and displacements in the close neighborhood of the smooth internal boundary of a planar crack in a linearly elastic solid under most general loading conditions may be expressed in terms of three stress intensity factors K_I, K_{II} and K_{III} (and three sets of related universal angular functions) associated with the symmetric opening, in-plane shear and anti-plane shear modes of deformation, respectively (WESTERGAARD 1939). He also evaluated the corresponding strain energy release rates G_I, G_{II} and G_{III} and their sum G for the general co-planar crack growth problem.

To make the energy balance theory, as modified by IRWIN (1957), an effective design tool, the concept of a realistic single parameter characterization of the material's resistance to fracture also needed to be developed. This required the additional assumption that, in solids fracturing in a brittle manner, the size and shape of the fracture process (or the energy dissipation) zone remain essentially constant as the crack propagates, leading to the hypothesis that in such solids the energy needed to create a unit fracture surface is a material constant. Irwin designated this fracture resistance energy as the fracture toughness, G_{Ic}. Thus, by the middle of the 1950s, nearly all pieces of a new field called fracture mechanics were in place and, by the late 1950s, the field was ready for rapid expansion.

During the 1950s and early 1960s, the immediate concern in applications was brittle fracture and fatigue crack growth. It turned out that the stress intensity factor could be used as an extremely effective correlation parameter to model both of these phenomena. Since the stress intensity factor is a product of linear elasticity solutions of crack problems, the initial efforts in fracture mechanics research were concentrated on developing and adapting methods for solving such problems. A fairly thorough description of the methods used in solving elastic crack problems may be found in various articles by ERDOGAN (1978), LIEBOWITZ (1968), SIH (1973) and ATLURI (1986). There are two major methods of solving the mixed boundary value problems in elasticity that arise from the formulation of the crack problems, namely the complex function theory and the integral transforms. The complex potentials were first introduced by GOURSAT (1898) to represent the biharmonic function. Their applications to problems in elasticity were, however, developed in detail by a school of Georgian mathematicians led by MUSKHELISHVILI (1933). The method is nearly indispensable for the examination of the singular nature of stresses at the crack tips, particularly in problems involving bonded dissimilar materials. However, the shortcoming of the method is that it is restricted to two-dimensional problems. There are a number of techniques used in the solution of two-dimensional crack problems which are also based on the complex function theory. Among these, one may mention conformal mapping, Laurent series expansion, boundary collocation method and certain applications of the Wiener-Hopf method. The method of integral transforms is one of the most widely used techniques in the formulation of the boundary value problems in mechanics. Depending on the crack geometry and the coordinate system, the most often used transforms are Fourier, Mellin and Hankel transforms. In simpler cases, the problem can very often be reduced to an Abel's equation and solved directly. In many cases, however, it may be necessary to reduce the resulting dual series or dual integral equations to singular integral equations, using the complex function theory to obtain the fundamental function and solving the problem numerically by taking advantage of the properties of the related orthogonal polynomials. Among other analytical methods used for solving linear elastic crack problems, one may also mention the method of eigenfunction expansion and the alternating method.

Theoretical methods are essential for solving crack problems for two main reasons. First, they provide the correct form of singularities and asymptotic results that may be needed to analyze and interpret the experimental results and to use for improving the

accuracy of purely numerical solutions. Secondly, they provide accurate solutions for relatively simple part/crack geometries and for certain idealized material behavior that could be used as benchmarks for numerical and approximate procedures. However, in practical applications, the geometry of the medium is seldom simple and realistic material models seldom lead to analytically tractable formulations. It is therefore necessary to develop purely numerical methods that can accommodate complicated part/crack geometries and material models. The finite element method, which is another major contribution of the solid mechanics community to the science and art of engineering within the past fifty years, appears to be ideal for this purpose and is widely used in fracture mechanics. One may also note that in certain problems, such experimental techniques as photoelasticity, moire interferometry and the method of caustics may prove to be very effective in estimating the stress intensity factors. In particular, the three-dimensional photoelasticity using frozen fringe technique was shown to be very useful in studying cracked structural components with relatively complex geometries.

Under operating temperatures and relatively high loads, most engineering materials exhibit some form of inelastic behavior. The main feature of the fracture process in such materials is that the characteristic length parameter of the inelastic region around the crack front, where the energy dissipation takes place, is generally of the same order of magnitude as the crack size. In elastic-plastic materials, the size of the plastic zone itself is very heavily dependent on the constraint conditions along the crack front. Thus, in relatively thick specimens, the interior region would be under plane strain conditions, whereas, near the surfaces, due to lack of constraints, there would be a transition to plane stress conditions, accompanied by greater plastic zone size and higher resistance to fracture. One would then observe a low energy flat fracture in the interior and shear lip formation and high energy ductile fracture near the surfaces. Very often, the terminology G_{Ic} used for fracture toughness in practice implies plane strain value of G_c, the critical strain energy release rate. The latter is rather heavily dependent on specimen constraints, particularly on thickness. Furthermore, the size of the plastic region around the crack front varies with growing crack size, generally increasing with the increasing crack size. This implies that a material's resistance to fracture would also increase with increasing crack size.

For ductile crack propagation, it appears that two essential conditions need to be satisfied. The first is a local condition needed for crack growth initiation. The mechanism for crack initiation may be the nucleation, growth and coalescence of voids or microcracks, or simply decohesion taking place at the crack tip. For this, in a small region ahead of the crack front, the mechanical conditions must reach a critical state regardless of what goes on in the surrounding plastic region. The initiation of crack growth can thus be characterized by a single strength parameter such as critical crack tip opening displacement, critical crack opening angle or work of separation. On the other hand, for further crack growth or unstable fracture, the condition of global energy balance must be satisfied. Since the material's resistance to ductile fracture is highly dependent on the crack size and the geometry of the medium, this second condition cannot be characterized by a single strength parameter.

The first important attempt at modeling the ductile fracture process, too, seems to have been made by Irwin and his associates. By recognizing the increase in fracture resistance with growing crack size, they introduced the concept of the crack extension resistance curve (R-curve), which consists of the plot of total energy dissipation rate (including the work of separation) as a function of the crack size. The fracture resistance is represented by energy (G_R, R, J_R) or sometimes by the equivalent stress intensity factor. The R-curve is thus a continuously distributed parameter characterization of ductile fracture growth. By including the crack driving force G or the stress intensity factors K in the same plot, the concept provides an effective tool to examine the processes of slow stable crack growth and fracture instability.

Even though it is based on a very sound physical concept, initially the R-curve was not widely used in applications. The main reasons for this are that it is generally dependent on the geometry of the component and the corresponding crack driving force is difficult to calculate. However, starting in the early 1970s, practicing engineers began to use the R-curve technique rather extensively. There seems to be a number of factors influencing this trend. It was during this period that fracture mechanics was becoming not only an interesting field to study but also an acceptable and effective design tool. There were some highly critical safety issues involving nuclear pressure vessels and other pressurized containers that needed a closer examination by a more rational technique. There were also some experimental studies indicating that, at least for some materials, the R-curve may indeed be the universal signature of the material's ductile fracture resistance. Finally, there was the very timely appearance of Rice's work on the so called J-integral (RICE 1968B).

The theoretical basis of the J-integral may be found in certain conservation laws previously studied by ESHELBY (1920) and GÜNTHER (1962). Also, physical concepts similar to that of the J-integral regarding the energy release rate were described earlier by SANDERS (1960) and CHEREPANOV (1968). However, for two-dimensional notch and crack problems in nonlinear elastic solids, RICE (1968B) have developed the concept of the path independent J-integral independently. Rice showed that in a general nonlinear elastic solid, the line integral encircling the crack tip is path independent and its value J represents the energy release rate for coplanar crack growth. Since nonlinear elasticity is equivalent to the deformation theory of plasticity (provided there is no unloading) and since the path integral can be calculated in a straightforward manner by using, for example, the finite element technique, J-integral gradually became an attractive alternative to G or K in studying elastic-plastic fracture.

It was also at this time that HUTCHINSON (1968) and RICE & ROSENGREN (1968) worked out the details of the singular behavior of stresses, strains and deformations around the crack tip for a particular nonlinear solid and showed that J is a measure of the strength of this so called HRR singularity. Even though the concept of J-integral is not valid in the plastic zone near the crack tip where loading is non-proportional, J would give a reasonably good approximation to the energy release rate, provided the charac-

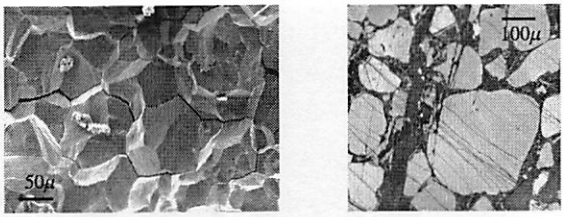

Figure 1.1: intergranular and transgranular spreading of brittle fracture

teristic size of the plastic zone with non-proportional loading is small compared to the size of the J-controlled region. This is somewhat analogous to the fracture process zone and K-controlled region in linear elastic fracture mechanics and provides further analytical justification for selectively using J-integral as the measure of crack driving force in certain elastic-plastic fracture problems.

Prior to the 1960s, the primary failure criteria used in mechanical design were tensile strength for brittle fracture, von Mises or Tresca criterion for yielding, energy absorption or toughness for impact and various versions of the Wöhler diagram for fatigue. Since, in most cases, the loading has a cyclic nature, fatigue has always been a major consideration in design. Thus, until the 1960s, the universally accepted criterion for design was the safe life criterion which required that time for crack initiation be longer than the expected operational life of the structure. In bulky components, nearly 95% of the life is consumed by the initiation of a detectable crack. Therefore, despite the heavy reliance on safety factors necessitated by large scale variabilities in observations, the technique is still used rather widely in conventional design. However, in some very highly critical application such as (civilian and military) aircraft components, nuclear pressure vessels, steel bridges and certain microelectronics devices, the existence of initial defects that may form the nuclei of fatigue cracking is practically unavoidable. The assumption then must be that the crack is always there and is growing and it becomes detectable only when it reaches a certain size. Consequently, in these structures a very significant part of the service life is consumed by subcritical crack propagation. It turns out that by using the stress intensity factor as the load parameter, the subcritical crack growth rate can be correlated much more tightly and hence, the service life can be estimated with much less uncertainty.

1.2 Process of fracture and crack growth

This section provides some elementary information about the various fracture mechanisms, which is an essential background for the study of fracture mechanics and the comprehension of the basic ideas and the limitations. Basically, there are two principal fracture mechanisms, namely cleavage fracture and ductile fracture. Cracking alone does not necessarily lead to fracture. When a crack due to propagation mechanisms such

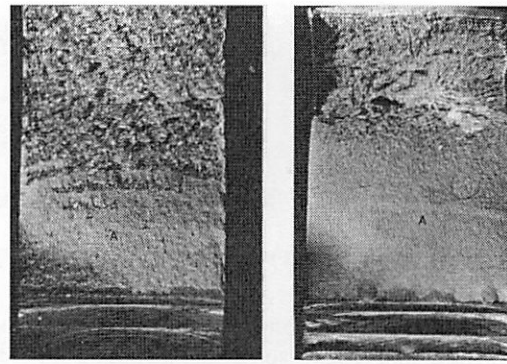

Figure 1.2: cleavage fracture left, and ductile fracture right, both initiated by fatigue crack

as fatigue, stress corrosion and hydrogen cracking has developed to a certain size, final fracture will take place by cleavage or by ductile fracture. Since a cleavage fracture is usually associated with little plastic deformation, it is called brittle fracture. But the term brittle fracture is often generalized to all fractures with little plastic deformation, although the final separation occurs in a ductile manner (BROEK 1974).

1.2.1 cleavage fracture and ductile fracture

Toughness is the term used to describe the ability of a material to deform plastically and to absorb energy before and during rupture. The adjectives *brittle* and *ductile* are used to distinguish failures of materials characterized by low and high toughness. Cleavage fracture is the most brittle form of fracture that can occur in crystalline materials. The likelihood of encountering cleavage fracture is increased by lower temperatures and higher strain rates as is illustrated by the well known ductile-brittle transition.

Cleavage fracture of metals occurs by direct separation along crystallographic planes due to a simple breaking of atomic bonds. Its main characteristic is that it is usually associated with a particular crystallographic plane. Iron for example cleaves along the cube planes (100) of its unit cell. This causes the relative flatness of a cleavage crack within one grain, as indicated in figure 1.1. Since neighboring grains will have slightly different orientations, the cleavage crack changes direction at a grain boundary to continue propagation on the preferred cleavage plane. The flat cleavage facets through the grains have a high reflectivity, giving the cleavage fracture a bright shiny appearance.

Fracture occurring under the single application of a continuously increasing load can either be brittle cleavage fracture or fracture associated with plastic deformation, which is essentially ductile. For the latter the amount of plastic deformation required to produce fracture may be so limited in certain cases, that relatively little energy is consumed. Then the fracture is still brittle in an engineering sense and can be initiated at a sharp notch

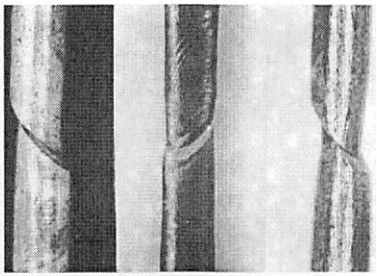

Figure 1.3: sheared single crystals of pure copper

or crack at a comparatively low nominal stress, particularly when a state of plane strain reduces the possibilities for plastic deformation.

The most familiar type of ductile fracture is by overload in tension, which produces the classic cup and cone fracture. After the maximum load has been reached the plastic elongation of a prismatic-tensile coupon becomes inhomogeneous and concentrates in a small portion of the specimen such that necking occurs. In extremely pure metals, which are virtually free of second phase particles, it is possible for plastic deformation on conjugate slip planes to continue until the specimen has necked down to an arrow point by 100 percent reduction of area. Such a failure is a geometric consequence of the slip deformations. As an example, figure 1.3 shows a single crystallin material that has almost failed by shear on a single slip plane.

Engineering materials always contain large amounts of second phase particles. Three types of particles can be distinguished. The first type are *Large particles*, visible under the optical microscope. Their size may vary from 1-20 μm. They usually consist of complicated compounds of the various alloying elements. The alloying elements may be added to improve castability or some other mechanical properties. Sometimes, however, particles of this size may be produced on purpose, as in the case of carbides in certain steels. The second type of particles are *Intermediate particles* which are only visible by means of the electron microscope. Their size is in the order of 500-5000 Ångstrøm units. These particles may also consist of complex compounds of the various alloying elements. Sometimes particles of this size are essential for the properties of the material, as in the case of dispersion strengthened metals (such as Ni-ThO_2,) and in the case of steels were carbides of this size are intentionally developed. The third type of particles are *Precipitate particles* which are in certain cases visible by means of the electron microscope. Their size is in the order of 50-500 Ångstrøm units. They are purposely developed by means of solution heat treatment and ageing, and they serve to give the alloy its required yield strength.

The large particles are often very brittle and therefore they cannot accommodate the plastic deformation of the surrounding matrix. As a result they fail early on, when the matrix has undergone only a small amount of plastic deformation. This means that voids

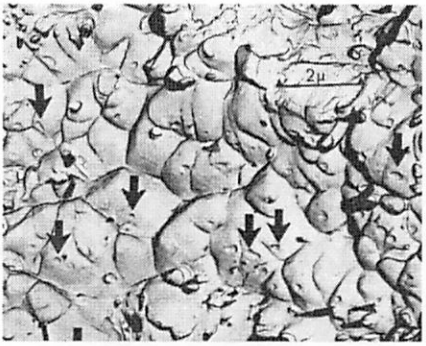

Figure 1.4: dimples initiated at intermediate size particles (arrows). Aluminium-alloy

are formed. The large inclusions visible in the optical microscope can determine the instant and location of ductile fracture and decrease the ductility of the material, but they do not play a role in the process of ductile fracture itself.

Fracture is induced by the much smaller intermediate particles of the sub-micron size. Since these particles cannot deform as easily as the matrix, they lose coherence with the matrix when extensive plastic flow takes place in their vicinity. In this way tiny voids are formed, which grow by slip, the material between the voids necks down to the full 100 percent in the same way as in figure 1.3. This necking takes place at a micro-scale and the resulting total elongation remains small.

The mechanism of initiation, growth and coalescence of microvoids gives rise to characteristic fractographic features. When observed in the electron microscope the fracture surface consists of small dimples which represent the coalesced voids (figure 1.4). In most of the dimples the small particle that initiated the void can easily be recognized. Dimples always have an irregular shape, due to the random occurrence of voids, and their profile gives an impression of the process of void growth and coalescence. Dimples can be roughly divided into two categories according to their apparent shape, namely equi-axed and parabolic. The shape in which the dimples appear in the microscope depends upon the stress systems that were active during their formation, and upon the angle of observation in the microscope. Equi-axed dimples may be formed if the stresses are predominantly tensile, and elongated dimples occur in the shear or tear mode.

Contrary to cleavage where the action of a tensile stress is sufficient for the separation, ductile fracture cannot occur without plastic deformation. The mechanism of final separation is a direct consequence of dislocation movements and slip displacements necessary for the growth and coalescence of voids. Apart from a stress to induce dislocation movement a certain plastic strain is required for ductile separation to occur. This plastic deformation may be confined to a small volume of material through which the fracture passes. Then failure occurs with relatively little plastic deformation on a macroscale,

Figure 1.5: striations on fatigue crack surface of Al-Cu-Mg alloy

requiring only little energy. The fracture is brittle in an engineering sense. Fractures induced by cracks in high strength materials are usually of this type.

1.2.2 fatigue cracking

Under the action of cyclic loads, cracks can be initiated as a result of cyclic plastic deformation. Even if the nominal stresses are well below the elastic limit, locally the stresses may be above yield due to stress concentrations at inclusions or mechanical notches. Consequently, plastic deformation occurs locally on a microscale, but it is insufficient to show in engineering terms. Several equivalent models have been proposed to explain the initiation of fatigue cracks by local plastic deformation, for example the slip mechanism proposed by WOOD (1958) which is followed by an extrusion or an intrusion in the metal surface (see also COTTRELL & HULL (1957) and (MOTT 1958)). A fatigue crack, once started, can also grow by a mechanism of reversed slip.

A sharp crack in a tension field causes a large stress concentration at its tip where slip can occur fairly easily. The material above the crack may slip along a favorable slip plane in the direction of maximum shear stress. Due to that slip the crack opens, but it also extends in length. Slip can now occur on another plane. Work hardening and increasing stress state will finally activate other parallel slip planes, which lead to a blunt crack tip. During the rising load part of the cycle the crack propagates by a certain amount and plastic deformation occurs in a small region which is embedded in elastic surroundings. During load release the elastic surroundings will contract and the plastically deformed region, which has become too large, does not fit any more in its surroundings. In order to make it fit, the elastic material will exert compressive stresses on the plastic region during the decreasing part of the cycle. These compressive stresses will be above yield again, at least locally at the crack tip. This means that reversed plastic deformation occurs, which will close and resharpen the crack tip.

The cyclic opening and closing of the crack will develop a typical pattern of ripples,

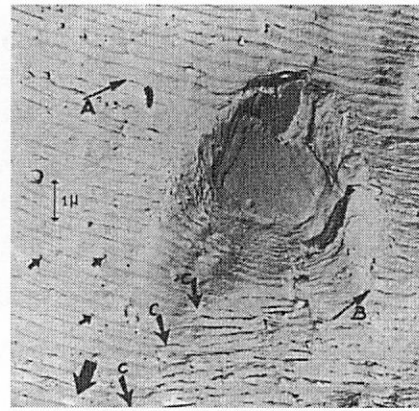

Figure 1.6: large cracked particle in fatigue crack surface at low fatigue crack growth rate in 2024-T3 aluminium alloy

every new cycle adding a new ripple. These ripples show up on the fracture surface in the electron microscope, and they are called fatigue striations. Figure (1.5) shows fatigue striations in a commercial Al-Cu-Mg alloy. In contrast, a mechanism of cleavage may sometimes be involved in fatigue crack propagation. This gives way to the formation of brittle striations as opposed to the ductile striations discussed above.

The question arises whether inclusions and second phase particles have an influence on fatigue cracking. As far as initiation of fatigue cracks is concerned they must be expected to have an influence. In the case of smooth specimens the inclusions are sites of stress concentration. At such locations, the required plastic deformation can occur. Fatigue cracking initiated at such particles was reported by GROSSKREUTZ & SHAW (1969), BOWLES & SCHIJVE (1973) and MCEVILY & BOETTNER (1963). If stress concentrations exist at mechanical notches it may be expected that particles are not strictly required for the initiation of a crack, since the extra stress concentration due to a particle is of limited importance. For the same reason it must be expected that particles have little influence on fatigue crack propagation. Indeed, at low crack rates their influence is very limited, figure (1.6).

The situation is completely different at high crack propagation rates in the order of 1 micron per cycle and above. High growth rates are a result of a high stress intensity at the crack tip. Due to the higher stress concentration, particles in front of the crack tip may cleave or lose coherence with the matrix, thus initiating a (large) void. The remaining material between the void and the crack tip now may rupture by ductile tearing, thus producing a local jump of the crack front. This is obvious from the areas with dimples in figure (1.7), which are evidence of a mechanism of void coalescence during ductile rupture. The influence of particles on fatigue crack propagation is limited to high crack propagation rates. This means that it is limited to the very last and small part of the crack

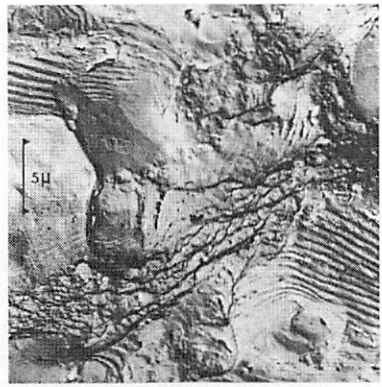

Figure 1.7: dimples around cracked large particles among fatigue striations at high fatigue crack growth rate in Aluminium-alloy

propagation life. Consequently, it is not very important technically. This is confirmed by tests on materials with very low particle content (EL-SOUDANI & PELLOUX 1973).

1.2.3 environment assisted cracking

Another way in which cracks can be initiated and grow at low stress levels is environmental cracking. A liquid metal environment may cause cracking even under zero stress. A corrosive environment, which would not normally attack the metal, may cause cracking under the assistance of mechanical stresses. Several theories have been put forward to explain this stress corrosion cracking, yet its mechanism is far from well understood. In particular, the role of the mechanical stresses is difficult to comprehend. It seems inconceivable that any single theory is likely to explain all observations and it seems reasonable that different mechanisms operate under different conditions and in different materials. In view of this, the discussion of stress corrosion cracking will be limited to it being mentioned as a mechanism for cracking. In many materials stress corrosion cracks are intergranular, which may be due to a potential difference between the grain boundary and the interior of the grains as a result of a segregation of the solute. Alternatively, it may be attributed to the presence of second phase particles at the grain boundaries.

There is some concurrence of opinion as to whether the hydrogen produced during corrosion in some cases may be the cause of stress corrosion cracking. The presence of hydrogen in steels can cause cracking even during processing. Hydrogen can also cause cracking of high strength steel after a considerable period of sustained loading known as static fatigue. Hydrogen cracking is usually intergranular, similar to stress corrosion cracking in steels. Other materials than steels can also be embrittled by hydrogen, but this embrittlement is often caused by the formation of brittle hydride particles. This means that the material has a low toughness, whereas in the case of steels the hydrogen serves

as a mechanism to produce a crack of sufficient length that the given toughness of the material will cause it to fail at the applied stress.

1.3 Crack and fracture mechanics

The linear fracture mechanics is based on the elastic analysis of the stress field for small deformations. It gives excellent results for brittle elastic materials, such as high strength steel, ceramic, glass and to a lesser extent, concrete and wood (LEMAITRE & CHABOCHE 1990). The crucial value of the energy release rate, the stress intensity factors, or the J-integral represents a precise condition of fracture by instability of the cracked medium. Similarly the fatigue model of PARIS (1962) and its derivatives, which express the crack growth rate per load cycle as a function of the amplitude of one of the above three variables, can be used to predict the propagation of cracks in structures subjected to periodic loading.

The case of plasticity or viscoplasticity are studied with the help of nonlinear fracture mechanics. This is the case for ductile materials like low carbon steel, stainless steel, certain aluminium alloys and polymers. The plasticity manifests itself into two ways: at the level of the plastic zone ahead of the crack tip (crack front in three-dimensional crack problems), being the source of history effect by virtue of the development of residual stresses, and at the level of the mechanisms of crack propagation. As long as the load is low enough, whether monotonically increasing or in a periodic manner, these effects can be neglected and linear fracture mechanics provides a good approximation to the physical problem. In contrast, for large and highly variable loads, the stable progression of ductile fracture cracks and the history effects due to overloads can be modeled only by taking plasticity into account. Average and high temperatures induce creep-fatigue interaction effects.

Dynamic effects become significant in two groups of crack problems, namely solids with a stationary crack under impact loading, and solids with a crack propagating at a sufficiently high velocity. In the former, the asymptotic stress field near the crack tip is identical to that of the corresponding elastostatic crack problem and there is generally an overshoot in the stress intensity factor. In the latter, the asymptotic crack tip behavior is dependent on the instantaneous crack velocity only (FREUND 1990). An important application of elastodynamics is in the area of nondestructive evaluation (NDE) of structural components, which generally involves the determination of the type, size, location and orientation of flaws in the medium using ultrasonic and acoustic emission test results (ACHENBACH 1973).

The next sections provide the fundamentals required for the following chapters of the thesis. For further details on nonlinear crack mechanics, elastodynamic crack mechanics and the related topics, the interested reader is referred to the pertinent literature by IRWIN (1948), RAVI-CHANDAR (1982), FREUND (1990), MAUGIN (1992),

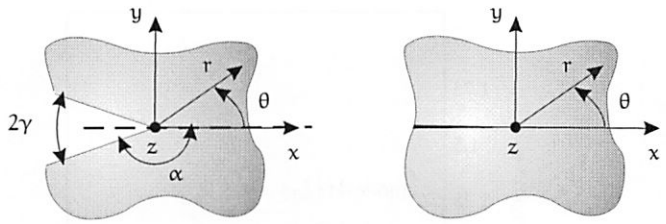

Figure 1.8: V-notch geometry and mathematical crack

BETEGON & HANCOCK (1991) and the works cited there.

1.3.1 linear elastostatic stress field of a crack

This section presents the asymptotic stress field of a V-notch. This field is due to WILLIAMS (1957) and can be reduced to the one of a traction free crack with a sharp tip. Figure 1.8-left shows a V-notch with traction free faces separated by an angle 2γ. The solution for a mathematical crack can be obtained from the one for the V-notch problem in the limit case as $\gamma \to 0$, figure 1.8-right. The origin of the coordinates is taken at the tip of the notch as shown in in figure 1.8. Neglecting the body forces, the solution of this problem is reduced to finding the Airy stress function satisfying the biharmonic equation, both for plane stress and plane strain problems. This can be formulated in Polar coordinates as

$$\Delta\Delta\Phi = \left(\frac{\partial^2}{\partial r^2} + \frac{1}{r}\frac{\partial}{\partial r} + \frac{1}{r^2}\frac{\partial^2}{\partial\theta^2}\right) \cdot \left(\frac{\partial^2}{\partial r^2} + \frac{1}{r}\frac{\partial}{\partial r} + \frac{1}{r^2}\frac{\partial^2}{\partial\theta^2}\right) \Phi = 0\,, \tag{1.1}$$

where the stress components in terms of the Airy stress function are

$$\begin{aligned} \sigma_{rr} &= \frac{1}{r}\frac{\partial\Phi}{\partial r} + \frac{1}{r^2}\frac{\partial^2\Phi}{\partial\theta^2}\,, \\ \sigma_{\theta\theta} &= \frac{\partial^2\Phi}{\partial r^2}\,, \\ \sigma_{r\theta} &= \frac{\partial}{\partial r}\left(\frac{1}{r}\frac{\partial\Phi}{\partial\theta}\right)\,. \end{aligned} \tag{1.2}$$

For this problem, the stress function can be written as

$$\Phi = \Phi(r,\theta,\lambda) = r^{(\lambda+1)}\,\Theta(\theta)\,, \tag{1.3}$$

where λ is a, as yet unknown, number. Substituting equation (1.3) into (1.1) gives

$$\Theta^{IV} + 2(\lambda^2+1)\,\Theta'' + (\lambda^2-1)^2\,\Theta = 0\,, \tag{1.4}$$

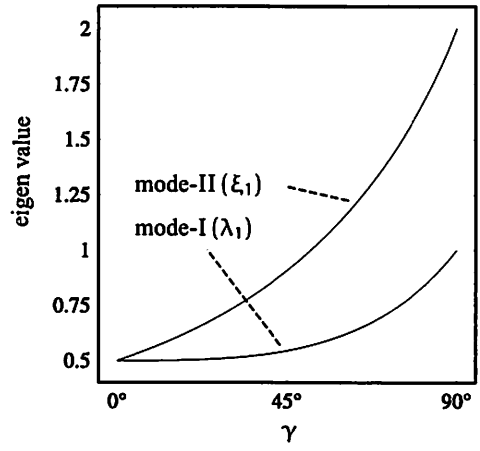

Figure 1.9: variation of the eigenvalues with notch angle

which is an ordinary differential equation (Euler equation). The general solution for this differential equation with $\lambda \neq 0$ and $\lambda \neq \pm 1$ is of the form

$$\Theta(\theta) = c_1 \cos(\lambda+1)\theta + c_2 \cos(\lambda-1)\theta + c_3 \sin(\lambda+1)\theta + c_4 \sin(\lambda-1)\theta\,, \tag{1.5}$$

where c_i's ($i = 1..4$) are the solution constants to be determined from the boundary conditions. Considering the relations (1.2) and prescribing the traction free boundary conditions on the notch faces, i.e $\sigma_{\theta\theta} = \sigma_{r\theta} = 0$ at $\theta = \pm\alpha$, leads to the following set of algebraic equation

$$\begin{pmatrix} (\lambda+1)e^{+i(\lambda+1)\alpha} & (\lambda+1)e^{-i(\lambda+1)\alpha} & (\lambda+1)e^{+i(\lambda-1)\alpha} & (\lambda+1)e^{-i(\lambda-1)\alpha} \\ (\lambda+1)e^{-i(\lambda+1)\alpha} & (\lambda+1)e^{+i(\lambda+1)\alpha} & (\lambda+1)e^{-i(\lambda-1)\alpha} & (\lambda+1)e^{+i(\lambda-1)\alpha} \\ -i(\lambda+1)e^{+i(\lambda+1)\alpha} & i(\lambda+1)e^{-i(\lambda+1)\alpha} & -i(\lambda-1)e^{+i(\lambda-1)\alpha} & i(\lambda-1)e^{-i(\lambda-1)\alpha} \\ -i(\lambda+1)e^{-i(\lambda+1)\alpha} & i(\lambda+1)e^{+i(\lambda+1)\alpha} & -i(\lambda-1)e^{-i(\lambda-1)\alpha} & i(\lambda-1)e^{+i(\lambda-1)\alpha} \end{pmatrix} \begin{pmatrix} c_1 \\ c_2 \\ c_3 \\ c_4 \end{pmatrix} = \begin{pmatrix} 0 \\ 0 \\ 0 \\ 0 \end{pmatrix}, \tag{1.6}$$

where $i = \sqrt{-1}$ is the imaginary unit of a complex number.

Obtaining the nontrivial solutions requires a singular coefficient matrix

$$\begin{aligned} &\lambda^2(1-\cos(4\alpha)) + \cos(4\alpha\lambda) - 1 = 0\,, \\ \Rightarrow\quad &\sin(2\alpha\lambda) \pm \lambda \sin(2\alpha) = 0\,. \end{aligned} \tag{1.7}$$

It is worth noting that if λ is a solution of (1.7) then $-\lambda$ is also a solution, however, the only admissible solutions are those that lead to a finite strain energy ($\mathrm{Re}(\lambda) > 0$). Let λ_n and ξ_n respectively be the eigenvalues for the symmetric and the antisymmetric loadings, which are complex numbers and have a real part ≥ 1. The eigenvalues λ_1 and ξ_1 are real

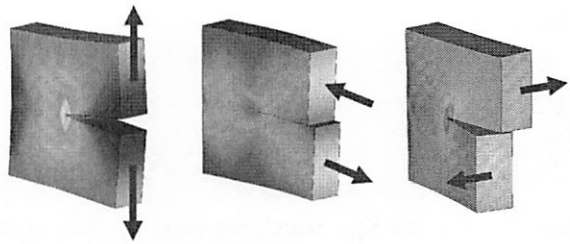

Figure 1.10: modes of crack deformation

for $\pi \leq \alpha \leq \pi/2$ and are $0.5 \leq \lambda_1 \leq 1$ and $0.5 \leq \xi_1 \leq 2$. This indicates that the stresses in equation (1.2) are singular at the notch tip, and the order of singularity is $\lambda - 1$. Figure 1.9 shows the variation of λ_1 and ξ_1 with respect to the notch angle γ. It can be seen that for a crack $\gamma = 0$, the order of singularity for symmetric and antisymmetric loading is -0.5.

For the case of a mathematical crack, the asymptotic stress field in the cartesian coordinates is

$$\begin{aligned}\sigma_{xx} =& \frac{K_I}{\sqrt{2\pi r}} \cos\frac{\theta}{2}\left(1 - \sin\frac{\theta}{2}\sin\frac{3\theta}{2}\right) \\ & - \frac{K_{II}}{\sqrt{2\pi r}} \sin\frac{\theta}{2}\left(2 + \cos\frac{\theta}{2}\cos\frac{3\theta}{2}\right) + O(1)\,,\end{aligned} \tag{1.8}$$

$$\begin{aligned}\sigma_{yy} =& \frac{K_I}{\sqrt{2\pi r}} \cos\frac{\theta}{2}\left(1 + \sin\frac{\theta}{2}\sin\frac{3\theta}{2}\right) \\ & + \frac{K_{II}}{\sqrt{2\pi r}} \sin\frac{\theta}{2}\cos\frac{\theta}{2}\cos\frac{3\theta}{2} + O(\sqrt{r})\,, \\ \sigma_{xy} =& \frac{K_I}{\sqrt{2\pi r}} \sin\frac{\theta}{2}\cos\frac{\theta}{2}\cos\frac{3\theta}{2} \\ & + \frac{K_{II}}{\sqrt{2\pi r}} \cos\frac{\theta}{2}\left(1 - \sin\frac{\theta}{2}\sin\frac{3\theta}{2}\right) + O(\sqrt{r})\,, \\ \sigma_{zz} =& \begin{cases} \nu(\sigma_{xx} + \sigma_{yy}) & \text{plane strain} \\ 0 & \text{plane stress}\,. \end{cases}\end{aligned}$$

The solution for the anti-plane shear is particularly simple to analyze, because the displacement vector is everywhere parallel to the crack edge (BROBERG 1999). The stress

field for mode III reads

$$\sigma_{xz} = -\frac{K_{III}}{\sqrt{2\pi r}} \sin\frac{\theta}{2}, \qquad \sigma_{yz} = \frac{K_{III}}{\sqrt{2\pi r}} \cos\frac{\theta}{2}. \tag{1.9}$$

The coefficients K_I, K_{II} and K_{III}, which represent the magnitude of the stress field singularities, are the so called stress intensity factors (IRWIN 1957), corresponding to different modes of crack deformation as presented in figure 1.10. The stress intensity factors indicate that the stresses near the crack tip increase proportional to K_α. Moreover, the stress intensity factors completely define the crack tip conditions. i.e. if they are known, it is possible to solve for all components of stress, strain and displacement as functions of r and θ. This single parameter description of crack tip conditions turns out to be one of the most important concept in fracture mechanics.

1.3.2 asymptotic stress field of an arbitrarily shaped 3-D crack

The stress expansion near the tip of a two-dimensional straight crack, given in section 1.3.1, is well known from the famous work of WILLIAMS (1957). The expansion formula near the tip of a curved crack in two-dimensions has been completed by TING (1985) who studied the general case of an arbitrary shaped crack. In three-dimensional crack problems, the stress expansion near the front is known to have the same form as in the two-dimensions. However, higher order terms of the expansion are involved in such questions as the crack tip plasticity, the path followed by a propagating crack or stability of such a path (RICE 1974), (LARSSON & CARLSSON 1973), (COTTERELL & RICE 1980), (LEBLOND 1989), (AYATOLLAHI, PAVIER & SMITH 1998).

LEBLOND & TORLAI (1992) have addressed the stress expansion formula in the most general three-dimensional arbitrary shaped crack with an arbitrary curved front, which lips are assumed to be free from traction (figure 1.11) up to the third order term, i.e. terms

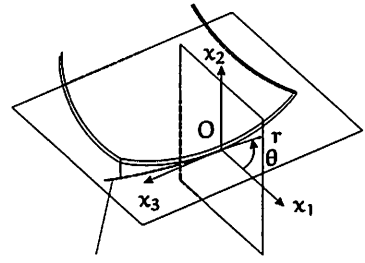

Figure 1.11: arbitrarily shaped crack

proportional to $r^{-1/2}$, r^0 and $r^{1/2}$.

$$\sigma_{ij} = K_\alpha f_{ij}^\alpha(\theta) r^{-1/2} + T_\alpha g_{ij}^\alpha(\theta) + \left(B_\alpha h_{ij}^\alpha(\theta) + K'_\alpha l_{ij}^\alpha(\theta) + C_{\lambda\mu} K_\alpha m_{ij}^{\alpha\lambda\mu}(\theta) + \Gamma K_\alpha n_{ij}^\alpha(\theta)\right) r^{1/2} + O(r), \tag{1.10}$$

where r, θ correspond to the local polar coordinates measured from the periphery of the crack front in the plane perpendicular to it, and the summation convention is employed for the index α that takes the values I, II and III, denoting the three crack deformation modes, i.e. opening, sliding and tearing, respectively. The constants K_I, K_{II} and K_{III} are the stress intensity factors corresponding to each mode, and T_I, T_{II} and T_{III} are the constant non-singular terms in the stress expansion, the so called T-stresses. T_I represents a uniform σ_{11} stress and a uniform σ_{33} stress equal to $\nu\,\sigma_{11}$ (plane strain solution), T_{II} a uniform σ_{13} stress (anti-plane solution), and T_{III} a uniform σ_{33} stress. The coefficients B_I, B_{II} and B_{III} have no special names , and $K'_\alpha = dK_\alpha/ds$ are the derivatives of the stress intensity factors along the crack front at point O. f_{ij}^α's, g_{ij}^α's, h_{ij}^α's, l_{ij}^α's, $m_{ij}^{\alpha\lambda\mu}$'s, and n_{ij}^α's are universal functions of θ, and are recalled in the appendix for completeness. $C_{\lambda\mu}$, where λ and μ take the values 1 and 3 are the components of the curvature tensor, and Γ is the curvature of the projected crack front to the tangent plane at point O. The terms $K'_\alpha l_{ij}^\alpha(\theta)$, $C_{\lambda\mu}K_\alpha m_{ij}^{\alpha\lambda\mu}(\theta)$ and $\Gamma K_\alpha n_{ij}^\alpha(\theta)$ are corrections to the stress expansion at the front of a plane crack (figure 1.11), arising from the non-uniformity of the stress intensity factors along the crack front, plus the curvatures of the surface and front of the crack. The point O is an arbitrary point on the crack front, so this expansion formula is valid in all planes perpendicular to the crack front. The stress expansion after kinking and propagation of the crack is of the same type, provided of course that the crack front is shifted to its new position and all coordinates and geometric parameters are changed accordingly.

Stress intensity factors are known to be sufficient parameters to describe the whole asymptotic stress and strain fields, but it is proved that beside the stress intensity factors, the non-singular constant terms in the stress expansion formula play also an important role in the subjects related to fracture mechanics and plasticity (LARSSON & CARLSSON 1973), (RICE 1974), (AYATOLLAHI, PAVIER & SMITH 1998). The analytical expressions for the stress intensity factors are given for many two-dimensional and three-dimensional crack problems (MURAKAMI 1987), but solutions for the T-stresses are available mostly for two-dimensional crack problems, and very limited solutions in three-dimensional case are available so far (WANG 2004), (SCHÜTTE & MOLLA-ABBASI 2007B), (MOLLA-ABBASI & SCHÜTTE 2008).

1.3.3 material force, and J-integral concept

On subjecting an elastic crystal containing dislocations to an appropriate external loading, some of the atoms will move and the dislocation line will move in the opposite direction

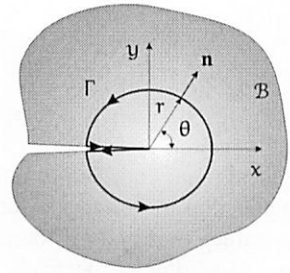

Figure 1.12: material force at a crack tip

(MAUGIN 1993). By virtue of the fundamental duality of mechanics, there is thus a force associated with this displacement via the space rate of change in the total energy of the system. This is not a force in the usual physical sense, and is called a material force. Material forces provide the basis for the study of inhomogeneities of continuous media.

Material forces acting on elastic singularities and inhomogeneities have been introduced in an elegant framework by ESHELBY (1951), who remarked that this kind of force, in a sense fictitious, is introduced to give a picturesque description of energy changes

$$\mathcal{F} = \int_\Gamma \boldsymbol{\mu}.\mathbf{n}\, d\Gamma = \int_A \nabla\boldsymbol{\mu}\, dA\,, \quad \boldsymbol{\mu} = W^e\mathbf{1} - \mathbf{u}\nabla.\boldsymbol{\sigma}\,, \tag{1.11}$$

where $\boldsymbol{\mu}$ is called the Eshelby's stress tensor in honor of ESHELBY (1951) who first introduced it as the Maxwell tensor of elasticity. Eshelby's stress tensor plays a fundamental role in the formulation of configurational or material forces, both for defects and material inhomogeneities. Γ is the contour encircling the inhomogeneity in the counter-clockwise sense, $\mathbf{n}$ the normal to the contour, $\mathbf{u}$ the displacement vectors, W^e is the strain energy density, $d\Gamma$ and dA represent the length element and the area element, respectively.

Considering a two-dimensional traction free sharp crack (figure 1.12), the tip of the crack qualifies as a defect. In the considered local Cartesian coordinates at the crack tip, the following scalar material force is resulting

$$\mathcal{F} = \int_\Gamma (W^e n_x - \mathbf{u}_{,x}.\boldsymbol{\sigma}.\mathbf{n})\, d\Gamma\,, \tag{1.12}$$

where $n_x = \mathbf{n}.\mathbf{e}_x$. It can be proved that this integral is independent of the path in the xy plane, so that the limit $\Gamma \to 0$ can be taken. The force $\mathcal{F}$ in the limit case

$$J = \lim_{\Gamma\to 0} \int_\Gamma (W^e n_x - \mathbf{u}_{,x}.\boldsymbol{\sigma}.\mathbf{n})\, d\Gamma\,, \tag{1.13}$$

is also called the Rice's J-integral after the work of RICE (1968B). This result were preceded by Eshelby's idea, and other works of deep insight by CHEREPANOV (1968), so it is also known as the Eshelby-Cherepanov-Rice's J-integral.

Following the reasoning of RICE (1968B), a virtual propagation δa of crack in the direction of n_x generates a material force G per unit length of the straight crack via an infinitesimal variation in the total potential energy. As the crack cannot repair, so the expenditure in potential energy goes into dissipation, and it can be shown

$$\delta\psi = -\delta E = G\,\delta a\,, \tag{1.14}$$

where G = J. The quantity G (dimensionally force per unit length or energy per unit area), the so called energy release rate, is indeed the thermodynamical dual of δa.

Comparing the computed value of G or J to a characteristic parameter G_c of the material, e.g. the surface energy proposed by GRIFFITH (1921), may state if the crack growth is possible. For further details on material inhomogeneities and the corresponding material forces in elasticity, interested readers are referred to the work of MAUGIN (1993).

1.3.4 path independent integrals in linear elasticity

The study of path independent integrals and their application to fracture mechanics is known by the concept of J-integral derived by ESHELBY (1951), CHEREPANOV (1967) and RICE (1968B) as a direct consequence of the application of the theory proposed by NÖTHER (1918) for material dilatation. Other material balance laws were deduced either directly or from Nöther's theorem for material dilatation and rotations. Additional material balance laws in elastostatics were introduced by GÜNTHER (1962), KNOWLES & STERNBERG (1972) and FLETCHER (1976) for homogeneous bodies in general, but BUDIANISKY & RICE (1973) were the first ones who have associated these balance laws with invariants of defect mechanics, called L- and M- integrals, respectively. The small strain assumption for these relations were established by EISCHEN & HERMANN (1987) by a direct calculation. RICE (1985) have discussed several applications of the J- and the M-integrals.

An extension of the J-integral to a path independent integral for a plate subjected to in-plane loading was given by BROBERG (1979) (see also BROBERG (1987)). This integral, known as the P-integral, is given by

$$P = \int_\Gamma \left(W^e_{av}\,dy - (u_{i,x}\,\sigma_{ij}.n_j)_{av}\right) d\Gamma\,, \quad (i = 1,2,3 \text{ and } j = 1,2)\,, \tag{1.15}$$

where the notations are the same as for the J-integral, and the subscript $\bullet_{av}$ indicates the average over the plate thickness. This integral for a general non-closed path has a non-zero value and for a closed path vanishes. It also takes on the same value for any path encircling the dissipative region at a crack tip.

Following the same methodology, the path independent M-integral, established by GÜNTHER (1962) and later by KNOWLES & STERNBERG (1972), is given by

$$M = \int_\Gamma \left(W^e\,\mathbf{n}.\mathbf{x} - \mathbf{u}\nabla.\boldsymbol{\sigma}.\mathbf{n}.\mathbf{x} - \frac{1}{2}\mathbf{n}.\boldsymbol{\sigma}.\mathbf{u}\right) d\Gamma\,. \tag{1.16}$$

Even though the M-integral vanishes for a closed path encircling a traction free crack tip, irrespective of the position of the coordinate system's origin, the value of the M-integral for a non-closed path depends on the position of the chosen coordinate system. The M-integral is used for expedient determination of the energy flux into the edge of an advancing crack, and thereby the stress intensity factors (see also the works by ESHELBY (1974) and FREUND (1978)).

KNOWLES & STERNBERG (1972) have shown that the L-integral is given as a vector by

$$\mathbf{L} = \int_{\Gamma} [(W^e \mathbf{n} - \mathbf{u}\nabla.\boldsymbol{\sigma}.\mathbf{n}) \times \mathbf{x} + (\boldsymbol{\sigma}.\mathbf{n}) \times \mathbf{u}] \, d\Gamma . \tag{1.17}$$

It can be proved that the L-integral is a path-independent integral and is independent of the selection of the coordinate system. BUDIANISKY & RICE (1973) have interpreted J-, L- and M-integrals as being the energy release rates when a cavity is translated, is rotated, and is expanded uniformly. In defect mechanics the integrals 1.16 and 1.17 can be associated with energy release rates in rigid rotation and in uniform (self similar) expansion such as the growth of cavities.

The path independent J-integral, presented in section 1.3.3, is indeed the first component of the J-integral vector (J_1, J_2, J_3), parallel to the crack plane and perpendicular to the crack front. KNOWLES & STERNBERG (1972) deduced that the Eshelby-Cherepanov-Rice's J-integral was actually a vector component of a more general conservation law, and found two additional laws which were subsequently associated with the L_k- and M-integrals of defect mechanics by BUDIANISKY & RICE (1973). The general form of the J-integral vector is given by

$$\mathbf{J} = \int_{\Gamma} \mu.\mathbf{n} \, d\Gamma , \quad \text{or} \tag{1.18}$$

$$J_k = \int_{\Gamma} (W^e n_k - u_{i,k} \, \sigma_{ij} n_j) \, d\Gamma ,$$

in the component notation. As mentioned, the path independency of J_1 holds true for traction free crack faces and a closed path encircling the crack tip. The same holds for J_2 and J_3, but it should be noted that the chosen path must necessarily include the crack faces and form a closed one, otherwise the path independency of these components is lost. For plane strain linear elastostatic crack problems, considering the linear elastic stress and displacement fields along with the definition of the J-integral, it can be shown

$$J_1 = \frac{1-\nu^2}{E} \left(K_I^2 + K_{II}^2 + \frac{1}{1-\nu} K_{III}^2 \right) , \tag{1.19}$$

$$J_2 = \frac{-(1-\nu^2)}{E} K_I \, K_{II} ,$$

$$J_3 = 0 ,$$

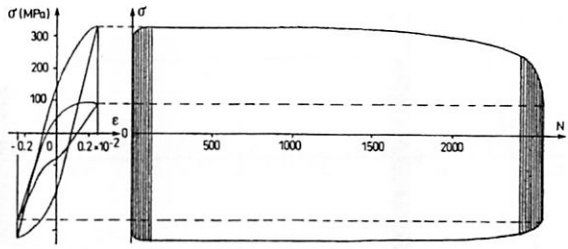

Figure 1.13: cyclic tension-compression test for low cycle fatigue of A316L stainless steel

and substituting $E/(1-\nu^2)$ with E, the same relations are applicable for the plane stress case.

For small scale and contained yielding, a path independent J-integral can be computed outside the plastic zone. This means that the path Γ has to be large enough to encircle the plastic zone and pass through the elastic region only. In gross plasticity, this is not possible, and some more or less pronounced path dependency will always occur.

1.3.5 fatigue crack growth and fracture mechanics

When materials are subjected to a cyclic loading, above a certain level of stress or strain, damage develops, in some cases together with cyclic plastic strain, proceeding the phases of nucleation and propagation of microcracks. Low cycle fatigue is characterized by a low number of loading cycles to rupture ($N_R < 10,000$). This is mainly due to the high stress levels. In contrast, when a material is loaded with a lower value of stress state, the plastic strain at the mesoscale level remains small and is often negligible. In this case, the number of loading cycles to failure may be very large ($N_R > 100,000$). As a consequence, the localization of damage is very high.

Characterization of fatigue crack propagation in engineering materials, with metals and polymers being of primary concern, has been a topic of rather extensive investigation during the past five decades. This has resulted in a substantial number of laws developed for analyzing fatigue crack propagation in terms of crack length, number of loading cycles, and variation of the stress intensity factors in a cycle. As already mentioned, stress intensity factors are sufficient parameters to describe the whole linear elastic stress and strain fields of the crack tip region. This is still meaningful if the size of the plastic zone at the crack tip is small, fulfilling the so called small scale yielding condition (RICE 1974). Then the rate of fatigue crack propagation per cycle may be determined by the stress intensity factors in the following form

$$\frac{da}{dN} = f(\Delta K) = f(K_{max} - K_{min}), \tag{1.20}$$

where K_{max} and K_{min} are the maximum and the minimum stress intensity factors in a

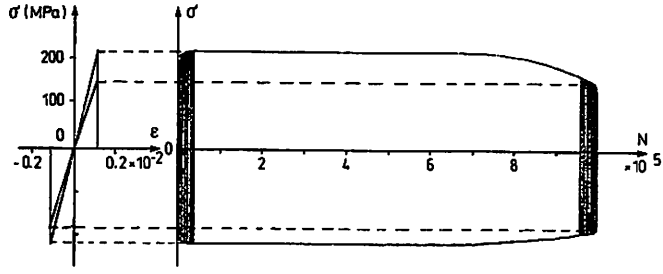

Figure 1.14: cyclic tension-compression test for high cycle fatigue of A316 stainless steel

cycle.

PARIS (1962) and PARIS, GOMEZ & ANDERSON (1961) were the first ones to point this out. Equation (1.20) is sometimes assumed to be a simple power function, known as Paris' law

$$\frac{da}{dN} = C\,(\Delta K)^{\eta}\,, \tag{1.21}$$

where C and η are supposed to be material constants. Despite popular acceptance of equation (1.21), too much emphasis should nevertheless not be placed on its merit as a satisfactory empirical representation of the test data. First of all, a single parameter ΔK is obviously insufficient for a complete characterization of crack tip fatigue response. Secondly, magnitudes of the so called material parameters, C and η, are noticeably influenced by changes in the operational conditions, such as specimen geometry and size, load history and stress level, Based on the mentioned points and the experimental observations, C and η cannot be viewed as material constants. Several researchers came to the realization that fatigue crack growth rate exhibits also a dependency on other parameters, such as the cycle ratio $R = K_{min}/K_{max}$. Several investigators have tried to establish empirical relations which attempt to incorporate the effect of the cycle ratio such that all data could be condensed to a single curve. BROEK & SCHIJVE (1963) proposed the following law

$$\frac{da}{dN} = C\,K_{max}^2\,\Delta K\,, \tag{1.22}$$

and a similar equation was given by ERDOGAN (1967).

WALKER (1969) proposed a more general equation

$$\frac{da}{dN} = C\,K_{max}^{\eta_1}\,(\Delta K)^{\eta_2}\,. \tag{1.23}$$

FORMAN, KEARNEY & ENGLE (1967) argued that da/dN should become infinite when the crack reaches a critical size, e.g. when K_{max} reaches the fracture toughness

of the material (K_{Ic}). With this argument, they suggested the following law

$$\frac{da}{dN} = \frac{C(\Delta K)^n}{(1-R)K_{Ic} - \Delta K} = \frac{C(\Delta K)^n}{(1-R)(K_{Ic} - K_{max})}. \tag{1.24}$$

The differences among these expressions are not large, and none of them has a general applicability. Each one may be found reasonably satisfactory in a limited region or for limited sets of data. The success of the application of fracture mechanics principles to arrive at a fracture safe design depends largely upon the reliability of fatigue crack growth predictions. In the case of constant amplitude fatigue loading, predictions can be made on the basis of empirical data, provided that safety factors are used to account for frequency and environmental effects. However, an improved crack growth theory that can be quantified is certainly needed to obtain a better appreciation of the factors affecting crack growth. In the case of variable amplitude fatigue loading, the prediction of retardation effects has to be based on a unified model of fatigue crack growth by plastic crack tip opening due to cyclic slip, in which crack closure by residual compressive stresses can be incorporated quantitatively.

The K-based empirical formulation of the fatigue crack growth does not deliver a compelled agreement with test results. One of the disadvantages of the fatigue evolution laws formulated in terms of the stress intensity factors is that the effect of the material parameters such as the Young's modulus and the Poisson's ratio are not taken into account. In experimental observations by JOHNSON & PARIS (1968), it has been stated that if ΔK is divided by the Young's modulus, the mid range fatigue data for various metals with diversified mechanical properties tend to congregate together within a relatively narrow scatter band. Another weakness of this formulation is that analyzing the fatigue crack growth using a K-based law is mathematically untraceable, since it is almost impossible to derive analytical solutions for the stress intensity factors of a crack propagated to an arbitrary shape.

To overcome the mentioned difficulties and to formulate the evolution equation in a more realistic manner considering the thermodynamics of the irreversible process of crack propagation, strain energy release rate or driving force seem to be the best choices. In this regard, instead of using stress intensity factors as a leading parameter for fatigue characterization, SUTTON (1974) and ARAD, RADON & CULVER (1974) have analyzed crack growth data for different polymers with respect to the strain energy release rate

$$\frac{da}{dN} = C(\Delta G)^n. \tag{1.25}$$

With this formulation varying degrees of success were achieved provided that the test data for different materials were analyzed separately. As in the case of K-based formulation, the absence of fracture toughness G_{Ic} seems to be the major weakness of this formulation. This was modified by WOO & CHOW (1984) as

$$\frac{da}{dN} = \frac{C(\Delta G)^n}{G_{Ic} - G_{max}}, \tag{1.26}$$

and later on another law was suggested by CHOW & LU (1990) in order to extend the applicability of the equation to cover wider range of materials, in the following form

$$\frac{da}{dN} = \frac{C(\Delta J)^{\eta}}{J_c - J_{max}}, \tag{1.27}$$

where G and J represent the energy release rate and the J-integral, respectively, and J_c is the critical value associated to the J-integral (RICE 1968B).

In this respect, another formulation was proposed by LEMAITRE & CHABOCHE (1990) in the form

$$\frac{da}{dN} = C\left(\sqrt{G_{max}} - \sqrt{G_o}\right)^{\eta}, \tag{1.28}$$

with G and G_o representing the strain energy release rate and its threshold value, respectively.

Considering the variational principle of a cracked body in equilibrium, SCHÜTTE (2001) extended equation (1.29) to take into account the effect of crack kinking

$$\frac{da}{dN} = C\left(\sqrt{G^*_{max}} - \sqrt{G^*_o}\right)^{\eta}, \tag{1.29}$$

where G^* represents the maximum driving force acting at the kinked crack tip.

Using the concept of energy release rate enables overcoming the dependency of the formulation on specimen geometry and size, crack configuration and size, and loading condition as well, and there is no need to calculate the stress intensity factors, since calculating the energy released during crack propagation requires nevertheless no stress field solution at the crack tip, and hence makes it applicable to any specimen with arbitrary crack shapes and loading conditions. The most important advantage of using a G-based evolution law is that the rate of crack propagation da/dN is given in terms of its thermodynamical dual G. This is best illustrated by considering the irreversible nature of the crack propagation process, where according to the continuum thermodynamics, there is an entropy production rate associated with this irreversibility. Thus introducing the crack propagation rate as a new internal variable, the driving force is considered as its thermodynamic conjugate force (thermodynamic dual) and the rate of the entropy production is given by $G \cdot \dot{a}$, and finally, with this kind of formulation the effect of the Young's modulus and the Poisson's ratio are automatically taken into account.

2 T-stress Solutions for Internal Elliptical and Circular Cracks

Contents

Natural cracks occurring in practice in the engineering structures posses often irregular geometrical shapes, however the geometry of elliptical and circular cracks are good approximations for the shape of a flaw in many engineering materials, hence they are important in the analysis. Indeed they represent idealization of the shape of internal flaws that are inherent in many engineering materials.

In this chapter, analytical expressions for the elastic constant stress terms of the asymptotic field, the so called T-stresses , for internal mixed-mode elliptical cracks in infinite homogeneous and isotropic elastic solids are addressed (MOLLA-ABBASI & SCHÜTTE 2008). Based on these results, the T-stresses for internal mixed-mode circular cracks are resulting and compared to the results in (SCHÜTTE & MOLLA-ABBASI 2007B). To solve the problem the mixed-mode crack problem is divided into sub-problems using the superposition method, and each sub-problem is then solved for the asymptotic stress field. Considering the expansion of the local stress field at the crack front, the elastic T-stress terms are derived for each sub-problem. The results are superimposed to give the analytical expressions of the so far missing elastic T-stresses for mixed-mode elliptical cracks.

The effect of the T-stresses on the size and shape of the plastic zone at the crack tip is discussed, and analytical results are compared to the ones from finite element analyses, both for the T-stress components and the size of the plastic zone. It is shown that for an accurate prediction of the plastic zone all singular and constant terms (T-stresses) in the

stress expansion formulae should be considered. It is observed that negative T-stresses increase the size of the plastic zone, while positive ones reduce it.

2.1 Introduction

The asymptotic stress expansion formula for the most general three-dimensional case of an arbitrary shaped crack with an arbitrary curved front was presented in chapter 1 as (LEBLOND & TORLAI 1992)

$$\sigma_{ij} = K_\alpha f_{ij}^\alpha(\theta) r^{-1/2} + T_\alpha g_{ij}^\alpha(\theta) + \Big(B_\alpha h_{ij}^\alpha(\theta) + K'_\alpha l_{ij}^\alpha(\theta) + C_{\lambda\mu} K_\alpha m_{ij}^{\alpha\lambda\mu}(\theta) + \Gamma K_\alpha n_{ij}^\alpha(\theta)\Big) r^{1/2} + O(r), \tag{2.1}$$

where r, θ correspond to the local polar coordinates measured from the periphery of the crack front in the plane perpendicular to it, and the summation convention is employed for the index α that takes the values I, II and III, denoting the three crack deformation modes, i.e. opening, sliding and tearing, respectively. The constants K_I, K_{II} and K_{III} are the stress intensity factors corresponding to each mode, and T_I, T_{II} and T_{III} are the constant non-singular terms in the stress expansion, the so called T-stresses. T_I represents a uniform σ_{11} stress and a uniform σ_{33} stress equal to $\nu\,\sigma_{11}$ (plane strain solution), T_{II} a uniform σ_{13} stress (anti-plane solution), and T_{III} a uniform σ_{33} stress. The coefficients B_I, B_{II} and B_{III} have no special names , and $K'_\alpha = dK_\alpha/ds$ are the derivatives of the stress intensity factors along the crack front at point O. f_{ij}^α's, g_{ij}^α's, h_{ij}^α's, l_{ij}^α's, $m_{ij}^{\alpha\lambda\mu}$'s, and n_{ij}^α's are universal functions of θ, and are recalled in the appendix for completeness. $C_{\lambda\mu}$, where λ and μ take the values 1 and 3 are the components of the curvature tensor, and Γ is the curvature of the projected crack front to the tangent plane at point O. The terms $K'_\alpha l_{ij}^\alpha(\theta)$, $C_{\lambda\mu}K_\alpha m_{ij}^{\alpha\lambda\mu}(\theta)$ and $\Gamma K_\alpha n_{ij}^\alpha(\theta)$ are corrections to the stress expansion at the front of a plane crack (figure 1.11), arising from the non-uniformity of the stress intensity factors along the crack front, plus the curvatures of the surface and front of the crack. The point O is an arbitrary point on the crack front, so this expansion formula is valid in all planes perpendicular to the crack front. The stress expansion after kinking and propagation of the crack is of the same type, provided of course that the crack front is shifted to its new position and all coordinates and geometric parameters are changed accordingly.

The T-stresses can be determined using the first two terms of the stress expansion, proportional to $r^{-1/2}$ and $r^0 = 1$. All remaining terms will have no contribution to the T-stresses, since they vanish on the crack front ($r \to 0$). The T-stresses are directly proportional to the loads applied to the cracked structure, crack length and overall geometry, and are depending on the material parameter ν, the Poisson's ratio of the material. For two-dimensional crack problems, they depend also on the thickness of the cracked solid. In the context of three-dimensional problems, the T-stresses depend on the crack front shape as well.

Sign of the first component of the T-stresses (T_I) is known to influence the stability of planar crack path under mode-I loading condition. This component is the well known T-stress (T) which has been considered by many authors to study its effect on the crack path stability, and to characterize the near tip elastic-plastic fields of two-dimensional and three-dimensional crack problems. COTTERELL & RICE (1980) have studied the stability of an initially straight crack under tensile loading (mode-I). They have shown that introducing a small shear perturbation, when T_I is positive the perturbation would be amplified and the departure from straight crack growth increases, while a negative T_I tends to stabilize the straight crack growth. LEBLOND & FRELAT (2000) have extended the Cotterell-Rice stability analysis to two-dimensional straight cracks under compressive loading. They have found that regardless of the sign of K_{II}, in the absence of T_{II}, cracks tend to further deviate from the initial direction if T_I is positive, and to come back to it if T_I is negative. For vanishing T_I and negative T_{II} (necessary for the crack to be initially closed), cracks tend to leave the initial direction. LEBLOND (1993) has shown that the T-stress stability criterion is also valid for three-dimensional internal crack problems under mode-I conditions.

SMITH, AYATOLLAHI & PAVIER (2001) have considered the effect of T_I in addition to K_I and K_{II} in their study to predict the fracture initiation of two-dimensional mixed-mode cracks. They have shown that for linear elastic materials, a negative T_I increases the apparent fracture toughness while a positive one decreases it. AYATOLLAHI, PAVIER & SMITH (1998) studied the influence of T_I on the fracture toughness of pure mode-II crack problems. AYATOLLAHI, PAVIER & SMITH (2002) have analyzed the growth of mode-I cracks subjected to large T_I, considering the maximum tensile stress criterion for linear elastic and moderate scale yielding. They have found that for both cases, beyond a critical value of T_I, cracks tend to deviate from the initial direction, for which a significant drop in the fracture toughness is predicted. Their results are in good agreement with the experimental findings. Recently, TIAN & CUI (2006) have studied the effect of T_I on fracture toughness of power-law hardening elastic-plastic materials, by deriving a critical value of J-integral in terms of T_I.

The first term of the elastic T-stresses has also been proved to be an important parameter to characterize the near tip elastic-plastic fields of two-dimensional and three-dimensional crack problems (SCHÜTTE & MOLLA-ABBASI 2007C). LARSSON & CARLSSON (1973) and RICE (1974) have shown that for two-dimensional problems the sign and magnitude of T_I substantially change the size and shape of the crack tip plastic zone at finite load levels. BILBY, CARDEW, GOLDTHORPE & HOWARD (1986) have shown that the T_I can strongly affect the magnitude of the hydrostatic triaxiality in the near crack tip elastic-plastic fields. The important feature resulting from these works is that the sign and magnitude of T_I can strongly alter the level of the crack tip stress triaxiality, hence influence the crack tip constraint. A positive T_I strengthens the level of the crack tip stress triaxiality and leads to a high crack tip constraint, while a negative one reduces the crack tip stress triaxiality and leads to the loss of the crack tip

constraint. WANG (1993), BETEGON & HANCOCK (1991), DU & HANCOCK (1991), and O'DOWD & SHIH (1991) have studied the elastic-plastic crack tip fields for different two-dimensional and three-dimensional crack problems using T_I in addition to the J-integral.

To be able to include the effect of the T-stresses in fracture mechanics studies, the analytical expressions for the T-stress components are to be addressed. The analytical expressions for the stress intensity factors are given for many two-dimensional and three-dimensional crack problems, but solutions for the T-stresses are available mostly for two-dimensional crack problems, and very limited solutions in three-dimensional case are available (MURAKAMI 1987).

In this chapter the complete set of the elastic T-stress terms for internal elliptical cracks under general mixed-mode loading are addressed. Many of the internal flaws in materials possess irregular geometrical shapes and many deviate substantially from being circular in profile. The elliptical boundary may be used as a good approximation to the shape of an actual internal crack. SCHÜTTE & MOLLA-ABBASI (2007B), recently, have addressed the complete set of the T-stress terms for mixed-mode internal circular cracks. Using the potential method and transformation technique, asymptotic solution for the stress components are derived (see also BENTHEM & KOITER (1973), KASSIR & SIH (1966), WANG (2004)), from which the T-stress terms are resulting.

To derive the elastic T-stresses of internal mixed-mode elliptical cracks, the problem is first decomposed into sub-problems, in which the internal crack is subjected to either pure shear loading or pure tensile loading. Solving for the asymptotic stress field for each individual sup-problem, and considering the stress expansion in the most general three-dimensional case (LEBLOND 1993), and with the help of the superposition technique, the complete set of the elastic T-stress terms for a mixed-mode internal elliptical crack in an infinite isotropic elastic solid are derived.

The impact of the T-stresses on the size and shape of the plastic zone at the crack tip is studied using the von Mises yield criterion. It is shown that the results are different

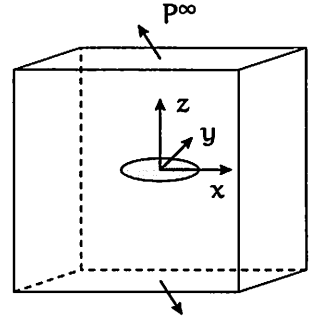

Figure 2.1: mixed-mode internal elliptical crack

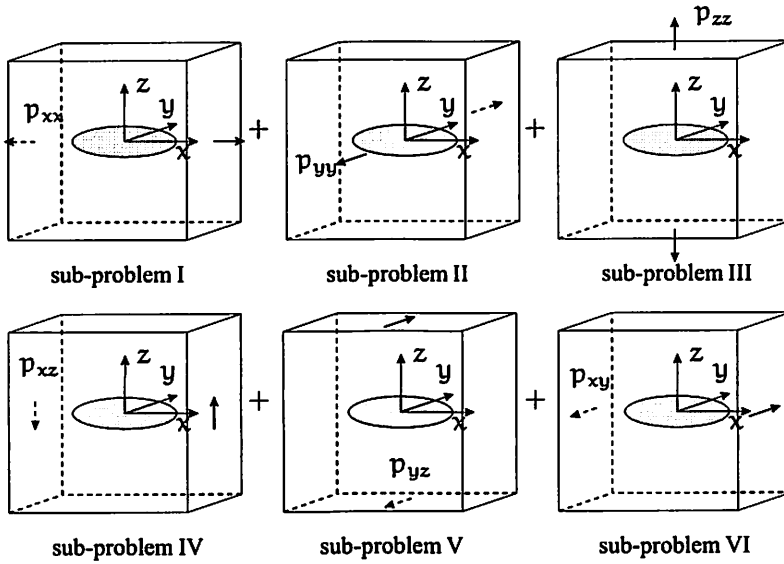

Figure 2.2: sub-problems of the mixed-mode internal elliptical crack

from the ones either neglecting all T-stress components or just considering the effect of T_I (which has been considered by most authors). Analytical results for the T-stress terms and their effect on the size and shape of the plastic zone are compared to the ones obtained from the finite element analysis for different mode-mixities.

2.2 Mixed-mode internal elliptical crack

Consider an internal elliptical crack in an infinite isotropic elastic solid under remote uniaxial traction, loading the crack in a mixed-mode manner (figure 2.1). Using the superposition technique, this problem can be divided into six sub-problems (figure 2.2), where the internal elliptical crack is located in the center of the xy-plane of an infinite unit cell subjected to either simple tension or simple shear, i.e. p_{xx}, p_{yy}, p_{zz} and p_{xy}, p_{yz}, p_{xz}, respectively (the p_{ij}'s are the projections of the remote loading into the rotated local coordinates at the center of the crack).

For this set of sub-problems, asymptotic expressions of the local stress field can be derived analytically. The formulation of this boundary-value problem can be expressed most conveniently using the cartesian coordinates (x, y, z) and the polar coordinates (r, θ, t) in conjugation with the symmetrical form of the ellipsoidal coordinates (ξ, η, ζ). The connection between these coordinate systems are known (KASSIR & SIH 1966), (WHITTAKER & WATSON 1962). The relation between different coordinate systems is

addressed in section 2.2.1.

Figure 2.3 shows a schematic of the elliptical crack geometry, with the crack centered at the origin of the cartesian coordinate system. The semi-major and semi-minor axes of the ellipse are denoted by α and β, respectively and points on the crack surfaces are described by the relations

$$\frac{x^2}{\alpha^2}+\frac{y^2}{\beta^2}\le 1, \quad z=\pm 0, \tag{2.2}$$

while points on the crack boundary are defined by the parametric relations

$$\frac{x^2}{\alpha^2}+\frac{y^2}{\beta^2}=1, \quad z=\pm 0 \quad \text{and} \tag{2.3}$$
$$x=\alpha\cos\varphi\,, \quad y=\beta\sin\varphi\,.$$

In the cartesian frame of reference, the components of the displacement vector are designated by (u_x, u_y, u_z) and those of the stress tensor by $(\sigma_{xx}, \sigma_{yy}, \sigma_{zz}, \sigma_{xy}, \sigma_{yz}, \sigma_{xz})$. The local stress field can be found by introducing a local triply orthogonal system of coordinates (n, t, z) with its origin at an arbitrary point along the crack front (figure 2.3). The system (n, t, z) forms a trihedral in such a way that the axes n, t, z are always directed along the principle normal, tangent and bi-normal of the crack front. The projection of the displacement vector and the stress tensor along this local axes are designated by (u_n, u_t, u_z) and $(\sigma_{nn}, \sigma_{tt}, \sigma_{zz}, \sigma_{nt}, \sigma_{tz}, \sigma_{nz})$, respectively.

Considering the first two terms of equation (2.1), i.e. terms proportional to $r^{-1/2}$ and r^0, for the points on the plane of the crack and outside the crack periphery ($\theta = 0$ and $\eta = 0$) the stress field components in the local coordinates (n, t, z) are

$$\sigma_{nn}=\frac{K_I}{\sqrt{2\pi r}}+T_I\,, \quad \sigma_{tt}=2\nu\frac{K_I}{\sqrt{2\pi r}}+\nu T_I+T_{III}\,, \quad \sigma_{zz}=\frac{K_I}{\sqrt{2\pi r}}\,, \tag{2.4}$$
$$\sigma_{nt}=T_{II}\,, \quad \sigma_{tz}=\frac{K_{III}}{\sqrt{2\pi r}}\,, \quad \sigma_{nz}=\frac{K_{II}}{\sqrt{2\pi r}}\,.$$

In the following sections, for each individual sub-problem the asymptotic stress field will be derived from which with the help of equations (2.4) the T-stress terms will be extracted.

2.2.1 coordinate systems

Ellipsoidal-Cartesian coordinate systems

Consider an ellipse located in the center of the xy-plane with semi-major and semi-minor axes α and β, respectively. The cartesian axes (x, y, z) are determined

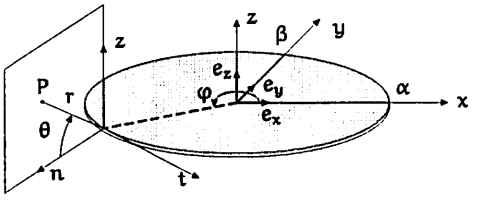

Figure 2.3: coordinate systems

in terms of the ellipsoidal axes (ξ, η, ζ) and vice versa by using the relations (WHITTAKER & WATSON 1962)

$$\begin{aligned} \alpha^2(\alpha^2-\beta^2)x^2 &= (\alpha^2+\xi)(\alpha^2+\eta)(\alpha^2+\zeta)\,, \\ \beta^2(\beta^2-\alpha^2)y^2 &= (\beta^2+\xi)(\beta^2+\eta)(\beta^2+\zeta)\,, \\ \alpha^2\beta^2 z^2 &= \xi\eta\zeta\,, \end{aligned} \tag{2.5}$$

where $-\alpha^2 \le \zeta \le -\beta^2 \le \eta \le 0 \le \xi \le \infty$. In the plane of the crack ($z = 0$), $\xi = 0$ corresponds to the points inside the ellipse, and $\eta = 0$ to the points outside the ellipse. The points on the periphery of the ellipse are identified by setting $\xi = \eta = 0$.

Ellipsoidal-Cylindrical coordinate systems

The derivation of the stress state around the border of an elliptical crack depends upon a knowledge of the limiting forms of the ellipsoidal coordinates (ξ, η, ζ) and the cylindrical coordinates (r, θ). It is observed from figure 2.3 that the coordinates of any point P(x, y, z) can be expressed by

$$\begin{aligned} x &= \alpha\cos\varphi + r\cos\theta\cos\vartheta_n\,, \\ y &= \beta\sin\varphi + r\cos\theta\sin\vartheta_n\,, \\ z &= r\sin\theta\,, \end{aligned} \tag{2.6}$$

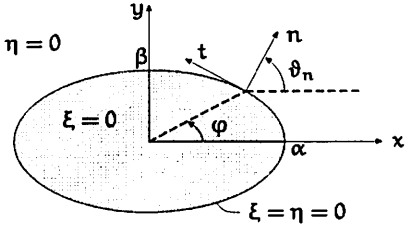

Figure 2.4: three coordinate systems in the plane of the crack

where ϑ_n is the angle between the outward unit normal vector to the crack border and the x-axis, figure 2.4. The angle ϑ_n is related to the parametric equations of an ellipse by

$$\begin{aligned} \alpha \sin\varphi &= \left(\alpha^2 \sin^2\varphi + \beta^2 \cos^2\varphi\right)^{1/2} \sin\vartheta_n , \\ \beta \cos\varphi &= \left(\alpha^2 \sin^2\varphi + \beta^2 \cos^2\varphi\right)^{1/2} \cos\vartheta_n . \end{aligned} \tag{2.7}$$

Upon adding, equations (2.5) give

$$x^2 + y^2 + z^2 = \xi + \eta + \zeta + \alpha^2 + \beta^2 , \tag{2.8}$$

and from (2.6) it follows that

$$\begin{aligned} \xi + \eta + \zeta = &- \left(\alpha^2 \sin^2\varphi + \beta^2 \cos^2\varphi\right) \\ &+ \frac{2\alpha\beta\cos\theta}{\left(\alpha^2 \sin^2\varphi + \beta^2 \cos^2\varphi\right)^{1/2}} r + r^2 . \end{aligned} \tag{2.9}$$

On the plane $z = 0$ (plane of the ellipse) for the points on the periphery of the ellipse, i.e. $r = 0$ and $\xi = \eta = 0$ (figure 2.4), without loss of generality equation (2.9) implies

$$\zeta = -\left(\alpha^2 \sin^2\varphi + \beta^2 \cos^2\varphi\right) , \tag{2.10}$$

and from (2.9) and (2.10)

$$\xi + \eta = \frac{2\alpha\beta\cos\theta}{\left(\alpha^2 \sin^2\varphi + \beta^2 \cos^2\varphi\right)^{1/2}} r + r^2 . \tag{2.11}$$

Combining equations $(2.5)_3$, $(2.6)_3$ and (2.10), a second relation between ξ and η is found

$$\xi\eta = \frac{-(\alpha\beta\sin\theta)^2}{\left(\alpha^2 \sin^2\varphi + \beta^2 \cos^2\varphi\right)} r^2 . \tag{2.12}$$

Solving equations (2.11) and (2.12) for ξ and η, the following expressions are resulting

$$\begin{aligned} \xi &= \frac{2\alpha\beta\cos^2\frac{\theta}{2}}{\left(\alpha^2 \sin^2\varphi + \beta^2 \cos^2\varphi\right)^{1/2}} r + \cos^2\frac{\theta}{2} r^2 + O(r^3) , \\ \eta &= \frac{-2\alpha\beta\sin^2\frac{\theta}{2}}{\left(\alpha^2 \sin^2\varphi + \beta^2 \cos^2\varphi\right)^{1/2}} r + \sin^2\frac{\theta}{2} r^2 + O(r^3) , \end{aligned} \tag{2.13}$$

where higher order terms have been neglected. Note should be taken that these expressions are asymptotic and are valid in the close vicinity of the crack front.

2.2.2 sub-problems I and II

Consider an internal elliptical crack in the center of the xy-plane of an infinite unit cell under remote uniaxial traction p_{xx} or p_{yy} parallel to the plane of the crack (figure 2.2: sub-problems I and II, respectively).

Evaluating the local stress field along the crack front, the elastic T-stresses are derived for each sub-problem. The stress field due to the uniaxial traction p_{xx} or p_{yy} is calculated with the help of the local orthogonal coordinates located at a point ($\alpha \cos\varphi$, $\beta \sin\varphi$, 0) on the crack front.

sub-problem I

For Sub-problem I, the non-zero local stress components along the crack front are

$$\begin{aligned}
\sigma_{nn} &= p_{xx} \frac{\beta^2 \cos^2\varphi}{\alpha^2 \sin^2\varphi + \beta^2 \cos^2\varphi}, \\
\sigma_{tt} &= p_{xx} \frac{\alpha^2 \sin^2\varphi}{\alpha^2 \sin^2\varphi + \beta^2 \cos^2\varphi}, \\
\sigma_{nt} &= -p_{xx} \frac{\alpha\beta \sin\varphi \cos\varphi}{\alpha^2 \sin^2\varphi + \beta^2 \cos^2\varphi},
\end{aligned} \tag{2.14}$$

It is easy to show that $K_I = K_{II} = K_{III} = 0$, and from (2.4) the T-stresses are

$$\begin{aligned}
T_I &= p_{xx} \frac{\beta^2 \cos^2\varphi}{\alpha^2 \sin^2\varphi + \beta^2 \cos^2\varphi}, \\
T_{II} &= -p_{xx} \frac{\alpha\beta \sin\varphi \cos\varphi}{\alpha^2 \sin^2\varphi + \beta^2 \cos^2\varphi}, \\
T_{III} &= p_{xx} \frac{\alpha^2 \sin^2\varphi - \nu\beta^2 \cos^2\varphi}{\alpha^2 \sin^2\varphi + \beta^2 \cos^2\varphi}.
\end{aligned} \tag{2.15}$$

sub-problem II

In an analogous way, the T-stresses for sub-problem II are derived from the local stress field

$$\begin{aligned}
\sigma_{nn} &= p_{yy} \frac{\alpha^2 \sin^2\varphi}{\alpha^2 \sin^2\varphi + \beta^2 \cos^2\varphi}, \\
\sigma_{tt} &= p_{yy} \frac{\beta^2 \cos^2\varphi}{\alpha^2 \sin^2\varphi + \beta^2 \cos^2\varphi}, \\
\sigma_{nt} &= p_{yy} \frac{\alpha\beta \sin\varphi \cos\varphi}{\alpha^2 \sin^2\varphi + \beta^2 \cos^2\varphi},
\end{aligned} \tag{2.16}$$

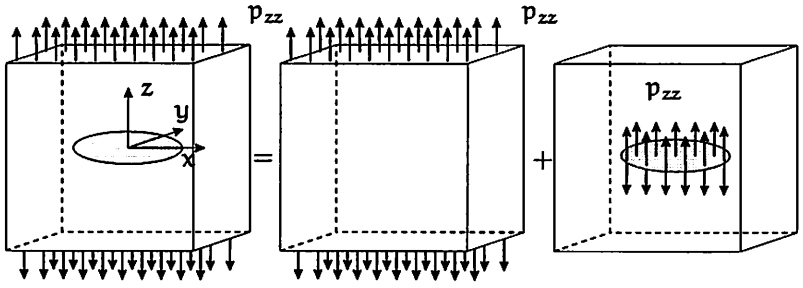

Figure 2.5: internal mode-I elliptical crack

and so

$$T_I = p_{yy} \frac{\alpha^2 \sin^2\varphi}{\alpha^2 \sin^2\varphi + \beta^2 \cos^2\varphi}, \qquad (2.17)$$
$$T_{II} = p_{yy} \frac{\alpha\beta \sin\varphi \cos\varphi}{\alpha^2 \sin^2\varphi + \beta^2 \cos^2\varphi},$$
$$T_{III} = p_{yy} \frac{\beta^2 \cos^2\varphi - \nu\alpha^2 \sin^2\varphi}{\alpha^2 \sin^2\varphi + \beta^2 \cos^2\varphi}.$$

2.2.3 sub-problem III

Consider an internal elliptical crack in the center of the xy-plane of an infinite unit cell under remote uniaxial traction p_{zz} normal to the plane of the crack, loading the crack in pure mode-I (figure 2.2: sub-problem III). This crack problem can be decomposed into two sub-problems; an un-cracked unit cell under remote tension and an internal elliptical crack whose faces are subjected to equal and opposite normal traction fields, figure 2.5.

For the first sub-problem all stress components vanish, except $\sigma_{zz} = p_{zz}$, which has no contribution to the T-stresses.

For the second sub-problem, the resulting stress field is symmetric with respect to the plane of the crack and is associated with mode-I stress intensity factor. Due to symmetry, this problem ($-\infty < z < \infty$) can be reduced to that of a half space ($z > 0$) with the following conditions on the plane of the crack ($z = 0$)

$$\begin{aligned} &\sigma_{xz} = \sigma_{yz} = 0, && \text{at } |x| < \infty, |y| < \infty, \\ &\sigma_{zz} = p_{zz}, && \text{at } \xi = 0, \\ &u_z = 0, && \text{at } \eta = 0. \end{aligned} \qquad (2.18)$$

The solution for the singular stress terms of this problem are presented in (KASSIR & SIH 1975). Here, a similar method is used to derive the expansion of

the components of the stress field, including both the singular stress terms and the T-stresses.

For a three-dimensional problem in elasticity, the displacement field is governed by the equilibrium equation which in vector form appears as

$$\nabla^2 \mathbf{u} + \frac{1}{1-2\nu} \nabla e = 0, \tag{2.19}$$

where the displacement vector is $\mathbf{u} = (u_x, u_y, u_z)$, and ∇ is the del-operator and ∇^2 the Laplace operator

$$\nabla^2 = \frac{\partial^2}{\partial x^2} + \frac{\partial^2}{\partial x^2} + \frac{\partial^2}{\partial z^2}, \tag{2.20}$$

and e is the dilatation

$$e = \frac{\partial u_x}{\partial x} + \frac{\partial u_y}{\partial y} + \frac{\partial u_z}{\partial z}. \tag{2.21}$$

A suitable displacement representation satisfying the field equation (2.19) and the symmetry requirement (2.18) depends on the knowledge of a single potential function $\mathcal{L}(x, y, z)$ (KASSIR & SIH 1975)

$$\begin{aligned} u_x &= (1-2\nu)\frac{\partial \mathcal{L}}{\partial x} + z\frac{\partial^2 \mathcal{L}}{\partial x \partial z}, \\ u_y &= (1-2\nu)\frac{\partial \mathcal{L}}{\partial y} + z\frac{\partial^2 \mathcal{L}}{\partial y \partial z}, \\ u_z &= -2(1-\nu)\frac{\partial \mathcal{L}}{\partial z} + z\frac{\partial^2 \mathcal{L}}{\partial z^2}, \end{aligned} \tag{2.22}$$

and the expressions for the corresponding stresses are

$$\begin{aligned} \frac{\sigma_{xx}}{2\mu} &= \frac{\partial^2 \mathcal{L}}{\partial x^2} + 2\nu\frac{\partial^2 \mathcal{L}}{\partial y^2} + z\frac{\partial^3 \mathcal{L}}{\partial x^2 \partial z}, \\ \frac{\sigma_{yy}}{2\mu} &= \frac{\partial^2 \mathcal{L}}{\partial y^2} + 2\nu\frac{\partial^2 \mathcal{L}}{\partial x^2} + z\frac{\partial^3 \mathcal{L}}{\partial y^2 \partial z}, \\ \frac{\sigma_{zz}}{2\mu} &= -\frac{\partial^2 \mathcal{L}}{\partial z^2} + z\frac{\partial^3 \mathcal{L}}{\partial z^3}, \\ \frac{\sigma_{xy}}{2\mu} &= (1-2\nu)\frac{\partial^2 \mathcal{L}}{\partial x \partial y} + z\frac{\partial^3 \mathcal{L}}{\partial x \partial y \partial z}, \\ \frac{\sigma_{yz}}{2\mu} &= z\frac{\partial^3 \mathcal{L}}{\partial y \partial z^2}, \\ \frac{\sigma_{xz}}{2\mu} &= z\frac{\partial^3 \mathcal{L}}{\partial x \partial z^2}. \end{aligned} \tag{2.23}$$

where ν and μ are the Poisson's ratio and the shear modulus of the elastic material, respectively, and $\mathcal{L}$ is an ellipsoidal harmonic function. An appropriate solution to this problem has been given by GREEN & SNEDDON (1950)

$$\mathcal{L} = \frac{A_{\mathcal{L}}}{2} \int_{\xi}^{\infty} \left(\frac{x^2}{\alpha^2 + s} + \frac{y^2}{\beta^2 + s} + \frac{z^2}{s} - 1 \right) \frac{ds}{\sqrt{Q(s)}}, \tag{2.24}$$

where

$$Q(s) = s(\alpha^2 + s)(\beta^2 + s), \tag{2.25}$$

and the constant $A_{\mathcal{L}}$ is evaluated from the boundary conditions (2.18). Application of the condition $(2.18)_2$ into equations $(2.23)_3$ and (2.24) results in

$$A_{\mathcal{L}} = -\frac{p_{zz}\, \alpha\, \beta^2}{4\, \mu\, E(k_1)}, \tag{2.26}$$

The quantity $E(k_1)$ is the complete elliptical integral of the second kind, and the following notations are considered hereafter

$$\begin{aligned} &k_1^2 = 1 - \frac{\beta^2}{\alpha^2}, \quad k_2^2 = \frac{\beta^2}{\alpha^2}, \quad k_3^2 = \frac{\alpha^2}{\beta^2}, \\ &k_1^2 + k_2^2 = 1, \quad k_2\, k_3 = 1. \end{aligned} \tag{2.27}$$

The equations (2.23)-(2.26) give the solution of the stress field. Performing the necessary integration with respect to the ellipsoidal axes (see the appendix), and considering the limit forms of the ellipsoidal axes, relations (2.10) and (2.13), the expansion of the stress field is resulting. On the plane $z = 0$ and outside the crack surface (corresponding to $\theta = 0$), the non-zero stress components would be

$$\begin{aligned} \frac{\sigma_{xx}}{2\mu A_{\mathcal{L}}} = &- \frac{\sqrt{2}\, \left(2\nu\, \alpha^2 \sin^2\varphi + \beta^2 \cos^2\varphi\right)}{\sqrt{\alpha^3\, \beta^3}\, \left(\alpha^2 \sin^2\varphi + \beta^2 \cos^2\varphi\right)^{3/4}} \frac{1}{\sqrt{r}} \\ &+ \frac{2\left((1-2\nu)\, \beta^2\, K(k_1) + (2\nu\, \alpha^2 - \beta^2) E(k_1)\right)}{\alpha\, \beta^2 (\alpha^2 - \beta^2)} + O(\sqrt{r}), \end{aligned} \tag{2.28}$$

$$\begin{aligned} \frac{\sigma_{yy}}{2\mu A_{\mathcal{L}}} = &- \frac{\sqrt{2}\, \left(\alpha^2 \sin^2\varphi + 2\nu\, \beta^2 \cos^2\varphi\right)}{\sqrt{\alpha^3\, \beta^3}\, \left(\alpha^2 \sin^2\varphi + \beta^2 \cos^2\varphi\right)^{3/4}} \frac{1}{\sqrt{r}} \\ &+ \frac{2\left((2\nu - 1)\, \beta^2\, K(k_1) + (\alpha^2 - 2\nu\, \beta^2) E(k_1)\right)}{\alpha\, \beta^2 (\alpha^2 - \beta^2)} + O(\sqrt{r}), \end{aligned}$$

$$\frac{\sigma_{zz}}{2\mu A_{\mathcal{L}}} = -\frac{\sqrt{2}\, \left(\alpha^2 \sin^2\varphi + \beta^2 \cos^2\varphi\right)^{1/4}}{\sqrt{\alpha^3\, \beta^3}} \frac{1}{\sqrt{r}} + \frac{2\, E(k_1)}{\alpha\, \beta^2} + O(\sqrt{r}),$$

$$\frac{\sigma_{xy}}{2\mu A_{\mathcal{L}}} = \frac{(2\nu-1)\sin 2\varphi}{\sqrt{2\alpha\beta}\left(\alpha^2\sin^2\varphi+\beta^2\cos^2\varphi\right)^{3/4}}\frac{1}{\sqrt{\tau}} + O(\sqrt{\tau}).$$

This, however, does not offer a physical interpretation. For a more intuitive knowledge of the crack front stress field, it is necessary to give the stress field in the local coordinate system (n, t, z). Upon transformation of the coordinate axes from (x, y, z) to (n, t, z), figure 2.3, the stress components σ_{xx}, σ_{yy}, σ_{zz}, σ_{xy}, σ_{yz}, σ_{xz} are combined to give

$$\begin{aligned}
\sigma_{nn} &= \frac{1}{2}(\sigma_{xx}+\sigma_{yy}) + \frac{1}{2}(\sigma_{xx}-\sigma_{yy})\cos 2\varphi + \sigma_{xy}\sin 2\varphi, \\
\sigma_{tt} &= \frac{1}{2}(\sigma_{xx}+\sigma_{yy}) - \frac{1}{2}(\sigma_{xx}-\sigma_{yy})\cos 2\varphi - \sigma_{xy}\sin 2\varphi, \\
\sigma_{zz} &= \sigma_{zz}, \\
\sigma_{nt} &= \frac{1}{2}(\sigma_{yy}-\sigma_{xx})\sin 2\varphi + \sigma_{xy}\cos 2\varphi, \\
\sigma_{nz} &= \sigma_{yz}\sin\varphi + \sigma_{xz}\cos\varphi, \\
\sigma_{tz} &= \sigma_{yz}\cos\varphi - \sigma_{xz}\sin\varphi.
\end{aligned} \tag{2.29}$$

Combination of equations (2.28)) and (2.29) result in the non-zero asymptotic stress components for a mode-I elliptical crack

$$\begin{aligned}
\frac{\sigma_{nn}}{p_{zz}} =& \sqrt{\frac{\beta}{\alpha}}\frac{\sqrt[4]{\alpha^2\sin^2\varphi+\beta^2\cos^2\varphi}}{\sqrt{2}\,E(k_1)}\frac{1}{\sqrt{\tau}} \\
&+ \mathcal{M}_1(\varphi)\left\{\left(2\nu-k_3^2+(1-2\nu)\frac{K(k_1)}{E(k_1)}\right)\sin^2\varphi\right. \\
&\left.+\left(-2\nu+k_2^2-(1-2\nu)k_2^2\frac{K(k_1)}{E(k_1)}\right)\cos^2\varphi\right\} + O(\sqrt{\tau}),
\end{aligned} \tag{2.30}$$

$$\begin{aligned}
\frac{\sigma_{tt}}{p_{zz}} =& \sqrt{\frac{\beta}{\alpha}}\frac{\sqrt[4]{\alpha^2\sin^2\varphi+\beta^2\cos^2\varphi}}{\sqrt{2}\,E(k_1)}\frac{2\nu}{\sqrt{\tau}} \\
&+ \mathcal{M}_1(\varphi)\left\{\left(1-2\nu\,k_3^2+(1-2\nu)\frac{K(k_1)}{E(k_1)}\right)\sin^2\varphi\right. \\
&\left.+\left(-1+2\nu\,k_2^2-(1-2\nu)k_2^2\frac{K(k_1)}{E(k_1)}\right)\cos^2\varphi\right\} + O(\sqrt{\tau}),
\end{aligned}$$

$$\frac{\sigma_{zz}}{p_{zz}} = \sqrt{\frac{\beta}{\alpha}}\frac{\sqrt[4]{\alpha^2\sin^2\varphi+\beta^2\cos^2\varphi}}{\sqrt{2}\,E(k_1)}\frac{1}{\sqrt{\tau}} - 1 + O(\sqrt{\tau}),$$

$$\frac{\sigma_{nt}}{p_{zz}} = (1-2\nu)\,\mathcal{M}_1(\varphi)\left(-\frac{k_2+k_3}{2} + k_2\frac{K(k_1)}{E(k_1)}\right)\sin 2\varphi + O(\sqrt{\tau}).$$

Considering equations (2.4), the T-stresses of an elliptical crack subjected to surface normal traction field are resulting

$$\begin{aligned}\frac{T_I}{p_{zz}} &= \frac{1}{p_{zz}} \lim_{r\to 0}\left(\sigma_{nn} - \frac{K_I}{\sqrt{2\pi r}}\right) \\ &= \mathcal{M}_1(\varphi)\left\{\left(2\nu - k_3^2 + (1-2\nu)\frac{K(k_1)}{E(k_1)}\right)\sin^2\varphi \right. \\ &\left. + \left(-2\nu + k_2^2 - (1-2\nu)\,k_2^2\frac{K(k_1)}{E(k_1)}\right)\cos^2\varphi\right\},\end{aligned} \tag{2.31}$$

$$\begin{aligned}\frac{T_{II}}{p_{zz}} &= \frac{1}{p_{zz}} \lim_{r\to 0} \sigma_{nt} \\ &= (1-2\nu)\,\mathcal{M}_1(\varphi)\left(-\frac{k_2+k_3}{2} + k_2\frac{K(k_1)}{E(k_1)}\right)\sin 2\varphi,\end{aligned}$$

$$\begin{aligned}\frac{T_{III}}{p_{zz}} &= \frac{1}{p_{zz}} \lim_{r\to 0}\left(\sigma_{tt} - \frac{2\nu K_I}{\sqrt{2\pi r}} - \nu T_I\right) \\ &= \frac{\mathcal{M}_1(\varphi)}{2}\left\{\nu(k_2^2 - k_3^2) + (2\nu^2+\nu-1)k_1^2\frac{K(k_1)}{E(k_1)} + \mathcal{M}_2(\varphi)\cos 2\varphi\right\}.\end{aligned}$$

where the following simplifications have been considered

$$\mathcal{M}_1(\varphi) = \frac{\alpha^2\beta^2}{(\alpha^2-\beta^2)\,(\alpha^2\sin^2\varphi + \beta^2\cos^2\varphi)}, \tag{2.32}$$

$$\mathcal{M}_2(\varphi) = \nu\,(k_2^2 + k_3^2) + 2\,(2\nu^2 - 1) - (2\nu^2+\nu-1)\,(1+k_2^2)\frac{K(k_1)}{E(k_1)}.$$

The well known mode-I stress intensity factor of internal elliptical cracks can also be resulting from $(2.30)_3$

$$K_I = \lim_{r\to 0}\left(\sqrt{2\pi r}\,\sigma_{zz}\right) = p_{zz}\sqrt{\frac{\beta}{\alpha}}\,\frac{\sqrt{\pi}\,\sqrt[4]{\alpha^2\sin^2\varphi + \beta^2\cos^2\varphi}}{E(k_1)}. \tag{2.33}$$

The T-stresses of mode-I internal circular cracks (SCHÜTTE & MOLLA-ABBASI 2007B) may also be derived from (2.31). In the limit case where $\beta \to \alpha$, the T-stresses of the internal circular cracks are resulting

$$\begin{aligned}(T_I)_{circular} &= \lim_{\beta\to\alpha} T_I = -\frac{1}{2}\,(1+2\nu)\,p_{zz}, \\ (T_{II})_{circular} &= \lim_{\beta\to\alpha} T_{II} = 0, \\ (T_{III})_{circular} &= \lim_{\beta\to\alpha} T_{III} = (1-\nu)\,T_I.\end{aligned} \tag{2.34}$$

which coincide with the results presented by SCHÜTTE & MOLLA-ABBASI (2007B).

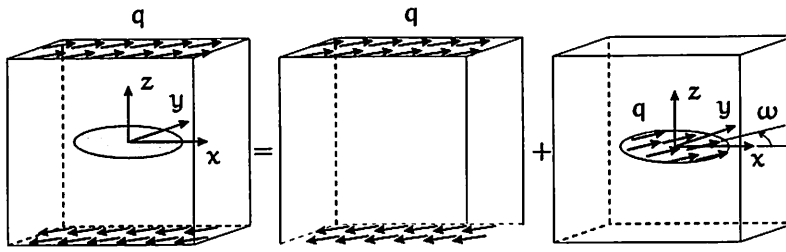

Figure 2.6: internal elliptical crack under remote shear tractions

2.2.4 sub-problems IV and V

Sub-problems IV and V present internal elliptical cracks in the center of the xy-plane of an infinite unit cells under simple shear loading p_{xz} or p_{yz} (figures 2.2: sub-problem IV and V). These two problems can be combined to one in which the unit cell embedding an internal elliptical crack in the center of the xy-plane is under simple shear q parallel to the plane of the crack and having a rotation angle ω with respect to the semi-major axis of the ellipse corresponding to the x-axis. In an analogous manner to the previous section, this combined problem can be decomposed into an un-cracked unit cell under simple shear and an internal elliptical crack in the xy-plane, whose faces are subjected to equal and opposite uniform shear loading q, and directed at an angle ω to the semi-major axis of the ellipse,figure 2.6.

The local stress field at a point ($\alpha \cos\varphi$, $\beta \sin\varphi$, 0) on the boarder of the ellipse due to the first problem is derived using the local orthogonal basis. The non-zero stress components are

$$\begin{aligned} \sigma_{nz} &= q\ (\alpha \sin\omega\, \mathcal{M}_3(\varphi) + \beta \cos\omega\, \mathcal{M}_4(\varphi))\ , \\ \sigma_{tz} &= q\ (-\alpha \sin\omega\, \mathcal{M}_3(\varphi) + \beta \cos\omega\, \mathcal{M}_4(\varphi))\ , \end{aligned} \tag{2.35}$$

where the following simplification have been considered

$$\begin{aligned} \mathcal{M}_3(\varphi) &= \frac{\sin\varphi}{\alpha^2 \sin^2\varphi + \beta^2 \cos^2\varphi}\ , \\ \mathcal{M}_4(\varphi) &= \frac{\cos\varphi}{\alpha^2 \sin^2\varphi + \beta^2 \cos^2\varphi}\ . \end{aligned} \tag{2.36}$$

These stress components have no contribution to the T-stresses.

For the second problem, the resulting stress field is skew-symmetric with respect to the plane of the crack and is associated with mode-II and mode-III stress intensity factors. The problem can be reduced to that of the half space with the following boundary conditions on the plane of the crack

a) the entire plane $z = 0$ is free of normal stresses

$$\sigma_{zz} = 0, \quad \text{for} \quad z = 0, \tag{2.37}$$

b) and for the points on the crack surface (inside the ellipse) and exterior to the ellipse one can write

$$\begin{cases} \sigma_{xz} = q \cos\omega \\ \sigma_{yz} = q \sin\omega \end{cases} \quad \text{for} \quad \left(\frac{x^2}{\alpha^2} + \frac{y^2}{\beta^2} \le 1 \text{ or } \xi = 0\right), z = 0, \tag{2.38}$$

$$\begin{cases} u_x = 0 \\ u_y = 0 \end{cases} \quad \text{for} \quad \left(\frac{x^2}{\alpha^2} + \frac{y^2}{\beta^2} \ge 1 \text{ or } \eta = 0\right), z = 0.$$

The solution for the singular stress terms of this problem has been given by KASSIR & SIH (1975). Here, a similar method is used to derive the complete expansion of the components of the stress field. An appropriate solution to this problem can be obtained by using a displacement field representation in terms of two harmonic functions $\mathcal{F}(x, y, z)$ and $\mathcal{H}(x, y, z)$

$$\begin{aligned} u_x &= -2(1-\nu)\frac{\partial \mathcal{F}}{\partial z} + z\frac{\partial \mathcal{G}}{\partial x}, \\ u_y &= -2(1-\nu)\frac{\partial \mathcal{H}}{\partial z} + z\frac{\partial \mathcal{G}}{\partial y}, \\ u_z &= -(1-2\nu)\mathcal{G} + z\frac{\partial \mathcal{G}}{\partial z}, \end{aligned} \tag{2.39}$$

and the expressions for the corresponding stress components are

$$\begin{aligned} \frac{\sigma_{xx}}{2\mu} &= -2(1-\nu)\frac{\partial^2 \mathcal{F}}{\partial x\,\partial z} - 2\nu\frac{\partial \mathcal{G}}{\partial z} + z\frac{\partial^2 \mathcal{F}}{\partial x^2}, \\ \frac{\sigma_{yy}}{2\mu} &= -2(1-\nu)\frac{\partial^2 \mathcal{F}}{\partial y\,\partial z} - 2\nu\frac{\partial \mathcal{G}}{\partial z} + z\frac{\partial^2 \mathcal{F}}{\partial y^2}, \\ \frac{\sigma_{zz}}{2\mu} &= z\frac{\partial^2 \mathcal{G}}{\partial z^2}, \\ \frac{\sigma_{xy}}{2\mu} &= -(1-\nu)\frac{\partial}{\partial z}\left(\frac{\partial \mathcal{F}}{\partial y} + \frac{\partial \mathcal{H}}{\partial x}\right) + z\frac{\partial^2 \mathcal{G}}{\partial x\,\partial y}, \\ \frac{\sigma_{xz}}{2\mu} &= -(1-\nu)\frac{\partial^2 \mathcal{F}}{\partial z^2} + \nu\frac{\partial \mathcal{G}}{\partial x} + z\frac{\partial^2 \mathcal{G}}{\partial x\,\partial y}, \\ \frac{\sigma_{yz}}{2\mu} &= -(1-\nu)\frac{\partial^2 \mathcal{H}}{\partial z^2} + \nu\frac{\partial \mathcal{G}}{\partial y} + z\frac{\partial^2 \mathcal{G}}{\partial y\,\partial z}, \end{aligned} \tag{2.40}$$

where the function $\mathcal{G}(x, y, z)$ designates the abbreviation

$$\mathcal{G} = \frac{\partial \mathcal{F}}{\partial x} + \frac{\partial \mathcal{H}}{\partial y}. \tag{2.41}$$

Similar to the case of the elliptical crack subjected to simple tension, the unknown functions $\mathcal{F}$ and $\mathcal{H}$ can be evaluated more expedient by the application of the ellipsoidal coordinates. An appropriate solution to the present problem has been given by GREEN & SNEDDON (1950)

$$\left\{ \begin{array}{c} \mathcal{F} \\ \mathcal{H} \end{array} \right\} = \frac{1}{2} \left\{ \begin{array}{c} A_{\mathcal{F}} \\ A_{\mathcal{H}} \end{array} \right\} \int_{\xi}^{\infty} \left(\frac{x^2}{\alpha^2+s} + \frac{y^2}{\beta^2+s} + \frac{z^2}{s} - 1 \right) \frac{ds}{\sqrt{Q(s)}}. \tag{2.42}$$

To evaluate the T-stresses in the asymptotic stress field, we are interested in the stress components outside the ellipse ($\eta = 0$) and on the plane of the crack ($z = 0$). Considering equations (2.40)-(2.42) and performing the necessary integration (see the appendix), the non-zero stress components in the plane of the crack, corresponding to the points both inside and outside the ellipse are

$$\begin{aligned} \frac{\sigma_{xx}}{2\mu} =& \frac{4 A_{\mathcal{F}}}{\alpha^2 \beta (\xi-\eta)(\xi-\zeta)} \sqrt{\frac{\eta \zeta (\beta^2+\xi)(\alpha^2+\eta)(\alpha^2+\zeta)}{\alpha^2-\beta^2}} \\ &+ \frac{4\nu A_{\mathcal{H}}}{\alpha \beta^2 (\xi-\eta)(\xi-\zeta)} \sqrt{\frac{\eta \zeta (\alpha^2+\xi)(\beta^2+\eta)(\beta^2+\zeta)}{\beta^2-\alpha^2}}, \end{aligned} \tag{2.43}$$

$$\begin{aligned} \frac{\sigma_{yy}}{2\mu} =& \frac{4\nu A_{\mathcal{F}}}{\alpha^2 \beta (\xi-\eta)(\xi-\zeta)} \sqrt{\frac{\eta \zeta (\beta^2+\xi)(\alpha^2+\eta)(\alpha^2+\zeta)}{\alpha^2-\beta^2}} \\ &+ \frac{4 A_{\mathcal{H}}}{\alpha \beta^2 (\xi-\eta)(\xi-\zeta)} \sqrt{\frac{\eta \zeta (\alpha^2+\xi)(\beta^2+\eta)(\beta^2+\zeta)}{\beta^2-\alpha^2}}, \end{aligned}$$

$$\begin{aligned} \frac{\sigma_{xy}}{2\mu} =& \frac{2(1-\nu) A_{\mathcal{F}}}{\alpha \beta^2 (\xi-\eta)(\xi-\zeta)} \sqrt{\frac{\eta \zeta (\alpha^2+\xi)(\beta^2+\eta)(\beta^2+\zeta)}{\beta^2-\alpha^2}} \\ &+ \frac{2(1-\nu) A_{\mathcal{H}}}{\alpha^2 \beta (\xi-\eta)(\xi-\zeta)} \sqrt{\frac{\eta \zeta (\beta^2+\xi)(\alpha^2+\eta)(\alpha^2+\zeta)}{\alpha^2-\beta^2}}, \end{aligned}$$

$$\begin{aligned} \frac{\sigma_{xz}}{2\mu} =& \frac{2 A_{\mathcal{F}} (1-\nu)}{\alpha \beta^2} \left(\frac{\eta \zeta \sqrt{Q(\xi)}}{\alpha \xi (\xi-\eta)(\xi-\zeta)} + E(\phi|k_1) - \frac{\alpha \sqrt{\beta^2+\xi}}{\sqrt{\xi(\alpha^2+\xi)}} \right) \\ &- \frac{2\nu A_{\mathcal{H}}}{\alpha \beta (\alpha^2-\beta^2)} \frac{\sqrt{-\xi(\alpha^2+\eta)(\alpha^2+\zeta)(\beta^2+\eta)(\beta^2+\zeta)}}{(\xi-\eta)(\xi-\zeta)} \\ &+ \frac{2\nu A_{\mathcal{F}}}{\alpha(\alpha^2-\beta^2)} \left(F(\phi|k_1) - E(\phi|k_1) - \frac{\xi(\beta^2+\xi)(\alpha^2+\eta)(\alpha^2+\zeta)}{\alpha \sqrt{Q(\xi)} (\xi-\eta)(\xi-\zeta)} \right), \end{aligned}$$

$$\frac{\sigma_{yz}}{2\mu} = \frac{2A_{\mathcal{H}}(1-\nu)}{\alpha\beta^2}\left(\frac{\eta\zeta\sqrt{Q(\xi)}}{\alpha\xi(\xi-\eta)(\xi-\zeta)} + E(\phi|k_1) - \frac{\alpha\sqrt{\beta^2+\xi}}{\sqrt{\xi(\alpha^2+\xi)}}\right)$$
$$- \frac{2\nu A_{\mathcal{F}}}{\alpha\beta(\alpha^2-\beta^2)}\frac{\sqrt{-\xi(\alpha^2+\eta)(\alpha^2+\zeta)(\beta^2+\eta)(\beta^2+\zeta)}}{(\xi-\eta)(\xi-\zeta)}$$
$$+ \frac{2\nu A_{\mathcal{H}}}{\beta(\alpha^2-\beta^2)}\left(\frac{\alpha}{\beta}E(\phi|k_1) - \frac{\beta}{\alpha}F(\phi|k_1) + \frac{\xi(\alpha^2+\xi)(\beta^2+\eta)(\beta^2+\zeta)}{\beta\sqrt{Q(\xi)}(\xi-\eta)(\xi-\zeta)}\right.$$
$$\left. - \frac{\alpha(\alpha^2-\beta^2)}{\beta}\frac{\xi}{\sqrt{Q(\xi)}}\right),$$

where the quantity $-(\beta^2+\zeta)$ is positive definite.

The constants $A_{\mathcal{F}}$ and $A_{\mathcal{H}}$ are derived by applying the boundary conditions $(2.38)_1$ to equations $(2.43)_{4,5}$. Performing the necessary integrations as addressed in the appendix the results would be

$$A_{\mathcal{F}} = \frac{\alpha\beta^2 k_1^2}{\left((k_1^2-\nu)E(k_1) + \nu k_2^2 K(k_1)\right)} q\cos\omega, \tag{2.44}$$

$$A_{\mathcal{H}} = \frac{\alpha\beta^2 k_1^2}{\left((k_1^2+\nu k_2^2)E(k_1) - \nu k_2^2 K(k_1)\right)} q\sin\omega.$$

The quantities $E(k_1)$ and $K(k_1)$ are the complete elliptical integrals of the second and first kind, respectively (BYRD & FRIEDMAN 1971). The solution to the problem is done, however, there remains to verify the conditions (2.37) and $(2.38)_2$. Since

$$\begin{Bmatrix} \frac{\partial\mathcal{F}}{\partial z} \\ \frac{\partial\mathcal{H}}{\partial z} \end{Bmatrix} = z\begin{Bmatrix} A_{\mathcal{F}} \\ A_{\mathcal{H}} \end{Bmatrix}\int_{\xi}^{\infty}\frac{ds}{\sqrt{s\,Q(s)}}, \tag{2.45}$$

for $z = 0$, the displacement components u_x and u_y (equations $(2.39)_{1,2}$) and the stress component σ_{zz} (equation $(2.40)_3$) would vanish, and the conditions (2.37) and $(2.38)_2$ are all satisfied. Performing the necessary integration, the stress field of the points of an infinite elastic solid containing an elliptical crack under simple shear is obtained from equations (2.40).

To find the corresponding T-stresses acting at the crack front, the local stress components at the crack front (in the plane of the crack $z = 0$ and outside of the ellipse $\eta = 0$) are to be derived. Using equations (2.29), and the application of equations (2.10) and (2.13) result in the expansion of the local stress components at the crack front. The non-zero asymptotic stress components are

$$\sigma_{nz} = \frac{-(A_{\mathcal{F}}\beta\cos\varphi + A_{\mathcal{H}}\alpha\sin\varphi)}{\sqrt{2\alpha^3\beta^3\sqrt[4]{\alpha^2\sin^2\varphi + \beta^2\cos^2\varphi}}}\frac{1}{\sqrt{r}} + O(\sqrt{r}), \tag{2.46}$$

$$\sigma_{tz} = \frac{(\nu-1)\,(A_{\mathcal{F}}\,\alpha\,\sin\varphi - A_{\mathcal{H}}\,\beta\,\cos\varphi)}{\sqrt{2\,\alpha^3\,\beta^3}\sqrt[4]{\alpha^2\,\sin^2\varphi + \beta^2\,\cos^2\varphi}}\frac{1}{\sqrt{r}} + O(\sqrt{r})\,,$$

where $A_{\mathcal{F}}$ and $A_{\mathcal{H}}$ are given by (2.44). Superimposing these results to the ones of the uncracked solid, the solution for stress components in the plane of the crack and outside the ellipse are resulting.

Considering equations (2.1) it is observed that for this crack problem there is no T-stresses along the crack front, since the corresponding stress terms are zero

$$\begin{aligned} T_I &= \lim_{r\to 0}\left(\sigma_{nn} - \frac{K_I}{\sqrt{2\pi r}}\right) = 0\,, \\ T_{II} &= \lim_{r\to 0}\sigma_{nt} = 0\,, \\ T_{III} &= \lim_{r\to 0}\left(\sigma_{tt} - \frac{2\nu\,K_I}{\sqrt{2\pi r}} - \nu\,T_I\right) = 0\,. \end{aligned} \tag{2.47}$$

From (2.46), the well known mode-II and mode-III stress intensity factors of internal elliptical cracks are resulting

$$\begin{aligned} K_{II} &= \lim_{r\to 0}\left(\sqrt{2\pi r}\,\sigma_{nz}\right) \\ &= \frac{-\sqrt{\pi}\,(A_{\mathcal{F}}\,\beta\,\cos\varphi + A_{\mathcal{H}}\,\alpha\,\sin\varphi)}{\sqrt{\alpha^3\,\beta^3}\sqrt[4]{\alpha^2\,\sin^2\varphi + \beta^2\,\cos^2\varphi}}\,, \end{aligned} \tag{2.48}$$

$$\begin{aligned} K_{III} &= \lim_{r\to 0}\left(\sqrt{2\pi r}\,\sigma_{tz}\right) \\ &= \frac{(\nu-1)\sqrt{\pi}\,(A_{\mathcal{F}}\,\alpha\,\sin\varphi - A_{\mathcal{H}}\,\beta\,\cos\varphi)}{\sqrt{\alpha^3\,\beta^3}\sqrt[4]{\alpha^2\,\sin^2\varphi + \beta^2\,\cos^2\varphi}}\,. \end{aligned}$$

2.2.5 sub-problem VI

This sub-problem presents an internal elliptical crack in the center of the xy-plane of an infinite unit cell under remote shear loadings p_{xy} (figure 2.2: sub-problem VI). For this problem, the local stress field along the crack front is

$$\begin{aligned} \frac{\sigma_{nn}}{p_{xy}} &= \frac{\alpha\,\beta\,\sin 2\varphi}{\alpha^2\,\sin^2\varphi + \beta^2\,\cos^2\varphi}\,, \\ \frac{\sigma_{tt}}{p_{xy}} &= \frac{-\alpha\,\beta\,\sin 2\varphi}{\alpha^2\,\sin^2\varphi + \beta^2\,\cos^2\varphi}\,, \\ \frac{\sigma_{nt}}{p_{xy}} &= \frac{-\alpha^2\,\sin^2\varphi + \beta^2\,\cos^2\varphi}{\alpha^2\,\sin^2\varphi + \beta^2\,\cos^2\varphi}\,. \end{aligned} \tag{2.49}$$

It is easy to show that $K_I = K_{II} = K_{III} = 0$ and considering (2.4), the T-stresses are

$$\begin{aligned}
\frac{T_I}{p_{xy}} &= \frac{\alpha\,\beta\,\sin 2\varphi}{\alpha^2\sin^2\varphi + \beta^2\cos^2\varphi}, \\
\frac{T_{II}}{p_{xy}} &= \frac{-\alpha^2\sin^2\varphi + \beta^2\cos^2\varphi}{\alpha^2\sin^2\varphi + \beta^2\cos^2\varphi}, \\
\frac{T_{III}}{p_{xy}} &= -(1+\nu)\,T_I = \frac{-(1+\nu)\,\alpha\,\beta\,\sin 2\varphi}{\alpha^2\sin^2\varphi + \beta^2\cos^2\varphi}.
\end{aligned} \tag{2.50}$$

2.2.6 complete set of T-stresses for a mixed-mode elliptical crack

The results of the previous sections can be superimposed to give the complete set of the T-stresses for internal elliptical cracks under general mixed-mode loading condition

$$\begin{aligned}
T_I =& p_{xx}\frac{\beta^2\cos^2\varphi}{\alpha^2\sin^2\varphi + \beta^2\cos^2\varphi} + p_{yy}\frac{\alpha^2\sin^2\varphi}{\alpha^2\sin^2\varphi + \beta^2\cos^2\varphi} + \\
& p_{zz}\,\mathcal{M}_1(\varphi)\left\{\left(2\nu - k_3^2 + (1-2\nu)\frac{K(k_1)}{E(k_1)}\right)\sin^2\varphi + \right. \\
& \left.\left(-2\nu + k_2^2 - (1-2\nu)\,k_2^2\frac{K(k_1)}{E(k_1)}\right)\cos^2\varphi\right\} + \\
& p_{xy}\frac{\alpha\,\beta\,\sin 2\varphi}{\alpha^2\sin^2\varphi + \beta^2\cos^2\varphi},
\end{aligned} \tag{2.51}$$

$$\begin{aligned}
T_{II} =& -p_{xx}\frac{\alpha\,\beta\,\sin\varphi\,\cos\varphi}{\alpha^2\sin^2\varphi + \beta^2\cos^2\varphi} + p_{yy}\frac{\alpha\,\beta\,\sin\varphi\,\cos\varphi}{\alpha^2\sin^2\varphi + \beta^2\cos^2\varphi} + \\
& p_{zz}(1-2\nu)\,\mathcal{M}_1(\varphi)\left(-\frac{k_2+k_3}{2} + k_2\frac{K(k_1)}{E(k_1)}\right)\sin 2\varphi + \\
& p_{xy}\frac{-\alpha^2\sin^2\varphi + \beta^2\cos^2\varphi}{\alpha^2\sin^2\varphi + \beta^2\cos^2\varphi},
\end{aligned}$$

$$\begin{aligned}
T_{III} =& p_{xx}\frac{\alpha^2\sin^2\varphi - \nu\,\beta^2\cos^2\varphi}{\alpha^2\sin^2\varphi + \beta^2\cos^2\varphi} + p_{yy}\frac{\beta^2\cos^2\varphi - \nu\,\alpha^2\sin^2\varphi}{\alpha^2\sin^2\varphi + \beta^2\cos^2\varphi} + \\
& p_{zz}\frac{\mathcal{M}_1(\varphi)}{2}\left\{\nu(k_2^2 - k_3^2) + (2\nu^2 + \nu - 1)k_1^2\frac{K(k_1)}{E(k_1)} + \mathcal{M}_2(\varphi)\cos 2\varphi\right\} - \\
& p_{xy}\frac{(1+\nu)\,\alpha\,\beta\,\sin 2\varphi}{\alpha^2\sin^2\varphi + \beta^2\cos^2\varphi}.
\end{aligned}$$

where the functions $\mathcal{M}_1(\varphi)$ and $\mathcal{M}_2(\varphi)$ are given in equation (2.32).

However, p_{ij}'s for each individual problem have to be addressed separately. Consider an internal elliptical crack in the center of the global xy-plane of an infinite unit cell under

remote tensile loading (P^∞) parallel to the global z-axis. The crack is initially in the plane $z = 0$, i.e. perpendicular to the direction of tension (mode-I). To have a general mode-mixity, the crack is first rotated by an angle γ_y about the global y-axis and then rotated γ_x about the rotated x-axis. The components of the projected load in the rotated local axes (xyz) can be derived with the help of the local orthonormal basis

$$\begin{pmatrix} p_{xx} & p_{xy} & p_{xz} \\ p_{yx} & p_{yy} & p_{yz} \\ p_{zx} & p_{yz} & p_{zz} \end{pmatrix} = P^\infty \begin{pmatrix} \cos^2\gamma_x \sin^2\gamma_y & -\sin\gamma_x \cos\gamma_x \sin\gamma_y & \cos^2\gamma_x \sin\gamma_y \cos\gamma_y \\ & \sin^2\gamma_x & \sin\gamma_x \cos\gamma_x \cos\gamma_y \\ \text{sym.} & & \cos^2\gamma_x \cos^2\gamma_y \end{pmatrix}. \quad (2.52)$$

2.3 Mixed-mode internal circular crack

Consider an internal circular crack in an infinite isotropic elastic solid under remote uniaxial traction, loading the crack in a mixed-mode manner. Using the superposition technique, this problem can be divided into six sub-problems (figure 2.2), where the internal circular crack is located in the center of the xy-plane of an infinite unit cell subjected to either simple tension or simple shear, i.e. p_{xx}, p_{yy}, p_{zz} and p_{xy}, p_{yz}, p_{xz}, respectively (the p_{ij}'s are the projections of the remote loading into the rotated local coordinates at the center of the crack).

The complete set of T-stress terms for mixed-mode internal circular cracks in an infinite isotropic elastic solid have been addressed by SCHÜTTE & MOLLA-ABBASI (2007B). Using the potential method and transformation technique, asymptotic solution for the stress components are derived (BENTHEM & KOITER 1973), (KASSIR & SIH 1966), (WANG 2004), from which the T-stress terms are resulting. T-stress terms for internal circular cracks, however, can be calculated from the ones for an elliptical crack in the limit case, where $\alpha \to \beta$. In this regard, the results of the previous sections can be summarized to give the complete set of the T-stress terms of internal circular cracks under the general mixed mode loading

$$\begin{aligned} T_I &= p_{xx} \cos^2\varphi - \frac{1}{2}(1+2\nu)\, p_{zz} + p_{yy} \sin^2\varphi - p_{xy} \sin 2\varphi\,, \\ T_{II} &= (p_{xx} - p_{yy}) \sin\varphi \cos\varphi + p_{xy} \cos 2\varphi\,, \\ T_{III} &= p_{xx}(\sin^2\varphi - \nu\cos^2\varphi) - \frac{1}{2}(1-\nu)(1+2\nu)\, p_{zz} \\ &\quad + p_{yy}(\cos^2\varphi - \nu\sin^2\varphi) + (1+\nu) p_{xy} \sin 2\varphi\,. \end{aligned} \quad (2.53)$$

For each individual problem, p_{ij}'s are derived in an analogous manner as for an elliptical crack, given in equation (2.52).

2.4 Impact of T-stresses

2.4.1 numerical evaluation of the T-stresses

In this section, distribution of the T-stresses along the crack front from the analytical solution and the effect of their magnitude and sign on the size and shape of the plastic zone at the crack tip are compared to the ones based on the finite element analysis, for different mode-mixities. Finite element simulations have been performed to determine the crack tip parameters (K_α's and T_α's) and the size of the plastic zone at the crack tip, based on the von Mises yield criterion (VON MISES 1913). To simulate the so called non-interacting crack, the size of the unit cell in the finite element model should be big enough with respect to the characteristic crack size, so that the crack tip fields are not influenced by the outer boundaries. To satisfy this condition, the size of the unit cell is taken here as 75 α, where α is respectively the radius of the circular crack and the semi-major axis of the elliptical crack, and the matrix of the unit cell is considered to be homogeneous, isotropic with a linear elastic response.

Hexahedral elements with quadratic displacement behavior are used to mesh the crack front region, where higher accuracy is needed. For this reason, crack front is embedded in a torus of radius $R_{torus} = \alpha/20$, figure 2.7. Inside this torus relatively fine elements are generated. The size of the elements in the radial direction is then $R_{torus}/n = \alpha/(20\,n)$, n being the number of elements in the radial direction. The rest of the model is meshed with quadratic tetrahedral elements which become coarser towards the outer boundaries of the unit cell. To reach errors of below 3 % for both T_α's and K_α's, the number of elements in the radial direction inside the torus n is chosen as 12, for which in average the maximum number of generated nodes is approximately 200,000.

To calculate the T-stresses along the crack front, the direct method is used which is based on the asymptotic stress field. The method is based on rearranging the equation (2.4) to calculate the local crack tip parameters (T_α's and K_α's) at a fixed θ. For example, for $\theta = 0°$ the T-stresses result from rearranging (2.4)

$$
\begin{aligned}
T_I &= \sigma_{nn} - \frac{K_I}{\sqrt{2\pi r}}, & K_I &= \sqrt{2\pi r}\,\sigma_{zz}, \\
T_{II} &= \sigma_{nt}, & K_{II} &= \sqrt{2\pi r}\,\sigma_{nz}, \\
T_{III} &= \sigma_{tt} - \frac{2\nu K_I}{\sqrt{2\pi r}} - \nu T_I, & K_{III} &= \sqrt{2\pi r}\,\sigma_{tz}.
\end{aligned}
\tag{2.54}
$$

K_α's and T_α's for the points along the crack front are evaluated by extrapolating the resulting nodal stresses back to the crack front in the planes perpendicular to the crack front for each point. This method is very efficient and fast, and for the considered degree of mesh refinement the maximum error for both K_α's and T_α's is less than 3% . Since no crack tip elements are used to mesh the crack front region, the results of the first rows of elements at the crack front should not be contributed in the calculation of the crack tip

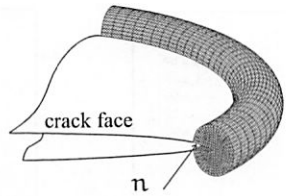

Figure 2.7: element design along the crack front

parameters. In this study, the results of the first three elements at the crack front in the radial direction are not considered in the evaluation of the crack tip parameters, i.e. for calculating the T-stresses and the stress intensity factors, the distance r at which the nodal stresses are extrapolated should be bigger than $\alpha/60 = 1.67\%\,\alpha$.

Following examples for different values of the rotation γ_y (see section 2.3) and Poisson's ratio of $\nu = 1/3$ are presented (figures 2.8, 2.9 and 2.10)

1. circular crack with a fixed rotation about the x-axis: $\gamma_x = 30°$,
2. elliptical crack with no rotation about the x-axis: $\gamma_x = 0°$,
3. elliptical crack with a fixed rotation about the x-axis: $\gamma_x = 30°$,

where continuous curves represent the analytical results, and finite element results are shown by cross-symbols. A loading level of $P^\infty/E = 1/100$ has been considered, and the aspect ratio β/α for the elliptical crack is chosen as and 0.5, respectively, where E is the Young's modulus.

Figures 2.8, 2.9 and 2.10 show that the results due to the finite element analyses are in very good agreement with the analytical solution.

2.4.2 effect of the T-stresses on the plastic zone

One of the basic assumptions behind the application of linear fracture mechanics to elastic-plastic materials is that the plastic deformation at the crack tip is governed by the intensity of the elastic stress singularities, i.e. the stress intensity factors. This is a valid argument, if the size of the plastic zone is small compared to other geometric dimensions of the problem, such as the crack length. The first order estimate of the size of the plastic zone, according to the approach of IRWIN (1961), for plane strain situations is $r_p = (K_I/\sigma_{yield})^2/6\pi$, where σ_{yield} is the tensile yield strength of the material. The shape of the plastic zone predicted by this model is, however, different from the actual one.

The shape and size of the plastic zone can be estimated by applying a yield criterion. For isotropic materials, considering von Mises yield criterion, the plastic zone is determined from the second associated homogeneous invariant of the deviatoric stress tensor

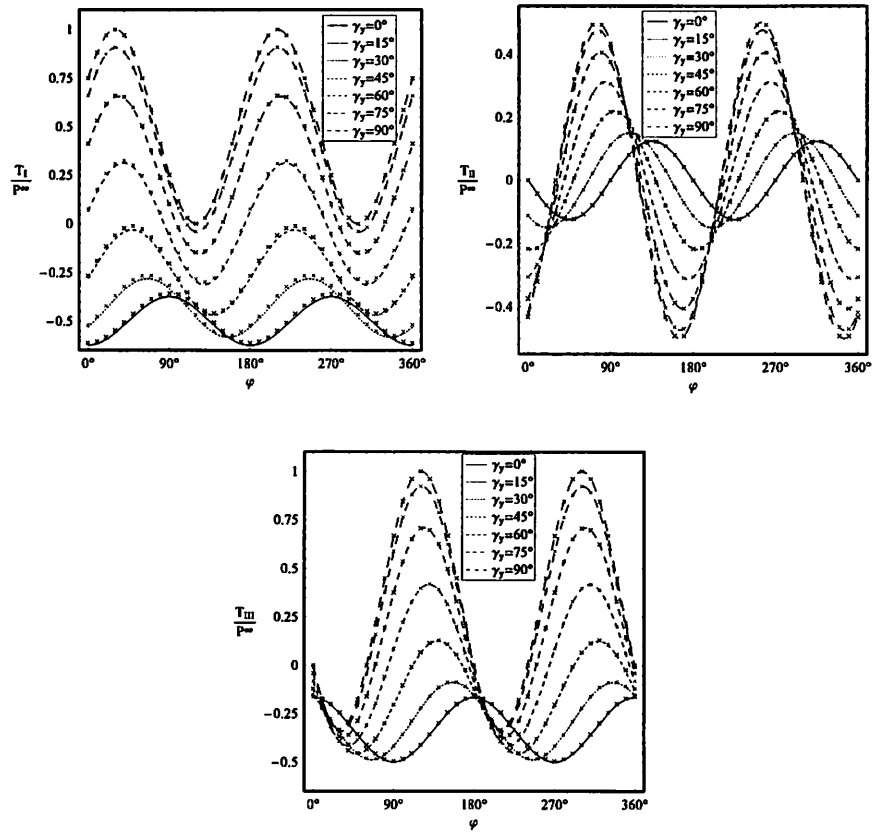

Figure 2.8: circular crack: T-stresses along the crack front ($\gamma_x = 30°$, and differing γ_y)

(LEMAITRE & CHABOCHE 1990)

$$J_2(\sigma) = (3\,p_{II})^{1/2} = \left(\frac{3}{2}\,\mathrm{Tr}(\sigma'^2)\right)^{1/2}, \text{and} \quad \sigma' = \sigma - \frac{1}{3}\,\mathrm{Tr}(\sigma)\mathbf{1}\,, \tag{2.55}$$

where σ' is the deviatoric part of the stress tensor σ. The size and shape of the plastic zone is found from

$$J_2(\sigma) - \sigma_{yield} = 0\,. \tag{2.56}$$

Solving equation (2.56) for r, gives an estimate of the radius of the plastic zone as a function of θ. A literature review shows that so far in the studies concerning the plastic zone at the crack tip, only the effect of the first component of the T-stresses (T_I), which is well known as the T-stress (LARSSON & CARLSSON 1973), (RICE 1974) has been

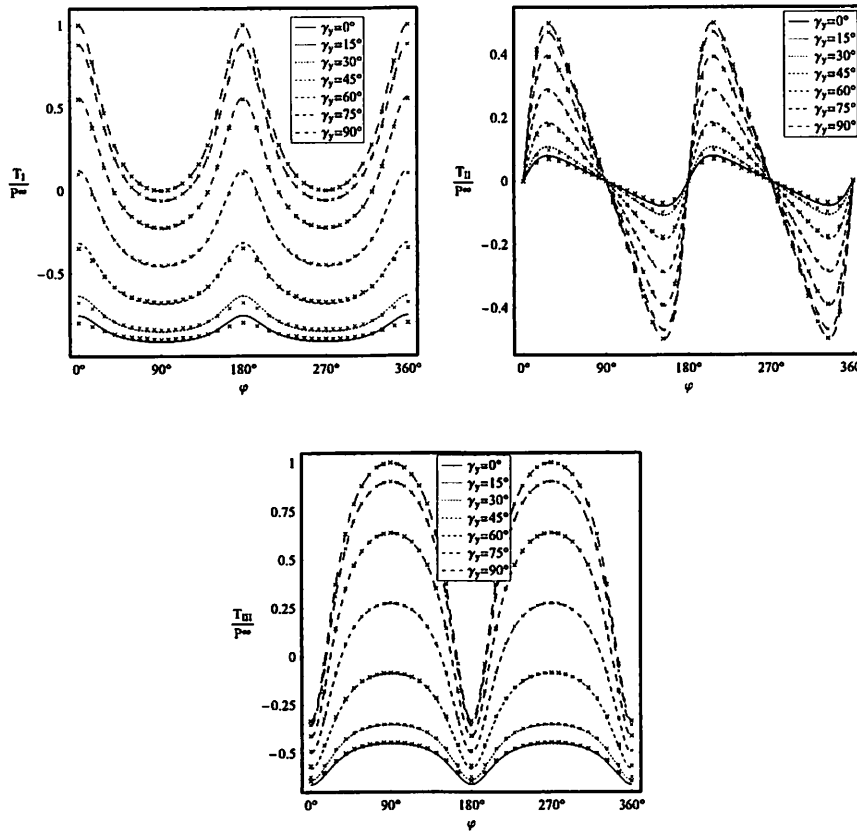

Figure 2.9: elliptical crack: T-stresses along the crack front ($\gamma_x = 0°$, and differing γ_y)

considered. This, however, does not result in an accurate estimate of the plastic zone. Here, it is shown that to have accurate results, beside considering the effect of the singular terms in the stress expansion formulae, the effect of the other components of the T-stresses should also be taken into account. To compare the effect of different terms on the resulting plastic zone at the crack tip, following combination of the singular terms and constant non-singular terms (T_α's) are considered (figures 2.11, 2.12, and 2.13)

case-1: considering the effect of pure singular stress terms (continuous gray lines)

case-2: considering the effect of the singular stress terms and T_I (black dashed lines)

case-3: considering the effect of the singular stress terms and all T-stresses (continuous black lines).

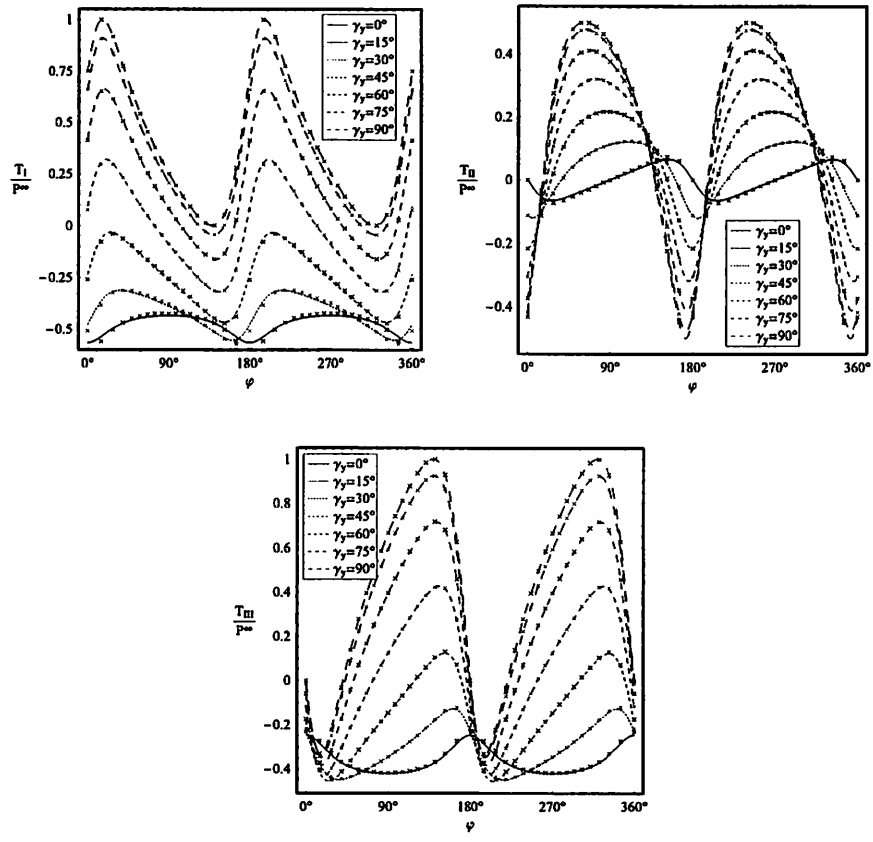

Figure 2.10: elliptical crack: T-stresses along the crack front ($\gamma_x = 30°$, and differing γ_y)

Following examples are presented

1. circular crack rotated 60° about the y-axis ($\gamma_x = 0°$ and $\gamma_y = 60°$),
2. elliptical crack under pure mode-I ($\gamma_x = \gamma_y = 0°$)
3. elliptical crack rotated 30° about the y-axis and 30° about the x-axis ($\gamma_x = \gamma_y = 30°$),

for which the load level is chosen as $P^\infty/\sigma_{yield} = 1/3$, Poisson's ratio $\nu = 1/3$ and aspect ratio for the considered elliptical cracks is chosen as $\beta/\alpha = 0.5$. Since it is difficult to compare the plastic zones due to different cases in a three-dimensional manner, only four representing cuts along the crack front are shown (points corresponding to $\varphi = 0°, 45°, 90°, 135°$).

It is observed that for all examples, the size and shape of the plastic zones from the

finite element analyses (cross-symbols) are in good agreement with the ones due to case-3, pointing out the fact that in three-dimensional crack tip plasticity problems, the impact of all T-stresses should be considered.

Figure 2.11 refers to the results of the penny shaped crack inclined 60° about the y-axis. At $\varphi = 0°$, the plastic zone due to all singular and T-stress terms (case-3) does not embed the other ones at all θ's. This is due to the change of the sign of individual T-stress terms. At points for which case-3 estimates a smaller r_p, there are positive T-stresses, which dominate and reduce r_p, and vice versa, at θ's with dominant negative T_α effect the magnitude of r_p increases. This behavior is observed in all examples. At $\varphi = 90°$, the plastic zones due to all cases are approximately identical. This is due to the fact that at this point T_{II} vanishes, and T_I is relatively small. Although T_{III} at this point is not negligible, it seems that it does not affect the plastic zone as significantly as the other two terms do.

Figure 2.12 shows that for a mode-I elliptical crack the plastic zone is maximum at $\varphi = 90°$ corresponding to the semi-minor axis and is minimum at the semi-major axis ($\varphi = 0°$), because both K_I and the non-zero T-stresses are maximum at the point on the semi-minor axis. The plastic zone due to all singular stress terms and the T-stresses (case-3) embeds the ones due to case-1 and case-2, showing the importance of considering the other two terms of the T-stresses, which normally have been neglected. Comparing the analytical results with the ones from the finite element analysis shows clearly, that only the solution presented here can correctly predict the size and shape of the plastic zone. It should also be mentioned that T_I and T_{III} for this example are negative along the crack front and bigger than T_{II} which its sign changes from a quarter to the next along the crack front. Comparing the results due to case-3 with the ones of case-1 and case-2 points out that negative T-stresses increase the size of the plastic zone.

Figure 2.13 shows the results of the last example ($\gamma_x = \gamma_y = 30°$). It is observed that the plastic zones due to different cases do not have a big difference. This is due to the point that for this problem T_α's are relatively small all along the crack front compared to the other examples, so the difference between the plastic zones becomes smaller. The presented observations suggest that for an accurate estimation of the size of the plastic zone, the effect of all T-stresses should be taken taken into account.

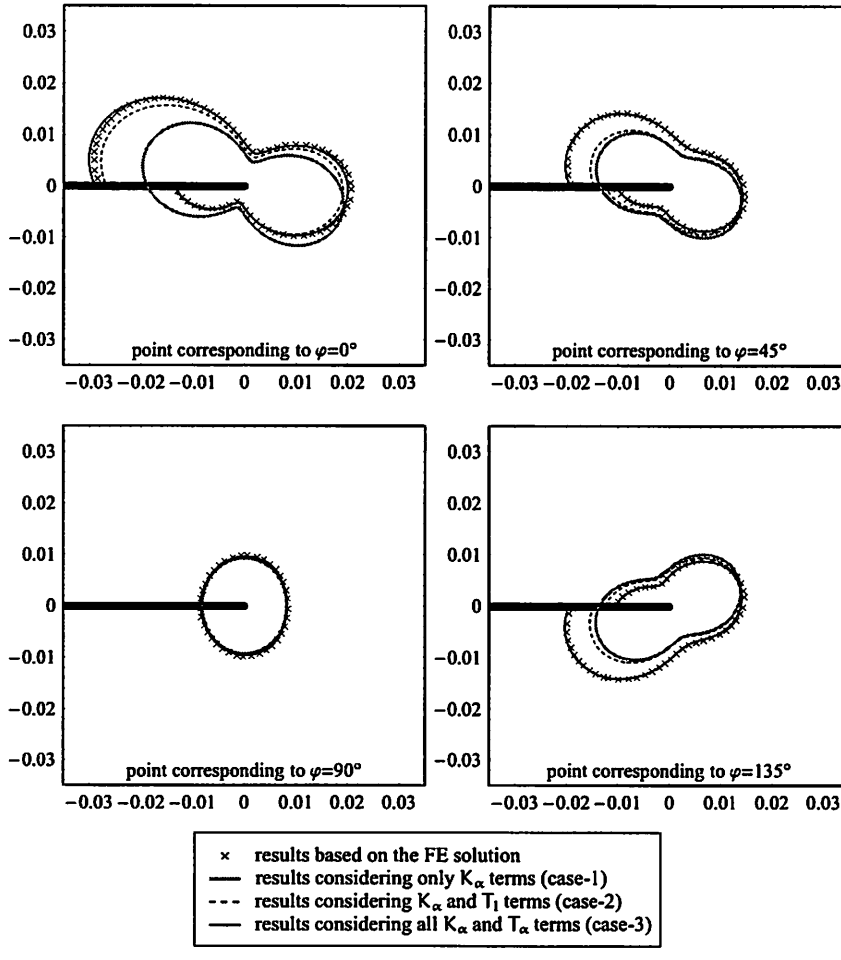

Figure 2.11: circular crack with $\gamma_x = 0°$, $\gamma_y = 60°$, normalized plastic zone $\frac{r_p}{\alpha}$

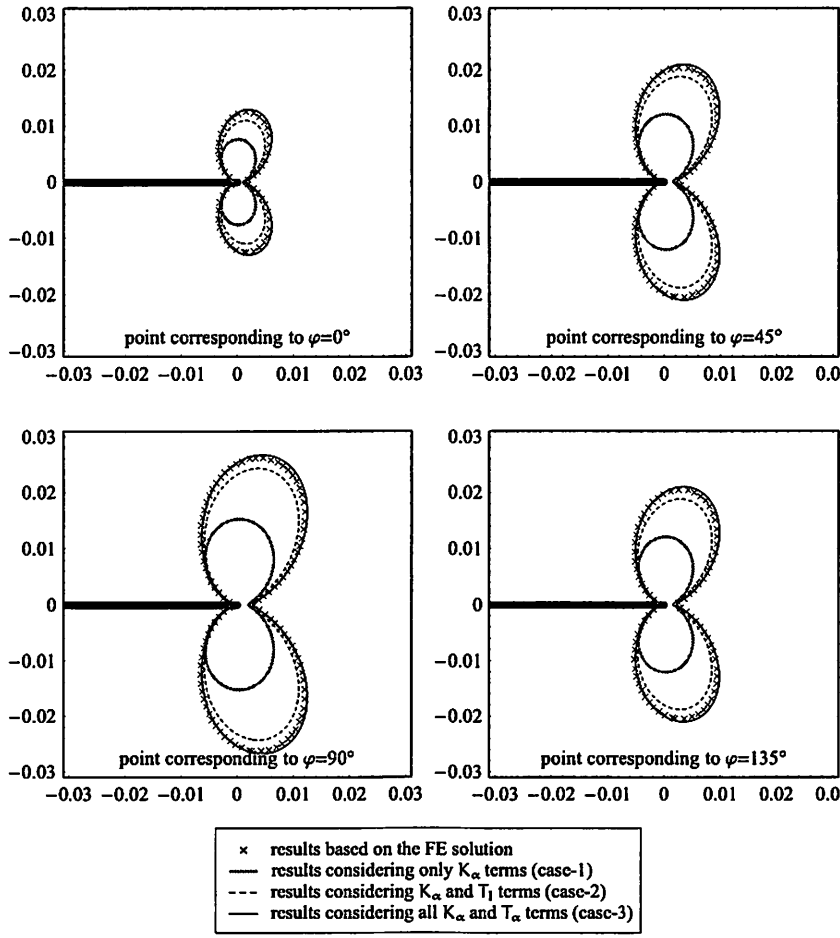

Figure 2.12: elliptical crack with $\gamma_x = \gamma_y = 0°$, normalized plastic zone $\frac{r_p}{\alpha}$

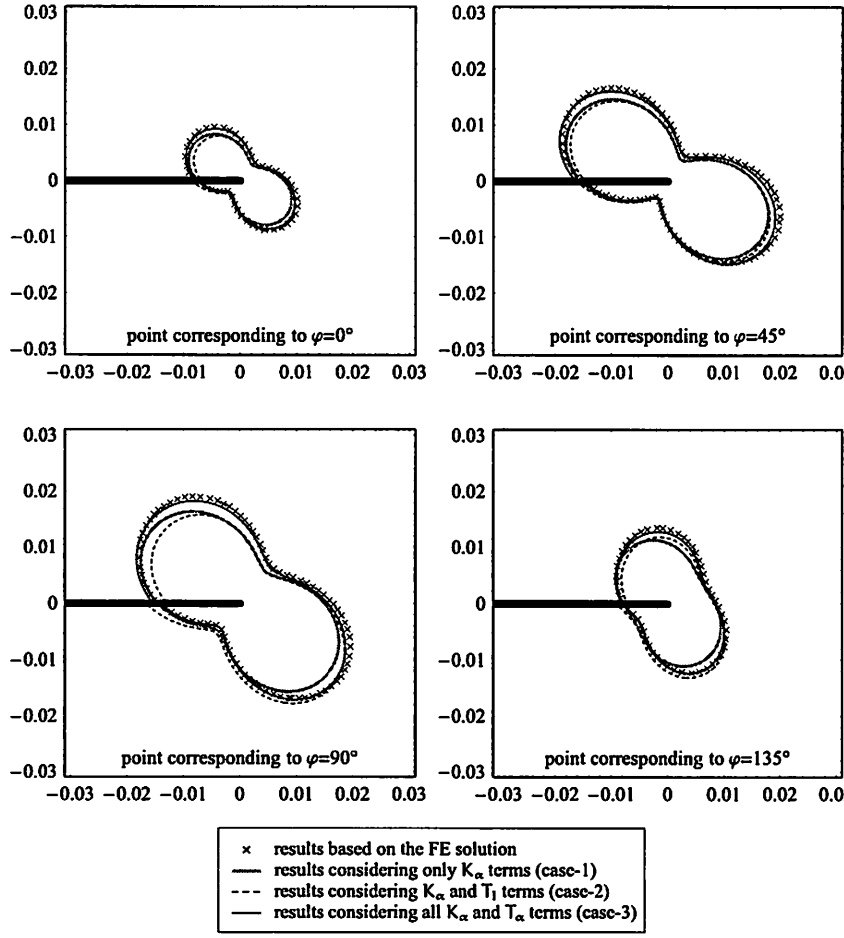

Figure 2.13: elliptical crack with $\gamma_x = \gamma_y = 30°$, normalized plastic zone $\frac{r_p}{\alpha}$

3 Crack Paths under Mixed-mode Loadings

Contents

The prediction of crack paths under general mixed-mode conditions, using the theory of linear elastic fracture mechanics, has been the subject of many investigations, both in two- and three-dimensions. These include both the theoretical works devoted to infinitesimal crack extension from a given geometry (COTTERELL & RICE 1980), (LEBLOND 1989), (AMESTOY & LEBLOND 1992), (LEBLOND & FRELAT 2000), (SUMI, NEMAT-NASSER & KEER 1983), and numerical studies simulating the propagation of cracks (ZIENKIEWICZ & TAYLOR 1989), (SUMI 1986), (ALIABADI 1997).

The aim of this chapter is to give the theoretical foundations for the prediction of crack paths within the theory of quasi-static linear elastic fracture mechanics, both in two- and three-dimensions, based mainly on the works of LE, STUMPF & WEICHER (1989), LE, SCHÜTTE & STUMPF (1999), LEBLOND (1989), AMESTOY & LEBLOND (1992) and LEBLOND & FRELAT (2000). In this respect, finite element simulation of two- and three-dimensional mixed-mode crack propagation is addressed. The models provide a general framework for mixed-mode linear elastic fracture mechanics, under small strain assumptions. Central straight cracks in two-dimensional case, and internal circular and elliptical cracks in three-dimensions with different mode-mixities are modeled in linearly elastic, homogeneous and isotropic solids, with or without inclusions, subjected to far field uniform traction field, to show the possible modes of crack propagation. The models enable us to give the evolution of the stress intensity factors and the T-stresses of mixed-mode internal cracks, as well (MOLLA-ABBASI & SCHÜTTE 2006).

3.1 Background on the simulation and crack growth criteria

The study of the prediction of crack paths within the theory of quasi-static linear elastic fracture mechanics in three-dimensions begun about two decades ago with the works of RICE (1985), GAO & RICE (1986), GAO & RICE (1987B), GAO & RICE (1987A), GAO (1988) and RICE (1989) who devoted their research to the question of the stability of the fundamental configuration of the crack front versus small perturbation within the crack plane, for semi-infinite, circular and external circular cracks in infinite bodies. Although all three modes were considered, except for the external circular crack geometry, the conclusions were mainly relevant in the case of pure mode-I, and the hypothesis of coplanar crack propagation was seldom verified in the presence of mode-II and III. All these works were based on two essential elements. First, asymptotic expressions of the stress intensity factors along the front of an arbitrary infinitesimal extension exhibiting the influence of its length, and second, use of some propagation criterion expressed in terms of the stress intensity factors. Slight deviations from coplanarity were envisaged in the works of GAO (1992), XU, BOWER & ORTIZ (1994) and BALL & LARRALDE (1995).

More recent and complete works on this subject are the series of papers by LEBLOND (1989), AMESTOY & LEBLOND (1992), LEBLOND & FRELAT (2000) and LEBLOND & FRELAT (2004) (see also the cited works therein), in which they have studied the theoretical foundation for the prediction of crack paths within the theory of quasi-static linear elastic fracture mechanics. In two-dimensional case different situations have been addressed, including the most general plane situation, crack kinking from an initially closed ordinary or interface crack in the absence or presence of friction. In three-dimensions, the case of an arbitrary three-dimensional geometry under arbitrary loading has been considered. LEBLOND (1989) has provided the formulae for the geometrical parameters including the branching angle and the curvature parameters of a crack propagating in the most general plane situation. Based on dimensional analysis (scale changes) and the regularity properties (continuity and differentiability) of the stresses with respect to the crack extension length, he has addressed the general form of the expansion of the stress intensity factors in powers of the crack extension length. Most terms of the expansion formulae are universal, in the sense that they depend only on the parameters characterizing the local geometry of the crack and its extension and the asymptotic stress field of the initial crack, without any explicit reference to the geometry of the body nor to the loading imposed on its boundary. LEBLOND & FRELAT (2004) have studied the crack kinking from an initially closed ordinary or interface crack in the absence of friction, or in the presence of friction (see also LEBLOND & FRELAT (2000) and LEBLOND & FRELAT (2001)). In an analogous way, based on the dimensional analysis and the regularity properties of the stresses with respect to the crack extension length, expansion formulae for the stress intensity factors in terms of the extension length have been derived, which in the presence of friction depend on the friction coefficient and for interface crack problems depends on the Dundurs parameters (DUNDURS 1969), as well. Using the principle of local symmetry proposed by GOLDSTEIN & SALGANIK (1974) to

predict the crack path, a theoretical value for the kink angle is derived for each case. In three-dimensions, LEBLOND (1999) has studied the prediction of crack paths in three-dimensional elastic solids, under the most general hypotheses of arbitrary geometry and arbitrary loading. For this, he has derived the expansion of the stress intensity factors along the crack front after an arbitrary infinitesimal propagation, in terms of the crack extension length up to the second term.

Numerical simulation of three-dimensional crack growth, especially the propagation law to determine the direction and growth rate of arbitrary three-dimensional mixed-mode cracks, are still interesting problems, mainly due to the need for an efficient modeling strategy to be employed as the crack propagates. A variety of numerical techniques have been used to establish a solution to this problem, including finite difference method (FDM) (LAPIDUS & PINDER 1982), finite element method (FEM) (ZIENKIEWICZ & TAYLOR 1989), boundary element method (BEM) (ALIABADI 1997), and boundary integral equation method (BIEM) (RIZZO 1967). LI, MEAR & XIAO (1998), and FRANGI, NOVATI, SPRINGHETTI & ROVIZZI (2002) have proposed a numerical simulation of crack propagation in three-dimensional linear elastic bodies by making use of the symmetric Galerkin boundary element method (SGBEM).

The BEM technique (ALIABADI 1997) involves discretization of the boundary alone, and the dimensions of the stiffness matrix formed in BEM is then reduced by one in comparison to a domain method, such as FEM, although the stiffness matrix is full and symmetric in general. An advantage of BEM in application to fracture problems over FEM is that domain remeshing is not necessary by crack growth and only elements at the crack tip are added to the already existing elements.

One of the most common approaches in simulating the crack propagation is the stepwise method, which consists of the succession of straight segments. In this method, the propagation path is considered to be a sequence of small steps. At each step of propagation, the crack extension length and its direction are predicted by the employed fracture criterion. The crack is then extended from the previous crack tip by a length increment in the plane perpendicular to the crack front. SCHÜTTE (2001) has studied the propagation of a central straight two-dimensional crack in a unit cell using the stepwise method. At each step, stress intensity factors are determined numerically by extrapolating the displacement field to the crack tip. The fracture criterion he has used is the maximum driving force criterion (LE, SCHÜTTE & STUMPF 1999). MOGILEVSKAYA (1997) has suggested a numerical algorithm to simulate two-dimensional crack growth, in which stepwise method based on local criterion of propagation is used. He has employed two crack propagation criteria. At the first step of propagation the maximum tensile stress criterion is used, and at subsequent steps the criterion of local symmetry (GOLDSTEIN & SALGANIK 1974) is employed.

There are several fracture criteria predicting the direction and the minimum load (limit load) required to extend a crack under mixed-mode loading, such as

the criteria of maximum strain energy release rate (ERDOGAN & SIH 1963), maximum driving force criterion (LE, SCHÜTTE & STUMPF 1999), maximum hoop stress (ERDOGAN & SIH 1963), maximum tensile stress (MAITI & SMITH 1983), local symmetry (GOLDSTEIN & SALGANIK 1974), and minimum strain energy density (SIH 1972). The first study of this problem goes back to ERDOGAN & SIH (1963) who have postulated that fracture is governed by the attainment of a critical circumferential stress, over a characteristic length surrounding the crack tip. This is the so called maximum hoop stress criterion. According to this criterion a crack propagates in the plane normal to the maximum hoop stress at a characteristic length. This critical stress is presumably a material constant and is determined by a pure mode-I test. The local symmetry criterion proposed by GOLDSTEIN & SALGANIK (1974) states that the crack tends to advance such that the in-plane shear stress in the vicinity of the crack tip vanishes. Another popular fracture criterion for mixed-mode problems is the maximum energy release rate criterion, or the Griffith theory (ERDOGAN & SIH 1963). It is postulated that a crack under mixed mode loading will grow along a direction which maximizes the energy release rate, and energy release rate is a material property and thus it is independent of the mode-mixity. The minimum strain energy density criterion, proposed by SIH (1974), states that the direction of crack extension coincides with the direction of minimum strain energy density along a constant radius around the crack tip. Since test results tend to show that a crack propagates in a direction perpendicular to the far field tensile load, it leads to the principal of maximum tensile stress criterion (MAITI & SMITH 1983). The maximum driving force criterion (LE, SCHÜTTE & STUMPF 1999) states that cracks propagate in the direction the driving force acting at the crack tip becomes maximum. This criterion is the direct consequence of a variational principle of a cracked body in equilibrium. Based on this work, the magnitude and the direction of the maximum driving force acting on a kinking crack are consistently determined.

In this chapter, the simulation of quasi-static propagation of mixed-mode internal cracks have been performed using the finite element method and the stepwise technique, considering small strain assumptions. The propagation of the crack is governed by the maximum driving force criterion (LE, SCHÜTTE & STUMPF 1999) along with a generalized Paris' law, from which the crack trajectory and the extension rate are resulting. With this, it can be shown that the local crack extension rate is proportional to its thermodynamic dual, the maximum driving force acting at the crack tip (SCHÜTTE 2001). This shows the connection of the maximum driving force criterion with the energy dissipated along the crack front by its kinking. Another advantage of this criterion is that it considers the effect of all stress intensity factors for general three-dimensional crack geometries. This is especially important, since K_{III} does not always tend to vanish, even for heavily grown cracks.

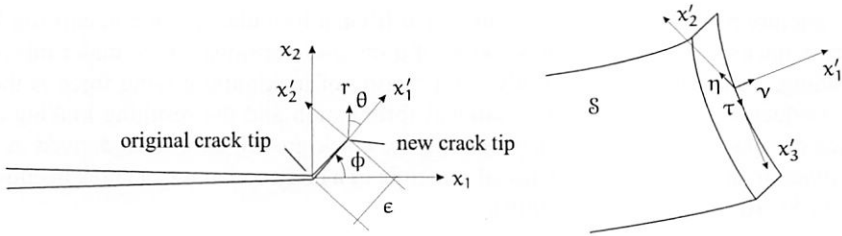

Figure 3.1: crack extension and new crack coordinates

3.1.1 variational principle of fracture mechanics in elastostatics

There are many situations in which a crack under remote loading may expand in directions not lying in the tangent plane to its initial surface. Tangential or non-tangential crack expansion can be categorized respectively by stating that a crack grows such that its expansion lies or does not lie in the tangent plane to its initial surface. In the case of non-tangential crack expansion the determination of the driving force is not simple. In this regard, the comparison of the energy stored in the body containing the kinked crack with that stored in the body prior to crack expansion is required. For small crack expansions, the change in energy depends strongly on the singular stress field and the displacement fields near the crack tip. It has been shown that the stress intensity factors for an infinitesimal kinked crack do not tend to those prior to crack expansion (BILBY & CARDEW 1957). The limiting stress intensity factors turn out to be a function of the kink angle and the stress intensity factors prior to crack kinking. The calculation of the energy change is the main difficulty in determining the driving force acting on a kinked crack.

This section summarizes the results of the works of LE, STUMPF & WEICHER (1989), LE & SCHÜTTE (1999) and LE, SCHÜTTE & STUMPF (1999), who considered the results of WU (1978) and LEBLOND (1993) in combination with the variational principles

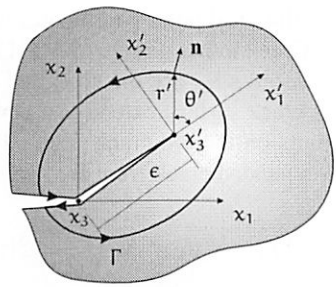

Figure 3.2: local coordinate system in the plane perpendicular to the front of the kinked crack

of fracture mechanics (LE 1989) to derive Irwin's formula, which contains the limiting stress intensity factor after the kinking of a three-dimensional crack under mixed mode loading. According to their study, the criterion of maximum driving force is the direct consequence of the proposed variational formulation and the resulting kinking angle is then computed. The equations governing the crack growth have been derived in straight forward manner from the variational principle of a body containing a crack in equilibrium (LE, SCHÜTTE & STUMPF 1999).

What follows gives a brief summary of the derivation of the formula for the maximum driving force acting on a kinked crack in three-dimensions as well as to determine the equilibrium criterion of a body containing a crack by means of the variational principles of fracture mechanics, under the assumption of small elastic strains.

Consider a linear elastic body occupying the region $\mathcal{B}_S = \mathcal{B}\backslash\bar{S}$ of the three dimensional Euclidean space with the exterior boundary $\partial\mathcal{B}$ and the interior boundary $S = S \cup \partial S$. The surface S is used to describe a crack surface in its initial configuration. The body is loaded such that it contains the displacement fields $u_i(x_j)$, where x_1, x_2, x_3 are the Cartesian coordinates, with the associated stress $\sigma_{ij}(x_k)$. Here, Latin indices $i, j, k, \ldots$ range over $1, 2, 3$ and the summation over repeated indices is understood. The governing equations are the three equilibrium conditions (in the absence of body forces) and the Hooke's law. Only such loading conditions are considered where the crack faces are traction free. Then the boundary conditions on the opposite sides of the crack read

$$\sigma_{ij}^{\pm} n_j = 0 \quad \text{on} \quad \partial S\,. \tag{3.1}$$

Here the indices $+$, $-$ indicate limit values of quantities on the two sides of S, and n_j is the normal vector pointing in the direction $+$. The singular stress field and the displacement field near the crack front prior to the crack extension are given by (WILLIAMS 1957), (RICE 1968A)

$$\sigma_{ij} = K_\alpha \frac{f_{ij}^\alpha(\theta)}{\sqrt{2\pi r}} + O(1)\,, \qquad u_i = K_\alpha \sqrt{\frac{r}{2\pi}}\, v_i^\alpha(\theta) + O(r)\,, \tag{3.2}$$

where r and θ correspond to the local polar coordinates in the plane perpendicular to the crack front (figure 3.1), and Greek indices range over I, II, III and denote the three crack deformation modes. The constants K_α are the so called stress intensity factors prior to the crack extension. Let the crack surface extend to a new surface, which is supposed to be smooth except at the points on the old crack front. The singular stress field and the displacement field near the expanded crack front are given by

$$\sigma_{i'j'} = K'_\alpha \frac{f_{i'j'}^\alpha(\theta')}{\sqrt{2\pi r'}} + O(1)\,, \qquad u_{i'} = K'_\alpha \sqrt{\frac{r'}{2\pi}}\, v_{i'}^\alpha(\theta') + O(r')\,, \tag{3.3}$$

where r' and θ' correspond to the polar coordinates of the shifted and rotated coordinate system and the indices with prim denote the projections onto the corresponding rotated

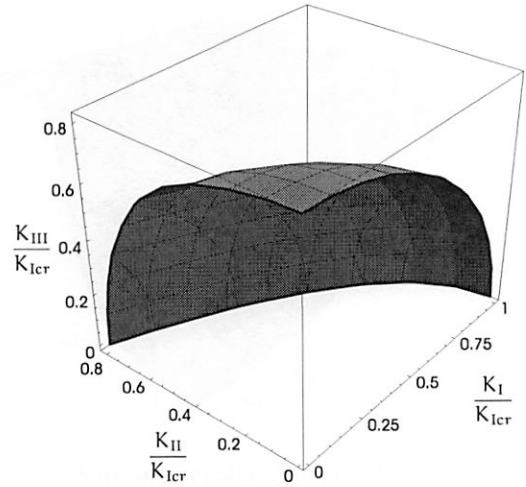

Figure 3.3: fracture locus in three-dimensions

coordinate axes. The radius of the domain, where equation (3.3) applies is of the order smaller than ϵ and tends to zero together with ϵ. However, the stress intensity factors do not tend to those prior to crack extension as ϵ tends to zero.

Based on the dimensional analysis (scale changes) and the regularity properties (continuity and differentiability) of the stresses with respect to the crack extension length ϵ, the general form of the expansion of the stress intensity factors can be derived in powers of the crack extension length (AMESTOY & LEBLOND 1992) and (LEBLOND 1993)

$$K'_\alpha = K_\alpha(\epsilon) = K^\star_\alpha + K^{(1/2)}_\alpha \sqrt{\epsilon} + O(\epsilon)\,, \tag{3.4}$$

where

$$\begin{aligned} K^\star_\alpha &= F_{\alpha\beta}(\phi)\, K_\beta\,, \\ K^{(1/2)}_\alpha &= G_{\alpha\beta}(\phi)\, T_\beta + a^\star\, H_{\alpha\beta}(\phi)\, K_\beta\,, \end{aligned} \tag{3.5}$$

where $F_{\alpha\beta}$, $G_{\alpha\beta}$, and $H_{\alpha\beta}$ are universal functions of the kinking angle ϕ, K_β and T_β are the stress intensity factors and the T-stresses of the crack prior to kinking, and $a^\star$ is the curvature parameter of the crack extension which for a straight extension vanishes ($a^\star = 0$). Most terms of the expansion formulae are universal, in the sense that they depend only on the parameters characterizing the local geometry of the crack and its extension and the asymptotic stress field of the initial crack, without any explicit reference to the geometry of the body nor to the loading imposed on its boundary.

Considering formula (3.4), the limiting value of K'_α as $\epsilon \to 0$ equals $K^\star_\alpha$

$$\lim_{\epsilon\to 0}(K'_\alpha = K_\alpha(\epsilon)) = K^\star_\alpha = F_{\alpha\beta}(\phi)\, K_\beta\,. \tag{3.6}$$

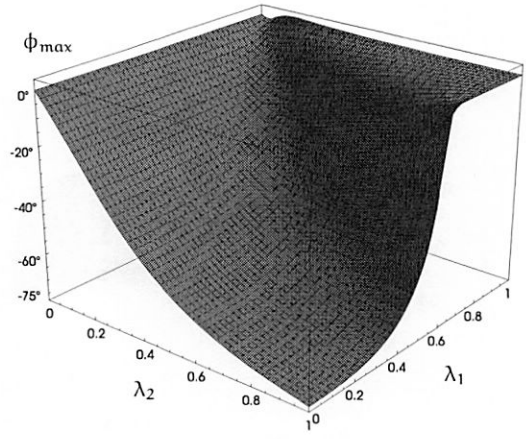

Figure 3.4: kinking angle in terms of λ_1 and λ_2

The total energy functional is then defined as follows

$$I[\mathbf{u}] = \int_{\mathcal{B}_\Sigma} W^e(\varepsilon_{ij}(u_i))\,dv - \int_{\partial\mathcal{B}_t} t_i u_i\,da + \int_\Sigma 2\gamma\,da, \tag{3.7}$$

with $W^e(\varepsilon_{ij}) = (1/2)\,\lambda\,\varepsilon_{ii}^2 + \mu\,\varepsilon_{ij}\,\varepsilon_{ij}$ and $\varepsilon_{ij} = (1/2)(u_{i,j} + u_{j,i})$ being the elastic energy density and the strain field, respectively, and t_i represents the external traction field. The last integral expresses the energy of the crack, which is assumed to be proportional to the area of the crack surface. Therefore γ can roughly be interpreted as the surface energy density, and the factor 2 appears because of two crack faces. Indeed the dissipation due to the plastic deformation and the separation in the plastic zone are proportional the area of the crack, and can be included in γ.

The variation of the energy functional (3.7) can be defined as

$$\delta I = \frac{d}{d\epsilon} I[\mathbf{u}(\epsilon)]\bigg|_{\epsilon=0}. \tag{3.8}$$

The variational principle of fracture mechanics states that the body containing a crack can only be in stable equilibrium, if the variation of its total energy functional is non-negative for all sets of admissible displacement fields (Le 1989)

$$\delta I \geq 0, \quad \forall\,\mathbf{u}(\epsilon) \in \mathcal{C}. \tag{3.9}$$

In the local rotated coordinate system x_i' with axes which coincide with the vectors ν, η, τ, where η is perpendicular to ν and τ (figure 3.1), the variation results in

$$\delta I = \int_{\partial S} (2\gamma - \lim_{\epsilon\to 0} J_{1'})\,\delta y\,ds \geq 0, \tag{3.10}$$

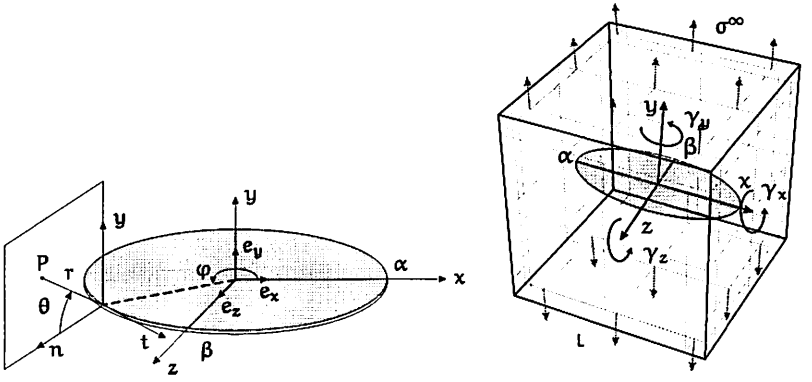

Figure 3.5: coordinate systems of the crack

where $J_{i'}$ is the corresponding component of the J-integral vector in the local coordinates at the new crack tip, given by (see also section 1.3.3)

$$J_{i'}(\phi) = \int_\Gamma \mu_{i'j'}\, n_{j'}\, ds = \int_\Gamma (W^{e\prime}\, n_{i'} - \sigma_{k'j'}\, u_{k',i'}\, n_{j'})\, d\Gamma\,, \tag{3.11}$$

with Γ the contour of radius $h = \epsilon/2$ surrounding the point of $\partial\mathcal{S}$, and $n_{i'}$ the unit normal vector on Γ. The expression

$$G_\phi = \lim_{\epsilon\to 0} J_{1'} = \lim_{\epsilon\to 0} \int_\Gamma (W^{e\prime}\, n_{1'} - \sigma_{k'j'}\, u_{k',1'}\, n_{j'})\, d\Gamma\,, \tag{3.12}$$

will be called the energy release rate for the non-tangential crack extension. Using the formulae (3.3) with the universal functions $f^{\alpha}_{i'j'}(\theta')$ and $\nu^{\alpha}_{i'}(\theta')$ one gets

$$G^* = \frac{1-\nu^2}{E}\left((K_I^*)^2 + (K_{II}^*)^2 + \frac{1}{1-\nu}(K_{III}^*)^2\right)\,. \tag{3.13}$$

where E and ν are respectively the Young's modulus and the Poisson's ratio of the matrix material.

According to the variational inequality (3.10), the body with a crack $\mathcal{S}$ can be in a state of stable equilibrium if and only if

$$G^* = \max_\phi G_\phi \le 2\gamma\,, \tag{3.14}$$

since $\delta y_i \ge 0$. This is analogous to the criterion of the maximum energy release rate, except that stress intensity factors are those for the kinked crack. The maximum of the driving force acting on the crack tip and the direction in which it is reached can be found, using formula (3.6).

Figure 3.3 shows the graphics of the dimensionless fracture locus in three-dimensions, in accordance with equation (3.14), and figure 3.4 gives the dependence of the angle ϕ_{max}, at which the driving force (formula (3.13)) reaches its maximum, on the mode-mixity factors

$$\lambda_1 = \frac{K_{II}}{K_I + |K_{II}|}, \qquad \lambda_2 = \frac{K_{III}}{K_I + |K_{II}| + |K_{III}|}. \tag{3.15}$$

Considering these mode-mixity factors, the following function may be resulting for the kinking angle from a curve fitting for the part of the surface in figure 3.4, where $0 < \lambda_1, \lambda_2 < 0.6$

$$\begin{aligned} \phi_{max} = \operatorname{sgn}(K_{II}) \{ & c_1 |\lambda_1|^3 \left(d_{11}\lambda_2^6 + d_{12}\lambda_2^4 + d_{13}\lambda_2^2 + d_{14}\right) \\ & + c_2 \left(d_{21}\lambda_2^6 + d_{22}\lambda_2^4 + d_{23}\lambda_2^2 + d_{24}\right) \\ & * \sin^2\left(c_3 |\lambda_1| \left(d_{31}\lambda_2^6 + d_{32}\lambda_2^4 + d_{33}\lambda_2^2 + d_{34}\right)\right) \\ & + c_4 \left(d_{41}\lambda_2^6 + d_{42}\lambda_2^4 + d_{43}\lambda_2^2 + d_{44}\right) \\ & * \tanh\left(c_5 |\lambda_1| \left(d_{51}\lambda_2^6 + d_{52}\lambda_2^4 + d_{53}\lambda_2^2 + d_{54}\right)\right) \}, \end{aligned} \tag{3.16}$$

with

$$(c_i) = \begin{pmatrix} 0.70966 \\ -0.0977254 \\ 3.91741 \\ -13.1588 \\ 0.15199 \end{pmatrix}, \quad (d_{ij}) = \begin{pmatrix} -6.33529 & +1.37583 & +3.29878 & +1 \\ -13.9737 & +16.0763 & -5.22639 & +1 \\ +2.54474 & -2.20079 & +1.78968 & +1 \\ -5.26771 & +8.21557 & -4.66357 & +1 \\ +60.6997 & +8.90186 & +5.60449 & +1 \end{pmatrix}, \tag{3.17}$$

where $i = 1,5$ and $j = 1,4$. This fits ϕ_{max} in figure 3.4 with a maximum relative error of 1%.

3.2 Simulation of mixed-mode crack growth

To simulate the propagation of mixed-mode internal cracks, the framework of the linear elastic fracture mechanics (LEFM) has been chosen. If no macroscopic plasticity occurs, there is no large plastic zone at the crack tip, i.e. the small scale yielding approach (RICE 1974) is suitable, and the crack problem can be treated within the framework of LEFM. The linear elastic crack tip displacement and stress fields are known to be governed by the stress intensity factors. However, it should be mentioned that for the general three-dimensional case of an arbitrary shaped crack with an arbitrary curved front, besides the three stress intensity factors, there are three constant non-singular stress terms commonly referred to as the T-stresses (see chapter 2), which play an important role in different areas of fracture mechanics such as the stability of the crack path, the two-parameter characterization of elastic-plastic crack tip deformation, and the crack tip plasticity. The number of T-stresses, however, reduces to one for a two-dimensional opened crack.

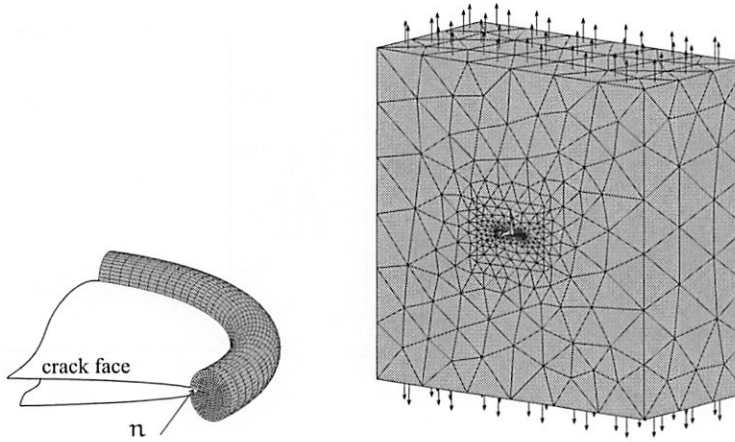

Figure 3.6: left: element design along the crack front, right:half-model of an internal crack

3.2.1 modeling mixed-mode internal cracks

To study the propagation of mixed-mode cracks and the evolution of the stress intensity factors and the T-stresses, the so called crack tip parameters, a unit cell containing a growing single internal elliptical or circular crack is considered, which is under uniform uniaxial remote tensile loading. Cracks are modeled as geometrical cuts in the center of the unit cell, and are initially perpendicular to the direction of the uniaxial tension, simulating a mode-I internal crack, figure 3.5. To have a general mode-mixity, cracks are rotated about the local x, y and z axes by γ_x, γ_y and γ_z, respectively. Hexahedral elements with quadratic displacement behavior are used to mesh the crack front region embedded in a torus of the radius $R_{torus} = a/20$ (figure 3.6-left), where higher accuracy is needed and the elements are refined towards the crack tip. a represents the semi-major axis of the elliptical crack and the radius of the circular crack, respectively. Generating n elements in the radial direction, the size of the elements would be $R_{torus}/n = a/(20\,n)$. The rest of the unit cell is meshed using quadratic tetrahedral elements, becoming coarser towards the outer boundaries of the unit cell. The number of elements in the unit cell is dependent on the number of elements in the torus (n), and choosing a higher n results an overall finer mesh. Figure 3.6-right shows half-model of an internal circular crack under pure mode-I loading.

To check the accuracy of the results, one possible way is comparing the evaluated stress intensity factors and T-stresses from the model to the analytical ones. This requires that the size of the cell with respect to the characteristic crack size is such that the crack tip fields are not affected by the outer boundaries. This, indeed, simulates the so called non-interacting crack which is later required to study the damage of a unit cell. To find the appropriate dimension of the unit cell with respect to the crack size fulfilling the

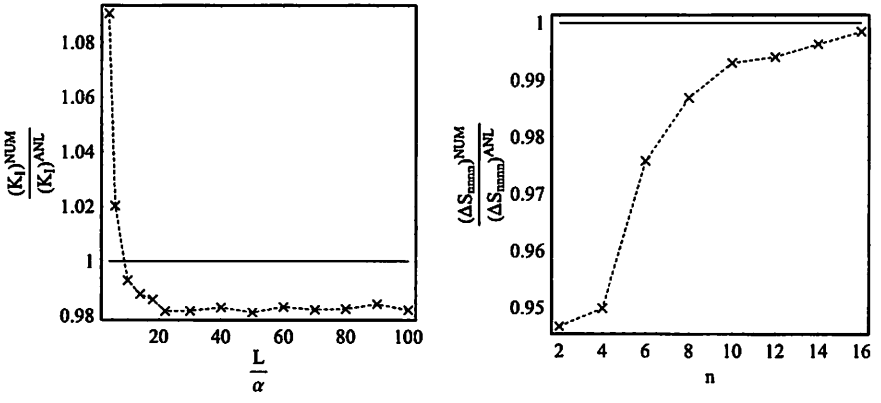

Figure 3.7: size effect (left), and mesh refinement effect (right)

mentioned requirement, a mode-I circular crack problem has been simulated for which the size of the unite cell embedding the crack is varying between 5α and 100α, and the resulting stress intensity factor (K_I) is compared to the analytical one. The number of elements n is chosen as 12. It is observed that if the relative size of the unit cell is not big enough, the resulting stress intensity factor from the model is bigger than what the analytical solution gives (figure 3.7-left), showing the fact that the crack tip stress field is affected by the outer boundaries. As the dimension of the unit cell increases ($L > 20\alpha$, figure 3.5) the stress intensity factor converges to the analytical one with an accuracy of 2%, pointing out the fact that the boundary effect on the crack tip fields vanishes. In our models, the characteristic size of the unit cell is chosen as 150 times the characteristic crack length α to ensure that there is no boundary effect on the crack tip fields, even for a heavily grown crack. Here, the cross-symbols and the continuous lines represent respectively the results from the simulation and the analytical solution.

Another possible way to validate the model is to compare the resulting change of compliance from the model (due to the initiation of the crack) to the analytical solution. Figure 3.7-right shows that the numerical results improve and converge relatively fast by increasing the number of elements.

3.2.2 numerical determination of the crack tip parameters

There are different methods to evaluate the stress intensity factors numerically, but a literature review shows that most of the methods suggested for the evaluation of the T-stresses deal with the calculation of T_I, and there is so far no efficient method for calculating all T-stress terms for mixed-mode crack problems.

The variational method suggested by LEEVERS & RADON (1982) is based on the min-

imization of the potential energy of the structure to determine the coefficients of the first 20 terms in the two-dimensional mode-I stress expansion for a given crack problem. The crack tip parameters K_I and T_I are indeed the first and second coefficients of the calculated set. A similar method was used by EWING, SWEDLOW & WILLIAMS (1976) for mixed-mode plane problems. For mode-I plane problems, the method suggested by KNSEL (1995) calculates the T_I by calculating the first few coefficients of the stress expansion using crack tip hybrid elements.

CARDEW, GOLDTHORPE, HOWARD & KFOURI (1984) and KFOURI (1986) developed a method for calculating the T-stress for two-dimensional crack problems making use of the properties of the path independent J-integral. In this method, the J-integral is determined for two elastic finite element analyses. The first one is for the actual geometry and loading configurations and the other for a semi infinite crack in an infinite plate subjected to a point force at the crack tip in the direction of the crack line. They proposed a formula to relate T_I to these two values of the J-integral to calculate the T-stress. This method has good accuracy, because the J-integral can be evaluated far from the crack tip. HALLBACK & JONSSON (1996) used a similar method for mixed mode crack problems to calculate the T_I. Path independent integrals were also employed by OLSEN (1994) and SLADEK, SLADEK & FEDELINSKI (1997) to compute K_I, K_{II} and T_I for mixed mode problems using the boundary element technique. These methods all require multiple finite element or boundary element analyses.

The weight function method considered by SHAM (1989) calculates T_I for two-dimensional crack problems using higher order weight functions by means of special integrals within a modified finite element procedure. The interaction integral method suggested by NAKAMURA & PARKS (1991) calculates T_I for three-dimensional crack problems. Using the local values of an interaction domain integral involving the stress, strain and displacement fields, the T_I component is derived along the crack front.

Most of the mentioned methods are limited to two-dimensional crack problems, and for three-dimensional problems they are only capable of calculating T_I. Therefore, here, the direct finite element method based on the stress distribution is applied in the crack front region, which results in accurate values for both T-stresses and stress intensity factors for relatively fine elements. The method is based on rearranging equation (1.10) for a fixed θ to calculate the local crack tip parameters from the stress field resulting from the finite element analysis. This method is very efficient and fast, and can be generalized to complicated three-dimensional crack problems with little programming effort. For example, for $\theta = 0°$, K_α's and T_α's are evaluated using the following equations

$$
\begin{aligned}
K_I &= \lim_{r\to 0}\left(\sqrt{2\pi r}\,\sigma_{yy}\right), \qquad T_I = \lim_{r\to 0}\left(\sigma_{nn} - \frac{K_I}{\sqrt{2\pi r}}\right), \\
K_{II} &= \lim_{r\to 0}\left(\sqrt{2\pi r}\,\sigma_{ny}\right), \qquad T_{II} = \lim_{r\to 0}\sigma_{nt}, \\
K_{III} &= \lim_{r\to 0}\left(\sqrt{2\pi r}\,\sigma_{ty}\right), \qquad T_{III} = \lim_{r\to 0}\left(\sigma_{tt} - \frac{2\nu K_I}{\sqrt{2\pi r}} - \nu T_I\right),
\end{aligned}
\tag{3.18}
$$

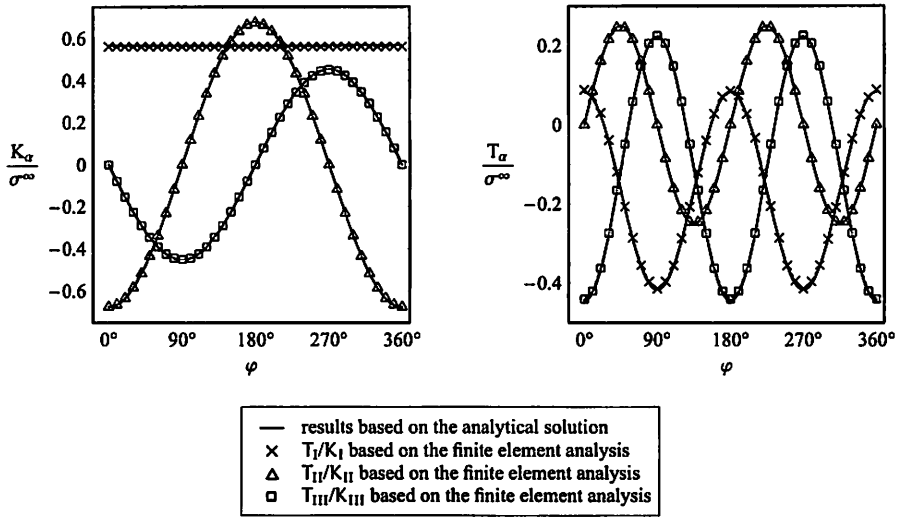

Figure 3.8: circular crack with $\gamma_z = 45°$ and $\gamma_x = \gamma_y = 0°$: distribution of the crack tip parameters along the crack front

where subscripts n, t, and y are respectively the directions of the local normal to crack front, the local tangent to the crack front, and the local normal to the crack plane (figure 3.5). K_α's and T_α's for the points along the crack front are evaluated by extrapolating the resulting nodal stresses back to the crack front in the planes perpendicular to the crack front for each point.

To validate the model, the resulting crack tip parameters from the simulation are compared to the analytical ones, for the initial crack geometry. For this, a circular crack having an inclination of 45° with respect to the loading direction ($\gamma_z = 45°$ and $\gamma_x = \gamma_y = 0°$), and an elliptical crack with an aspect ratio of $\beta/\alpha = 0.5$ which its major axis has an inclination of 60° with respect to the uniform uniaxial remote tension ($\gamma_z = 30°$ and $\gamma_x = \gamma_y = 0°$) are considered. The matrix is considered to be homogeneous, isotropic and linear elastic. The Poisson's ratio is chosen as $\nu = 1/3$, and the loading level as $\sigma^\infty/E = 1/100$, where E is the Young's modulus of the matrix material. For these crack geometries, the analytical expressions for the stress intensity factors and T-stresses are known, see for example MURAKAMI (1987) for the stress intensity factors and chapter 2 for the complete set of T-stresses of internal elliptical and circular crack.

It is observed that by choosing $n \geq 6$ (figure 3.6), the resulting stress intensity factors and T-stresses are acceptable (errors smaller than 6%), and choosing $n = 12$ improves the results considerably and the maximum error is in the range of 2%, for both the K_α's and T_α's. Considering this degree of mesh refinement, in average the maximum number of generated nodes is approximately 300,000. The distribution of the stress intensity factors

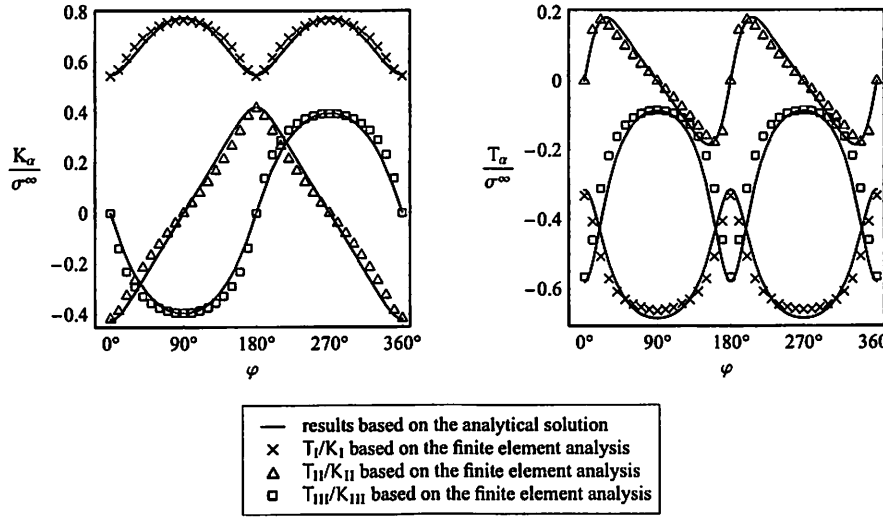

Figure 3.9: elliptical crack with $\beta/\alpha = 0.5$, $\gamma_z = 30°$ and $\gamma_x = \gamma_y = 0°$: distribution of the crack tip parameters along the crack front

and the T-stresses for the considered degree of mesh refinement ($n = 12$) are given along the crack front in figures 3.8 and 3.9, respectively for the considered circular and elliptical crack geometries. The cross-symbol represents the first component of the stress intensity factors and T-stresses (K_I, T_I), and triangle and square symbols, respectively the second and third components (K_{II}, T_{II} and K_{III},T_{III}). Results based on the analytical solution are shown with continuous lines. This notation is considered for other graphs as well.

To check the accuracy of the results for the propagated crack geometry, there is no exact analytical solution giving the stress intensity factors and the T-stresses. However, the stress intensity factors at the kinked crack tip may be approximated analytically using the expansion formula (3.4) in terms of the extension length ϵ and the crack tip parameters prior to kinking. Based on this, it is possible to validate the accuracy of the model for the propagated geometry as well. Having validated the model at each step, this error measure may be used in further propagation steps to validate the stress intensity factors. Figure 3.10 compares the resulting stress intensity factors for the first propagated geometry to the analytical approximation, respectively for the circular crack (left curves) and the elliptical crack (right curves).

It should be mentioned that the concern of this study is not giving an efficient method for the determination of the stress intensity factors and the T-stresses, so basically any method resulting a good level of accuracy could be used to evaluate the required crack tip parameters. It should be mentioned that relatively fine elements should be generated to obtain accurate results, and the distance from the crack tip at which the stress results

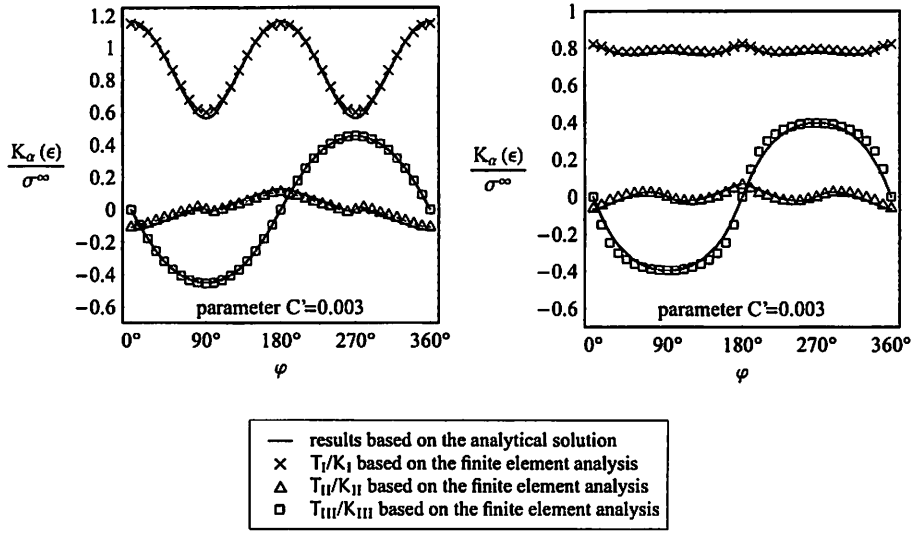

Figure 3.10: distribution of $K_\alpha(\epsilon)$ for the circular crack (left) and the elliptical crack (right)

are extrapolated is also crucial in the accuracy of the results. To obtain results within the mentioned level of accuracy, the distance r from the crack tip at which the nodal stresses are extrapolated should be bigger than $\alpha/60 = 1.67\%\,\alpha$. This is because the stress field in the first two rows of elements at the crack front does not represent equation (2.1) accurately enough.

3.2.3 quasi-static propagation of cracks

As mentioned, propagation of the crack is governed by the maximum driving force criterion given in section 3.1.1, according to which a crack grows in the direction of the local maximum driving force. To calculate the crack propagation rate in terms of the number of cycle and the associated material parameters, this criterion can be coupled with a crack evolution law (see section 1.3.5). For example, considering Paris' law, the local propagation rate is obtained

$$\frac{da}{dN} = C\,(K_{Imax} - K_{Io})^{\eta}\,, \tag{3.19}$$

where a and N are the crack length and the number of the load cycles, K_{Imax} and K_{Io} represent the stress intensity factors due to the maximum load and the threshold value, respectively, and C and η are material constants. A thermodynamic generalization of

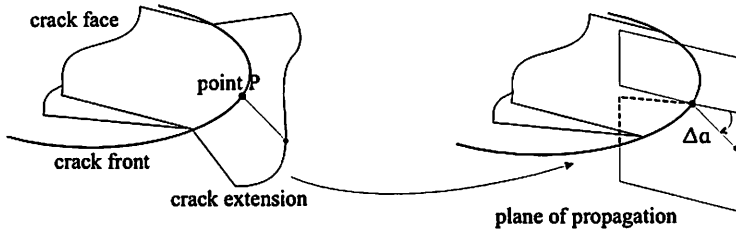

Figure 3.11: local crack propagation

Paris' law is presented by LEMAITRE & CHABOCHE (1990). The advantage of such a generalization is that the formulation would not be restricted to cyclic loading with constant loading amplitude, but it could also be applied to arbitrary loading amplitude and cycle. The fundamental of the thermodynamic formulation is the flow-rule like in plasticity and the dissipation of the growing crack. From a generalization of Paris's law following evolution law can be deduced (SCHÜTTE 2001)

$$\frac{da}{dN} = C\left(\sqrt{G^*_{max}} - \sqrt{G^*_o}\right)^{\eta}, \tag{3.20}$$

where G^*_{max} and G^*_o represent the maximum value and the threshold value for the maximum driving force, respectively. For vanishing threshold values, and $\eta = 2$, the crack growth rate is resulting as

$$\frac{da}{dN} = C\,G^*_{max} \qquad \text{or} \qquad \dot{a} = C\,G^*_{max}, \tag{3.21}$$

where $\dot{a}$ is the crack propagation rate. This is identical to the proportionality between the thermodynamic flux $\dot{a}$ and the corresponding thermodynamic force G^*. The advantages of a G based fatigue crack evolution law was explained in section 1.3.5 in detail.

3.2.4 crack growth algorithm and examples

The procedure of simulating the quasi-static propagation of cracks, using the stepwise method, can be summarized as follows. At each step of crack propagation, the stress intensity factors at a certain number of geometrical points on the crack front are evaluated numerically using the direct method based on the extrapolation of the stress field. The propagation rate and the propagation angle for each point are then determined using equations (3.13), (3.16)and (3.20). Points are then propagated in the planes perpendicular to the crack front in a local sense, figure 3.11. After propagating all points on the crack front, the new crack geometry is built and the model is re-meshed according to the new crack geometry. It is assumed here, that the crack front remains continuously differentiable, so crack front rotation, segmentation and the forming of vertexes are prohibited.

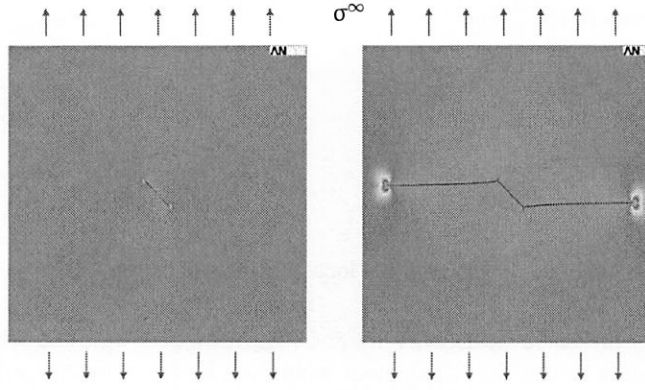

Figure 3.12: growth of the central straight crack with $\gamma_z = 45°$

Solving the new model enables us to repeat the procedure in further steps to propagate the crack.

This propagation algorithm is applied to four crack problems to show the propagation of cracks under mixed-mode loading conditions. The matrix material is considered to be homogeneous, isotropic and linear elastic. The Poisson's ratio is chosen as $\nu = 1/3$, and the loading level as $\sigma^\infty/E = 1/100$. To satisfy the non-interacting crack assumption even for a heavily grown crack, the size of the unit cell is chosen as 150α, α being the characteristic crack size.

The first example is a two dimensional central straight having an inclination of 45° with respect to the direction of the remote uniaxial tensile loading. Figure 3.12 shows the growth of the mixed-mode central crack. It is observed that crack propagates in a symmetric manner, and the final path becomes perpendicular to the direction of the remote tension.

As the second example, two inclusions are introduced along the path of the first crack problem to see the effect of soft and hard inclusions on the selected path by a propagating crack. The hard inclusion, which is closer to the tip of the initial crack, is considered to be smaller with a radius of $0.5\,\alpha$ and a Young's modulus of $1000\,E$, with E being the Young's modulus of the matrix material. The second inclusion is a soft one with a Young's modulus of $E/100,000$ and a radius of $0.75\,\alpha$. For both inclusions the Poisson's ratio is chosen as $1/3$. In figure 3.13, it is observed that crack chooses a path to avoid the hard inclusion, if possible. Passing by the region, where the stress field due to the soft inclusion is dominant, crack is attracted to the soft inclusion. Finally, in the last phase of crack growth, by entering to a region where the surrounding material is homogeneous, a stabilization in the crack path is observed.

The third and fourth examples are the considered circular and elliptical crack problems, respectively, which were already introduced in section 3.2.2, i.e circular crack with $\gamma_z =$

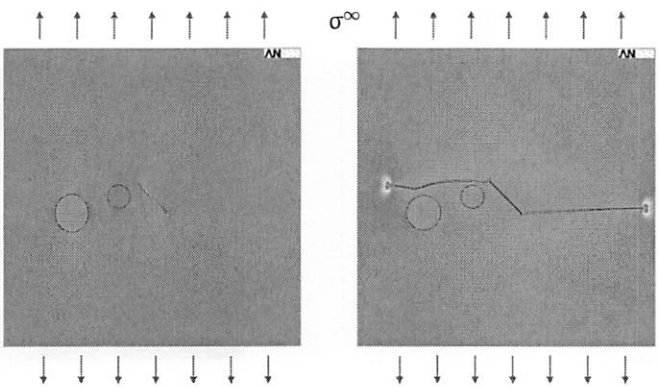

Figure 3.13: growth of the central straight crack with $\gamma_z = 45°$ in the presence of inclusions

45° and $\gamma_x = \gamma_y = 0°$, and elliptical crack with an aspect ratio of $\beta/\alpha = 0.5$, and $\gamma_z = 30°$ and $\gamma_x = \gamma_y = 0°$. Figures 3.14 and 3.15 show respectively the growth of the circular crack and the elliptical crack. The same behavior as in the two-dimensional examples are observed, showing that cracks, loaded cyclically with a load of constant amplitude and direction, grow to a mode-I crack.

The models also enable us to give the evolution of the stress intensity factors and the T-stresses of mixed-mode internal cracks. Figure 3.19 shows the evolution of the crack tip parameters for the circular crack problem. The evolution of the T-stresses shows that as the crack grows, T_{II} vanishes along the crack front. T_I and T_{III} become negative constant values along the crack front; their values are approximately the same as for a mode-I circular crack. The evolution of the stress intensity factors show that mode-II stress intensity factor vanishes along the crack front, as it is for a mode-I circular crack. However, the mode-III stress intensity factor does not vanish and comparing its value to K_I shows that its effect should be considered in the propagation of the crack. It should be noted that although K_{III} may not have an impact on the direction of crack growth, but its value influences the resulting propagation rate. Similar to the T-stresses, evolution of K_I is also in good agreement with a mode-I growing circular crack. It is observed that for a crack propagated to approximately 5 times its initial size, at each propagation step K_I is approximately constant along the crack front and by crack growth K_I grows in the same manner as in the case of a self-similar growth of a circular crack. The same behavior is observed for the elliptical crack, figures 3.20. The evolution of the stress intensity factors and the T-stresses show that the inclined elliptical crack turns also to a mode-I circular crack.

Considering different values for the step size parameter $C' = C\,\Delta N$, it is possible to investigate the state of the kinking, and see how this influences the crack path. For this, the circular crack is considered again. The paths followed by the circular crack choosing C' as 0.003, 0.005, 0.0011, and 0.025 are given in figure 3.16. To have a more

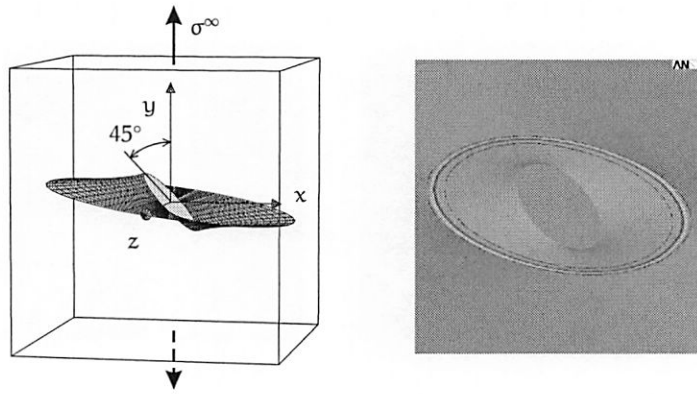

Figure 3.14: growth of the circular crack with $\gamma_z = 45°$ and $\gamma_x = \gamma_y = 0°$

clear picture of the paths, the cut of the crack geometries in the xy-plane is shown. It is observed that choosing the step size parameter $C' = C\,\Delta N$ in equation (3.21) bigger than a certain value, here $C' \geq 0.01$, results in a somehow different crack path, which in the case of non-proportional loading may lead to other crack paths than expected. In the case of proportional loading, however, this may not influence the results very heavily, since after a few propagation steps the paths followed by cracks for different values of C' approximately coincide, and the difference is in the number of steps to reach a certain crack length (figure 3.16). However, simulation of crack growth phenomena in the case of non-proportional loading, and even proportional loading in a solid with inclusions and/or holes, requires that the extension length be small enough, so that the curvature of the crack path is captured correctly. An example of such a problem is the fatigue crack growth in airplane panels with windows.

3.3 Impact of fracture criterion

As mentioned in section 3.1, there are different fracture criteria. Some of them neglect the effect of K_{III}, or they are based on two-dimensional reasonings. They are, however, widely used for three-dimensional problems.

In this section, comparison is made between different fracture criteria and how they influence the results by crack growth. To show the effect of K_{III}, the maximum driving force criterion leaving out the effect of K_{III} is considered as a separate criterion. The maximum hoop-stress and local symmetry criteria are considered as well. The Griffith maximum energy release rate criterion, which considers the effect of K_{III} is considered to show its difference with the maximum driving force. It is shown that the difference is in the first few steps, where there is still considerable kinking as the crack grows. By

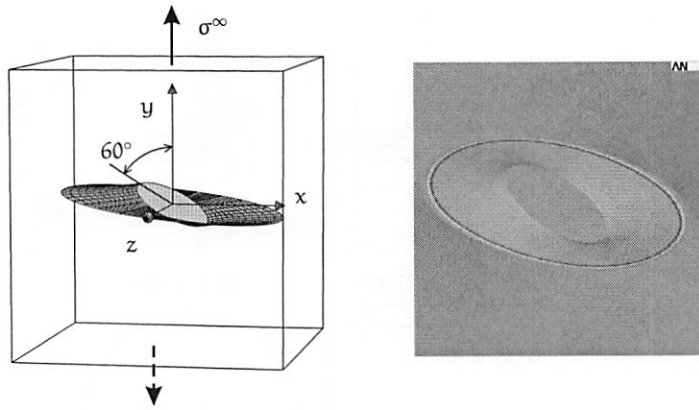

Figure 3.15: growth of the elliptical crack with $\beta/\alpha = 0.5$, $\gamma_z = 30°$ and $\gamma_x = \gamma_y = 0°$

tending the kinking angle to zero, the results due to these two criteria converge. It should be mentioned that the convergence of the paths is due to the good nature of the problem under consideration, as all criteria will tend to cracks growing in a direction perpendicular to the axis of tension in a homogeneous sample. To summarize, the following fracture criteria are considered

1. maximum driving force criterion (3D D.F.),
2. maximum driving force criterion neglecting the effect of K_{III} (2D D.F.),
3. maximum hoop-stress criterion (Hoop-S),
4. maximum energy release rate criterion considering the effect of K_{III} (JINT),
5. Local symmetry criterion (LSYM).

To compare the impact of different fracture criteria on the evolution of the compliance tensor of a unit cell due to a growing mixed-mode crack, again the circular crack problem in section 3.2.1 is considered. To show the impact of different criteria on the kinking angle and crack growth rate, a representative point on the crack front is considered for which none of the stress intensity factors vanishes. The impact of different fracture criteria on the evolution of compliance in the principle directions of the unit cell as the circular crack grows is presented, as well.

Figures 3.18 show the evolution of the compliance components in the principle directions, which are normalized with the compliance of the matrix (virgin) material. This can be considered as a measure of damage due to a growing circular crack. It is obvious that leaving out the effect of K_{III} from the maximum driving force criterion, i.e 2D D.F., Hoop-S and LSYM, the resulting damage is smaller than the one obtained from the criteria considering the effect of K_{III} (3D D.F. and JINT). Results from the criteria LSYM and 2D D.F. are in good agreement. This can be explained by considering the fact that both criteria estimate nearly the same propagation rate (figure 3.17). The evolution of

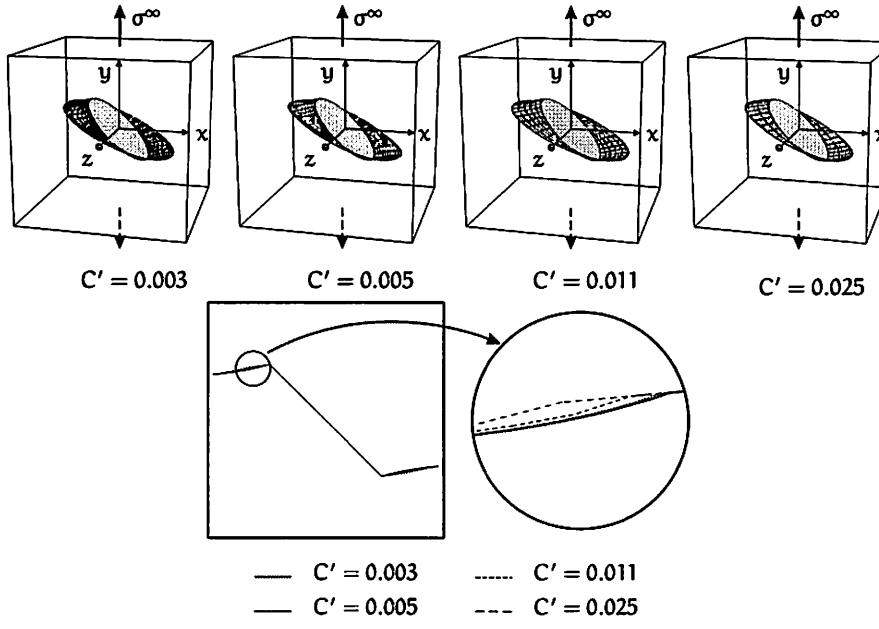

Figure 3.16: evolution of the crack geometry considering different C′s

compliance due to 3D D.F. and JINT criteria are nearly the same, but a closer look to the first few steps states that damage due to JINT is slightly smaller. This is due to the fact that in the first steps of propagation, the growth rate resulting from JINT is lower than the one of 3D D.F. (figure 3.17-right), since the stress intensity factors presented in the JINT are the ones of the crack prior to kinking, which are smaller than the ones of the kinked crack (in 3D D.F.).

The evolution of the kinking angle and the growth rate using different criteria are shown in figure 3.17-left. As expected, different criteria result in different kinking angles, but after some steps of propagation the kinking angles due to different criteria converge all to zero. The behavior for the growth ratio is somehow different. Figure 3.17-right, explains the behavior observed in figures 3.18. As stated before, the propagation rate for 3D D.F. and JINT are different for the first steps, but afterwards they converge to the same values. The same behavior is observed for the other three criteria that neglect the effect of K_{III}. This is due to the fact that the values of stress intensity factors of the propagating crack are different for these criteria (due to the difference in the kinking angle and propagation length), but after a few steps, as K_{II} tend to vanish, the results due to 2D D.F., Hoop-S and LSYM criteria converge. Figure 3.17-right shows that estimated growth rates due to the criteria which neglect the effect of K_{III} reduce at the first few steps, which is contrary to the fact that crack growth rate increases by crack growth, i.e. growth rate of a bigger crack

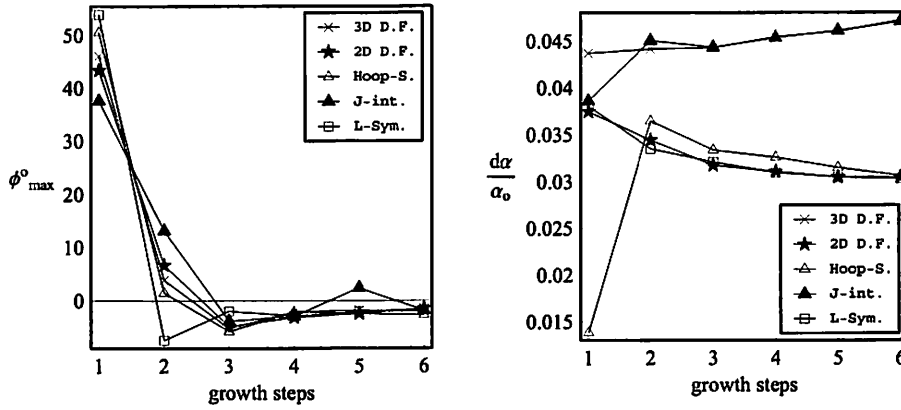

Figure 3.17: evolution of the kinking angle (left), and the growth rate (right)

is larger than a smaller one, under the same loading conditions. The estimated growth rate due to 3D D.F. and JINT are in good agreement with the mentioned point, showing the fact that for three-dimensional crack problems, the effect of K_{III} should be considered.

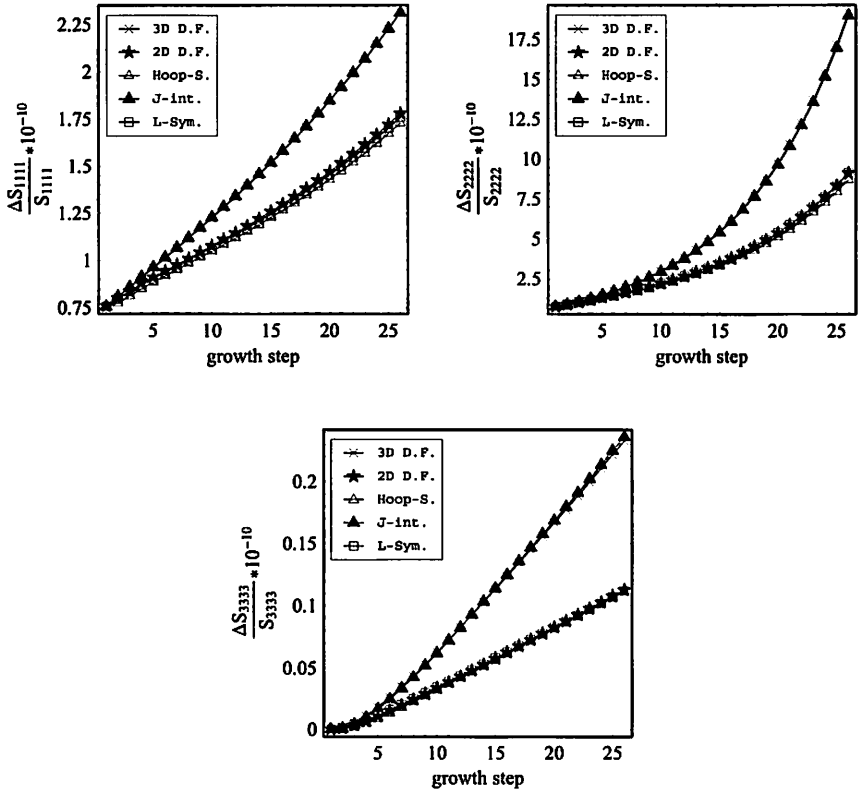

Figure 3.18: evolution of the compliance components in the principle directions for the circular crack with $\gamma_z = 45°$ and $\gamma_x = \gamma_y = 0°$

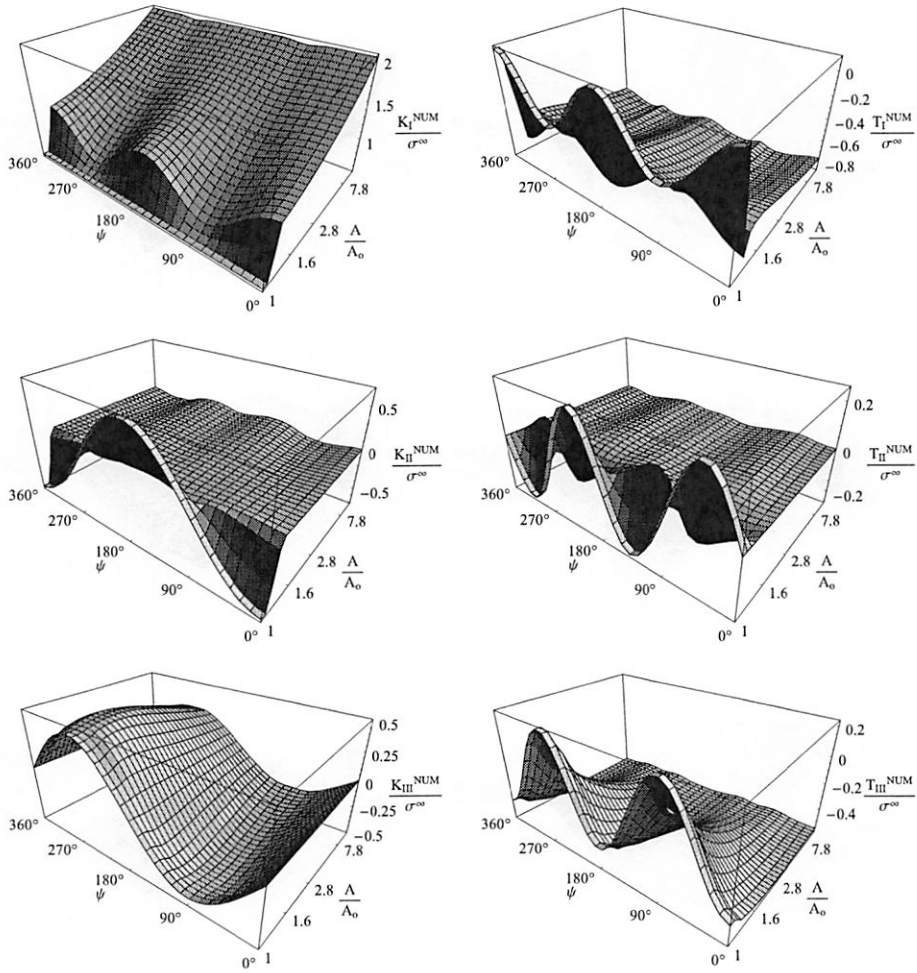

Figure 3.19: circular crack with $\gamma_z = 45°$: evolution of the K_α's and T_α's

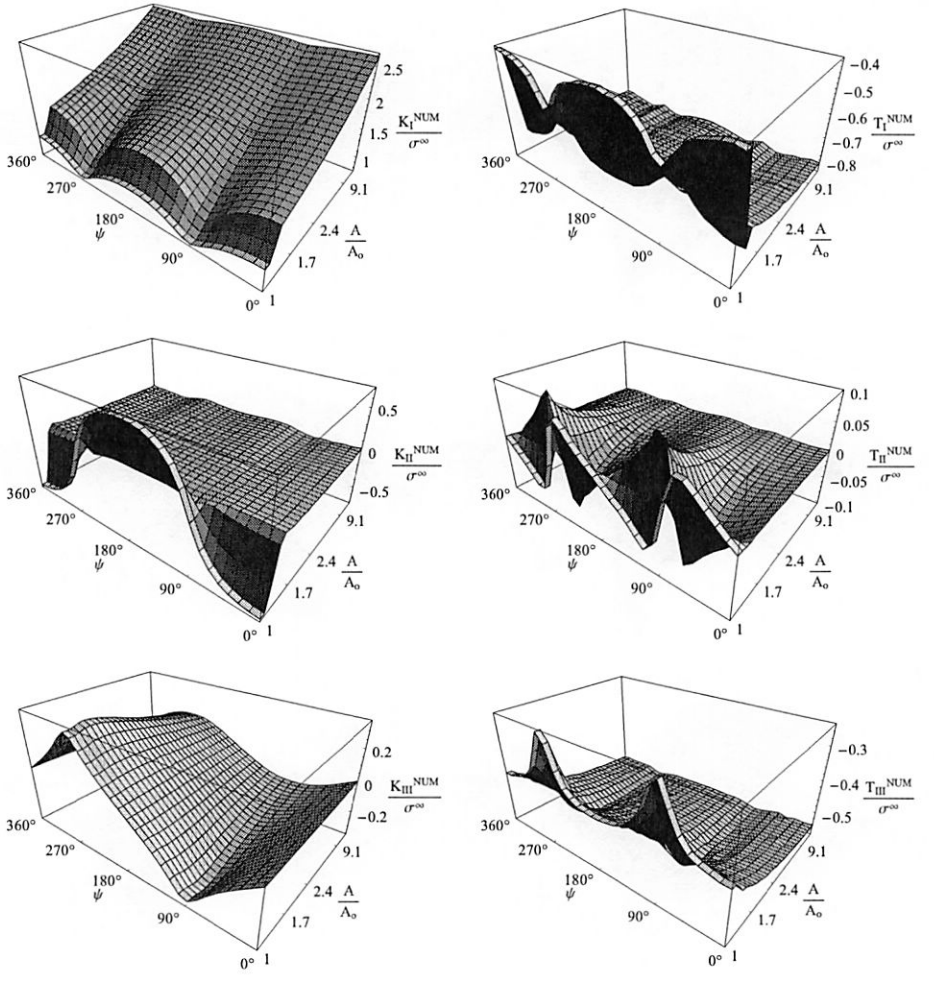

Figure 3.20: elliptical crack with $\beta/\alpha = 0.5, \gamma_z = 30°$: evolution of the K_α's and T_α's

4 Analysis of the Anisotropic Damage Evolution

Contents

This chapter is concerned with the numerical analysis of the evolution of anisotropic damage due to a single growing internal mixed-mode elliptical or circular crack in a unit cell, as presented in the previous chapter. This provides a better insight to the process of damage from the microscale to the macroscale level. For this, the concept of unit cell damaged by a growing single mixed-mode internal crack is considered.

Finite element simulation of quasi-static propagation of internal cracks under mixed-mode loading condition was addressed in chapter 3. At each step of crack propagation, the compliance tensor of the unit cell modified by the damage due to the growing crack can be calculated by applying six loadings, i.e. three simple shearings and three simple tractions. This enables us to study the effect of damage evolution due to a growing microcrack on the mechanical behavior of materials and the corresponding elastic properties in a local sense (MOLLA-ABBASI & SCHÜTTE 2007). Considering the fact that all materials under special loading conditions and most brittle materials develop anisotropic damage, the presented model results in the evolution of the type of the material symmetries. To identify the type of material symmetry, the approach proposed by COWIN & MEHRABADI (1987) is used, which is based on the characterization of the eigenvalues and eigenvectors of the elasticity tensor. The results are then verified with the help of an optimization procedure.

4.1 Anisotropic materials

Many materials are anisotropic and inhomogeneous due to the presence of varying composition of their constituents, or become anisotropic during the manufacturing process or

during the loading history, due to the accumulation of damage or initiation and growth of microcracks, microvoids and microdefects in general.

Man made composite materials are often designed to be anisotropic, because their intended use is to carry a particular type of loading that requires stiffness and strength in one direction more than in the others. Wood is a natural composite composed of cylindrical layers associated with each year's growth. The micro-structure of many natural materials such as bone tissue, wood, teeth and muscle endow the material with a particular anisotropic material symmetry for resisting the loadings to which the material is subjected. These materials evolve their particular micro-structures in response to the environmental forces.

The method of formation of geological materials generally provides them with a definite layering (natural composite) which makes them elastically anisotropic. Gravity is the force that gives geological sediments their initial layering. Plate tectonic forces then move these layers in directions other than that in which they were formed. Macroscopic man-made materials such as reinforces concreted, skis and helicopter blades are other examples of anisotropic elastic materials.

Constitutive relations in linear elasticity are given by the generalized Hooke's law which linearly relates the components of the second-rank stress and strain tensors with the help of the fourth-rank elasticity or compliance tensor. The number of independent components of the linear stiffness or compliance tensor is 21 for the most general case, where the elastic material possesses no symmetry. For materials with a certain number of planes of symmetry, the number of distinct components of this tensor will reduce further accordingly, e.g. for isotropic elastic materials, where every plane is a plane of symmetry, there are only two distinct elastic constants, the so called Lamé constants. In general, in a coordinate system other than the symmetry coordinate system of the material, with a known material symmetry, there will be 21 non-zero components for the elasticity tensor. However, for a given elasticity tensor relative to a known but arbitrary coordinate system it is possible to determine the symmetry coordinate system. Once the symmetry coordinate system has been determined the fourth-rank tensor transformation can be applied to obtain the elasticity tensor in the symmetry coordinate system.

In this section, different notations for the Hooke's law are given. The method for the identification of material symmetries for a given elasticity tensor relative to a known but arbitrary coordinate system is described next. A short summary on the determination of the eigentensors for the anisotropic elastic material symmetries is given. These provide the fundamentals required for the analysis of anisotropic damage evolution presented in the following sections.

4.1.1 different notations for the generalized Hooke's law

The generalized Hooke's law in fourth-rank tensorial notation relates the components of the second-rank stress and strain tensors by a fourth-rank tensor, the so called elasticity

type of material symmetry	Nr. of distinct elastic coefficients	Nr. of planes of symmetry
Isotropy	2	∞^2
Transverse Isotropy	5	$\infty + 1$
Cubic	3	9
Tetragonal 6	6	5
Tetragonal 7	7	5
Hexagonal 6	6	3
Hexagonal 7	7	3
Orthotropic	9	3
Monoclinic	13	1
Triclinic	21	0

Table 4.1: characterization of the material symmetries

tensor or compliance tensor depending on its definition, and it reads

$$\boldsymbol{\sigma} = \mathbb{C} : \boldsymbol{\varepsilon} \quad \text{or} \quad \boldsymbol{\varepsilon} = \mathbb{S} : \boldsymbol{\sigma} \quad \text{where} \quad \mathbb{S} = \mathbb{C}^{-1}, \tag{4.1}$$

where the superscript -1 indicates the inverse operation, and

$$\boldsymbol{\sigma} = \begin{pmatrix} \sigma_{11} & \sigma_{12} & \sigma_{13} \\ \sigma_{21} & \sigma_{22} & \sigma_{23} \\ \sigma_{31} & \sigma_{32} & \sigma_{33} \end{pmatrix}, \qquad \boldsymbol{\varepsilon} = \begin{pmatrix} \varepsilon_{11} & \varepsilon_{12} & \varepsilon_{13} \\ \varepsilon_{21} & \varepsilon_{22} & \varepsilon_{23} \\ \varepsilon_{31} & \varepsilon_{32} & \varepsilon_{33} \end{pmatrix}, \tag{4.2}$$

and

$$\mathbb{C} = \begin{pmatrix} \begin{pmatrix} C_{1111} & C_{1112} & C_{1113} \\ C_{1121} & C_{1122} & C_{1123} \\ C_{1131} & C_{1132} & C_{1133} \end{pmatrix} & \begin{pmatrix} C_{1211} & C_{1212} & C_{1213} \\ C_{1221} & C_{1222} & C_{1223} \\ C_{1231} & C_{1232} & C_{1233} \end{pmatrix} & \begin{pmatrix} C_{1311} & C_{1312} & C_{1313} \\ C_{1321} & C_{1322} & C_{1323} \\ C_{1331} & C_{1332} & C_{1333} \end{pmatrix} \\ \begin{pmatrix} C_{2111} & C_{2112} & C_{2113} \\ C_{2121} & C_{2122} & C_{2123} \\ C_{2131} & C_{2132} & C_{2133} \end{pmatrix} & \begin{pmatrix} C_{2211} & C_{2212} & C_{2213} \\ C_{2221} & C_{2222} & C_{2223} \\ C_{2231} & C_{2232} & C_{2233} \end{pmatrix} & \begin{pmatrix} C_{2311} & C_{2312} & C_{2313} \\ C_{2321} & C_{2322} & C_{2323} \\ C_{2331} & C_{2332} & C_{2333} \end{pmatrix} \\ \begin{pmatrix} C_{3111} & C_{3112} & C_{3113} \\ C_{3121} & C_{3122} & C_{3123} \\ C_{3131} & C_{3132} & C_{3133} \end{pmatrix} & \begin{pmatrix} C_{3211} & C_{3212} & C_{3213} \\ C_{3221} & C_{3222} & C_{3223} \\ C_{3231} & C_{3232} & C_{3233} \end{pmatrix} & \begin{pmatrix} C_{3311} & C_{3312} & C_{3313} \\ C_{3321} & C_{3322} & C_{3323} \\ C_{3331} & C_{3332} & C_{3333} \end{pmatrix} \end{pmatrix}. \tag{4.3}$$

The elasticity tensor has certain symmetry properties, which follows from the symmetry of the stress and strain tensors and the thermodynamic requirement that no work should be produced by the elastic material in a closed loading cycle. The number of independent components will then reduce from 81 components to 21 for the most general form, where the elastic material possesses no symmetry (Triclinic materials). For materials with a certain number of planes of symmetry , the number of distinct components of the tensor $\mathbb{C}$ will reduce further accordingly, e.g. for orthotropic elastic materials (three planes of symmetry) $\mathbb{C}$ has nine distinct components, for Cubic elastic materials (nine planes of symmetry) the number of distinct components reduces to three, and for isotropic elastic materials where every plane is a plane of symmetry, there are only two distinct elastic constants, the so called Lamé constants λ and μ.

Referring to the Voigt matrix notation, the Hooke's law is given as

$$\begin{pmatrix} \sigma_{11} \\ \sigma_{22} \\ \sigma_{33} \\ \sigma_{12} \\ \sigma_{23} \\ \sigma_{13} \end{pmatrix} = \begin{pmatrix} \mathbb{C}_{1111} & \mathbb{C}_{1122} & \mathbb{C}_{1133} & \mathbb{C}_{1112} & \mathbb{C}_{1123} & \mathbb{C}_{1113} \\ \mathbb{C}_{2211} & \mathbb{C}_{2222} & \mathbb{C}_{2233} & \mathbb{C}_{2212} & \mathbb{C}_{2223} & \mathbb{C}_{2213} \\ \mathbb{C}_{3311} & \mathbb{C}_{3322} & \mathbb{C}_{3333} & \mathbb{C}_{3312} & \mathbb{C}_{3323} & \mathbb{C}_{3313} \\ \mathbb{C}_{1211} & \mathbb{C}_{1222} & \mathbb{C}_{1233} & \mathbb{C}_{1212} & \mathbb{C}_{1223} & \mathbb{C}_{1213} \\ \mathbb{C}_{2311} & \mathbb{C}_{2322} & \mathbb{C}_{2333} & \mathbb{C}_{2312} & \mathbb{C}_{2323} & \mathbb{C}_{2313} \\ \mathbb{C}_{1311} & \mathbb{C}_{1322} & \mathbb{C}_{1333} & \mathbb{C}_{1312} & \mathbb{C}_{1323} & \mathbb{C}_{1313} \end{pmatrix} \begin{pmatrix} \varepsilon_{11} \\ \varepsilon_{22} \\ \varepsilon_{33} \\ 2\,\varepsilon_{12} \\ 2\,\varepsilon_{23} \\ 2\,\varepsilon_{13} \end{pmatrix}, \tag{4.4}$$

or

$$\tilde{\sigma} = \tilde{\mathbb{C}} : \tilde{\varepsilon} \quad \text{or} \quad \tilde{\varepsilon} = \tilde{\mathbb{S}} : \tilde{\sigma}, \quad \text{and} \quad \tilde{\mathbb{C}} = \tilde{\mathbb{S}}^{-1}, \tag{4.5}$$

where the stiffness matrix $\tilde{\mathbb{C}}$ or the compliance matrix $\tilde{\mathbb{S}}$ do not represent the components of a second-rank tensor in six-dimensions. The stress and strain are considered as vectors in six-dimensional cartesian space. This representation is obtained from (4.1) by making use of the index-notation conventions of the free and summation indices. The Voigt matrix notation is important because much of the data on the elastic properties of anisotropic elastic materials are reported and recorded in this notation.

The second-rank tensor notation in six-dimensions due, in principle, to KELVIN (1856) (see also KELVIN (1878)), which was expressed by RYCHLEWSKI (1984) and MEHRABADI & COWIN (1990) in contemporary linear algebra notation, converts the non-tensorial Voigt notation to the tensorial notation, given in equation (4.6). Using this notation, stress and strain components form vectors in six-dimensional cartesian space, as well as second-rank tensors in a three-dimensional cartesian system

$$\begin{pmatrix} \sigma_{11} \\ \sigma_{22} \\ \sigma_{33} \\ \sqrt{2}\,\sigma_{12} \\ \sqrt{2}\,\sigma_{23} \\ \sqrt{2}\,\sigma_{13} \end{pmatrix} = \begin{pmatrix} \mathbb{C}_{1111} & \mathbb{C}_{1122} & \mathbb{C}_{1133} & \sqrt{2}\,\mathbb{C}_{1112} & \sqrt{2}\,\mathbb{C}_{1123} & \sqrt{2}\,\mathbb{C}_{1113} \\ \mathbb{C}_{2211} & \mathbb{C}_{2222} & \mathbb{C}_{2233} & \sqrt{2}\,\mathbb{C}_{2212} & \sqrt{2}\,\mathbb{C}_{2223} & \sqrt{2}\,\mathbb{C}_{2213} \\ \mathbb{C}_{3311} & \mathbb{C}_{3322} & \mathbb{C}_{3333} & \sqrt{2}\,\mathbb{C}_{3312} & \sqrt{2}\,\mathbb{C}_{3323} & \sqrt{2}\,\mathbb{C}_{3313} \\ \sqrt{2}\,\mathbb{C}_{1211} & \sqrt{2}\,\mathbb{C}_{1222} & \sqrt{2}\,\mathbb{C}_{1233} & 2\,\mathbb{C}_{1212} & 2\,\mathbb{C}_{1223} & 2\,\mathbb{C}_{1213} \\ \sqrt{2}\,\mathbb{C}_{2311} & \sqrt{2}\,\mathbb{C}_{2322} & \sqrt{2}\,\mathbb{C}_{2333} & 2\,\mathbb{C}_{2312} & 2\,\mathbb{C}_{2323} & 2\,\mathbb{C}_{2313} \\ \sqrt{2}\,\mathbb{C}_{1311} & \sqrt{2}\,\mathbb{C}_{1322} & \sqrt{2}\,\mathbb{C}_{1333} & 2\,\mathbb{C}_{1312} & 2\,\mathbb{C}_{1323} & 2\,\mathbb{C}_{1313} \end{pmatrix} \begin{pmatrix} \varepsilon_{11} \\ \varepsilon_{22} \\ \varepsilon_{33} \\ \sqrt{2}\,\varepsilon_{12} \\ \sqrt{2}\,\varepsilon_{23} \\ \sqrt{2}\,\varepsilon_{13} \end{pmatrix}, \tag{4.6}$$

or

$$\hat{\sigma} = \hat{\mathbb{C}} : \hat{\varepsilon} \quad \text{or} \quad \hat{\varepsilon} = \hat{\mathbb{S}} : \hat{\sigma}, \quad \text{and} \quad \hat{\mathbb{C}} = \hat{\mathbb{S}}^{-1}, \tag{4.7}$$

The factor $\sqrt{2}$ which multiplies the shearing components of the six-dimensional stress and strain vectors in the Voigt notation assures that the scalar product of the two six-dimensional vectors is equal to the trace of the product of the corresponding second-rank tensors ($\mathrm{Tr}(\sigma : \varepsilon)$). This correction also permits the conversion of three-dimensional second-rank tensor components directly to six-dimensional vector components, and vice versa. The six-dimensional second-rank tensor of elasticity is constructed from the one of the Voigt notation multiplying $\sqrt{2}$ and 2 factors to the components of the upper-right, lower-left and lower right matrices, respectively. In (MEHRABADI & COWIN 1990), it has been proved that the symmetric matrices $\hat{\mathbb{C}}$ and $\hat{\mathbb{S}}$ are representing the components of second-rank tensors in six-dimensional space.

4.1.2 identification of material symmetries

As mentioned, the elasticity tensor of a linear anisotropic elastic material with known type of material symmetry, in general, has 21 non-zero components in a coordinate system other than the symmetry coordinate system. For a given elasticity tensor relative to an arbitrary coordinate system with known type of material symmetry, it is possible to determine the number and orientation of the planes of symmetry (COWIN & MEHRABADI 1987). A plane of symmetry at a point in an elastic material is a plane with respect to which the material has reflective symmetry. The number of planes of symmetry associated with the number of distinct elastic symmetries propose which type of symmetry the material possesses. If every vector in a plane is a normal to a plane of symmetry, the plane is said to be a plane of isotropy, which itself is a plane of symmetry.

According to COWIN & MEHRABADI (1987), there are ten traditional and distinct elastic symmetries identified so far. Given the form of the elasticity tensor for a material relative to an arbitrary coordinate system, it is possible to determine to which of the elastic symmetries it belongs. Here, the method proposed by COWIN & MEHRABADI (1987) is used to determine the type of the material symmetry.

A material is said to have a plane of symmetry at a point, if the structure of the material shows reflective (mirror) symmetry with respect to a plane passing through this point. The necessary and sufficient conditions for a vector a_i to be the normal to a plane of symmetry of a material of given elasticities $\mathbb{C}_{ijmn}$ are

$$\begin{aligned}
&\mathbb{C}_{irst}\, a_r\, a_s\, a_t = (\mathbb{C}_{rstu}\, a_r\, a_s\, a_t\, a_u)\, a_i\,, \\
&\mathbb{C}_{immj}\, a_j = (\mathbb{C}_{tmmu}\, a_t\, a_u)\, a_i\,, \\
&\mathbb{C}_{immj}\, a_j = (\mathbb{C}_{tumm}\, a_t\, a_u)\, a_i\,, \\
&\mathbb{C}_{ijmn}\, b_j\, b_m\, a_n = (\mathbb{C}_{rstu}\, b_s\, b_t\, a_r\, a_u)\, a_i
\end{aligned} \tag{4.8}$$

where the vector b_i is any vector perpendicular to a_i, and the indices range over 1, 2, 3.

Conditions $(4.8)_2$ and $(4.8)_3$ show that a_i must be an eigenvector of the symmetric second rank tensors $\mathbb{C}_{imnj}$ and $\mathbb{C}_{ijmn}$, respectively. These two conditions allow one to calculate a set of possible vectors a_i. If one of the vectors of the set of a_i also is an eigenvector of $\mathbb{C}_{irst}\, a_r\, a_s\, a_t$ and $\mathbb{C}_{ijmn}\, b_j\, b_m$, i.e. satisfies the conditions $(4.8)_1$ and $(4.8)_4$, respectively, then it represents a normal to a plane of symmetry of a material for which its elasticity tensor $\mathbb{C}_{ijmn}$ is given.

Using this theorem, one can characterize the traditional and distinct elastic symmetries by their planes of symmetry. The ten traditional and distinct elastic symmetries with the number of non-zero components of the elasticity tensor are triclinic(21), monoclinic(13), orthotropic(9), hexagonal(7), hexagonal(6), tetragonal(7), tetragonal(6), hexagonal(5), cubic(3), and isotropic(2).

Traditional anisotropic elastic material symmetries are characterized by the planes of symmetry. Triclinic materials have no planes of symmetry. Monoclinic symmetry is characterized by one plane of symmetry. In the case of three mutually orthogonal planes of symmetry the material has orthotropic or rhombic symmetry. Hexagonal(7) symmetry is characterized by three planes of symmetry whose normals all lie in one plane and make angles that are multiples of 60° with each other. Hexagonal(6) symmetry is also characterized by three planes of symmetry whose normals all lie in one plane and make angles that are multiples of 60° with each other, but differs from hexagonal(7) in that, for Hexagonal(6) symmetry one of the normals to a plane of symmetry is a coordinate axis of the symmetry coordinate system. Tetragonal(7) symmetry is characterized by five planes of symmetry, four of which have normals that lie in one plane and make angles which are multiples of 45° with each other. The fifth plane is the plane in which the other four normals lie. Tetragonal(6) symmetry is also characterized by five planes of symmetry of the type described for tetragonal(7) symmetry, but the difference is that for tetragonal(6) three of the normals to the planes of symmetry are coordinate axes of the symmetry coordinate system, while for tetragonal(7) only one normal to a plane of symmetry is a coordinate axis. Materials with cubic symmetry have nine planes of symmetry, which all intersect at either 90° or 45°. For Isotropic materials, any plane passing through a point is both a plane of symmetry and a plane of isotropy.

Table 4.2 indicates the type of material symmetry for given number of planes of symmetry and the distinctness of the eigenvalues of the second-rank tensors $\mathbb{C}_{imnj}$ and $\mathbb{C}_{ijmn}$, where S is the set of all a_i's which satisfy the conditions (4.8), and e_{III} denotes the eigenvector corresponding to the distinct eigenvalue.

4.1.3 eigentensors of linear elastic anisotropic materials

The eigenvectors of the three-dimensional fourth-rank anisotropic elasticity tensor, considered as a second-rank tensor in six-dimensional space, are called eigentensors when projected back into the three-dimensional space. The maximum number of eigentensors

type of material symmetry (distinct elastic coef.)	Nr. of planes of symmetry	Eigenvalues of $\mathbb{C}_{imnj}$ & $\mathbb{C}_{ijmn}$	remarks on eigenvectors
Isotropic(2)	∞^2	three equal	any vector is an eigenvector
Transverse Isotropy(5)	$\infty + 1$	two equal	e_{III} is in S
Cubic(3)	9	three equal	any vector is an eigenvector
Tetragonal(6)	5	two equal	e_{III} is in S
Tetragonal(7)	5	two equal	e_{III} is in S
Hexagonal(6)	3	two equal	e_{III} is not in S
Hexagonal(7)	3	two equal	e_{III} is not in S
Orthotropic(9)	3	three distinct	three coincide
Monoclinic(13)	1	three distinct	one coincides
Triclinic(21)	0	three distinct	non coincides

Table 4.2: characterization of the material symmetries

for any elastic symmetry is therefore six. The concept of eigentensor was introduced by KELVIN (1856), who determined the eigentensors for many elastic symmetries. The eigentensors are useful in the design of composite materials. The invariants of eigentensors are useful in formulating the phenomenological theories of fracture for brittle anisotropic materials.

The eigentensors of particular elastic symmetries are significant because they identify preferred modes of deformation associated with particular anisotropic elastic symmetries. The eigentensors of a linear isotropic elastic material are familiar. They are the deviatoric second-rank tensor and a tensor proportional to the unit tensor, the so called hydrostatic (or dilatational or spherical) part of the tensor.

The problem of finding the eigentensors and eigen-elastic constants for a given elastic symmetry is addressed by seeking those strain states ε for which ε and σ are parallel in the six-dimensional cartesian space. Especially, we seek the values of the number Λ and the strain states ε that satisfy the equation

$$\sigma = \Lambda\,\varepsilon, \quad \text{or} \qquad (\mathbb{C} - \Lambda\mathbb{I}) \cdot \varepsilon = 0. \tag{4.9}$$

Since $\mathbb{C}$ is a positive definite symmetric second-rank tensor in six-dimensions, there will be a maximum of six positive values of Λ (Λ_N, $N = 1, \ldots, 6$) satisfying equation (4.9) and a maximum of six associated values of ε, denoted by the vector $\hat{\varepsilon}^N$ in six-dimensional space, and by the second-rank tensor $\varepsilon^{(N)}$ in three-dimensions. The values of Λ_N are called the eigen-elastic constants and, if possible, are ordered by the inequality

$\Lambda_1 \geq \cdots \geq \Lambda_6 \geq 0$, and the values of $\varepsilon^{(N)}$ are called the strain eigentensors of linear elastic material characterized by $\mathbb{C}$. The eigenvalues of the compliance tensor $\mathbb{S}$ are the inverse of the eigenvalues of $\mathbb{C}$.

Symmetry	eigenvalues	multiplicity	mode
Isotropy	$c_{11} + 2c_{12}$	1	D
	$2c_{44}$	5	I
Cubic	$c_{11} + 2c_{12}$	1	D
	$c_{11} - c_{12}$	2	I
	$2c_{44}$	3	I
Transversely	$c_{33} + \sqrt{2}c_{13}(\tan\alpha + \sec\alpha)$	1	D
isotropy	$c_{33} - \sqrt{2}c_{13}(\tan\alpha + \sec\alpha)$	1	D
	$c_{11} - c_{12}$	2	I
	$2c_{44}$	2	I
Hexagonal(7) &	$c_{33} + \sqrt{2}c_{13}(\tan\alpha + \sec\alpha)$	1	D
Hexagonal(6)	$c_{33} - \sqrt{2}c_{13}(\tan\alpha + \sec\alpha)$	1	D
	$0.5(c_{11}-c_{12})(1+\sec\beta)+c_{44}(1-\sec\beta)$	2	I
	$0.5(c_{11}-c_{12})(1-\sec\beta)+c_{44}(1+\sec\beta)$	2	I
Tetragonal(7)	$c_{33} + \sqrt{2}c_{13}(\tan\alpha + \sec\alpha)$	1	D
	$c_{33} - \sqrt{2}c_{13}(\tan\alpha + \sec\alpha)$	1	D
	$0.5(c_{11}-c_{12})(1+\sec\gamma)+c_{66}(1-\sec\gamma)$	1	I
	$0.5(c_{11}-c_{12})(1-\sec\gamma)+c_{66}(1+\sec\gamma)$	1	I
	$2c_{44}$	2	I
Tetragonal(6)	$c_{33} + \sqrt{2}c_{13}(\tan\alpha + \sec\alpha)$	1	D
	$c_{33} - \sqrt{2}c_{13}(\tan\alpha + \sec\alpha)$	1	D
	$c_{11} - c_{12}$	1	I
	$2c_{66}$	1	I
	$2c_{44}$	2	I

Table 4.3: properties of the eigenvalues for different elastic symmetries

The stress eigentensors $\sigma^{(N)}$ are obtained by multiplying $\varepsilon^{(N)}$ by the eigenvalues Λ_N. KELVIN (1856) called the the constants Λ_N the six principle elasticities of the material, and he called the stress and strain eigentensors the principle types of stress and strain. The eigentensors associated with distinct values of Λ_N are orthogonal. For example for the strain eigentensors

$$\hat{\varepsilon}^{(N)} \cdot \hat{\varepsilon}^{(M)} = 0\,, \quad \text{or} \quad \operatorname{tr}\left(\varepsilon^{(N)} \cdot \varepsilon^{(M)}\right) = 0\,, \quad \text{for } N \neq M\,, \tag{4.10}$$

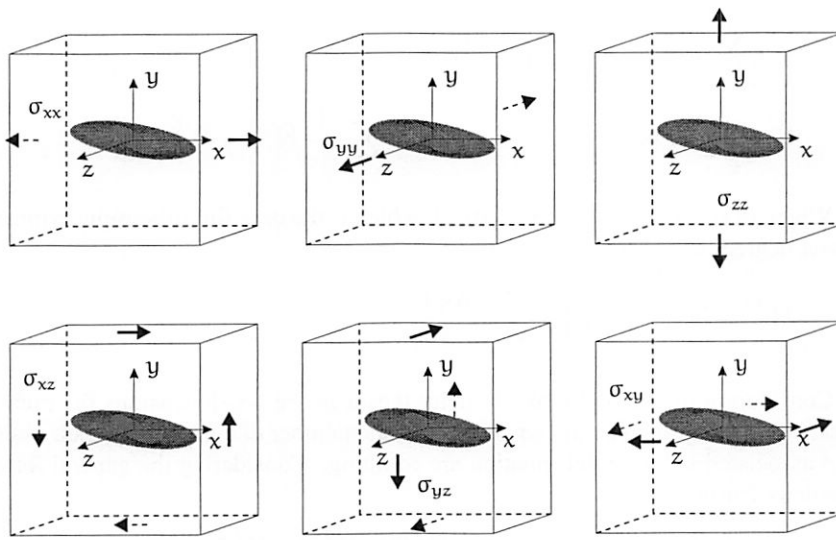

Figure 4.1: six deformation modes to calculate the compliance tensor

and similar relations hold for stress eigentensors. The strain eigenvector $\hat{\varepsilon}^{(N)}$ is not required to be a unit vector in the six-dimensions. A Cartesian basis can be constructed from the normalized eigentensors. The normalization of $\hat{\varepsilon}$ is denoted by $\hat{\mathbf{N}}$,

$$\hat{\varepsilon} = \hat{\mathbf{N}}\, |\hat{\varepsilon}| \,, \quad \text{where} \quad |\hat{\varepsilon}|^2 = \hat{\varepsilon} \cdot \hat{\varepsilon} \,. \tag{4.11}$$

The stress eigenvector can be written in terms of the normalized strain eigenvector

$$\hat{\sigma} = \Lambda\, |\hat{\varepsilon}|\, \hat{\mathbf{N}} \,. \tag{4.12}$$

The set of six $\hat{\mathbf{N}}$ form a Cartesian basis in six-dimensional space, where

$$\sum_{K=1}^{6} \hat{\mathbf{N}}^{(K)} \otimes \hat{\mathbf{N}}^{(K)} = \hat{\mathbb{I}} \,. \tag{4.13}$$

With respect to such a space, $\hat{\sigma}$, $\hat{\varepsilon}$ and $\hat{\mathbb{C}}$ or $\hat{\mathbb{S}}$ have the representation

$$\hat{\sigma} = \sum_{K=1}^{6} \Lambda_K\, \hat{\varepsilon}^{(K)} = \sum_{K=1}^{6} \Lambda_K \left|\hat{\varepsilon}^{(K)}\right| \hat{\mathbf{N}}^{(K)} \,,$$

$$\hat{\varepsilon} = \sum_{K=1}^{6} \hat{\varepsilon}^{(K)} = \sum_{K=1}^{6} \left|\hat{\varepsilon}^{(K)}\right| \hat{\mathbb{N}}^{(K)}, \tag{4.14}$$

$$\hat{\mathbb{C}} = \sum_{K=1}^{6} \Lambda_K \hat{\mathbb{N}}^{(K)} \otimes \hat{\mathbb{N}}^{(K)}, \quad \text{or} \quad \hat{\mathbb{S}} = \sum_{K=1}^{6} \frac{1}{\Lambda_K} \hat{\mathbb{N}}^{(K)} \otimes \hat{\mathbb{N}}^{(K)}.$$

When all six values of Λ_K are distinct, which is the case for orthotropic symmetry and lesser degrees of symmetry

$$\hat{\mathbb{N}}^{(K)} \otimes \hat{\mathbb{N}}^{(K)} = \prod_{N=1(N\neq K)}^{6} \frac{\hat{\mathbb{C}} - \Lambda_N \hat{\mathbb{I}}}{\Lambda_K - \Lambda_N}. \tag{4.15}$$

Considering the second-rank elasticity tensor in the six-dimensions for each type of elastic symmetry and solving equation (4.9) the number of eigenvalues, their multiplicity and associated mode of deformation are resulting. Considering the general form of the elasticity tensor

$$\hat{\mathbb{C}} = \begin{pmatrix} c_{11} & c_{12} & c_{13} & \sqrt{2}c_{14} & \sqrt{2}c_{15} & \sqrt{2}c_{16} \\ c_{21} & c_{22} & c_{23} & \sqrt{2}c_{24} & \sqrt{2}c_{25} & \sqrt{2}c_{26} \\ c_{31} & c_{32} & c_{33} & \sqrt{2}c_{34} & \sqrt{2}c_{35} & \sqrt{2}c_{36} \\ \sqrt{2}c_{41} & \sqrt{2}c_{42} & \sqrt{2}c_{43} & 2c_{44} & 2c_{45} & 2c_{46} \\ \sqrt{2}c_{51} & \sqrt{2}c_{52} & \sqrt{2}c_{53} & 2c_{54} & 2c_{55} & 2c_{56} \\ \sqrt{2}c_{61} & \sqrt{2}c_{62} & \sqrt{2}c_{63} & 2c_{64} & 2c_{65} & 2c_{66} \end{pmatrix}, \tag{4.16}$$

the eigenvalues for different elastic symmetries (MEHRABADI & COWIN 1990) are listed in table 4.3, where D and I represent the dilatational and isochoric modes of deformation, respectively, and the angle α is defined by

$$\alpha = \frac{\sqrt{2}}{4c_{13}}(c_{11} + c_{12} - c_{33}). \tag{4.17}$$

For Hexagonal(7) and Hexagonal(6) the angle β are respectively defined by

$$\beta^{H7} = \arctan \frac{4\sqrt{c_{14}^2 + c_{15}^2}}{c_{11} - c_{12} - 2c_{44}}, \tag{4.18}$$

$$\beta^{H6} = \arctan \frac{4c_{14}}{c_{11} - c_{12} - 2c_{44}},$$

and for Tetragonal(7) symmetry γ is obtained from

$$\gamma = \arctan \frac{4c_{16}}{c_{11} - c_{12} - 2c_{66}}. \tag{4.19}$$

The associated eigentensors for individual elastic symmetries are obtained by solving the eigenvalue problem (4.9) for each tensor $\mathbb{C}$ associated with a distinct linear elastic anisotropy.

4.2 Evolution of the material symmetries

In this section, the evolution of the compliance tensors modified by the damage due to a growing internal mixed-mode crack is given first, which is based on the simulation results presented in chapter 3. For this, the circular and elliptical crack problems given in chapter 3 are considered further, i.e circular crack with $\gamma_z = 45°$ and $\gamma_x = \gamma_y = 0°$, and elliptical crack with an aspect ratio of $\beta/\alpha = 0.5$, and $\gamma_z = 30°$ and $\gamma_x = \gamma_y = 0°$. Evolution of the type of material symmetries for the calculated compliance tensors is then given with the help of the method based on the characteristics of the eigenvalues and eigenvectors presented in section 4.1.2 (COWIN & MEHRABADI 1987).

For a given elasticity tensor with a known type of symmetry, it is possible to calculate the location of the normals to the planes of symmetry with the help of an optimization procedure. The idea of this method is to find the coordinate transformation that yields the best symmetry representation of the given tensor. As mentioned, this method requires the type of material symmetry as a priori known, hence cannot be generalized to problems without information on the type of elastic symmetry. The evolution of the axes of symmetry for the presented examples are also calculated with the help of this method, and the results are compared to the ones based on the COWIN & MEHRABADI (1987) method.

4.2.1 evaluation of the compliance tensor

The components of the compliance tensor of the unit cell at each propagation step can be computed by applying six basic modes of deformation to the unit cell (three uniaxial tensile loadings and three simple shear loadings). Application of each tensile loading results in 9 components of the compliance tensor, and each shear loading results in 18 components.

For example, applying $\sigma_{11} = \sigma_{xx}$ results the following components

$$\mathbb{S}_{1111} = \frac{\varepsilon_{11}}{\sigma_{11}}, \qquad \mathbb{S}_{1211} = \mathbb{S}_{2111} = \frac{\varepsilon_{12} + \varepsilon_{21}}{2\,\sigma_{11}},$$

$$\begin{aligned} \mathbb{S}_{2211} &= \frac{\varepsilon_{22}}{\sigma_{11}}, \qquad \mathbb{S}_{2311} = \mathbb{S}_{3211} = \frac{\varepsilon_{23} + \varepsilon_{32}}{2\,\sigma_{11}}, \\ \mathbb{S}_{3311} &= \frac{\varepsilon_{33}}{\sigma_{11}}, \qquad \mathbb{S}_{1311} = \mathbb{S}_{3111} = \frac{\varepsilon_{13} + \varepsilon_{31}}{2\,\sigma_{11}}, \end{aligned} \tag{4.20}$$

and applying $\sigma_{12} = \sigma_{xy}$ results

$$\begin{aligned}
\mathbb{S}_{1112} = \mathbb{S}_{1121} &= \frac{\varepsilon_{11}}{2\,\sigma_{12}}, & \mathbb{S}_{1212} = \mathbb{S}_{1221} = \mathbb{S}_{2112} = \mathbb{S}_{2121} &= \frac{\varepsilon_{12} + \varepsilon_{21}}{4\,\sigma_{12}}, \\
\mathbb{S}_{2212} = \mathbb{S}_{2221} &= \frac{\varepsilon_{22}}{2\,\sigma_{12}}, & \mathbb{S}_{2312} = \mathbb{S}_{2321} = \mathbb{S}_{3212} = \mathbb{S}_{3221} &= \frac{\varepsilon_{23} + \varepsilon_{32}}{4\,\sigma_{12}}, \\
\mathbb{S}_{3312} = \mathbb{S}_{3321} &= \frac{\varepsilon_{33}}{2\,\sigma_{12}}, & \mathbb{S}_{1312} = \mathbb{S}_{1321} = \mathbb{S}_{3112} = \mathbb{S}_{3121} &= \frac{\varepsilon_{13} + \varepsilon_{31}}{4\,\sigma_{12}}.
\end{aligned} \tag{4.21}$$

4.2.2 numerical results

This section presents the evolution of the compliance tensor and the evolution of the type of material symmetry for the considered crack problems. The components of the compliance tensor are given in six-dimensional second-rank tensorial notation with respect to the principle loading coordinate system of the unit cell, coincident with the global coordinate system, figure 4.1. The Poisson's ratio is chosen as $\nu = 1/3$ and the loading level as $\sigma^{\infty}/E = 1/100$, where E is the Young's modulus of the homogenous linear elastic isotropic matrix material.

The six-dimensional second-rank compliance tensor of the homogeneous isotropic matrix material in its pristine state is

$$\begin{aligned}
\mathbb{S}^{\text{Matrix}} &\triangleq \frac{1}{E}\begin{pmatrix} 1 & -\nu & -\nu & 0 & 0 & 0 \\ -\nu & 1 & -\nu & 0 & 0 & 0 \\ -\nu & -\nu & 1 & 0 & 0 & 0 \\ 0 & 0 & 0 & 1+\nu & 0 & 0 \\ 0 & 0 & 0 & 0 & 1+\nu & 0 \\ 0 & 0 & 0 & 0 & 0 & 1+\nu \end{pmatrix} \\
&= \frac{1}{E}\begin{pmatrix} 1 & -1/3 & -1/3 & 0 & 0 & 0 \\ -1/3 & 1 & -1/3 & 0 & 0 & 0 \\ -1/3 & -1/3 & 1 & 0 & 0 & 0 \\ 0 & 0 & 0 & 4/3 & 0 & 0 \\ 0 & 0 & 0 & 0 & 4/3 & 0 \\ 0 & 0 & 0 & 0 & 0 & 4/3 \end{pmatrix}.
\end{aligned} \tag{4.22}$$

As the crack grows, the compliance tensor modified by damage is calculated with the help of the procedure given in section 4.2.1. The change of the compliance tensors associated to the damage due to the initiation of the circular and the elliptical cracks are

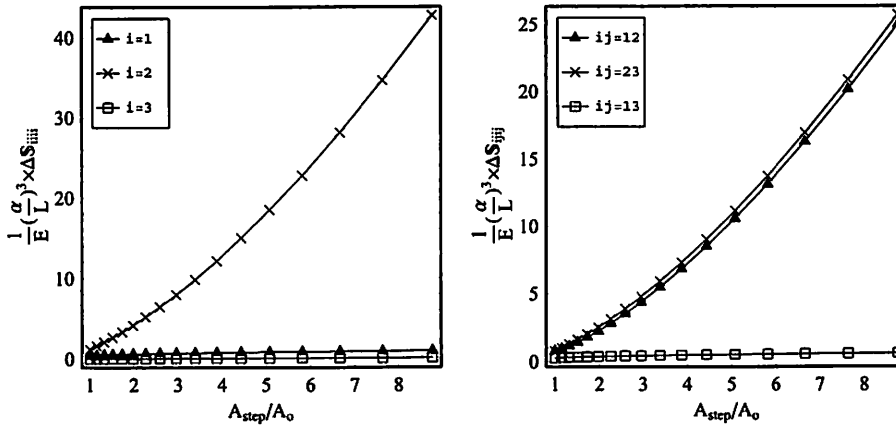

Figure 4.2: elliptical crack: evolution of the diagonal components of the compliance tensor

respectively

$$\Delta \mathbb{S}_C^{Crack} = \frac{1}{E}\left(\frac{\alpha}{L}\right)^3 \begin{pmatrix} 2.6050 & -0.2365 & 0 & 1.6740 & 0 & 0 \\ -0.2365 & 2.6047 & 0 & 1.6741 & 0 & 0 \\ 0 & 0 & 0 & 0 & 0 & 0 \\ 1.6740 & 1.6741 & 0 & 2.3693 & 0 & 0 \\ 0 & 0 & 0 & 0 & 1.4216 & 1.4201 \\ 0 & 0 & 0 & & 1.4201 & 1.4201 \end{pmatrix}, \tag{4.23}$$

and

$$\Delta \mathbb{S}_E^{Crack} = \frac{1}{E}\left(\frac{\alpha}{L}\right)^3 \begin{pmatrix} 0.41044 & -0.02732 & 0 & 0.49054 & 0 & 0 \\ -0.02732 & 1.1797 & 0 & 0.44827 & 0 & 0 \\ 0 & 0 & 0 & 0 & 0 & 0 \\ 0.49054 & 0.44827 & 0 & 0.78721 & 0 & 0 \\ 0 & 0 & 0 & 0 & 0.76571 & 0.44096 \\ 0 & 0 & 0 & & 0.44096 & 0.25479 \end{pmatrix}, \tag{4.24}$$

where the tolerance is set as 10^{-7}. These results are in good agreement with the ones based on the analytical solutions for an isotropic homogenous infinite solid damaged by a single circular crack (KRAJCINOVIC 1996), and a single elliptical crack (BUDIANISKY & O'CONNELL 1976). The detailed analytical solutions for the effective continuum elastic properties of homogenous isotropic elastic solids corresponding to the damage due to a circular and an elliptical internal cracks are given in section 5.3.

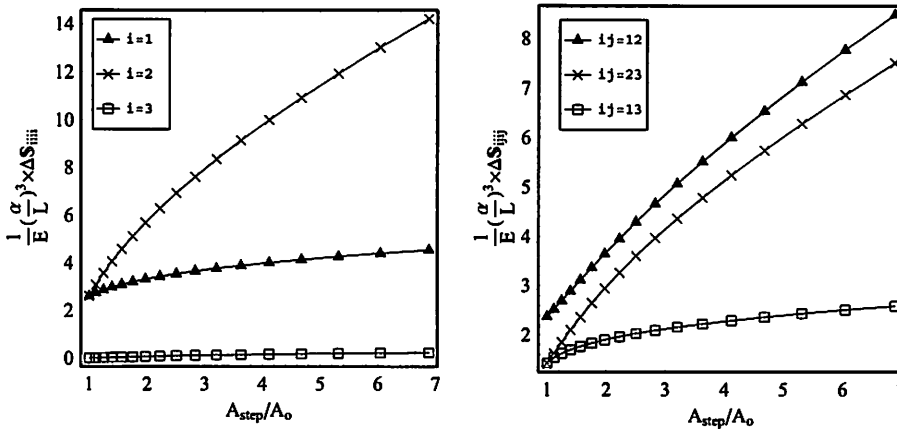

Figure 4.3: circular crack: evolution of the diagonal components of the compliance tensor

Figures 4.3 and 4.2 show the evolution of the diagonal components of the change of compliance tensor, respectively for the circular and elliptical cracks. The left hand curves in figures 4.3 and 4.2 show the change of the compliance components of the unit cell in the principle loading directions, and the right hand ones represent the shear components.

4.2.3 Cowin-Mehrabadi approach

To see if there exists a plane of symmetry for the calculated tensors, the Cowin-Mehrabadi method based on the characterization of the eigenvalues and eigenvectors of the compliance tensor is considered here. For this, the eigenvectors of the second-rank tensors $\mathbb{S}_{imnj}$ and $\mathbb{S}_{ijmn}$ are to be calculated first.

For the compliance tensor modified by the damage due to the initial elliptical crack, the eigenvectors of the two tensors are coincident

$$\begin{aligned} n_1^{(1)} &= n_1^{(2)} = (0.866 \quad -0.500 \quad 0.000)\ , \\ n_2^{(1)} &= n_2^{(2)} = (0.500 \quad 0.866 \quad 0.000)\ , \\ n_3^{(1)} &= n_3^{(2)} = (0.000 \quad 0.000 \quad 1.000)\ , \end{aligned} \tag{4.25}$$

so all three vectors could be normals to the planes of symmetry. These eigenvectors also satisfy the conditions $(4.8)_1$ and $(4.8)_4$, showing that all three eigenvectors are normals to the planes of symmetry. This indicates that the damaged unit cell has at least three planes of symmetry. The eigenvalues of the two tensors are distinct, so no more than three planes of symmetry can exist (COWIN & MEHRABADI 1987). Since there are three mutually orthogonal planes of symmetry for the unit cell embedding the el-

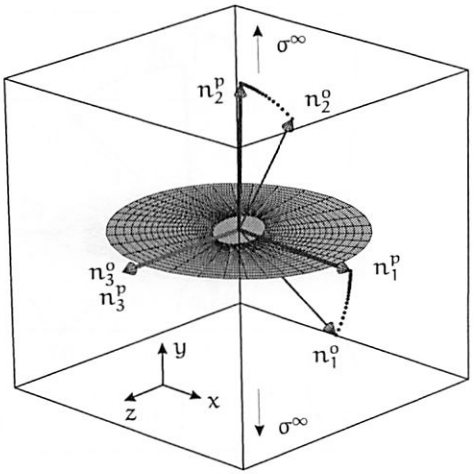

Figure 4.4: elliptical crack: evolution of the normals to the planes of orthotropy

liptical crack, it follows that the material has orthotropic symmetry, for which the normals to the planes of symmetry are aligned with the ones of the crack coordinates (n_1 is aligned with the semi-minor axis, n_2 is perpendicular to the plane of the crack and n_3 is aligned with the semi-major axis of the ellipse. These results were also predicted by BUDIANISKY & O'CONNELL (1976).

As the crack grows, the same procedure can be undertaken to determine the evolution of the material symmetries. It is observed that for each step of crack growth, the type of material symmetry is approximately orthotropic. Figure 4.4 shows the evolution of the normals to the planes of orthotropic symmetry as the elliptical crack grows. The thin arrows (n_i^o's) show the normals to planes of symmetry due to the initial crack, the thick ones (n_i^p's) show the ones of the last propagation step and the dots in between show the evolution path. It is observed that by crack growth, the normal vectors are rotating to align with the principle loading directions.

In an analogous way, the conditions (4.8) are checked for the initial circular crack. For this case, the eigenvectors of the tensor $\mathbb{S}_{imnj}$ and $\mathbb{S}_{ijmn}$ are identical as well

$$\begin{aligned} n_1^{(1)} &= n_1^{(2)} = (0.707 \quad -0.707 \quad 0.000)\ , \\ n_2^{(1)} &= n_2^{(2)} = (0.707 \quad 0707 \quad 0.000)\ , \\ n_3^{(1)} &= n_3^{(2)} = (0.000 \quad 0.000 \quad 1.000)\ , \end{aligned} \tag{4.26}$$

so all three vectors could be normals to planes of symmetry. The eigenvectors also satisfy the conditions $(4.8)_1$ and $(4.8)_4$, showing that all three eigenvectors are normals to the planes of symmetry, so the damaged unit cell has at least three planes of symmetry. The tensors $\mathbb{S}_{imnj}$ and $\mathbb{S}_{ijmn}$ both have two identical eigenvectors. This indicates

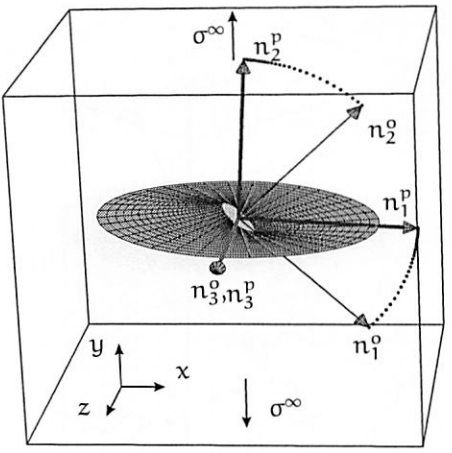

Figure 4.5: circular crack: evolution of the normals to the planes of orthotropy

that the material damaged by the single circular crack becomes transversely isotropic (COWIN & MEHRABADI 1987). This could be further checked, by considering the eigenvector associated with the distinct eigenvalue of the tensor $\mathbb{S}_{imnj}$ or $\mathbb{S}_{ijmn}$. This vector is normal to the plane of the crack, and it is easy to show that in the plane of the crack, where every vector is orthogonal to this vector, any chosen vector is an eigenvector of the tensor $\mathbb{C}_{imnj}$ or $\mathbb{C}_{ijmn}$. This indicates that the number of the planes of symmetry is $\infty + 1$, which is the case for a transversely isotropic material.

However, for the growing circular crack the type of material symmetry is different than for the initial circular crack. It is observed that at each step of crack growth the type of material symmetry is approximately orthotropic, as was the case for the elliptical crack. Figure 4.5 shows the evolution of the normals to the planes of orthotropic material symmetry as the circular crack grows.

4.2.4 optimization approach

Considering the fact that the damage associated with a growing elliptical or circular crack changes the virgin isotropic material properties into orthotropic one, it is possible to find the orthotropy axes using an optimization method. The idea of the optimization procedure is to find the coordinate transformation that yields the best symmetry representation of a tensor with a known type of symmetry. So at each step of crack propagation, the optimization algorithm consists of finding the appropriate coordinate transformation for the measured compliance tensor in the principle loading coordinate system of the unit cell that yields the best orthotropic representation. The compliance tensor transformed to the axes of orthotropy is denoted with $\mathbb{S}'$, which is calculated using the fourth-rank tensor

transformation rule

$$\mathbb{S}'_{ijmn} = R_{ir}\, R_{js}\, R_{mt}\, R_{nu}\, \mathbb{S}_{rstu}\,, \tag{4.27}$$

where $\mathbf{R}$ is an orthogonal transformation including all three Euler rotation angles about the three cartesian axes ($\mathbf{R} = \mathbf{R}_z(\gamma_z).\mathbf{R}_y(\gamma_y).\mathbf{R}_x(\gamma_x)$). As an optimization criterion, the following target function is defined (SCHÜTTE & MOLLA-ABBASI 2007A)

$$\begin{aligned}\mathcal{F}_{ORT} &= \sum_{i,j,m,n}^{non.ORT} \left(\mathbb{S}'_{ijmn}\left(\mathbf{R}(\gamma_x, \gamma_y, \gamma_z)\right)\right)^2 \\ &= (\mathbb{S}'_{1213})^2 + (\mathbb{S}'_{1223})^2 + (\mathbb{S}'_{1323})^2 + \sum_{i=1}^{3} (\mathbb{S}'_{ii12})^2 + (\mathbb{S}'_{ii23})^2 + (\mathbb{S}'_{ii13})^2\,,\end{aligned} \tag{4.28}$$

where the summation applies only to the non-orthotropic terms that deviate from zero in the orthotropic coordinate system, and for perfect orthotropy the target function becomes zero. By finding the appropriate coordinate transformation by the set of angles ($\gamma_x, \gamma_y, \gamma_z$) that minimizes the target function, the orthonormal basis resulting the best orthotropic approximation is found

$$\begin{aligned}&\mathbf{R}^{ORT} = \arg\min\left\{\mathcal{F}_{ORT}(\mathbf{R}) \,\middle|\, \det\mathbf{R} = 1,\ \mathbf{R}^T = \mathbf{R}^{-1}\right\}\,, \\ &\Rightarrow \quad \mathbb{S}^{ORT}_{ijmn} = ORT\left\{\mathbb{S}'_{ijmn}\left(\mathbf{R}^{ORT}\right)\right\}\,,\end{aligned} \tag{4.29}$$

where $ORT(\bullet)$ is the operator that nulls out the non-orthotropic components of $\mathbb{S}'_{ijmn}$ deviating from zero. This gives the best orthotropic representation of $\mathbb{S}'_{ijmn}$ in the resulting orthotropic coordinate system.

This method is applied to the considered examples to find the evolution of orthotropic coordinate system. For both examples, the resulting rotation angles about the x and y axes are zero (γ_x and γ_y). The evolution of the non-zero rotation, which is about the z-axis, for the best representation of orthotropy is given by the left hand curves in figures 4.6 and 4.7, respectively for the elliptical and circular cracks. To compare the accuracy of the results, the resulting approximate orthotropic compliance tensor $\mathbb{S}'$ is compared to the best orthotropic tensor $\mathbb{S}^{ORT}$ which is resulting from $\mathbb{S}'$ by setting all non-orthotropic components to zero. For this, the following error function is considered

$$Error^{ORT} = \frac{\| \mathbb{S}^{ORT} - \mathbb{S}^{ISO} \|}{\| \mathbb{S}' - \mathbb{S}^{ISO} \|}, \qquad \text{where} \qquad \| \mathbb{S} \| = \sqrt{\sum_{i,j,m,n=1}^{3} \mathbb{S}_{ijmn}\, \mathbb{S}_{ijmn}}\,, \tag{4.30}$$

and $\mathbb{S}^{ISO}$ is the compliance tensor for the undamaged matrix. The right hand curves in figures 4.6 and 4.7 compare the errors due to the Cowin-Mehrabadi approach and the

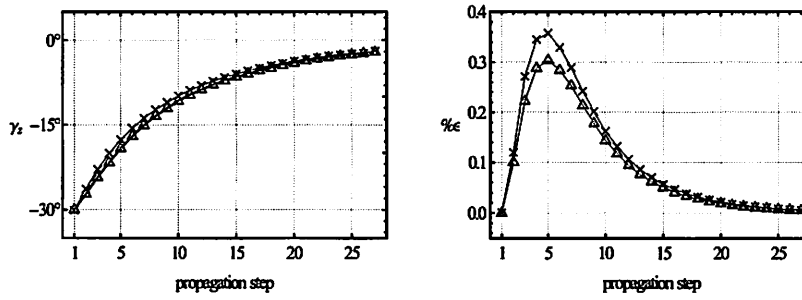

Figure 4.6: elliptical crack: evolution of the orthotropic transformation angle

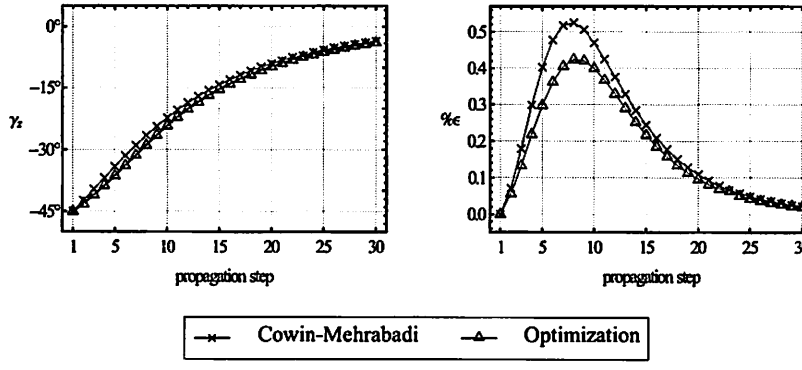

Figure 4.7: circular crack: evolution of the orthotropic transformation angle

optimization procedure. It is observed that the difference between the Cowin-Mehrabadi approach and the optimization procedure is very small. This deviation may be due to the numerical errors in processing of the results.

Summarizing the results of this chapter, the following points should be mentioned. The evolution of the compliance tensor shows that the damage associated with the initiation of a single mixed-mode internal circular crack changes the virgin isotropic properties into transversely isotropic ones (KRAJCINOVIC 1996), and the damage associated with a single elliptical crack results in orthotropic material symmetry (BUDIANISKY & O'CONNELL 1976). Thus, changing the type of material symmetry from isotropic to orthotropic may imply the existence of local damage due to an elliptical crack. This result is the cornerstone for the proposed continuum damage model in the next chapter. The evolution of damage due to a growing internal elliptical or circular crack shows that at each step of crack growth material possesses orthotropic symmetry, and for heavily grown cracks the axes of orthotropy rotate towards the principle loading coordinates of the unit cell.

The advantage of using the approach of Cowin-Mehrabadi is that the type of elastic material symmetry is directly identified from the character of the eigenvectors and eigenvalues, and there is no need for a priori assumptions. Using the optimization procedure, however, the type of material symmetry should be a priori known and this method cannot be generalized for problems without prior information on the type of elastic symmetry

5 A Consistent Micromechanical Based Continuum Damage Model

Contents

Failure of most structural members on the macroscale follows the irreversible heterogeneous microprocesses of time and environment dependent deterioration of materials. The existence of distributed microscopic voids, cavities, or cracks of the size of crystal grains is referred to as material damage, whereas the process of void nucleation, growth, and coalescence, which initiates the macrocracks and causes progressive material degradation through the reduction of strength and stiffness, is called damage evolution (CHABOCHE 1988), (SKRZYPEK & GANCZARSKI 1999).

On the atomic scale, the material structure is not continuous at all, but is represented by a configuration of atoms ordered in a crystal lattice or molecular chains bonded by the interatomic forces. The state of material damage on this level is determined by the configuration of atomic bonds, the breaking and re-establishing of which constitutes the damage evolution. On the microscale, the damage is due to the accumulation of the microstresses at the neighborhood of microdefects and microinclusions, and material structure is piecewise discontinuous and heterogeneous. The state of damage in a volume of material can be determined by the number of microcracks or microvoids and their size and configuration. On the mesoscale, damage process is concerned with the growth and coalescence of microcracks or microvoids which together initiate one crack. On the macroscale, growth of the initiated cracks is the main mechanism of damage and a concept of quasi-continuum

is introduced. In this regard, the discontinuous and heterogeneous solid suffering from damage evolution, is approximated by the ideal pseudo undamaged continuum using the couples of effective state variables, such as $\tilde{\varepsilon}$ and $\tilde{\sigma}$, in the current damaged state and dissipation potential instead of the classical state variables, such as ε and σ, representing the strain and stress tensors for the idealized (pseudo undamaged) and the true (damaged) solids, respectively. To derive the behavior of the material at the mesoscale, specific mechanisms at the microscale are studied (LEMAITRE 1992). The mechanical modeling of these mechanisms is performed with common constitutive equations and a crack growth criterion at the meso- or macroscale. The crucial step is the interaction between different mechanisms and the homogenization binding the gap between the micro- and the mesoscale.

Damage of crystalline metallic materials can basically be distinguished introducing two main mechanisms. The first damage mechanism, called the ductile or transgranular damage mode, is predominant at high stress level tests when the slipbands of plasticity are formed in favorably oriented grains. The microslips are inclined roughly at 45° to the main stress direction and the coupled damage-(visco)plasticity mechanism may approximately be described by the isotropic (scalar) damage internal variable $\mathcal{D}$, the evolution of which may be governed by the elastic energy release rate (LEMAITRE & CHABOCHE 1990) or the total (elastic and inelastic) energy release (SAANOUNI, FORSTER & BEN-HATIRA 1994) in a more general case. The material instability from microslips initiation eventually yields a discontinuous bifurcation of the velocity field (RUNESSON, OTTOSEN & PERIC 1991). The plastic strain localization in zones of microvoid concentration leads to a failure mode with material separation and the formation of free surfaces (decohesion) on the macrolevel. The macrocracks are formed in a transgranular mode with a preferable inclination that coincides with the directions of slipbands of plasticity.

The second damage mechanism, usually identified for simplicity with brittle or intergranular damage, is representative for rather low stress level loading conditions. It is mainly based on the microcracking process initiated at the grain (or subgrain) boundaries, and it is recognized to be controlled by the local maximum stress, rather than the effective stress, such that the normal to the microcrack direction coincides with the principal stress direction at the point considered. The macrocracking process may be observed at selected grain boundaries to result from the coalescence of microcracks of similar average orientation. No or negligibly small plastic deformations precede the damage evolution, hence pure brittle failure mechanism occurs. The discontinuous and heterogeneous damaged solid is approximated by the pseudo undamaged continuum by the use of the couples of effective state variables, the definitions of which depend on the equivalence principles employed. In such a case, however, the damage evolution in the elastic-brittle or creep materials is no longer isotropic, hence unlike the ductile damage phenomenon, brittle damage behavior is anisotropic in nature, so that the description by scalar internal variables is insufficient. The essentially anisotropic description of damage in the elastic-brittle or creep solids by the development of distributed and

oriented microscopic cracks require damage variables ranging from a vector to second-rank or higher-rank tensors (KACHANOV 1958), (VAKULENKO & KACHANOV 1971), (DAVISON & STEVENS 1973), (MURAKAMI & OHNO 1981), (CHABOCHE 1988), (KRAJCINOVIC 1996).

Basically, there are two ways to model the failure of materials, either in a discrete or a continuum format. The latter approach has the advantage that the early stages of the failure process, for example the onset of microcracking or void nucleation, can be modeled adequately. Various classes of constitutive models are available (SKRZYPEK & GANCZARSKI 1999), (KRAJCINOVIC 1996). Attempts to capture damage phenomena such as shear bands, microcracks and other localization phenomena with numerical methods for continuum damage and continuum plasticity models have started in the mid-1980s. The original concept of continuum damage mechanics was introduced by KACHANOV (1958), and it was further developed by HULT (1979), CHABOCHE (1988), and KRAJCINOVIC (1989). The general purpose of continuum damage mechanics is to describe the coupling effects of damage processes and the stress-strain behavior of a material. Two basic approaches have been developed within this framework.

The first method is the micromechanical approach pioneered by MCCLINTOCK (1968) and RICE & TRACEY (1969), is based upon the micromechanisms of void nucleation and growth. Within this approach, the effective elastic properties of the material are derived by using the pertinent results of micro-constituent analysis, such as that of a planar crack embedded in an infinite medium. Various averaging schemes are utilized in the transition from micro to macro response, depending on the density of the cracks and their interactions (BUDIANISKY & O'CONNELL 1976), (HORI & NEMAT-NASSER 1983). At the microscale, a good representation of the local effects and the physical mechanisms can be introduced. However, due to the overwhelming complexity of the physical phenomena reflecting the growth and interaction of the microcracks, difficulties often arise when the micromechanical approach is implemented into a practical scale structural analysis.

The second approach of continuum damage mechanics is essentially a phenomenological one. With this approach, the effect of damage on the deformation processes is taken into account by introducing damage variables into the constitutive equations of the continuum (LEMAITRE & CHABOCHE 1985), (CHABOCHE 1988), (CHOW & LU 1989), (KRAJCINOVIC 1989). It is assumed that the response of a material depends only on the current state of the micro-structural arrangement, which is approximated by a set of internal state variables that reflect the macroscopic effects of the microdefects. However, the exact description of each individual microcrack evolution would be meaningless in view of the fact that the details of the cracking pattern differs from one crack to the other. The useful homogenization (averaging) concept is applied for describing the macroscopic behavior of the material. Hence, instead of trying to reproduce the fine details of the microdefect and macrocrack patterns, continuum damage mechanics attempts to formulate a theory that will reflect the influence of these defects in a brittle solid in an approximate

manner.

Five decades of research on the identification of different damage mechanisms have provided this field with a wealth of damage models and concepts to study the evolution of damage and failure analysis of materials and structures. However, there is still a need for new material models and ideas covering the physical aspects of the irreversible damage process, with which one can describe the accumulation and the growth of damage more accurately in practical scale structures. In the framework of brittle and quasi-brittle continuum damage mechanics, which is the concern of this chapter, beside the advantages of the so far proposed models and their applicability for certain problems, most of these models are based on simplifying and ad hoc assumptions, without considering the irreversible damage process in their formulation in a thermodynamically correct way. To mention some shortcomings of these models, the following points can be pointed out. Some models are based on the assumption of isotropic damage evolution, in the sense that the initial type of the material symmetry is preserved during the total load history. Considering the directional characteristic of microcracks and microvoids in three-dimensional state of deformation, the application of isotropic damage model is very limited and for multi-dimensional stress state the need for anisotropic models arises. Some of these models are based on the degradation of elastic properties due to microcracks with a fixed orientation and/or self-similar growth of microcracks, without allowing these microdefects to grow and kink to different planes or shapes. This, however, is in contrast with reality and experimental observations proving the fact that mixed-mode microcracks in brittle and quasi-brittle materials grow in a kinking manner. Anisotropic material damage is known to affect the apparent Young's modulus and the Poisson's ratio of the solids. This is neglected in some of the so far proposed damage models, which is in contrast with the experimental observation (KRAJCINOVIC & FONSEKA 1982). The simplifying and ad hoc assumptions which some damage models are based on, neither take the thermodynamics of the damage phenomena into account, nor properly describe the real irreversible process of the material degradation in a thermodynamically correct way.

It is known from experiments that most materials, and in more special case brittle and quasi-brittle materials, under general loading conditions develop anisotropic damage (KRAJCINOVIC & FONSEKA 1982). For a given stress state, materials damaged by microcracks in general accumulate additional damage through the growth of these microcracks. Considering this and the mentioned points, the concern of this chapter is to provide a consistent, continuum damage model based on the micromechanical framework and the local anisotropy (orthotropy) induced by kinking and growing elliptical and/or circular microcracks. For clarity purposes and to explain the main issues of the proposed model in a more clear mathematical way, the complexity of the proposed damage model is reduced here by leaving out the thermal effects and other non-mechanical phenomena. Strains and rotations are assumed to be small, hence the framework of linear elastic fracture mechanics can be applied. Furthermore, viscous effects and permanent deformations are neglected and the material behavior is assumed to be linear elastic in its pristine state. The small strain assumption, and the lack of permanent deformations in this model makes

it suitable to show the evolution of damage in structures with brittle and quasi-brittle fracture behavior experiencing high-cycle fatigue.

Generally, it is impossible to formulate a damage model covering the mixed-mode propagation of microcracks in a fully traceable way. Considering microcracks in the form of elliptical and circular cracks, one may calculate the kinking of the initial cracks analytically only for the first load increment. After the kinking of the initial cracks, however, the mathematical formulation of the next kinking steps is no longer possible. To overcome this difficulty, some researchers have introduced models based on simplifying assumption such as fixing the plane of the initiated microcracks, so that microcracks may only grow in a self-similar manner. This assumption may be acceptable for the case of monotonic loading or cyclic loading with a constant loading direction, but for loads with changing direction and amplitude, as is the case for non-proportional loads or even sequential loads, this assumption leads to underestimating the damage, since it does not allow for crack kinking. The assumption of self-similar growth of mixed-mode cracks, in general, results in a smaller damage accumulation than what the real mixed-mode kinking results in.

To cover the mentioned shortcomings of other models, and to overcome the difficulties in the formulation of a damage model, which accounts for the kinking and growth of microcracks in a mathematical traceable manner, a micromechanical based continuum damage model is proposed here, which is based on the reduction of stiffness due to kinking elliptical microcracks. To be able to formulate the model in a fully mathematical traceable way, the concept of an equivalent elliptical crack is introduced in the sense that a kinked crack is replaced with an equivalent elliptical crack, resulting in an equivalent dissipation of energy. Basically, eight degrees of freedom can be considered for each equivalent elliptical microcrack replacing the kinking one. These are the major and minor axes of the ellipse, orientation of the microcrack given by three Eulerian rotation angles, and the position of the crack in space. Considering the concept of unit cell and assuming that the microcrack is located in the center of the cell, the position of the microcrack can be fixed and may be left out of the formulation. This is because in the case of non-interacting cracks, the position of the crack does not have an impact on the elastic properties of the material. To calculate the other five unknown characteristics of the equivalent crack, different postulates may be proposed. Here, to determine the geometry and orientation of the equivalent elliptical crack, the postulates of equivalent dissipation and equivalent damage induced anisotropy are considered. Such a formulation of the dissipative damage process due to kinking equivalent elliptical microcracks, taking into account the damage induced orthotropy of an elliptical crack in a local sense, results in a consistent damage model capturing the load history through the local orthotropic degradation of the mechanical material properties.

This chapter is organized as follows. The principles of continuum damage mechanics are presented first, which provide the required fundamentals for the discussions in the general continuum damage mechanics. Based on the micromechanical approach, the components of the tensors for the change of compliance due to the initiation and the kink-

ing of an elliptical crack are addressed in an analytical way. These results can be reduced to give the ones corresponding to a circular crack in the limit case as the major axis of the ellipse approaches its minor axis. Based on these and the results given in the previous chapters, a micromechanical based three-dimensional damage model for brittle and quasi-brittle solids weakened by kinking elliptical microcracks is developed. In the implementation of the continuum damage model, the hypothesis of statistical homogeneity and weak interaction of microdefects is considered, which is reasonable for a modest distribution of heterogeneities (NEMAT-NASSER & HORI 1993). With this, the assumption of non-interacting defects is fulfilled. A variety of numerical examples is then presented to explain the proposed damage model in more detail and also to show its applicability to real components subjected to fatigue conditions, by comparing the results based on the proposed model with the experiments.

5.1 Damage variables

Continuum damage models are developed in either phenomenological or micromechanical framework. In either case, the choice of the damage variables is of crucial importance, since it reflects the nature of damage and determines the degree of simplicity and feasibility of the theory for application purposes. In all cases of various equivalence principles it is assumed that in a quasi-continuum the true distribution of defects is smeared out and homogenized by properly defined internal variables that characterize the damage state. Scalar (KACHANOV 1958), vector (DAVISON & STEVENS 1973), second-rank tensor (VAKULENKO & KACHANOV 1971), (MURAKAMI & OHNO 1981), fourth-rank tensor (CHABOCHE 1988) and even eighth-rank tensor variables (KRAJCINOVIC 1996) have been used to represent damage variables. While vector and higher rank tensors are predominately used for the representation of anisotropic damage, the scalar damage variable has been reserved for isotropic damage.

It was KACHANOV (1958) and later RABOTNOV (1969), who for the first time introduced the concept of the scalar damage variable to represent damage progression in creep of metals. To characterize a gradual deterioration process of a micro-structure, via microcracks and microvoids nucleation and evolution through the surface area δA of intersection of the plane of normal $\mathbf{n}$ with the representative volume element (RVE), surrounding a material point M, KACHANOV (1958) introduced the continuity parameter ω, the magnitude of which is determined as the ratio of the effective (remaining) area $\delta\widetilde{A} = \delta A - \delta A_{\mathcal{D}}$ to the total (undamaged) area δA (figure 5.1)

$$\omega = \frac{\delta\widetilde{A}}{\delta A}, \quad 0 \leq \omega \leq 1, \tag{5.1}$$

such that $\omega = 1$ corresponds to the undamaged (virgin) state, whereas the continuity decreases with damage growth to eventually reach zero for a completely damaged surface element $\delta A_{\mathcal{D}} = \delta A$.

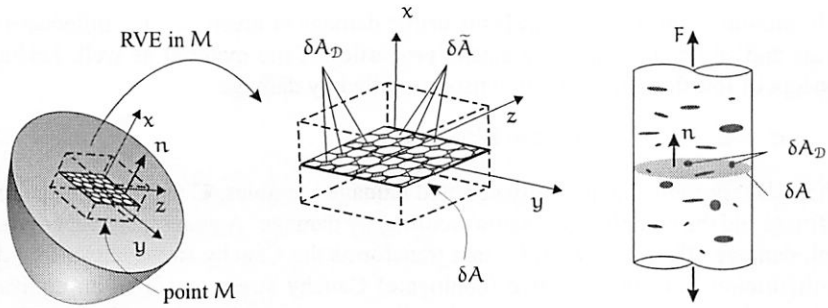

Figure 5.1: surface damage measure

Considering planes of various normals n_x, the surface damage in an arbitrary direction x can be defined

$$\mathcal{D}(M, \mathbf{n}, x) = \frac{\delta A_{\mathcal{D}_x}}{\delta A}, \tag{5.2}$$

where $\mathcal{D} = 1 - \omega = 0$ corresponds to the undamaged state of the surface element considered, and $\mathcal{D} = 1$ to the completely damaged element (fully broken). The above definition is mainly applicable for crystalline materials in which, on the microscale, microscopic cracks develop both in metal grains (transgranular damage) and on intergranular boundaries (intergranular damage). These microcracks have different orientations, such that the surface damage parameter also changes with the normal vector orientation when the more developed vectorial or tensorial damage measures are introduced. This concept received prompt acceptance and became the cornerstone for further isotropic damage models.

Consider a one-dimensional volume element, e.g a bar of cross-sectional area δA with a distribution of microdefects measured by the damaged surface portion $\delta A_{\mathcal{D}}$, subjected to tension F. The stress, without considering the effect of damage, is $\sigma = F/\delta A$. For the damaged element subjected to the same traction field, with $\delta A - \delta A_{\mathcal{D}}$ as the effective area and considering equation (5.6), the stress is defined as

$$\tilde{\sigma} = \frac{F}{\delta A - \delta A_{\mathcal{D}}} = \frac{\sigma}{1 - \mathcal{D}}, \tag{5.3}$$

which is the so called effective stress principle in one-dimensions.

The concept of scalar damage variable $\mathcal{D}$ can be generalized to study three-dimensional anisotropic damage. CHABOCHE (1988), LECKIE & ONAT (1981) and other researchers have given different fourth-rank tensorial representation of damage. In an analogous way to equation (5.3)

$$\tilde{\boldsymbol{\sigma}} = (\mathbb{I} - \mathbb{D})^{-1} : \boldsymbol{\sigma} = \mathbb{M} : \boldsymbol{\sigma}, \tag{5.4}$$

where $\mathbb{I}$ represents the fourth-rank identity tensor, and $\mathbb{D}$ and $\mathbb{M}$ are the fourth rank damage and damage effect tensors, respectively.

Evolution of the anisotropic elastic brittle damage or creep damage influences both the stress and strain states and the elastic properties of the material as well, leading to the concept of fourth-rank elasticity tensor modified by damage

$$\sigma = \widetilde{\mathbb{C}}(\mathcal{D}) : \varepsilon, \quad \text{or} \quad \varepsilon = \widetilde{\mathbb{S}}(\mathcal{D}) : \sigma, \tag{5.5}$$

where $\mathcal{D}$ represents the properly selected damage variables, $\widetilde{\mathbb{C}}$ and $\widetilde{\mathbb{S}}$ are respectively the stiffness and the compliance tensors modified by damage. A general concept of the fourth-rank damage effect tensor $\mathbb{M}(\mathcal{D})$ that transforms the Cauchy stress tensor in a damaged configuration σ to the effective (conjugate) Cauchy stress tensor in an equivalent fictive pseudo undamaged solid $\widetilde{\sigma}$, based on the appropriate damage equivalence hypothesis (strain or stress or complementary energy or total energy equivalence) takes into account the fully anisotropic nature of damage in the form (CHOW & LU 1992)

$$\widetilde{\sigma} = \mathbf{M}(\mathcal{D}) : \sigma, \tag{5.6}$$

where $\mathbb{M}(\mathcal{D})$ is an isotropic fourth-rank tensor valued function of a damage state variable $\mathcal{D}$, and the effective stress tensor $\widetilde{\sigma}(\sigma, \mathcal{D})$ is an isotropic second-rank tensor valued function of σ and $\mathcal{D}$.

5.2 Equivalence principles of continuum damage mechanics

Consider a damaged solid in a current configuration, the mechanical state of which is defined by the couple of external state variables (ε, σ), where ε is the small strain tensor and its associated variable σ is the Cauchy tress tensor. The damaged state can be replaced with a fictive pseudo undamaged state characterized by the effective state variables $(\widetilde{\varepsilon}, \widetilde{\sigma})$, the definition of which depends on the damage equivalence principle. This section gives the various damage equivalence principles more systematically, to generalize the above definitions to three-dimensional problems.

5.2.1 principle of strain equivalence - the effective stress concept

The hypothesis of strain equivalence (figure 5.2) states that the strain associated with a damaged state under the applied stress σ is equivalent to the strain associated with the undamaged state under the effective stress $\widetilde{\sigma}$ (LEMAITRE 1992).

In the general case of a linear anisotropic elastic solid in three-dimensional space, the stress-strain relation is characterized by the generalized Hooke's law

$$\sigma = \mathbb{C} : \varepsilon \quad \text{or} \quad \varepsilon = \mathbb{S} : \sigma, \quad \text{where} \quad \mathbb{S} = \mathbb{C}^{-1}, \tag{5.7}$$

which relates the components of the second-rank elastic stress tensor σ to the components of the second-rank elastic strain tensor ε by a linear fourth-rank tensor $\mathbb{S}$ or $\mathbb{C}$, the so called compliance and stiffness tensors, respectively.

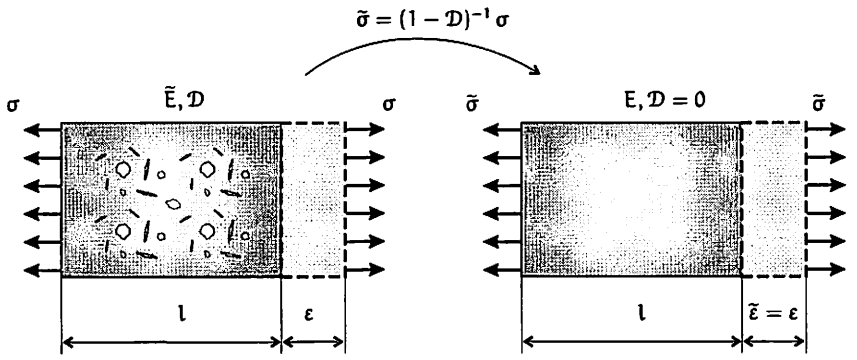

Figure 5.2: one-dimensional strain equivalent concept

Hooke's law for the damaged material follows

$$\sigma = \tilde{\mathbb{C}} : \varepsilon , \tag{5.8}$$

and considering the principle of strain equivalence, $\tilde{\varepsilon}(\tilde{\sigma}, 0) = \varepsilon(\sigma, \mathbb{D})$, the stress-strain relation for the undamaged state yields

$$\tilde{\sigma} = \mathbb{C} : \varepsilon . \tag{5.9}$$

Combining equations (5.8) and (5.9) results in

$$\tilde{\sigma} = \mathbb{C} : \tilde{\mathbb{C}}^{-1} : \sigma . \tag{5.10}$$

This together with the definition of effective stress result in the damage tensor

$$\mathbb{D} = \mathbb{I} - \tilde{\mathbb{C}} : \mathbb{C}^{-1} , \tag{5.11}$$

and reformulating this, the elasticity tensor for the damaged state is resulting

$$\tilde{\mathbb{C}} = (\mathbb{I} - \mathbb{D}) : \mathbb{C} . \tag{5.12}$$

It should be emphasized, however, that the principle of strain equivalence leads to the restrictive conclusion that the Poisson's ratio is not affected by damage, so $\tilde{\nu} = \nu$, and consequently under uniaxial tension test a material suffers only from damage in the direction of tensile stresses. However, for most engineering materials this is not true, since nucleation and growth of microscopic damage not only results in the redistribution of stresses due to the cross sectional area reduction but also decreases the stiffness of the material (CHOW & LU 1992). Hence, the strain equivalence principle is considered as just one possible principle in continuum damage mechanics.

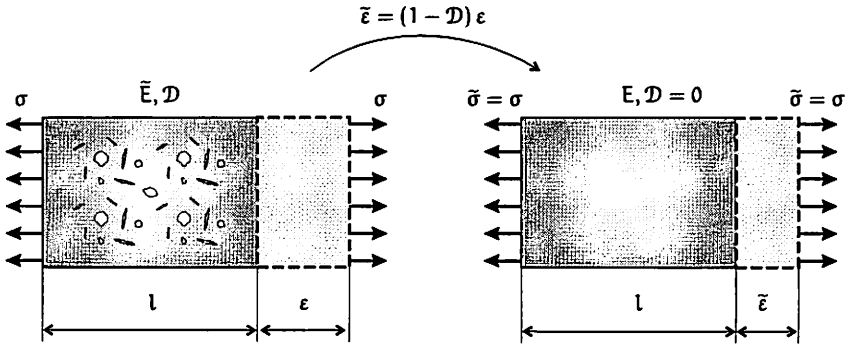

Figure 5.3: one-dimensional stress equivalent concept

5.2.2 principle of stress equivalence - the effective strain concept

The hypothesis of stress equivalence (figure 5.3) states that the stress associated with a damaged state under the applied strain ε is equivalent to the stress associated with the undamaged state under the effective strain $\tilde{\varepsilon}$ (CORDEBOIS & SIDOROFF 1979), (SIMO & JU 1987).

In an analogous manner to the principle of strain equivalence, the damage tensor and the elasticity tensor for the damaged state are resulting. For the undamaged state, the stress-strain relation may be written in the form

$$\tilde{\varepsilon} = \mathbb{C}^{-1} : \sigma\,, \tag{5.13}$$

and considering the principle of stress equivalence $\tilde{\sigma}(\tilde{\varepsilon}, 0) = \sigma(\tilde{\varepsilon}, \mathbb{D})$, and

$$\varepsilon = \tilde{\mathbb{C}}^{-1} : \sigma\,, \tag{5.14}$$

it results

$$\tilde{\varepsilon} = \tilde{\mathbb{C}}^{-1} : \mathbb{C} : \varepsilon\,. \tag{5.15}$$

Considering the definition of effective strain $\tilde{\varepsilon} = (\mathbb{I} - \mathbb{D}) : \varepsilon$, the damage tensor is expressed by

$$\mathbb{D} = \mathbb{I} - \mathbb{C}^{-1} : \tilde{\mathbb{C}}\,, \tag{5.16}$$

and the elasticity tensor for the damaged state is given by

$$\tilde{\mathbb{C}} = \mathbb{C} : (\mathbb{I} - \mathbb{D})\,. \tag{5.17}$$

It should be noted that in constitutive equations and damage evolution laws, replacing the nominal stress with the effective stress in the framework of the strain equivalence

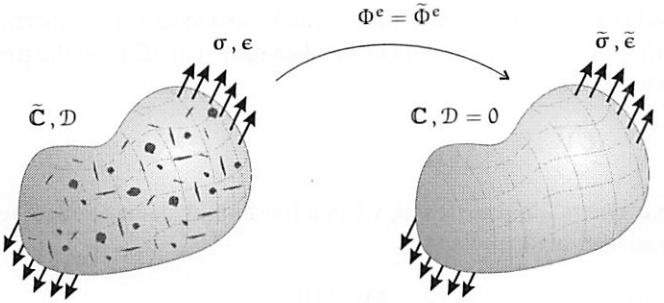

Figure 5.4: elastic energy equivalence in three-dimensions

principle or the nominal strain with the effective strain in the framework of the stress equivalence principle generally increases the complexity of the governing equations. Although the effective stress or strain concepts can be converted to an effective stiffness concept via the strain or stress equivalence principles, and vice versa, choosing and consistently applying one of these principles can be confusing. These simplified models do not properly describe the real irreversible thermodynamic material degradation processes in an appropriate manner. Hence in general, the hypothesis of the elastic (or total) energy equivalence might be considered as more realistic than that of strain or stress equivalence (CORDEBOIS & SIDOROFF 1979), (SIDOROFF 1981).

5.2.3 principle of elastic energy equivalence

The hypothesis of elastic energy equivalence (figure 5.4) states that the elastic energy associated with a damaged state under the applied stress σ and the resulting stress ϵ is equivalent to the elastic energy associated with the undamaged state under the effective stress $\tilde{\sigma}$ and the resulting strain $\tilde{\epsilon}$ (CORDEBOIS & SIDOROFF 1979). This hypothesis is also known as the principle of complementary energy equivalence.

The complementary elastic energy potentials for the damaged and the pseudo undamaged states are, respectively given by

$$\Phi^e(\sigma, \mathcal{D}) = \frac{1}{2}\sigma : \tilde{\mathbb{C}}^{-1} : \sigma, \quad \text{and} \tag{5.18}$$
$$\tilde{\Phi}^e(\tilde{\sigma}, 0) = \frac{1}{2}\tilde{\sigma} : \mathbb{C}^{-1} : \tilde{\sigma},$$

where $\mathcal{D}$ represents a set of damage variables.

Considering the hypothesis of elastic energy equivalence ($\tilde{\Phi}^e(\tilde{\sigma}, 0) = \Phi^e(\sigma, \mathcal{D})$) and the damage coupled Hooke's law, the following definitions for the effective variables $\tilde{\sigma}$ and $\tilde{\epsilon}$ are resulting

$$\tilde{\sigma} = (\mathbb{I} - \mathbb{D})^{-1} : \sigma, \quad \text{and} \quad \tilde{\epsilon} = (\mathbb{I} - \mathbb{D}) : \epsilon, \tag{5.19}$$

where $\mathbb{I}$ and $\mathbb{D}$ are the fourth-rank identity and damage tensors, respectively. $\mathbb{D}$ is related to the fourth-rank elasticity tensors of the damaged state ($\widetilde{\mathbb{C}}$) and the pseudo undamaged (fictive) state ($\mathbb{C}$) through

$$\mathbb{D} = \mathbb{I} - (\widetilde{\mathbb{C}})^{\frac{1}{2}} : (\mathbb{C})^{-\frac{1}{2}}. \tag{5.20}$$

In a more general representation, when a fourth-rank damage effect tensor is used, the effective variables are expressed as

$$\widetilde{\sigma} = \mathbf{M}(\mathcal{D}) : \sigma, \quad \text{and} \quad \widetilde{\varepsilon} = \mathbb{M}^{-1}(\mathcal{D}) : \varepsilon, \tag{5.21}$$

with $\mathcal{D}$ denoting the properly selected damage variables.

Note that in the energy based damage equivalence model, growth of microcracks and microvoids influences both stress and strain distributions, which is more realistic than in the strain or stress damage equivalence postulate, where the drop of local stiffness results in a local stress decrease or local strain increase, exclusively. Nevertheless, this hypothesis is limited as it does not allow for the physically adequate description of phenomena other than damage coupled elasticity (CHOW & LU 1992).

5.3 Effective continuum elastic properties of damaged media

Most materials under special loading conditions and most brittle materials develop anisotropic damage. One way to model the anisotropic damage is to consider its influence on the compliance or stiffness of the material in a local sense. Continuum damage models based on the reduction of stiffness are assumed to involve the degradation of the elastic properties due to the nucleation and the growth of microcracks and microdefects in general, which ultimately coalesce to form macrocracks. Most of these damage models are based on the self-similar crack growth assumption, and they do not consider the kinking and propagation of mixed-mode microcracks and the corresponding effect on the evolution of the elastic stiffness tensor. For a given stress state, however, it is known that materials damaged by microcracks in general accumulate additional damage through the kinking and growth of these microdefects. Considering the kinking and growth of microcracks in the formulation of a damage model is especially important in the case of loads with changing direction and amplitude (non-proportional loading). In such cases, the assumption of self-similar growth of microcracks is not sufficient to describe the irreversible thermodynamic process of the material degradation due to the kinking and growth of microcracks to other planes and shapes. This idea is one of the important cornerstones for the continuum damage model presented in this work.

The micromechanical models are commonly referred to a class of analytical models which give the relation between the macroscopic state of a specimen and its microstructure (BUDIANSKY 1983). One of the goals of the micromechanical models is to

provide relatively simple constitutive laws. Within this approach, the effective elastic properties are derived by using the pertinent results of microconstituent analysis, such as that of a planar crack embedded in an infinite medium. Using the concept of micromechanics, continuum damage models based on the framework of fracture mechanics and elasticity can give the local details of the damage response within a representative volume element. These class of models are based on the hypothesis of statistical homogeneity and weak interaction of defects, which are justifiable for reasonably modest concentration of heterogeneities (NEMAT-NASSER & HORI 1993). In this respect, the first step in the formulation of the proposed continuum damage model requires the formulation of the change of continuum elastic properties due to the presence, kinking and growth of elliptical and/or circular microcracks.

Applying the approach of micromechanics, the components of the effective compliance tensor of an infinite, homogeneous, isotropic (in its pristine state) and elastic continuum damaged by a single internal circular crack is given in (KRAJCINOVIC 1996). Here, applying the same method, the components of the tensor for the change of compliance due to the presence of a single internal elliptical crack are derived, from which the results corresponding to a single circular crack can be reproduced (see also BUDIANISKY & O'CONNELL (1976)). Within the approach of micromechanics, the effective elastic properties of a solid damaged by a planar internal elliptical crack are derived from the contribution to the complementary strain energy corresponding to the quasi-static, selfsimilar growth of the crack. For this, the stress intensity factors suffice to give the energy released during the quasi-static, selfsimilar growth of the crack. However, for the formulation of the complementary strain energy corresponding to the kinking of a crack, the analytical expressions for the so called T-stresses are required as well. The complete set of the T-stresses for internal elliptical and circular cracks embedded in a homogenous isotropic infinite solid have been addressed in chapter 2.

5.3.1 presence of a single internal elliptical crack

Consider a single internal elliptical crack in an infinite, homogeneous, isotropic and elastic continuum subjected to mechanical loads applied at infinity. This problem can be decomposed into two sub-problems: that of the continuum without a crack subjected to the remote traction field, and that of the same continuum, where only the crack faces are subjected to the traction field. The traction field of the second sub-problem is determined from the condition requiring that the total tractions over the mating faces of the crack vanish.

Within the framework of linear elastic fracture mechanics, the total, local and average stress and strain fields admit superposition. Under the same traction field, the presence of an active crack will typically increase the total strains. This implies that the average strain of the second sub-problem is a non-zero second-rank tensor, so the total average strain

tensor is given by

$$\varepsilon = \varepsilon^e + \varepsilon^d = \widetilde{\mathbb{S}} : \sigma, \quad \text{where} \quad \widetilde{\mathbb{S}} = \mathbb{S}^{\text{Matrix}} + \Delta\mathbb{S}^{\text{Crack}}, \tag{5.22}$$

where $\widetilde{\mathbb{S}}$ represents the effective compliance of the continua considering the effect of the crack, $\mathbb{S}^{\text{Matrix}}$ is the compliance tensor associated to the matrix material in its pristine state, and $\Delta\mathbb{S}^{\text{Crack}}$ is the change of compliance due to the presence of the crack.

The components of the tensor $\Delta\mathbb{S}^{\text{Crack}}$ can be derived from the contribution to the complementary strain energy corresponding to this sub-problem. The complementary energy is indeed the energy released during the quasi-static, selfsimilar growth of an elliptical crack (dissipated energy), and is given by (BUDIANISKY & O'CONNELL 1976), (KRAJCINOVIC 1996)

$$\psi^* = \frac{1}{V}\int_0^r \left(\oint_c \vec{J}_1 \, dl\right) . d\vec{r}. \tag{5.23}$$

Applying the concept of the local driving force acting in the plane normal to the crack front, it can be shown (SCHÜTTE & MOLLA-ABBASI 2007A)

$$\psi^* = \frac{1}{V}\int_0^r \left(\oint_c J_1 \, \mathbf{e}_n \cdot \mathbf{e}_r \, dl\right) dr, \tag{5.24}$$

where J_1 is the first component of the J-integral vector, and c is the path encircling the ellipse boarder. $\mathbf{e}_n$ and $\mathbf{e}_r$ are the unit vectors showing the normal and radial directions to the ellipse, and dl and dr are the length elements along the ellipse boarder and radius. Considering the local coordinate system given in figure 5.5, the following expressions for the directional unit vectors and the length increments are resulting

$$\mathbf{e}_r = \frac{1}{\sqrt{\alpha^2 \cos^2\varphi + \beta^2 \sin^2\varphi}} (\alpha \cos\varphi, \beta \sin\varphi, 0), \tag{5.25}$$
$$\mathbf{e}_n = \frac{1}{\sqrt{\alpha^2 \sin^2\varphi + \beta^2 \cos^2\varphi}} (\beta \cos\varphi, \alpha \sin\varphi, 0),$$

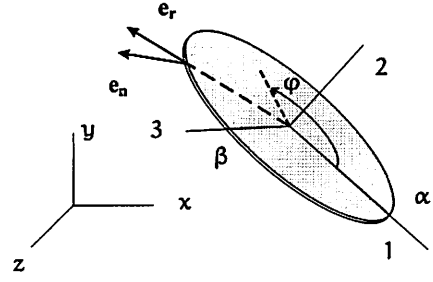

Figure 5.5: elliptical crack and local coordinates

$$dr = \frac{\sqrt{\alpha^2 \cos^2\varphi + \beta^2 \sin^2\varphi}}{\alpha} d\alpha,$$
$$dl = \sqrt{\alpha^2 \sin^2\varphi + \beta^2 \cos^2\varphi}\, d\varphi.$$

In the neighborhood of the crack front, the stress and strain states are a combination of plane strain and anti-plane shear, and J_1 for homogenous and isotropic elastic solids can be expressed in terms of the stress intensity factors

$$J_1 = \frac{1-\nu^2}{E}\left(K_I^2 + K_{II}^2 + \frac{1}{1-\nu}K_{III}^2\right), \tag{5.26}$$

where E and ν represent the Young's modulus and the Poisson's ratio, respectively. Equation (5.26) can be rewritten in index notation as

$$J_1 = M_{\alpha\beta}K_\alpha K_\beta, \quad \text{where} \quad (M_{\alpha\beta}) = \frac{1-\nu^2}{E}\begin{pmatrix} 1 & 0 & 0 \\ 0 & 1 & 0 \\ 0 & 0 & \frac{1}{1-\nu} \end{pmatrix}. \tag{5.27}$$

The symmetric forms of the expressions for the stress intensity factors of an internal elliptical crack in a homogenous, isotropic and elastic material are (KASSIR & SIH 1966)

$$K_I = \sigma_{22}\sqrt{\frac{\beta}{\alpha}}\frac{\sqrt{\pi}\sqrt[4]{\alpha^2 \sin^2\varphi + \beta^2 \cos^2\varphi}}{E(k_1)}, \tag{5.28}$$

$$K_{II} = \frac{-\sqrt{\pi}\left((\sigma_{12}+\sigma_{21})\,B_{\mathcal{F}}\,\beta\,\cos\varphi + (\sigma_{23}+\sigma_{32})\,B_{\mathcal{H}}\,\alpha\,\sin\varphi\right)}{2\sqrt{\alpha^3\beta^3}\sqrt[4]{\alpha^2 \sin^2\varphi + \beta^2 \cos^2\varphi}},$$

$$K_{III} = \frac{(\nu-1)\sqrt{\pi}\left((\sigma_{12}+\sigma_{21})\,B_{\mathcal{F}}\,\alpha\,\sin\varphi - (\sigma_{23}+\sigma_{32})\,B_{\mathcal{H}}\,\beta\,\cos\varphi\right)}{2\sqrt{\alpha^3\beta^3}\sqrt[4]{\alpha^2 \sin^2\varphi + \beta^2 \cos^2\varphi}},$$

where α and β are the semi-major and semi-minor axes of the ellipse, respectively, φ is the geometric angle along the ellipse border, and

$$B_{\mathcal{F}} = \frac{\alpha\,\beta^2\,k_1^2}{\left((k_1^2-\nu)\,E(k_1) + \nu\,k_2^2 K(k_1)\right)}, \tag{5.29}$$

$$B_{\mathcal{H}} = \frac{\alpha\,\beta^2\,k_1^2}{\left((k_1^2+\nu\,k_2^2)\,E(k_1) - \nu\,k_2^2 K(k_1)\right)},$$

where $K(\bullet)$ and $E(\bullet)$ are the complete elliptical integrals of the first and second kind respectively, and σ_{ij} $(i,j=1,2,3)$ are the stress components in the local crack coordinates

(figure 5.5). Care should be taken that in the expression for K_I, the sign of σ_{22} is positive, hence to express it in a mathematically correct manner it should be multiplied with the Heaviside step function $H(\sigma_{22})$. This leads to a vanishing K_I for the pure cleavage mode, where the stress normal to the crack faces is compressive.

Substituting the expressions for the stress intensity factors and equations (5.25) into (5.24) and performing the requisite integration, the strain energy released (complementary energy) by a single elliptical crack in an infinite, homogeneous, isotropic solid in its pristine state is resulting (KASSIR & SIH 1966)

$$\psi^* = \frac{1}{V}\frac{4\pi\alpha\beta^2(1-\nu^2)}{3E}\left(G_{22}\sigma_{22}^2 + G_{12}\left(\frac{\sigma_{12}+\sigma_{21}}{2}\right)^2 + G_{23}\left(\frac{\sigma_{23}+\sigma_{32}}{2}\right)^2\right), \tag{5.30}$$

where

$$G_{22} = \frac{1}{E(k_1)}, \tag{5.31}$$

$$G_{12} = \frac{k_1^2}{(k_1^2-\nu)\,E(k_1)+\nu k_2^2 K(k_1)},$$

$$G_{23} = \frac{k_1^2}{(k_1^2+\nu k_2^2)\,E(k_1)-\nu k_2^2 K(k_1)},$$

$$k_1 = \sqrt{1-\frac{\beta^2}{\alpha^2}}, \quad k_2 = \frac{\beta}{\alpha}.$$

These results are identical to the ones derived on the basis of the self-consistent method given by BUDIANISKY & O'CONNELL (1976). The components of the fourth-rank compliance tensor attributed to the presence of a single elliptical crack are resulting from

$$\mathbb{S}_{ijmn} = \frac{\partial^2\psi^*}{\partial\sigma_{ij}\,\partial\sigma_{mn}}, \tag{5.32}$$

and considering equations (5.24)-(5.25), it results

$$\Delta\mathbb{S}_{ijmn}^{Crack} = \frac{\partial^2\psi^*}{\partial\sigma_{ij}\,\partial\sigma_{mn}} = \frac{1}{V}\int_0^r\left(\oint_c M_{\alpha\beta}\frac{\partial K_\alpha}{\partial\sigma_{ij}}\frac{\partial K_\beta}{\partial\sigma_{mn}}\,e_n\cdot e_r\,dl\right)dr \tag{5.33}$$

$$= \frac{1}{V}\int_0^\alpha\left(\int_0^{2\pi} M_{\alpha\beta}\frac{\partial K_\alpha}{\partial\sigma_{ij}}\frac{\partial K_\beta}{\partial\sigma_{mn}}\,\beta\,d\varphi\right)d\alpha.$$

In the local coordinate system of the ellipse, the expression for the compliance tensor attributable to the presence of a planar elliptical crack of semi-major and semi-minor axes

of α, β is derived by substituting relations (5.27)-(5.32) into (5.33) and performing the requisite integrations. The fourth-rank tensor of the change of compliance attributed to the presence of a single elliptical crack is

$$\begin{aligned}\Delta\mathbb{S}^{\text{Crack}} =& \Delta\mathbb{S}^{\text{Crack}}_{2222}\,(\mathbf{e}_2\mathbf{e}_2\mathbf{e}_2\mathbf{e}_2) + \\ & \Delta\mathbb{S}^{\text{Crack}}_{1212}\,(\mathbf{e}_1\mathbf{e}_2\mathbf{e}_1\mathbf{e}_2 + \mathbf{e}_2\mathbf{e}_1\mathbf{e}_2\mathbf{e}_1 + \mathbf{e}_1\mathbf{e}_2\mathbf{e}_2\mathbf{e}_1 + \mathbf{e}_2\mathbf{e}_1\mathbf{e}_1\mathbf{e}_2) + \\ & \Delta\mathbb{S}^{\text{Crack}}_{2323}\,(\mathbf{e}_2\mathbf{e}_3\mathbf{e}_2\mathbf{e}_3 + \mathbf{e}_3\mathbf{e}_2\mathbf{e}_3\mathbf{e}_2 + \mathbf{e}_2\mathbf{e}_3\mathbf{e}_3\mathbf{e}_2 + \mathbf{e}_3\mathbf{e}_2\mathbf{e}_2\mathbf{e}_3)\,,\end{aligned} \tag{5.34}$$

where

$$\Delta\mathbb{S}^{\text{Crack}}_{2222} = \frac{8\pi\left(1-\nu^2\right)}{3\,E}\,\frac{E\left(k_3\right)}{\left(E\left(k_1\right)\right)^2}\,\frac{\beta^3}{V}\,, \tag{5.35}$$

$$\Delta\mathbb{S}^{\text{Crack}}_{1212} = \frac{2\pi\left(1-\nu^2\right)\,k_1^2}{3\,E}\,\frac{\left(k_1^2-\nu\right)E\left(k_3\right)+\nu\,K\left(k_3\right)}{\left(\left(\nu-k_1^2\right)E\left(k_1\right)-\nu\,k_2^2\,K\left(k_1\right)\right)^2}\,\frac{\beta^3}{V}\,,$$

$$\Delta\mathbb{S}^{\text{Crack}}_{2323} = \frac{2\pi\left(1-\nu^2\right)\,k_1^2}{3\,E}\,\frac{\left(k_1^2-\nu\,k_2^2\right)E\left(k_3\right)-\nu\,K\left(k_3\right)}{\left(\left(k_1^2+\nu\,k_2^2\right)E\left(k_1\right)-\nu\,k_2^2\,K\left(k_1\right)\right)^2}\,\frac{\beta^3}{V}\,,$$

where the components of the compliance tensor satisfy the symmetry properties imposed by the symmetries of the stress and strain tensors, i.e $\mathbb{S}_{ijmn} = \mathbb{S}_{jimn} = \mathbb{S}_{ijnm} = \mathbb{S}_{mnij}$.

In terms of a general coordinates system, the tensor may be derived using the law of coordinate transformation

$$\mathbb{S}^{\text{Global}}_{ijmn} = R_{ir}\,R_{js}\,R_{mt}\,R_{nu}\,\mathbb{S}^{\text{Local}}_{rstu}\,, \tag{5.36}$$

where R_{ij} are the components of an orthogonal transformation matrix.

The expression for the compliance tensor attributable to the presence of a planar circular crack (KRAJCINOVIC 1996) can be reproduced from (5.34) in the limit case where $\alpha \to \beta$

$$\Delta\mathbb{S}^{\text{Crack}}_{2222} = \frac{8\left(1-\nu^2\right)}{3\,E}\,\frac{\alpha^3}{V}\,, \tag{5.37}$$

$$\Delta\mathbb{S}^{\text{Crack}}_{1212} = \Delta\mathbb{S}^{\text{Crack}}_{2323} = \frac{16\left(1-\nu^2\right)}{3\,E\left(3-\nu\right)}\,\frac{\alpha^3}{V}\,.$$

The structure of the resulting tensors indicate that the presence of an elliptical crack in a homogenous and isotropic volume element in its pristine state changes the type of the reflective material symmetry from isotropy to orthotropy, where the axes of orthotropy are aligned with the local coordinates of the ellipse. Considering the circular crack since $\mathbb{S}_{1212} = \mathbb{S}_{2323}$, the type of symmetry changes to a transversely isotropic one, where in the plane of the crack any vector is a normal to a plane of symmetry.

5.3.2 kinking of an internal elliptical crack

To study the degradation of the elastic material properties due to the kinking and growth of elliptical and/or circular microcracks, consider a single elliptical crack in an infinite, homogeneous, isotropic and elastic continuum subjected to mechanical loads applied at infinity. For a stress state outside the damage surface, the considered crack will kink and propagate to a new geometry, and the local kinking angle ϕ and the local crack extension length Δa can be calculated from the considered fracture criterion coupled with a fatigue crack evolution law. In an analogous manner to the previous section, this problem can be decomposed into two sub-problems: that of the continuum without a crack subjected to the remote traction field, and that of the same continuum, where only the crack faces are subjected to the traction field.

In the framework of linear elasticity, the compliance tensor of a material containing a kinked crack can be decomposed into three parts (SCHÜTTE & MOLLA-ABBASI 2007A)

$$\widetilde{\mathbb{S}} = \mathbb{S}^{\text{Matrix}} + \Delta\mathbb{S}^{\text{Crack}} + \Delta\mathbb{S}^{\text{Kink}}, \tag{5.38}$$

where $\mathbb{S}^{\text{Matrix}}$ and $\Delta\mathbb{S}^{\text{Crack}}$ refer respectively to the compliance tensor of the matrix material in its pristine state and the change of compliance due to the presence of the microcrack, and $\Delta\mathbb{S}^{\text{Kink}}$ is the change of compliance due to the kinking and growth of the microcrack with local kinking angle ϕ and local crack extension Δa.

The analytical expression for the tensor of the change of compliance due to the presence of a single active elliptical or circular microcrack was given in the previous section. In a similar way, the tensor of the change of compliance due to the kinking of a crack can be calculated from the contribution to the complementary strain energy corresponding to the kinking of the crack, which is the energy released during the kinking of the crack.

The rate of the change of the compliance tensor for a volume element V of elastic material, attributable to the extension rate $\dot{s}$, through which a point on the perimeter of a single crack kinks to a new position is given by (SCHÜTTE & MOLLA-ABBASI 2007A)

$$\dot{\mathbb{S}}^{\text{Kink}}_{ijmn} = \frac{\partial^2 \dot{\psi}^{**}}{\partial\sigma_{ij}\,\partial\sigma_{mn}} = \frac{1}{V}\frac{\partial^2 (G(s)\dot{s})}{\partial\sigma_{ij}\,\partial\sigma_{mn}}, \tag{5.39}$$

where ψ^{**} is the complementary energy associated with the kinking of the crack.

Integrating this along the crack perimeter, the rate of the change of compliance due to the growth of an internal crack is resulting

$$\dot{\mathbb{S}}^{\text{Kink}}_{ijmn} = \frac{1}{V}\oint_c \left(\frac{\partial^2 G(s)}{\partial\sigma_{ij}\,\partial\sigma_{mn}}\,\dot{s}\right) dl, \tag{5.40}$$

where $G(s)$ is the energy released during the kinking of crack with a local extension of s, and is given by

$$G(s) = \frac{1-\nu^2}{E}\left(K_I^2(s) + K_{II}^2(s) + \frac{1}{1-\nu}K_{III}^2(s)\right) = M_{\alpha\beta}\,K_\alpha(s)\,K_\beta(s), \tag{5.41}$$

with $K_\alpha(s)$ being the stress intensity factors at the propagated crack front, given by (see section 3.1.1)

$$K_\alpha(s) = K_\alpha^* + K_\alpha^{(1/2)}\sqrt{s} + O(s)\,, \tag{5.42}$$

and $M_{\alpha\beta}$ is given in (5.27). Unlike the case of a single elliptical crack, the stress intensity factors alone would not suffice to give the complementary strain energy corresponding to the kinking of the crack, and the analytical expressions for the T-stresses of the elliptical crack (prior to kinking) are required as well (see chapter 2 for the complete set of the T-stresses for mixed-mode internal elliptical and circular cracks in homogeneous, isotropic linear elastic solids).

Considering the expansion of the stress intensity factors in terms of the extension length and the crack tip parameters prior to kinking (see section 3.1.1), equation (5.40) can be rewritten as

$$\dot{S}_{ijmn}^{Kink} = \frac{1}{V}\oint_c M_{\alpha\beta}\left(\frac{\partial K_\alpha(s)}{\partial \sigma_{ij}}\frac{\partial K_\beta(s)}{\partial \sigma_{mn}}\dot{s}\right) dl\,, \tag{5.43}$$

with

$$\begin{aligned}\frac{\partial K_\alpha(s)}{\partial \sigma_{ij}} &= \frac{\partial\left(F_{\alpha\lambda}(\phi)\,K_\lambda + G_{\alpha\lambda}(\phi)\,T_\lambda\sqrt{s}\right)}{\partial \sigma_{ij}} \\ &= F_{\alpha\lambda}(\phi)\frac{\partial K_\lambda}{\partial \sigma_{ij}} + G_{\alpha\lambda}(\phi)\frac{\partial T_\lambda}{\partial \sigma_{ij}}\sqrt{s}\,,\end{aligned} \tag{5.44}$$

where K_α and T_α are the stress intensity factors and the T-stresses of the crack prior to propagation, and $F_{\alpha\beta}(\phi)$ and $G_{\alpha\beta}(\phi)$ are universal functions in terms of the kinking angle ϕ.

The local propagation rate $\dot{s}$, measured in the direction normal to the crack front at a considered point, can be calculated using a fatigue crack evolution law coupled with the selected fracture criterion. For example considering the modified Paris' law given by equation (3.20) in combination with the fracture criterion of maximum driving force (equation (3.13)), and setting a threshold value for crack growth, it results (SCHÜTTE 2001)

$$\dot{s} = \frac{ds}{dN} = C\left(\sqrt{G^*} - \sqrt{G_{th}}\right)^\eta\,, \tag{5.45}$$

where C and η are material constants, N represents the number of load cycles, G^* is the maximum driving force acting at the kinked crack tip, and G_{th} is the threshold value, below which there is no damage growth. Here, the threshold value G_{th} is considered to take into account the load history and is varying by crack growth. Indeed, its value is decreasing by damage growth for brittle and quasi-brittle materials.

The expression for the fourth-rank tensor of the rate of the change of compliance due to the kinking of an elliptical crack with a local growth rate $\dot{s}$ is derived by substituting

relations (5.44) and (5.45) into (5.43), and performing the requisite integration along the crack front in the following form

$$\dot{\mathbb{S}}^{\text{Kink}}_{ijmn} = \frac{1}{V}\int_0^{2\pi} M_{\alpha\beta}\sqrt{\alpha^2\sin^2\varphi + \beta^2\cos^2\varphi} \tag{5.46}$$
$$\left\{ F_{\alpha\lambda}F_{\beta\mu}\frac{\partial K_\lambda}{\partial\sigma_{ij}}\frac{\partial K_\mu}{\partial\sigma_{mn}} + \right.$$
$$\left(F_{\alpha\lambda}G_{\beta\mu}\frac{\partial K_\lambda}{\partial\sigma_{ij}}\frac{\partial T_\mu}{\partial\sigma_{mn}} + G_{\alpha\lambda}F_{\beta\mu}\frac{\partial T_\lambda}{\partial\sigma_{ij}}\frac{\partial K_\mu}{\partial\sigma_{mn}}\right)\sqrt{s} +$$
$$\left. G_{\alpha\lambda}G_{\beta\mu}\frac{\partial T_\lambda}{\partial\sigma_{ij}}\frac{\partial T_\mu}{\partial\sigma_{mn}}s\right\}\dot{s}\,d\varphi\,,$$

where the T_α and K_α are given in equations (2.51) and (5.28), respectively.

The expression for the compliance tensor corresponding to the kinking of a planar circular crack can be obtained from (5.46) in the limit case where $\alpha \to \beta$. It should be noted that for the growing crack problem, it is not possible to give a closed form solution for the compliance tensor attributable to the kinking of a crack, since depending on the crack problem and the resulting mode-mixity, the kinking angle ϕ and the propagation rate $\dot{s}$ change. Hence for each crack problem integral (5.46) should be solved individually.

5.4 A fracture based anisotropic continuum damage model

It is known from experiments that most materials, and in more special case brittle and quasi-brittle materials, under general loading conditions develop anisotropic damage (KRAJCINOVIC & FONSEKA 1982), for which damage variable can no longer be expressed as a scalar. The micromechanical approach of modeling the evolution of the damage in brittle and quasi-brittle materials consists of studying the growth of a single crack or material defect, and at the continuum level, modeling is obtained by applying the homogenization technique to an ensemble of cracks or defects. A given stress state causes the opposite faces of cracks and defects to open, slide or close, resulting a change in the material stiffness. A way to model the anisotropic damage is to consider the influence of the kinking and growth of microcracks on the stiffness of the material at the mesoscale (KRAJCINOVIC 1996). For a stress state outside the damage surface, materials accumulate additional damage through the growth of the microcracks and the material defects, which generally happens in a kinking manner.

Analytical formulation of the interaction of microcracks and microdefects, in general, is a difficult task. This becomes almost impossible for propagating cracks, due to the overwhelming complexity of the physical phenomena reflecting the growth and the interaction of the microcracks. Some limited solutions have been proposed for very specific case, such as two parallel elliptical cracks in an infinite solid subjected to tension (ISIDA & ET AL. 1984), and plates containing random array of cracks (ISIDA 1970).

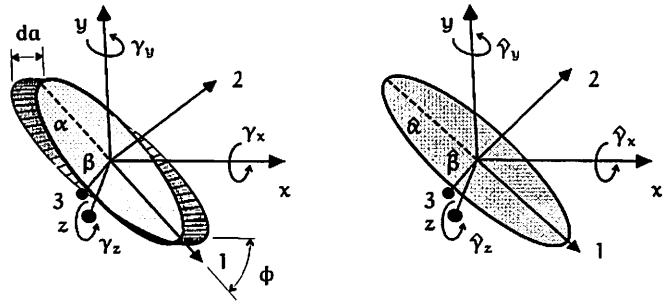

Figure 5.6: kinked crack and its equivalent elliptical crack

However, the proposed solutions are not always analytical, and some of them are empirical formulae (MURAKAMI 1987).

Based on the hypothesis of statistical homogeneity and weak interaction of microcracks, and in more general case microdefects, which is reasonable for a modest distribution of heterogeneities (NEMAT-NASSER & HORI 1993), the first step in the formulation of the proposed damage model requires the formulation of the change of continuum elastic properties due to the presence, kinking and growth of elliptical and/or circular microcracks. In the previous section, based on the assumption of noninteracting cracks, the effect of a single mixed-mode elliptical crack and its kinking on the effective elastic properties of materials was formulated in an analytical manner. After the kinking of the initial cracks, however, mathematical formulation of the next kinking steps is no longer possible. To overcome this difficulty in the formulation of a damage model, which accounts for the kinking and growth of microcracks in a mathematical traceable way, the concept of an equivalent elliptical crack may be considered. In this regard, a kinked crack is replaced with an equivalent elliptical crack in a thermodynamically consistent manner, resulting equivalent dissipation of energy and equivalent damage induced anisotropy. Basically, eight degrees of freedom can be considered for each equivalent elliptical microcrack replacing the kinking one. These are the major and minor axes of the ellipse (2 unknowns), orientation of the microcrack given by three Eulerian rotation angles (3 unknowns), and the position of the crack in the space (3 unknowns). Considering the concept of the unit cell and assuming that the microcrack is located in the center of the cell, the position of the microcrack can be considered a priori known (fixed) and be left out of the formulation.

To calculate the other five unknowns characteristics of the equivalent crack, i.e. the geometry and orientation of the equivalent crack, different postulates may be considered. SCHÜTTE (2001) has proposed a damage model based on a two-dimensional equivalent straight crack, where the number of degrees of freedom in his model reduces to two. These are the crack length, and its orientation about its center. He has considered different possibilities to find the rotation and the geometry of the equivalent replacement crack

- equivalent stress intensity factors $\hat{K}_\alpha = K^*_\alpha$,
- equivalent driving forces $\hat{G} = G^*$,
- equivalent mode-mixities $\hat{\lambda} = \lambda^*$,
- equivalent propagation rates $\dot{\hat{a}} = \dot{a}^*$,
- equivalent dissipations,

where quantities with a hat indicate the ones corresponding to the equivalent replacement crack. His damage model is based on the assumptions of equivalent propagation rates combined with equivalent dissipations, resulting the length of the equivalent crack and its orientation, respectively.

Considering the anisotropic nature of damage in the three-dimensional stress state and the postulate of equivalent dissipations, the following postulates may be proposed further

- equivalent damage induced anisotropy, and
- equivalent change of compliance tensors $\Delta\hat{\mathbb{S}}^{\text{Crack}}_{ijmn} = \Delta\mathbb{S}^{\text{Crack}}_{ijmn} + \Delta\mathbb{S}^{\text{Kink}}_{ijmn}$.

In this work, the equivalent replacement crack model is based on the postulates of equivalent dissipations and equivalent damage induced anisotropy. The geometry and the orientation of the equivalent elliptical crack replacing the kinked one then result considering two optimization problems. The first problem takes into account the fact that the local damage associated with a single planar elliptical crack results in an orthotropic material symmetry, thus it can be argued that changing the type of material symmetry from isotropy to orthotropy may imply the existence of local damage due to an elliptical crack. In section 4.2, it was shown that the damage associated with the growth of a mixed-mode elliptical or circular crack also changes the virgin isotropic material into approximately orthotropic one. Thus it is deduced that the orientation of the equivalent crack replacing the kinked one is such that the resulting orthotropy axes are aligned with the ones due to the damage associated with the kinked crack. It is reminded that for a single elliptical crack in an initially isotropic material, the axes of orthotropy are aligned with the axes of the ellipse, i.e. two axes of orthotropy are aligned with the major and minor axes of the ellipse and the third one is the normal to the plane of the ellipse. The second optimization problem results in the geometry of the equivalent elliptical crack in the sense that the components of the change of compliance due to the kinked crack and the equivalent crack are approximately identical. Such a formulation of the dissipative damage process due to kinking elliptical microcracks, taking into account the damage induced orthotropy of an elliptical crack in a local sense, results in a consistent damage model capturing the load history through the local orthotropic degradation of the mechanical properties.

The proposed continuum damage model based on the reduction of stiffness due to the kinking of equivalent elliptical microcracks results the effective elastic properties of a damaged material volume element in a completely analytical and consistent way. Based on the incremental analysis of the effective elasticity tensor for the given cur-

rent values of the local stress and strain tensors, and taking the load history into account by introducing the concept of an equivalent elliptical crack, the propagation of microcrack is calculated by considering a crack evolution law. In this study, the propagation of microcracks is governed by the modified Paris' law given by equation (3.20) coupled with the fracture criterion of maximum driving force given by equation (3.13) (LE, SCHÜTTE & STUMPF 1999).

5.4.1 optimization subroutines

As mentioned in the previous section, based on the assumption of equivalent damage induced anisotropy, here orthotropy, the orientations of the equivalent crack are resulting. For this the optimization procedure addressed in section 4.2 is considered again, in the sense that the appropriate orthogonal rotation is calculated which results in the best orthotropic representation of the compliance tensor corresponding to the damage due to the kinked crack. Considering the transformation law for fourth-rank tensors, one possible way is considering the following optimization procedure which looks for the best Eulerian rotation angles minimizing the non-orthotropic components of the corresponding compliance tensor

$$\mathcal{F}_1 = \sum_{i,j,m,n}^{non.ORT} \left(\mathbb{S}'_{ijmn}\left(\mathbf{R}(\gamma_x, \gamma_y, \gamma_z)\right)\right)^2 \tag{5.47}$$

$$= (\mathbb{S}'_{1213})^2 + (\mathbb{S}'_{1223})^2 + (\mathbb{S}'_{1323})^2 + \sum_{i=1}^{3} (\mathbb{S}'_{ii12})^2 + (\mathbb{S}'_{ii23})^2 + (\mathbb{S}'_{ii13})^2 ,$$

$$\mathbf{R}^{ORT}(\hat{\gamma}_x, \hat{\gamma}_y, \hat{\gamma}_z) = \arg\min \left\{ \mathcal{F}_1(\mathbf{R}) \,\middle|\, \det \mathbf{R} = 1,\ \mathbf{R}^T = \mathbf{R}^{-1} \right\} ,$$

$$\Rightarrow \quad \mathbb{S}^{ORT}_{ijmn} = ORT\left\{ \mathbb{S}'_{ijmn}\left(\mathbf{R}^{ORT}\right) \right\} ,$$

$$\text{where} \quad \mathbb{S}'_{ijmn} = R_{ir}\, R_{js}\, R_{mt}\, R_{nu}\, \mathbb{S}_{rstu} ,$$

where $\mathbf{R}$ is an orthogonal transformation including all rotations about the three cartesian axes ($\mathbf{R}(\gamma_x, \gamma_y, \gamma_z)$), figure 5.6, and $\mathbb{S}$ and $\mathbb{S}'$ are the compliance tensors in the considered global coordinate system and the local orthotropic coordinate system, respectively.

The geometry of the equivalent crack is resulting from the postulate of equivalent tensors for the change of compliance. This is done by a direct comparison of the change of compliance tensors associated with the damages due to the kinked crack and due the equivalent elliptical crack, given with respect to a known coordinate system (local coordinates of the equivalent crack may be a good choice). In this regard, the following

given: $\begin{cases} \Delta\varepsilon^{n+1}, \varepsilon^n, \sigma^n \\ \alpha^n, \beta^n, \gamma_x^n, \gamma_y^n, \gamma_z^n \end{cases}$

- map σ^n to the local crack coordinate system
- check for damage/crack growth $G^* > G_{th}$.
- continue in case of damage growth
- calculate the propagation of crack with the help of a crack evolution law coupled with a fracture criterion, i.e obtaining the functions $\Delta a(\varphi)$ and $\phi(\varphi)$
- calculate the compliance tensors attributable to the presence and kinking of the current elliptical crack with $\alpha^n, \beta^n, \gamma_x^n, \gamma_y^n, \gamma_z^n$, through equations (5.34) and (5.46)
- first optimization algorithm resulting the orientation of the equivalent elliptical crack, $\gamma_x^{n+1}, \gamma_y^{n+1}, \gamma_z^{n+1}$, through equation (5.47)
- second optimization algorithm resulting the geometry of the equivalent elliptical crack, $\alpha^{n+1}, \beta^{n+1}$, through equation (5.48)
- update the stiffness matrix C^{n+1} and the stress state σ^{n+1}

Table 5.1: algorithm for a consistent fracture based continuum damage model

optimization problem should be solved

$$\mathcal{F}_2 = \sum_{i,j,m,n}^{3} \left(\hat{\mathbb{S}}_{ijmn}\left(\hat{\alpha}, \hat{\beta}\right) - \mathbb{S}_{ijmn}^{ORT}\right)^2 , \tag{5.48}$$

$$\left\{\hat{\alpha}, \hat{\beta}\right\} = \arg\min\left\{\mathcal{F}_2 \middle| \hat{\alpha} \geq \alpha_o, \hat{\beta} \geq \beta_o\right\} ,$$

where $\hat{\mathbb{S}}$ is the tensor of the change of compliance due to the equivalent elliptical crack with an aspect ratio of $\hat{\lambda} = \hat{\beta}/\hat{\alpha}$, the components of which are given in the local crack coordinates in equation (5.34), and α_o and β_o are the semi-major and semi-minor axes of the elliptical crack prior to kinking.

The proposed continuum damage model based on the reduction of stiffness due to kinking elliptical microcracks can be easily implemented in a finite element code. In the incremental formulation, to have a more stable algorithm and for a faster convergence, the tangent stiffness of the damage material should be introduced, the so called algorithmic tangent (SIMO & TAYLOR 1986). The algorithm of the proposed damage model based is summarized in table 5.1 in an incremental manner.

The proposed damage model can also capture the unilateral effect observed in tension-compression tests, observed for a certain classes of materials including ceramics and concrete (BROUTMAN, KRISHNAKUMAR & MALLICK 1970), (HORIBE 1990), provided

that for a passive crack the corresponding components of the compliance components are recovered, and they return to their degraded state upon the activation of the crack. To see if the state of a crack is passive or active, a criterion based on the stress or strain state may be considered. CHABOCHE (1988) has proposed both strain based and stress based methods as activation and deactivation criteria. According to the strain based criterion, the damage can be considered as fully active if the normal strain associated to that direction1 is positive. This criterion holds true only under uniaxial compression and tension, where the crack plane is perpendicular to the loading, and cannot be considered for multi-axial stress state. Under multi-axial state of stress with increasing confining stress, the active damage due to positive normal strain would lead to an erroneous result. The stress based crack closure criterion can be defined using the normal traction to the plane of the crack. According to this criterion, a crack becomes active if the corresponding normal stress to its plane is positive.

The criterion considered here is based on the fact that a closed crack can still kink due to the influence of mode-II and III crack deformations. According to this criterion, if the mode I deformation of a crack vanishes, it may still be considered as an active crack if the effect of mode-II and III deformations can overcome the energy barrier needed for crack kinking, and else it is a passive crack. In both cases, it should be checked, which components of the compliance tensor are recovered and which ones are influenced by the damage. It is reminded that in this work, the effect of friction for a closed crack is considered to be negligible.

5.5 Numerical examples

The proposed continuum damage model, based on the reduction of stiffness due to kinking elliptical microcracks can be easily implemented in a finite element code. This has been performed here in the commercial finite element analysis software *Ansys* as a user material subroutine.

In the following sections, a variety of numerical examples is presented. The first two examples are illustrative examples, which explain the proposed model in a fully analytical manner. The first example addresses the determination of the equivalent crack after a single kink step. As the second example, a unit cell damaged by a single mixed-mode circular crack is subjected to four stages of cyclic loadings with changing directions. With this, the degradation of the material properties and the evolution of the considered damage parameters are presented. This example is especially important, since it provides the reader with the details of the irreversible damage process due to growing microcracks subjected to cyclic loading with changing directions. The third example shows the mesh sensitivity of the model. The objective of the other examples is to show the applicability of the proposed model to real components subjected to fatigue conditions. This is performed by calibrating the model at the first step. For this, the results of two fatigue experiments conducted by JEELANI & MUSIAL (1986) have been considered. These experiments

ultimate tensile strength (MPa)	yield strength (MPa)	shear strength (MPa)	fracture toughness (MPa$\sqrt{m}$)	Poisson's ratio	Young's modulus in tension (MPa)	Young's modulus in tension (MPa)	shear modelus (MPa)
1232	1036	756	162	0.32	203,000	203,000	77,000

Table 5.2: mechanical properties of AISI 4130 steel

enable one to estimate a domain for the constants in the proposed damage model. To check if the calibrated model leads to valid results, it is then applied to study the evolution of damage leading to final failure by considering two other experiments chosen from (JEELANI & MUSIAL 1986).

All experiments are conducted on AISI 4130 steel with the mechanical properties and the chemical composition given in tables 5.2 and 5.3, respectively (HUDSON & FERRAINOLO 1991), (JEELANI & MUSIAL 1986), except the first illustrative example, which for comparison purposes the mechanical properties are chosen to be the same as the ones considered in chapters 3 and 4.

5.5.1 example-1

The objective of this section is to explain the proposed continuum damage model by giving an illustrative example in a fully analytical manner. The considered crack problem is the circular crack presented in chapters 3, 2 and 4, i.e. $\gamma_z = 45°$ and $\gamma_x = \gamma_y = 0°$. The loading level is $\sigma^\infty/E = 1/1000$, the Poisson's ratio $\nu = 1/3$, and the initial crack size is considered to be $\alpha_o/L = 1/150$ with L being the characteristic length of the volume element.

To avoid more complexity, it is assumed that the stress state is outside the damage surface, thus the considered circular microcrack will propagate, and at this step due to simplicity purposes, the Wöhler's limit stress is assumed to be negligible. The first step in the model is calculating the propagation of the crack under the given local stress state, which is resulting from a crack evolution law, e.g. Paris' law, coupled with a fracture

Fe	C	Mn	P	S	Si	Cr	Mo
balance	0.305	0.500	0.035	0.04	0.275	0.950	0.20

Table 5.3: chemical composition of AISI 4130 steel (wt %)

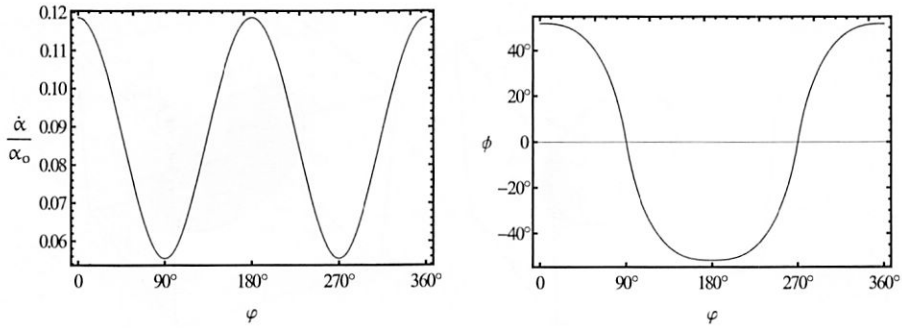

Figure 5.7: circular crack: propagation parameters along the crack front

criterion, e.g. maximum driving criterion which is considered in this work. Considering equations (3.20) and (3.13), the rate of crack growth is

$$\dot{\alpha} = C\left(\sqrt{G^*}\right)^{\eta}, \tag{5.49}$$

where C and η are the Paris' parameters. For clarity purposes, the propagation of the crack is exaggerated by selecting these parameters as $C = 0.01$ and $\eta = 2$. This and the considered loading level and material parameters result in crack extension length of approximately 12% of initial crack radius α_o. The propagation parameters, i.e. the extension length and the kinking angle are resulting as functions of the geometrical angle φ along the crack front. Figure 5.7 gives the distributions of these parameters along the crack front, and with these the new crack geometry is resulting (figures 5.9-left).

The next step is to calculate the influence of crack growth on the compliance tensor through relations (5.37), (5.46). These result in the effective compliance tensor modified by the damage due to the propagated circular crack. In six-dimensional tensorial notation,

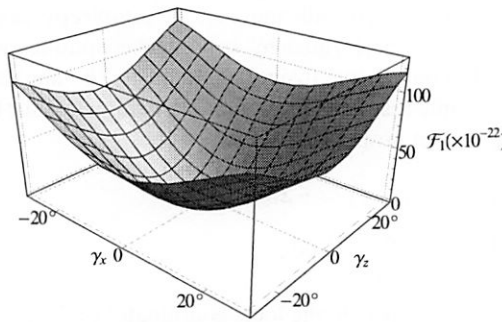

Figure 5.8: target function in the optimization algorithm

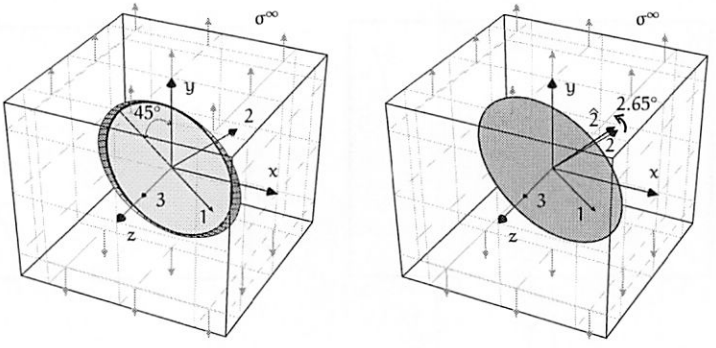

Figure 5.9: growth of the circular crack and its equivalent elliptical crack

normalizing the components of the compliance tensor with the tensile compliance component of the pristine material $1/E$, and the factor $(\alpha/L)^3$, where α and L are respectively the characteristic size of the crack and the length of the unit cell, results in:

$$\Delta\mathbb{S}_C = \frac{1}{E}\left(\frac{\alpha_o}{L}\right)^3 \begin{pmatrix} 0.05270 & 0.01853 & -0.00338 & 0.18844 & 0 & 0 \\ 0.01853 & 5.57268 & 0.00920 & 0.29881 & 0 & 0 \\ -0.00338 & 0.00920 & 0.01928 & 0.00743 & 0 & 0 \\ 0.18844 & 0.29880 & 0.00743 & 3.79581 & 0 & 0 \\ 0 & 0 & 0 & 0 & 3.59953 & 0.12201 \\ 0 & 0 & 0 & & 0.12201 & 0.03956 \end{pmatrix} . \tag{5.50}$$

To find the equivalent elliptical crack which replaces the propagated crack, it suffices to perform two further steps. The first step is finding the axes of orthotropy due to the damage induced by crack growth which can be deduced as the local coordinates of the equivalent crack. The second step is to find the geometry of the equivalent crack, the local axes of which are aligned with the axes of orthotropy calculated at the previous step. These two steps are performed by solving the optimization problems, given by equations (5.47) and (5.48), respectively (figure 5.8). The application of this procedure to the considered example results in the following parameters for the equivalent elliptical crack replacing the current propagated crack

$$\hat{\gamma}_x \simeq 0^\circ\,, \quad \hat{\gamma}_y \simeq 0^\circ\,, \quad \hat{\gamma}_z \simeq -2.65^\circ\,, \tag{5.51}$$
$$\frac{\hat{\alpha}}{\alpha_o} = 1.14755\,, \quad \frac{\hat{\beta}}{\beta_o} \simeq 1.00\,,$$

where $\hat{\gamma}$'s are given with respect to the local coordinates of the crack prior to propagation. The resulting local Eulerian angles result in the best approximate orthotropic representation of tensor (5.49), which is indeed given in the local coordinate system of the equivalent

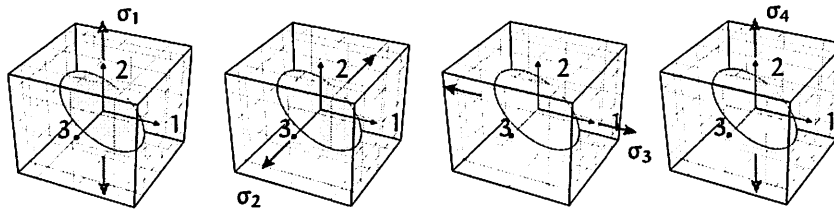

Figure 5.10: order of the considered sequential loading

elliptical crack replacing the propagated one

$$\Delta\widehat{\mathbb{S}}_C^{ORT} = \frac{1}{E}\left(\frac{\alpha_o}{L}\right)^3 \begin{pmatrix} 0.04412 & 0.00708 & -0.0033 & 0 & 0 & 0 \\ 0.00708 & 5.60415 & 0.00966 & 0 & 0 & 0 \\ -0.0033 & 0.00966 & 0.01928 & 0 & 0 & 0 \\ 0 & 0 & 0 & 3.77292 & 0 & 0 \\ 0 & 0 & 0 & 0 & 3.60319 & 0 \\ 0 & 0 & 0 & & 0 & 0.03590 \end{pmatrix}, \tag{5.52}$$

5.5.2 example-2

The objective of this example is to provide a better insight to the irreversible process of brittle damage in a local sense. For this a representative volume element of AISI 4130 steel is considered which embeds a single circular crack. The circular crack in its initial configuration has an inclination angle of 45° with respect to the 2-axis (figure 5.10). The initial size of the crack is considered to be L/500, L being the characteristic size of the unit cell. The mechanical properties of the matrix material in its pristine state are given in table 5.2, and the constants in the modified Paris' equation (3.20) are chosen as $C = 10^{-5}$ and $\eta = 2$.

stage 1		stage 2		stage 3		stage 4	
stress σ_1 (MPa)	cycles N_1	stress σ_2 (MPa)	cycles N_2	stress σ_3 (MPa)	cycles N_3	stress σ_4 (MPa)	cycles N_4
1500	100,000	1400	100,000	1350	100,000	1450	100,000

Table 5.4: characteristics of the applied sequential loading

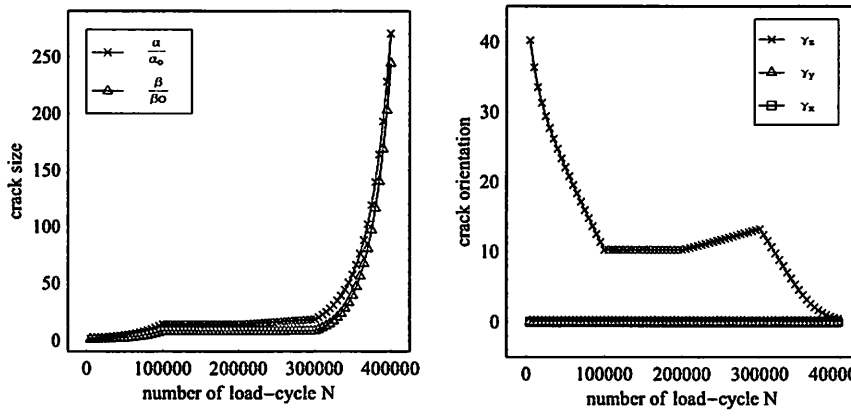

Figure 5.11: evolution of the geometry and the orientations of the equivalent elliptical crack

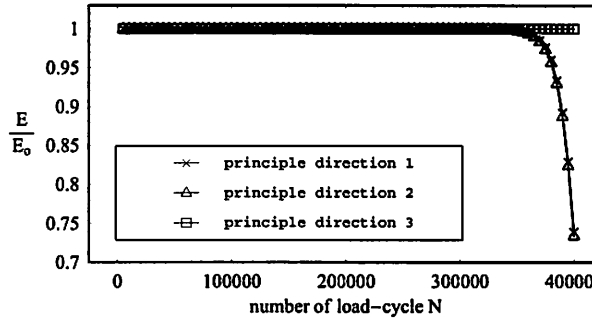

Figure 5.12: evolution of the stiffness components in the principle directions

To study the local degradation of the considered material under fatigue conditions with the help of the proposed model, the unit cell is subjected to four stages of cyclic loading as presented in table 5.4 and figure 5.10. In the load stage 1, a stress of 1500 (MPa) is applied in the direction of 2-axis for 100,000 cycles, and in the subsequent stages the direction of the applied stress is parallel to the 3-axis, 1-axis, and 2-axis, respectively. The applied stresses are 1400 (MPa), 1350 (MPa), 1450 (MPa) and the corresponding number of cycles are the same as for the stage 1.

The proposed optimization subroutines are solved at each load increment, in order to calculate the geometry and the rotation of the equivalent elliptical crack replacing the kinked one. Figure 5.11 shows the evolution of the geometrical parameters and the orientation of the equivalent elliptical crack with respect to the number of cycles. It is observed

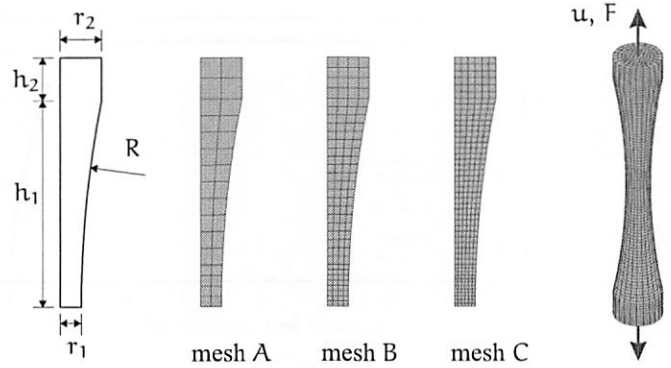

Figure 5.13: specimen geometry and different mesh patterns

that up to approximately 300, 000 loading cycles, the evolution of the corresponding damage is relatively smooth, and at this moment application of the load stage 4 accelerates the accumulation of damage.

To explain this, lets review each load stage separately. The load stage 1, is identical to the propagation of the circular crack presented in chapters 3, 4. It was observed that by crack growth, the equivalent elliptical crack rotates to become perpendicular to the direction of σ_1. This is more evident in figure 5.11-right, where at $N = 100,000$ the equivalent crack has an inclination of approximately $\gamma_z = 10°$ with direction-1. Changing the load to the load stage 2 results in no observable damage accumulation in the material, because at this stage, the equivalent crack is parallel to σ_2. Hence, very small changes in the presented parameters are induced, which due to the scaling of the curves is not observable. The load stage 3, similar to the load stage 2 has small contribution to the process of damage growth, since at this stage, plane of the crack is inclined nearly 10° with respect to the direction of σ_3 (identical to the direction-1). This small angle induces a relatively small normal stress on the plane of the equivalent crack, leading to a relatively small driving force along the crack front, which consequently results in a slow propagation of the crack. This is observed between cycles 200, 000 and 300, 000 in figure 5.11, as γ_z grows again bigger. At the end of this stage, γ_z has reached a value of approximately 15°. Application of the load stage 4, however, accelerates the propagation of the crack, since at this stage the orientation of the equivalent crack is such that the local normal stress acting on the plane of the crack induces a strong driving force on the crack front. As can be deduced from figure 5.11, the dimensions of the crack evolve very fast to damage the whole material volume.

Figure 5.12 shows the degradation of the stiffness components in the principle loading directions. It is observed that at the end of the load stage 4, the stiffness in direction-3 does not show a considerable change, while in directions 1 and 2, the degradation of stiffness is obvious.

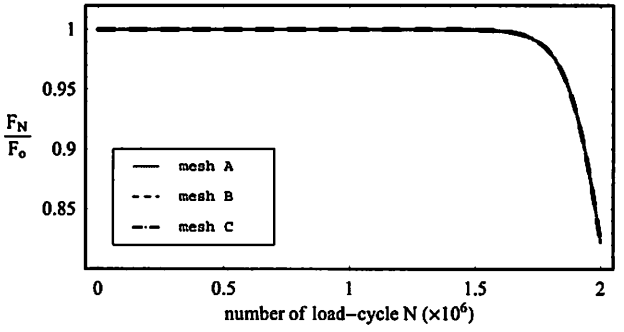

Figure 5.14: load-cycle curves for different mesh patterns

5.5.3 mesh sensitivity

The objective of this example is to show the degree of the mesh dependency for the proposed damage model. For this, the specimen of the form given in figure 5.13 is considered, where

$$r_1 = 10\,\text{mm}, \quad r_2 = 20\,\text{mm}, \quad h_1 = 100\,\text{mm}, \quad h_2 = 20\,\text{mm}, \quad R = 505\,\text{mm}.$$

Displacement controlled analyses have been performed for different discretization levels (figure 5.13), where a constant displacement with the magnitude of 2% of the specimen's initial length $h_1 + h_2$ is applied for 2,000,000 cycles. All models are meshed with the help of hexahedral elements with quadratic displacement behavior. Considering mesh pattern A, 48 hexahedral elements are generated, and mesh patterns B and C result in 384 and 1728 elements, respectively. The corresponding constants of the damage model are chosen as $\eta = 2, C = 7.39 \times 10^{-9}$. The resulting force-cycle curves for these experiments are given in figure 5.14, where F_N and F_o are the resultant forces at the end cross section of the specimen (r_2), which correspond respectively to the current load-cycle and the initial load-cycle. The good agreement between the results corresponding to different discretization levels demonstrate the mesh independency of the model. This is due to the fact that in the considered fatigue microcrack evolution law, the rate of the driving force is not appearing.

5.5.4 calibration and validation of the model

The aim of the presented examples here is to show the applicability of the proposed model to real components subjected to fatigue conditions. This is performed by calibrating the model at the first step. For this two experiments are considered. It is then checked if the calibrated model leads to valid results by considering two other experiments.

For the calibration and validation of the model, the cumulative fatigue data of the experiments conducted by JEELANI & MUSIAL (1986) have been considered. These experiments enable one to estimate a domain for the material constants in the proposed damage model, leading to valid results for all the considered experiments. For this, the specimen of the form given in figure 5.15 has been considered, where

$$r_1 = 2.5\,\text{mm}, \quad r_2 = 20\,\text{mm}, \quad h_1 = 45\,\text{mm}, \quad h_2 = 2.5\,\text{mm}, \quad R = 70\,\text{mm}.$$

The laboratory experiments have been conducted on AISI 4130 steel to generate cumulative fatigue data. The tests have been performed in four stages (JEELANI & MUSIAL 1986). In the first, second and third stages, the loads and the number of cycles applied at each load stage have been predetermined. In the fourth stage, the load has been preselected and the experiment has been continued until the final failure of the specimen. Tests have been conducted with low-to-high, low-to-high-mixed, high-to-low and high-to-low-mixed stress sequences. All the experiments have been conducted in the elastic range. For more details on these experiments, the reader is referred to JEELANI & MUSIAL (1986).

In order to calibrate and validate the proposed damage model, four experiments have been chosen from (JEELANI & MUSIAL 1986), where for all experiments the stress ratio is $R = 0$. These are given in tables 5.5 and 5.6, where the first set of data (table 5.5) is considered to calibrate the model and the second set (table 5.6) is applied for the validation of the calibrated model. All models are meshed with the help of hexahedral elements with quadratic displacement behavior, and the considered degree of mesh refinement leads to 1539 elements. For each experiment, at each stage of loading the specimen is subjected to a surface load of the amplitude $F = \bar{\sigma} A$, where $A = \pi r_2^2$, and r_2 is the bigger radius of the specimen (figure 5.15).

In order to calibrate the model, by considering different values for the constants in the damage model the cumulative fatigue data corresponding to the first two experiments presented in table 5.5 are generated. This gives a domain for the constants in the proposed damage model. Fitting the resulting damage data from the model to the experiments

test Nr	stage 1		stage 2		stage 3		stage 4	
	stress (MPa)	cycles	stress (MPa)	cycles	stress (MPa)	cycles	stress (MPa)	cycles to failure
1	455	635,800	595	232,300	700	5,500	750	11,000
2	490	467,200	630	189,200	560	289,000	770	82,400

Table 5.5: calibration of the model: cumulative fatigue data for the stress ratio of 0

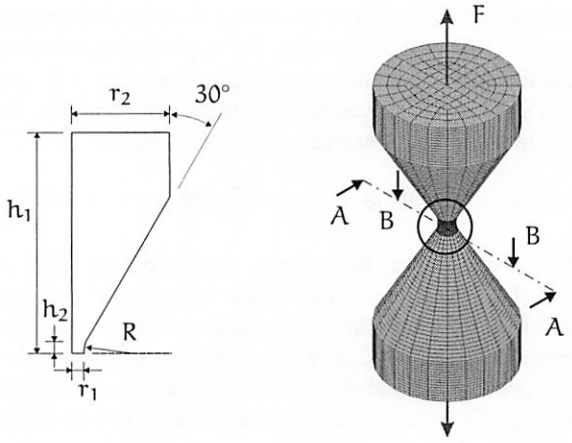

Figure 5.15: geometry of the specimen and its discretization

results in the following material parameters for these experiments

$$\eta = 2.18\,, \qquad C = 1.73 \times 10^{-9}\,.$$

The next step is to validate the resulting fatigue parameters. This is performed by considering the fatigue data of experiments 3 and 4 given in table 5.6. To see if these parameters lead to valid results, the corresponding model for each experiment is loaded by the first three load stages, and at the final step it is loaded with the load stage 4 and the required number of load cycles to final failure are determined. This is given in the last row of table 5.6, where the resulting number of cycles to final failure from the model are in good agreement with the experimental data. The maximum deviation is nearly 3.6%, which for application purposes is acceptable.

Figures 5.16, 5.18, 5.20, 5.22 show the applied loading and the resulting elongation

test Nr	stage 1		stage 2		stage 3		stage 4		
	stress (MPa)	cycles	stress (MPa)	cycles	stress (MPa)	cycles	stress (MPa)	cycles to failure	
								experiment	model
3	700	32,500	630	189,200	560	89,000	490	682,300	657,800
4	770	1,900	630	108,200	700	29,500	560	647,300	629,500

Table 5.6: validation of the parameters: cumulative fatigue data for the stress ratio of 0

with the number of loading cycles corresponding to each experiment, respectively. $\Delta l = 2\,\Delta h_l$ is the elongation of the specimen in the direction of the applied load F. For all experiments, it is observed that at some point in the final stage of loading, the elongation Δl increases very fast. This corresponds, indeed, to the final failure of the specimen. The analysis is interrupted when the elongation has reached 6% of the initial specimen's length $2\,h_l$, as the proposed model is no longer valid in the presence of big plastic deformations at the macroscopic crack tip.

Figures 5.17, 5.19, 5.21, 5.23 show different views of the state of damage in the neck cross section (the weakest cross section) of the specimen at the end of each load stage (figure 5.15-right: views A – A and B – B). Here, 0 corresponds to the pristine state and 1 represents the fully damaged state.

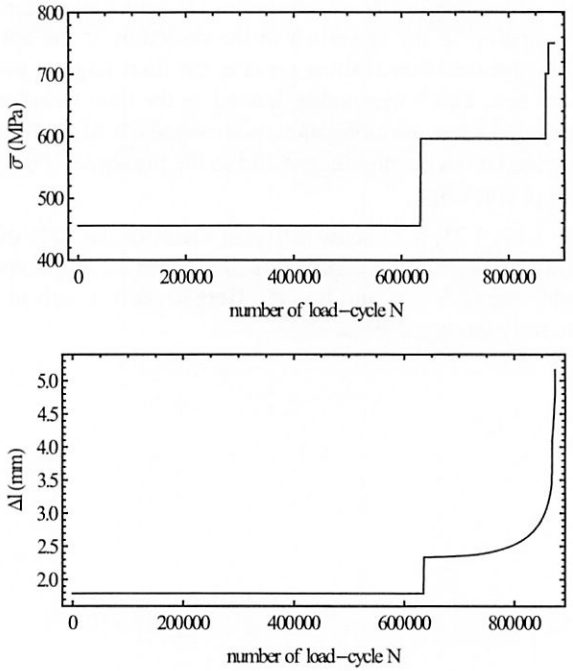

Figure 5.16: experiment 1: stress-cycle and elongation-cycle curves

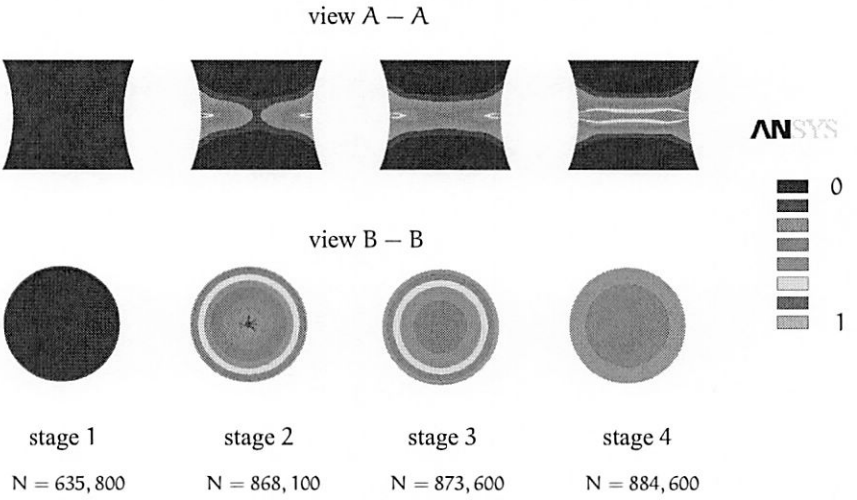

Figure 5.17: experiment 1: evolution of damage

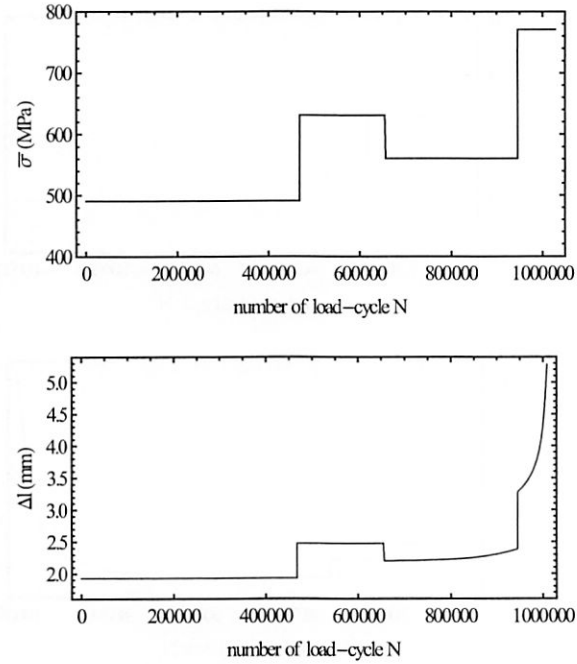

Figure 5.18: experiment 2: stress-cycle and elongation-cycle curves

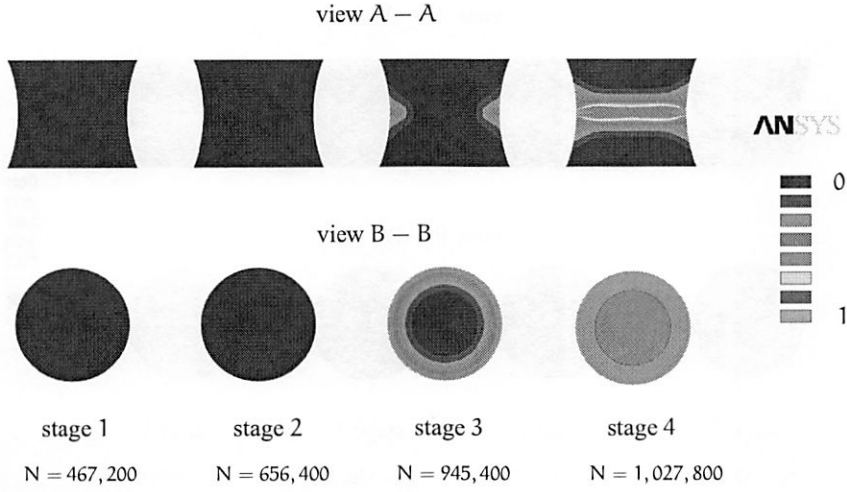

Figure 5.19: experiment 2: evolution of damage

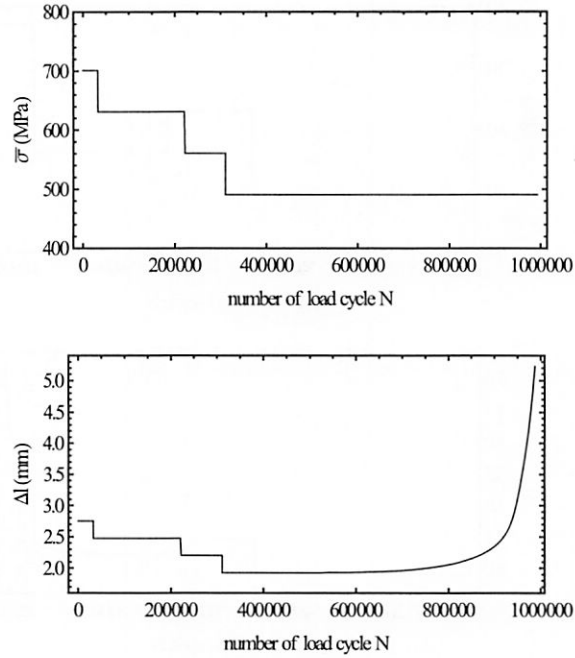

Figure 5.20: experiment 3: stress-cycle and elongation-cycle curves

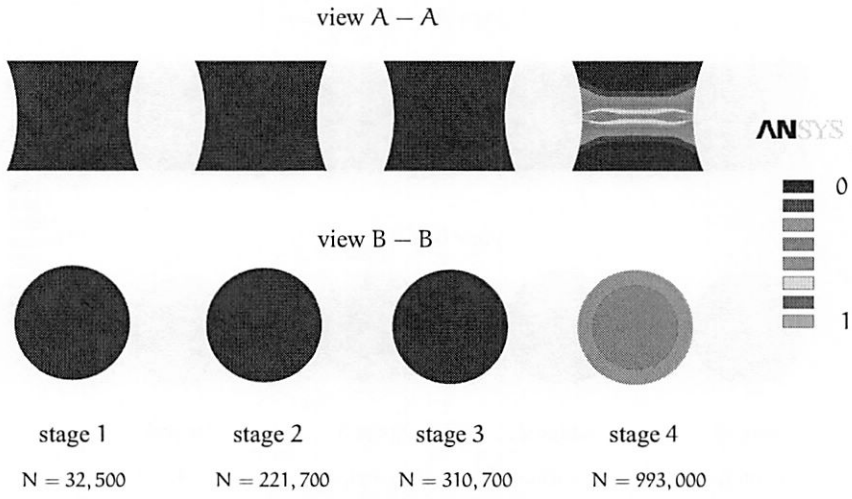

Figure 5.21: experiment 3: evolution of damage

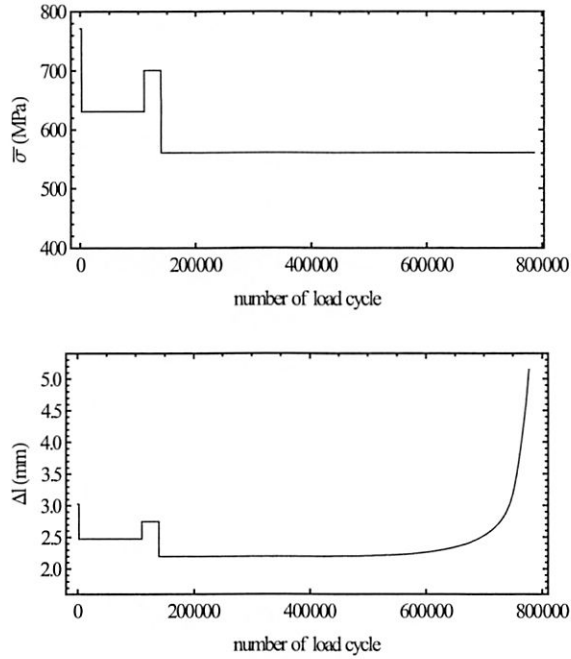

Figure 5.22: experiment 4: stress-cycle and elongation-cycle curves

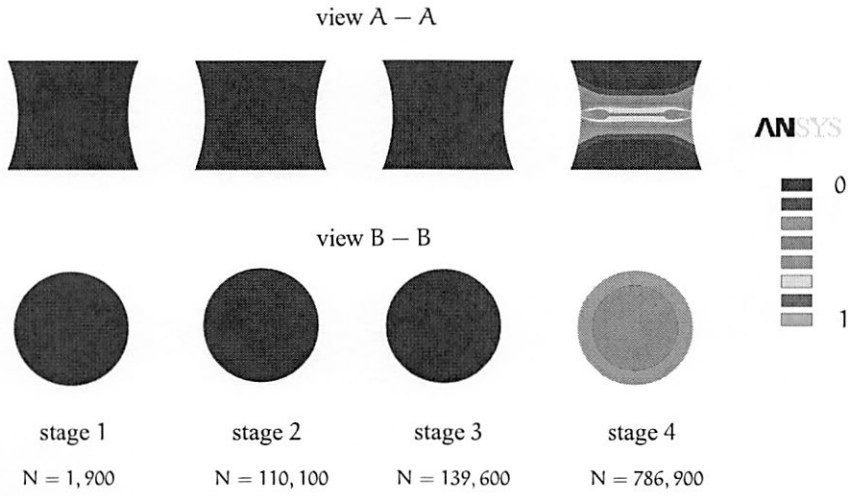

Figure 5.23: experiment 4: evolution of damage

6 Discussions and Outlooks

A micromechanical based continuum damage model based on the reduction of stiffness due to kinking elliptical microcracks has been proposed to show the anisotropic irreversible process of damage accumulation due to microcrack kinking and growth in brittle and quasi-brittle materials. It is known from experiments that all materials, and in more special case brittle materials, under general loading conditions develop anisotropic damage (KRAJCINOVIC & FONSEKA 1982). For a given stress state, materials damaged by microcracks in general accumulate additional damage through the kinking and growth of the initiated microcracks. The model is formulated consistently in a fully analytical way and the degradation of the elastic properties is associated with the irreversible process of crack kinking and growth. In order to make the formulation of the model mathematically traceable, the concept of an equivalent elliptical crack is proposed. The geometry and the orientation of the equivalent cracks are resulting from the postulates of equivalent dissipation and equivalent damage induced anisotropy. The proposed formulation yields a consistent damage model suitable for predicting the failure of structures and mechanical components subjected to fatigue conditions, independent of the type of loading. Accounting for the kinking and growth of microcracks and the type of damage induced anisotropy in the formulation of damage models is especially important in the case of non-proportional loads or even sequential loads, since the assumption of self-similar growth of mixed-mode cracks may underestimate the accumulated damage.

The micromechanical models are commonly referred to a class of analytical models which give the relation between the macroscopic state of a specimen and its microstructure (BUDIANSKY 1983). These class of models are based on the hypothesis of statistical homogeneity and weak interaction of defects, which are justifiable for reasonably modest concentration of heterogeneities (NEMAT-NASSER & HORI 1993). Within the approach of micromechanics, the effective elastic properties of a solid damaged by microcracks are derived by using the pertinent results of microconstituent analysis, such as that of a planar elliptical crack embedded in an infinite medium. The components of the effective compliance tensor can be derived from the contribution to the complementary strain energy corresponding to the quasi-static, selfsimilar growth of an elliptical crack. For this, the stress intensity factors suffice to give the energy released during the quasi-static, selfsimilar growth of an elliptical crack. However, for the formulation of the complementary strain energy corresponding to the kinking of a crack, the non-singular constant terms in the stress expansion formula, the so called T-stresses, are required as well. To be able to include the effect of the T-stresses, the analytical expressions for the T-stress components are to be addressed. The analytical expressions for the stress

intensity factors are given for many two-dimensional and three-dimensional crack problems, but solutions for the T-stresses are available mostly for two-dimensional crack problems, and very limited solutions in three-dimensions are available (MURAKAMI 1987). In chapter 2, the complete set of the elastic T-stresses for elliptical and circular cracks embedded in a homogenous isotropic infinite solid have been addressed (SCHÜTTE & MOLLA-ABBASI 2007B), (MOLLA-ABBASI & SCHÜTTE 2008). Using the potential method and a transformation technique, the asymptotic solutions for the stress components are derived, from which the T-stresses for elliptical and circular cracks in infinite isotropic linear elastic solids are resulting. It has been shown that beside the stress intensity factors, the T-stresses play also an important role in the subjects related to fracture mechanics and plasticity (LARSSON & CARLSSON 1973), (RICE 1974), (AYATOLLAHI, PAVIER & SMITH 1998), (SCHÜTTE & MOLLA-ABBASI 2007C).

The evolution of the cracks is governed by the criterion of maximum driving force coupled with a fatigue crack evolution law. In this regard, instead of using the stress intensity factors as the leading parameter for fatigue characterization, the maximum driving force concept has been considered (LE, SCHÜTTE & STUMPF 1999). The advantage of using such a formulation is that the effect of the material parameters such as the Young's modulus and the Poisson's ratio are taken into account. In experimental observations by JOHNSON & PARIS (1968), it has been observed that by dividing ΔK by the Young's modulus, the mid range fatigue data for various metals with diversified mechanical properties tend to congregate together within a relatively narrow scatter band. Using the concept of driving force or energy release rate enables overcoming the dependency of the formulation on specimen geometry and size, crack configuration and size, and loading condition as well, and there is no need to calculate the stress intensity factors, since calculating the energy released during crack propagation requires nevertheless no stress field solution at the crack tip, and hence makes it applicable to any specimen with arbitrary crack shapes and loading conditions. The most important advantage of using a G-based evolution law is that the rate of crack propagation is given in terms of its thermodynamical dual G. This is best illustrated by considering the irreversible nature of the crack propagation process, where according to the continuum thermodynamics, there is an entropy production rate associated with this irreversibility. Thus introducing the crack propagation rate as a new internal variable, the driving force is considered as its thermodynamic conjugate force (thermodynamic dual). Finally, with this kind of formulation the effect of mode III stress intensity factor is automatically taken into account. This is especially important, since for general three-dimensional crack problems K_{III} does not always tend to vanish, even for heavily grown cracks.

For clarity purposes and to explain the main issues of the proposed model in a more clear mathematical way, the complexity of the proposed damage model has been reduced here by leaving out the thermal effects and other non-mechanical phenomena. Strains and rotations have been assumed to be small, hence the framework of the linear elastic fracture mechanics can be applied. Furthermore, viscous effects and permanent deformations have been neglected and the material behavior is assumed to be linear elastic in its

pristine state. The small strain assumption, and the lack of permanent deformations in this model makes it suitable to show the evolution of damage in structures with brittle and quasi-brittle fracture behavior experiencing high-cycle fatigue. As the first extension, the proposed damage model can be modified to account for the effects of friction and temperature. The implementation of the model can also capture the unilateral effect observed in tension-compression tests, observed for a certain class of materials including ceramics and concrete, provided that for a passive crack the components of the corresponding compliance components are recovered, and they return to their degraded state upon the activation of the crack.

Bibliography

Achenbach, J. D. (1973). *Wave Propagation in Elastic Solids*. North-Holland, Amsterdam.

Aliabadi, M. H. (1997). Boundary element formulations in fracture mechanics. *Applied Mechanics Review* **50**, 83–96.

Amestoy, M. & J. B. Leblond (1992). Crack paths in plane situations - II: Detailed form of the expansion of the stress intensity factors. *International Journal of Solids and Structures* **29**, 465–501.

Arad, S., J. C. Radon & L. E. Culver (1974). Growth of fatigue cracks in metals and polymers. *Engineering Fracture Mechanics* **6**(1), 195–208.

Atluri, S. N. (1986). *Computational Methods in the Mechanics of Fracture*. North Holland.

Ayatollahi, M. R., M. J. Pavier & D. J. Smith (1998). Determination of T-stress from finite element analysis for mode-I and mixed-mode loading. *International Journal of Fracture* **91**, 293–298.

Ayatollahi, M. R., M. J. Pavier & D. J. Smith (2002). Mode-I cracks subjected to large T-stresses. *International Journal of Fracture* **117**, 159–174.

Ball, R. C. & H. Larralde (1995). Linear stability analysis of planar straight cracks propagating quasistatically under type I loading. *International Journal of Fracture* **71**, 365–377.

Benthem, J. P. & W. T. Koiter (1973). *Mechanics of fracture - Method of analysis and solutions of crack problems (ed. Sih, G. C.)*, Volume 1:131-178. Noordhoff international publishing Leyden.

Betegon, C. & J. W. Hancock (1991). Two-parameter characterization of elastic-plastic crack tip fields. *Journal of Applied Mechanics* **58**, 104–110.

Bilby, B. A. & G. E. Cardew (1957). The crack with a kinked tip. *International Journal of Fracture* **11**, 708–712.

Bilby, B. A., G. E. Cardew, M. R. Goldthorpe & I. C. Howard (1986). *A finite element investigation of the effect of speciemen geometry on the fields of stress and strain at the tips of stationary cracks, Size Effects in Fracture*. Mechanical Engineering Publications Limited, London.

Bowles, C. Q. & J. Schijve (1973). The role of inclusions in fatigue crack initiation in an aluminium alloy. *International Journal of Fracture* **9**, 171–1798.

Broberg, K. B. (1979). Mathematical methods in fracture mechanics. *Trends in Applications of Pure Mathematics to Mechanics* **2**, 57–78.

Broberg, K. B. (1987). A path independent integral for plates. *Journal of Applied Mechanics* **54**, 458–459.

Broberg, K. B. (1999). *Cracks and Fracture*. Academic Press.

Broek, D. (1974). *Elementary Engineering Fracture Mechanics*. Noordhoff international publishing Leyden.

Broek, D. & J. Schijve (1963). The influence of the mean stress on th epropagation of fatigue cracks in aluminium alloy sheets. *Nat. Aerospace Inst. Amsterdam* (TR-M-2111).

Broutman, L. J., S. M. Krishnakumar & P. K. Mallick (1970). Effects of combined stresses on fracture of alumina and graphite. *Journal of the American Ceramic Society* **53**(12), 649–654.

Budianisky, B. & J. R. O'Connell (1976). Elastic moduli of a cracked solid. *International Journal of Solids and Structures* **12**, 81–97.

Budianisky, B. & J. R. Rice (1973). Conservation laws and energy release rates. *Journal of Applied Mechanics* **40**, 201–203.

Budiansky, B. (1983). Micromechanics. *Computers and Structures* **16**, 3–12.

Byrd, P. F. & M. D. Friedman (1971). *Handbook of Elliptical Integrals for Engineers and Scientists* (2nd ed.), Volume Band-67. Springer.

Cardew, G. E., M. R. Goldthorpe, I. C. Howard & A. P. Kfouri (1984). On the elastic T-term. *Fundamentals of Deformation and Fracture*, 465–476.

Chaboche, J. L. (1988). Continuum damage mechanics: part I: general concepts, part II: damage growth, crack initiation, and crack growth. *Journal of Applied Mechanics* **55**(3), 59–71.

Cherepanov, G. P. (1967). Crack propagation in continous media. *Applied Mechanics and Mechanics* **31**, 476–488.

Cherepanov, G. P. (1968). Cracks in solids. *International Journal of Solids and Structures* **4**, 811–831.

Chow, C. L. & T. J. Lu (1989). On evolution laws of anisotropic damage. *Engineering Fracture Mechanics* **3**(3), 679–701.

Chow, C. L. & T. J. Lu (1990). A unified approach to fatigue crack propagation in metals and polymers. *Journal of Materials and Science Letters* **9**, 1427–1430.

Chow, C. L. & T. J. Lu (1992). An analytical and experimental study of mixed-mode ductile fracture under non-proportional loading. *International Journal of Damage Mechanics* **1**, 191–236.

Cordebois, J. P. & F. Sidoroff (1979). Damaged induced elastic anisotropy. *Coll. Euromech 115, Villard de Lnas*.

Cotterell, B. & J. R. Rice (1980). Slightly curved or kinked cracks. *International Jurnal of Fracture* **16**(2), 155–169.

Cottrell, A. H. & D. Hull (1957). Extrusion and intrusion by cyclic slip in copper. *Proceedings of the Royal Society of London* (A242), 211–217.

Cowin, S. C. & M. M. Mehrabadi (1987). On the identification of material symmetry for anisotropic elastic materials. *Quarterly Journal of Mechanics and Applied Mathematics* **40**, 451–476.

Davison, L. & A. L. Stevens (1973). Thermomechanical constitution of spalling elastic

bodies. *Journal of Applied Physics* **44**, 668–674.

Drucker, D. & W. Prager (1952). Soil mechanics and plastic analysis or limit design. *Quarterly of Applied Mathematics* **10**, 157–165.

Du, Z. Z. & J. W. Hancock (1991). The effect of non-singular stresses on crack tip constraint. *Journal of Mechanics and Physics of Solids* **39**, 555–567.

Dundurs, J. (1969). Edge-bonded dissimilar orthogonal elastic wedges under normal and shear loading. *Journal of Applied Mechanics* **36**, 650–652.

Eischen, J. W. & G. Hermann (1987). Energy release rates and related balance laws in linear defect mechanics. *ASME Journal of Applied Mechanics* **54**, 388–392.

El-Soudani, S. M. & R. M. N. Pelloux (1973). Influence of inclusion content on fatigue crack propagation in aluminium alloys. *Metallurgical Transactions* **4**, 519–531.

Erdogan, F. (1967). Crack propagation theories. *NASA reports* (CR-901).

Erdogan, F. (1978). Mixed boundary value problems in mechanics. *Mechanics Today* **4**, 1–86.

Erdogan, F. & G. C. Sih (1963). On the crack extension in plates under plane loading and transverse shear. *ASME Journal of Basic Engineering* **85**, 519–527.

Eshelby, J. D. (1920). The force on an elastic singularity. *Philosophical Transactions of the Royal Society of London* **A221**, 163–198.

Eshelby, J. D. (1951). The force on an elastic singularity. *Philosophical Transactions of the Royal Society of London* **A244**, 87–112.

Eshelby, J. D. (1974). The calculation of energy release rate. *Prospects of Fracture Mechanics*, 69–84.

Ewing, P. D., J. L. Swedlow & J. G. Williams (1976). Further results on the angled crack problem. *International Journal of Fracture* **12**, 85–93.

Fletcher, D. C. (1976). Conservation laws in linear elastodynamics. *Archive for Rational Mechanics and Analysis* **60**, 329–353.

Forman, R., V. E. Kearney & R. M. Engle (1967). Numerical analysis of carck propagation in cyclic loaded structure. *Transactions of the ASME, Journal of Basic Engineering* (89D), 459.

Frangi, A., G. Novati, R. Springhetti & M. Rovizzi (2002). 3-D fracture analysis by the symmetric galerkin bem. *Computational Mechanics* **28**, 221–231.

Freund, L. B. (1978). Stress intensity calculations based on a conservation integral. *International Journal of Solids and Structures* **14**, 241–250.

Freund, L. B. (1990). *Dynamic Fracture Mechanics*. Cambridge University Press.

Gao, H. (1988). Nearly circular shear mode cracks. *International Journal of Solids and Structures* **24**, 177–193.

Gao, H. (1992). Three-dimensional slightly non-planar cracks. *ASME Journal of Applied Mechanics* **59**, 335–343.

Gao, H. & J. R. Rice (1986). Shear stress intensity factors for a planar crack with slightly curved front. *ASME Journal of Applied Mechanics* **53**(774-778).

Gao, H. & J. R. Rice (1987a). Nearly circular connections of elastic half spaces. *ASME Journal of Applied Mechanics* **54**, 627–634.

Gao, H. & J. R. Rice (1987b). Somewhat circular tensile cracks. *International Journal of Fracture* **33**, 155–174.

Goldstein, R. V. & R. K. Salganik (1974). Brittle fracture of solids with arbitrary cracks. *International Journal of Fracture* **10**(4), 507–523.

Goursat, E. (1898). Sur l'équation $\nabla^2\nabla^2 w = 0$. *Bulletin de la Société Mathématique France* **26**, 236.

Green, A. E. & I. N. Sneddon (1950). The distribution of stress in the neighborhood of a flat elliptical crack in an elastic solid. *Proceedings of the Cambridge Philosophical Society* **46**, 159–164.

Griffith, A. A. (1921). The phenomena of rupture and flow in solids. *Philosophical Transactions, Series A* **221**, 163–198.

Griffith, A. A. (1924). The theory of rupture. *Proceedings of First International Congress of Applied Mechanics*, 55–63.

Grosskreutz, J. C. & C. Shaw (1969). Critical mechanisms in the development of fatigue cracks in 2024-T4 aluminium. *Fracture, Chapman and Hall*, 620–629.

Günther, W. (1962). Über einige randintegrale der elastomechanik. *Abh. Brauchschw. Wiss. Ges.* **14**, 53–72.

Hallback, N. & N. Jonsson (1996). T-stress evaluations of mixed mode I/II fracture specimens and T-effects on mixed mode failure of aluminium. *International Journal of Fracture* **76**, 141–168.

Hori, M. & S. Nemat-Nasser (1983). Overall moduli of solids with microcracks: Load-induced anisotropy. *Journal of Mechanics and Physics of Solids* **31**, 155–171.

Horibe, S. (1990). A new method for tension-compression fatigue testing of ceramic materials. *Journal of Materials Science* **9**, 745–747.

Hudson, C. M. & J. J. Ferrainolo (1991). A compendium of sources of fracture toughness and fatigue crack growth data for metallic alloys, part IV. *International Journal of Fracture* **48**, R19–R43.

Hult, J. (1979). *"CDM-capabilities, limitations and promises", Mechanics of Deformation and Fracture*. Pergamen Press, NY.

Hutchinson, J. W. (1968). Singular behaviour at the end of a tensile crack in hardening material. *Journal of Mechanics and Physics of Solids* **16**, 13–31.

Inglis, C. E. (1913). Stress in a plate due to presence of cracks and shape corners. *Transactions of the Institute of Naval Architects* **55**, 219–241.

Irwin, G. R. (1948). Fracture dynamics, fracturing of metals. *ASM Publications*, 147–166.

Irwin, G. R. (1957). Analysis of stresses and strains near the end of a crack traversing a plate. *ASME Journal of Applied Mechanics* **24**, 361–364.

Irwin, G. R. (1961). Plastic zone near a crack and fracture toughness. *Sagamore Research Conference Proceedings*.

Isida, M. (1970). Analysis of stress intensity factors for plates containing random array of cracks. *Bulletin of the Japan Society of Mechanical Engineers* **13**(59), 635–642.

Isida, M. & et al. (1984). Two parallel elliptical cracks in an infinite solid subjected to

tension. *International Journal of Fracture* **27**(31), 31–48.

Jeelani, S. & M. Musial (1986). A study of cumulative fatigue damage in ASIS 4130 steel. *Journal of Materials Science* **21**, 2109–2113.

Johnson, H. H. & P. C. Paris (1968). *Engineering Fracture Mechanics* **1**, 3.

Kachanov, L. M. (1958). On the creep rupture time. *Izv. Akad. Nauk. (SSSR)* **8**, 2631.

Kassir, M. K. & G. C. Sih (1966). Three-dimensional stress distribution around an elliptical crack under arbitrary loadings. *Journal of Applied Mechanics*, 601–611.

Kassir, M. K. & G. C. Sih (1975). *Mechanics of Fracture - Three-Dimensional Crack Problems*, Volume 2. Noordhoff international publishing Leyden.

Kelvin, L. (1856). Elements of a mathematical theory of elasticity, part1 on stresses and strains. *Philosophical Transactions of the Royal Society of London* **166**, 481–498.

Kelvin, L. (1878). Mathematical theory of elasticity. *Elasticity, Encyclopedia Britannica* **7**, 819–825.

Kestin, J. & J. Bataille (1977). Irreversible thermodynamics of continnum and internal variables. *In Continuum Models of Discrete Systems* (12).

Kfouri, A. P. (1986). Some evaluations of elastic T-term using eshelby's method. *International Journal of Fracture* **30**, 301–315.

Knowles, J. K. & E. Sternberg (1972). On a class of conservation laws in linearized and finite elastostatics. *Archive for Rational Mechanics and Analysis* **44**, 187–211.

Knsel, Z. (1995). Evaluation of the elastic T-stress using a hybrid finite element approach. *International Journal of Fracture* **70**, R9–R14.

Kommers, J. B. (1912). Repeated stress testing, parts I and II. *Sixth Congress of the International Association for Testing Materials, New York.*

Krajcinovic, D. (1983a). Constitutive equations for damaging materials. *Journal of Applied Mechanics* **50**, 355–360.

Krajcinovic, D. (1983b). Creep of structure-a continuous damage mechanics approach. *Journal of Structural Mechanics* **11**(1), 1–11.

Krajcinovic, D. (1985). Continuum damage mechanics revisited : basic concepts and definitions. *Journal of Applied Mechanics* **52**, 829–834.

Krajcinovic, D. (1989). Damage mechanics. *Mechanics of Materials* **8**, 117–197.

Krajcinovic, D. (1996). *Damage Mechanics*. North-Holland.

Krajcinovic, D. & G. U. Fonseka (1981). The continuous damage theory of brittle materials. *ournal of Apphed Mechanics* **48**, 809–824.

Krajcinovic, D. & G. U. Fonseka (1982). The continuous damage theory of brittle materials; parts I and II. *Journal of Applied Mechanics* **48**, 809–824.

Lapidus, L. & G. F. Pinder (1982). *Numerical solution of partial differential equations in science and engineering*. John Willy & Sons-New York.

Larsson, S. G. & A. J. Carlsson (1973). Influence of non-singular stress terms and speciemen geometry on small scale yielding at crack tips in elastic-plastic materials. *Journal of Mechanics and Physics of Solids* **21**, 263–278.

Le, K. C. (1989). Equilibrium criterion for a nonlinear elastic slitted body. *Advances in Fracture - Oxford: Pergamon Press*, 49–53.

Le, K. C. & H. Schütte (1999). Variational formulation of the crack problem with a virtual crack kinking. *Proceedings of 9th International Symposium on Continuum Models and Discrete Systems*, 727–735.

Le, K. C., H. Schütte & H. Stumpf (1999). Determination of the driving force acting on a kinked crack. *Archive of Applied Mechanics* **69**(1), 337–344.

Le, K. C., H. Stumpf & D. Weicher (1989). Variational principles of fracture mechanics. *Mitteilungen Institute für Mechanik, Rihr Universität Bochum* (64).

Leblond, J. B. (1989). Crack paths in plane situations - I: General form of the expansion of the stress intensity factors. *International Journal of Solids and Structures* **25**, 1311–1325.

Leblond, J. B. (1993). Crack kinking and curving in three-dimensional elastic solids - application to the study of crack path stability in hydraulic fracturing. *Mixed-mode fatigue and fracture-ESIS 14 (Edited by H.P. Rossmanith and K.J. Miller), Mechanical Engineering Publications, London*, 219–243.

Leblond, J. B. (1999). Crack paths in three-dimensional elastic solids. I: two-term expansion of the stress intensity factors–application to crack path stability in hydraulic fracturing. *International Journal of Solids and Sructures* **36**, 79–103.

Leblond, J. B. & J. Frelat (2000). Crack kinking from an initially crcak. *International Journal of Solids and Sructures* **37**, 1595–1614.

Leblond, J. B. & J. Frelat (2001). Crack kinking from an interface crack with initial contact between the crack lips. *European Journal of Mechanics A/Solids* **20**, 937–951.

Leblond, J. B. & J. Frelat (2004). Crack kinking from an initially closed, ordinary or onterface crack, in the presence of friction. *Engineering Fracture Mechanics* **71**, 289–307.

Leblond, J. B. & O. Torlai (1992). The stress field near the front of an arbitrarily shaped crack in a three-dimensional elastic body. *Journal of Elasticity* **29**, 97–131.

Leckie, F. A. & E. T. Onat (1981). Tensorial nature of damage measuring internal variables. *Physical Nonlinearities in Structural Analysis, Springer*, 140–155.

Leevers, P. S. & J. C. Radon (1982). Inherent stress biaxiality in various fracture specimen geometries. *International Journal of Fracture* **9**, 311–325.

Lemaitre, J. (1985). A continuous damage mechanics model for ductile fracture. *ournal of Engineering Materials and Technology* **107**, 83–89.

Lemaitre, J. (1992). *A course on damage mechanics*. Springer.

Lemaitre, J. & J. L. Chaboche (1985). *Mecanique des Materiaux Solides*. Dunod, Paris.

Lemaitre, L. & J. L. Chaboche (1990). *Mechanics of Solid Materials*. Cambridge University Press.

Li, S., M. E. Mear & L. Xiao (1998). Symmetric weak-form integral equation method for three-dimentional fracture analysis. *Computer Methods Applied Mechanics Engineering* **151**, 435–459.

Liebowitz, H. (1968). *Fracture*. Academic Press.

Maiti, S. K. & R. A. Smith (1983). Criteria for mixed mode brittle fracture based on

the pre-instability stress-strain field - I and II. *International Journal of Fracture* **23**, 281–295.

Maugin, G. A. (1992). *The Thermomechanics of Plasticity and Fracture*. Cambridge University Press.

Maugin, G. A. (1993). *Material inhomogeneities in elasticity* (1st ed.). St. Edmundsbury Press - Great Britain.

McClintock, F. A. (1968). A criterion for ductile fracture by the growth of holes. *Journal of Applied Mechanics*, 363–371.

McEvily, A. J. & R. C. Boettner (1963). A note on fatigue and microstructure. *Fracture of Solids* **1963**(Interscience Publications), 383–389.

Mehrabadi, M. M. & S. C. Cowin (1990). Eigentensors of linear anisotropic elastic materials. *Quarterly Journal of Mechanics and Applied Mathematics* **43**, 15–41.

Miner, M. A. (1945). Cumulative damage in fatigue. *Journal of Applied Mechanics* **12**(3), A159–A164.

Mogilevskaya, S. G. (1997). Numerical modelling of 2-D smooth crack growth. *International Journal of Fracture* **87**, 389–405.

Mohr, O. (1900). Welche umstände bedingen die elastizitätsgrenze und den bruch eines materials? *Zeitschrift des Vereins Deutscher Ingenieure* (24), 1524–1530.

Molla-Abbasi, K. & H. Schütte (2006). Evolution of elstic T-stresses of growing mixed-mode cracks. *Proceedings in Applied Mathematics and Mechanics* **6**, 179–180.

Molla-Abbasi, K. & H. Schütte (2007). Numerical analyses of the anisotropic damage evolution due to a growing mixed-mode crack. *Key Engineering Materials* **348-349**, 701–404.

Molla-Abbasi, K. & H. Schütte (2008). On the full set of elastic non-singular stress terms of internal elliptical cracks under mixed-mode loading condition. *Engineering Fracture Mechanics* **75**(6), 1545–1568.

Mott, N. F. (1958). A theory of the origin of the fatigue cracks. *Acta Metallurgica* **6**, 195–197.

Murakami, S. & N. Ohno (1981). A continuum theory of creep and creep damage. *Creep in Structures*, 422–434.

Murakami, Y. (1987). *Stress Intensity Factors Handbook*. Pergamon Press.

Muskhelishvili, N. I. (1933). *Some basic problems of the mathematical theory of elasticity*. Noordhoff.

Nakamura, T. & D. M. Parks (1991). Determination of elastic T-stress along 3-D crack fronts using an interaction integral. *International Journal of Solids and Structures* **29**, 1597–1611.

Nemat-Nasser, S. & M. Hori (1993). *Micromechanics, Overal Properties of Heterogeneous Materials*. North-Holland.

Nöther, E. (1918). Invariante variations-probleme. *Nachrichtender der Königlicher Gesellschaft der Wissenschaften, Göttingen* (235-257).

O'Dowd, N. P. & C. F. Shih (1991). Family of crack tip fields characterized by triaxial-

ity parameter-I. structure of fields. *Journal of Mechanics and Physics of Solids* **39**, 989–1015.

Olsen, P. C. (1994). Determining the stress intensity factors k_I, k_{II} and the t-term via the conservation laws using the boundary element method. *Engineering Fracture Mechanics* **49**(1), 49–60.

Orowan, E. (1948). Fracture and strength of solids. *Reports on Progress in Physics XII* **34**, 185–232.

Palmgreen, A. (1924). Die lebensdauer von kugellagern. *VDI Zeitschrift* **68**, 339–341.

Paris, P. C. (1962). *The Growth of Fatigue Growth due to Variations in Load.* Ph. D. thesis, Lehigh University, Bethlehem, USA.

Paris, P. C., M. P. Gomez & W. E. Anderson (1961). A rational analytic theory of fatigue. *The Trend in Engineering* **13**, 9–14.

Rabotnov, Y. N. (1968). Creep rupture. *Proceedings of the 12th International Congress of Applied Mechanics*, 342–349.

Rabotnov, Y. N. (1969). Creep problems in structural members. *Amsterdam: North Holland Publishing Co.*.

Ravi-Chandar, K. (1982). *An Experimental Investigation into the Mechanics of Dynamic Fracture.* Ph. D. thesis, California Institute of Technology, California, USA.

Rice, J. (1985). Conserved integrals and energetic forces. *Fundamentals of Deformation and Fracture, Eshelby Memorial Symposium*, 33–56.

Rice, J. (1989). Weight function theory for three-dimensional elastic crack analysis. *Fracture Mechanics: Perspectives and Directions*, 29–57.

Rice, J. R. (1968a). *Fracture: An Advanced Treatise, ed. Liebowitz, H., Chapter 3: Mathematical analysis in the mechanics of fracture (191-311)*, Volume 7. Academic Press, New York.

Rice, J. R. (1968b). A path independent integral and the approximate analysis of strain concentration by notches and cracks. *Journal of Applied Mechanics* **35**, 379–386.

Rice, J. R. (1974). Limitations to the small scale yielding approximation for crack tip plasticity. *Journal of the Mechanics and Physics of Solids* **22**, 17–26.

Rice, J. R. & G. F. Rosengren (1968). Plane strain deformation near a crack tip in a power-law hardening material. *Journal of Mechanics and Physics of Solids* **16**, 1–12.

Rice, J. R. & D. M. Tracey (1969). On the ductile enlargement of voids in triaxial stress fields. *Journal of Mechanics and Physics of Solids* **17**, 201–217.

Rizzo, F. J. (1967). An integral equation approach to boundary value problems of classical elastostatics. *Quarterly of Applied Mathematics* **25**, 83–95.

Robinson (1952).

Runesson, K., N. S. Ottosen & D. Peric (1991). Plane strain and stress discontinuous bifurcations in elastic-plastic materials at plane stress and plane strain. *International Journal of Plasticity* **27**, 9–121.

Rychlewski, J. (1984). On hook's law. *Prikl. Matem. Mekhan.* **48**, 303–314.

Saanouni, K., C. H. Forster & F. Ben-Hatira (1994). On the anelastic flow with damage.

International Journal of Damage Mechanics **3**, 140–169.

Sanders, J. L. (1960). On the griffith-irwin fracture theory. *Journal of Applied Mechanics* **27**, 352–353.

Schütte, H. (2001). *Ein finites Modell für spröde Schädigung basierend auf der Ausbreitung von Mikrorissen*. Ph. D. thesis, Ruhr Universität Bochum, Bochum, Germany.

Schütte, H. & K. Molla-Abbasi (2007a). On the evolution of elastic symmetries of growing mixed-mode cracks. *8th International Conference on Multiaxial Fatigue and Fracture*.

Schütte, H. & K. Molla-Abbasi (2007b). On the full set of elastic non-singular stress terms of internal circular cracks under mixed-mode loading condition. *Engineering Fracture Mechanics* **74**(17), 2770–2787.

Schütte, H. & K. Molla-Abbasi (2007c). On the influence of corner singularity on kinking mixed-mode crack propagation. *Key Engineering Materials* **348-349**, 585–588.

Sham, T. L. (1989). The determination of the elastic T-term using higher order weight functions. *International Journal of Fracture* **48**, 81–102.

Sidoroff, F. (1981). Description of anisotropic damage application to elasticity. *IUTAM - Physical Nonlinearities in Structural Analysis, Springer*, 237–244.

Sih, G. C. (1973). *Mechanics of Fracture - Methods of analysis and solutions of crack problems*, Volume 1. Noordhoff international publishing Leyden.

Sih, G. S. (1972). *Mechanics of Fracture - A Special Theory of Crack Propagation*. Noordhoff international publishing Leyden.

Sih, G. S. (1974). Strain energy density factor applied to mixed mode crack problems. *International Journal of Fracture* **10**(3), 305–321.

Simo, J. C. & J. W. Ju (1987). Strain- and stress- based continuum damage models. *International Journal of Solids and Structures* **23**(7), 821–869 and 841–869.

Simo, J. C. & R. L. Taylor (1986). A return mapping algorithm for plane stress elastoplasticity. *International Journal for Numerical Methods in Engineering* **22**, 649–670.

Skrzypek, J. & A. Ganczarski (1999). *Modeling of Material Damage and Failure od Structures, Theory and Applications*. Springer.

Sladek, J., V. Sladek & P. Fedelinski (1997). Contour integrals for mixed-mode crack analysis: effect of nonsingular terms. *Theoretical and Applied Fracture Mechanics* **27**, 115–127.

Smith, D. J., M. R. Ayatollahi & M. J. Pavier (2001). The role of T-stress in brittle fracture for linear elastic materials under mixed-mode loading. *Fatigue and Fracture of Engineering Materials and Structures* **24**, 137–150.

Sneddon, I. N. (1946). The distribution of stress in the neighbourhood of a crack in an elastic solid. *Proceedings of the Royal Society* **60**, 187–222.

Sumi, Y. (1986). Computational crack path prediction, applied to crack arrestabilty by a circular hole. *Proceedings of the International Conference on Computational Mechanics, Tokyo*, 241.

Sumi, Y., S. Nemat-Nasser & L. M. Keer (1983). On crack branching and curving in a finite body. *International Journal of Fracture* **21**, 67–79.

Sutton, S. A. (1974). Fatigue crack propagation in an epoxy polymer. *Engineering Fracture Mechanics* **6**(3), 587–595.

Tian, C. & W. Cui (2006). T-stress in elastic-plastic crack-tip fields. *International Journal of Fracture* **136**, 9–14.

Timoshenko, S. P. (1953). *History of the Strength of Materials*. McGraw-Hill.

Ting, T. C. T. (1985). Asymptotic solution near the apex of an elastic wedge with curved boundaries. *Quarterly of Applied Mathematics* **42**, 467–476.

Tresca, H. (1872). sur les godets graisseurs présentés par m. ermond rous. *Acad. Sci. Paris* **20**, 75–135.

Vakulenko, A. A. & M. L. Kachanov (1971). Continual theory of medium with cracks. *Mechanics of Solids* **6**, 145–151.

von Mises, R. (1913). Mechanik der festen körper im plastischen deformablen zustand. *Nachrichten von der Gesellschaft der Wissenschaten zu Göttingen* (Mathematisch-Physikalische Klasse), 582–592.

Walker, E. K. (1969). An effective strain concept for crack propagation and fatigue with specific application to biaxial stress fatigue. *Air Force Conference on Fracture and Fatigue* (TR-70-144), 225–233.

Wang, X. (2004). Elastic T-stress solutions for penny-shaped cracks under tension and bending. *Engineering Fracture Mechanics* **71**, 2283–2298.

Wang, Y. Y. (1993). On the two-parameter characterization of elastic-plastic crack front field in surface cracked plates. *ASTM - Constraint Effects in Fracture*, 120–138.

Westergaard, H. M. (1939). Bearing pressure and cracks. *Journal of Applied Mechanics* **61**, A49–A53.

Whittaker, E. T. & G. N. Watson (1962). *Modern Analysis*. Cambridge University Press, 548-552.

Wieghardt, K. (1907). Über das Spalten und Zerreissen elastischer Körper. *Zeitschrift für Mathematik und Physik* **55**, 60–103. (Translated in Fatigue and Fracture of Engineering Materials and Structures. On splitting and cracking of elastic bodies (1995) 18, 1371-1405.).

Williams, M. L. (1957). On the stress distribution at the base of a stationary crack. *Journal of Applied Mechanics* **24**, 109–114.

Wöhler, A. (1860). Über die festigkeits-versuche mit eisen und stahl. *Zeitschrift für Bauwesen* **8,10,13,16,20**.

Woo, C. W. & C. L. Chow (1984). Fatigue crack propagation in aluminium and pmma. *International Journal of Fracture* **26**(R), 37–42.

Wood, W. A. (1958). Recent observations on fatigue fracture in metals. *American Society of Testing Materials* **237**, 110–121.

Wu, C. H. (1978). Elasticity problems od slender Z-crack. *Journal of elasticity* **8**, 183–205.

Xu, G., A. F. Bower & M. Ortiz (1994). An analysis of non-planar crack growth un-

der mixed-mode loading. *International Journal of Solids and Structures* **31**, 2167–2193.

Ziegler, H. (1983). *North-Holland Publishing Co.*

Zienkiewicz, O. C. & R. L. Taylor (1989). *Finite Element Method* (4^{th} ed.). McGraw-Hill. New York.

Appendix

Appendix A

Expressions of f_{ij}^{α} and g_{ij}^{α}

The non-zero expression of the universal functions are given in (LEBLOND & TORLAI 1992). The functions for f are expressed in the Polar-coordinates and the g-functions in both Polar- and Cartesian-coordinates.

Functions f_{ij}^{α}:

$$f_{rr}^{I}(\theta) = \frac{1}{4\sqrt{2\pi}}\left(5\cos\frac{\theta}{2} - \cos\frac{3\theta}{2}\right), \quad f_{\theta\theta}^{I}(\theta) = \frac{1}{4\sqrt{2\pi}}\left(3\cos\frac{\theta}{2} + \cos\frac{3\theta}{2}\right), \tag{A-1}$$

$$f_{r\theta}^{I}(\theta) = \frac{1}{4\sqrt{2\pi}}\left(\sin\frac{\theta}{2} + \sin\frac{3\theta}{2}\right), \quad f_{zz}^{I}(\theta) = \frac{2\nu}{\sqrt{2\pi}}\cos\frac{\theta}{2},$$

$$f_{rr}^{II}(\theta) = \frac{1}{4\sqrt{2\pi}}\left(-5\sin\frac{\theta}{2} + 3\sin\frac{3\theta}{2}\right), \quad f_{\theta\theta}^{II}(\theta) = \frac{-3}{4\sqrt{2\pi}}\left(\sin\frac{\theta}{2} + \sin\frac{3\theta}{2}\right), \tag{A-2}$$

$$f_{r\theta}^{II}(\theta) = \frac{1}{4\sqrt{2\pi}}\left(\cos\frac{\theta}{2} + 3\cos\frac{3\theta}{2}\right), \quad f_{zz}^{II}(\theta) = \frac{-2\nu}{\sqrt{2\pi}}\sin\frac{\theta}{2},$$

$$f_{rz}^{III}(\theta) = \frac{1}{\sqrt{2\pi}}\sin\frac{\theta}{2}, \quad f_{\theta z}^{III}(\theta) = \frac{1}{\sqrt{2\pi}}\cos\frac{\theta}{2}. \tag{A-3}$$

Functions g_{ij}^{α} in the Cartesian coordinates:

$$g_{xx}^{I}(\theta) = 1, \quad g_{zz}^{I}(\theta) = \nu \tag{A-4}$$
$$g_{xz}^{II}(\theta) = 1,$$
$$g_{zz}^{III}(\theta) = 1.$$

Functions g_{ij}^{α} in the Polar coordinates:

$$g_{rr}^{I}(\theta) = \cos^2(\theta), \quad g_{\theta\theta}^{I}(\theta) = \sin^2(\theta), \tag{A-5}$$
$$g_{zz}^{I}(\theta) = \nu, \quad g_{r\theta}^{I}(\theta) = \frac{-1}{2}\sin(2\theta),$$
$$g_{\theta z}^{II}(\theta) = -\sin(\theta), \quad g_{rz}^{II}(\theta) = \cos(\theta),$$
$$g_{zz}^{III}(\theta) = 1,$$

Universal functions proportional to $\sqrt{\tau}$

Functions h_{ij}^{α}:

$$h_{rr}^{I}(\theta)=\frac{1}{4\sqrt{2\pi}}\left(3\cos\frac{\theta}{2}+\cos\frac{5\theta}{2}\right),\quad h_{\theta\theta}^{I}(\theta)=\frac{1}{4\sqrt{2\pi}}\left(5\cos\frac{\theta}{2}-\cos\frac{5\theta}{2}\right), \tag{A-6}$$

$$h_{r\theta}^{I}(\theta)=\frac{1}{4\sqrt{2\pi}}\left(\sin\frac{\theta}{2}-\sin\frac{5\theta}{2}\right),\quad h_{zz}^{I}(\theta)=\frac{2\nu}{\sqrt{2\pi}}\cos\frac{\theta}{2},$$

$$h_{rr}^{II}(\theta)=\frac{1}{4\sqrt{2\pi}}\left(3\sin\frac{\theta}{2}+5\sin\frac{5\theta}{2}\right),\quad h_{\theta\theta}^{II}(\theta)=\frac{5}{4\sqrt{2\pi}}\left(\sin\frac{\theta}{2}-\sin\frac{5\theta}{2}\right), \tag{A-7}$$

$$h_{r\theta}^{II}(\theta)=\frac{1}{4\sqrt{2\pi}}\left(-\cos\frac{\theta}{2}+5\cos\frac{5\theta}{2}\right),\quad h_{zz}^{II}(\theta)=\frac{2\nu}{\sqrt{2\pi}}\sin\frac{\theta}{2},$$

$$h_{rz}^{III}(\theta)=\frac{1}{\sqrt{2\pi}}\sin\frac{3\theta}{2},\quad h_{\theta z}^{III}(\theta)=\frac{1}{\sqrt{2\pi}}\cos\frac{3\theta}{2}. \tag{A-8}$$

Functions l_{ij}^{α}:

$$l_{\theta z}^{I}(\theta)=\sqrt{\frac{1}{2\pi}}\left(2\nu-\frac{3}{2}\right)\left(\sin\frac{\theta}{2}+\sin\frac{3\theta}{2}\right), \tag{A-9}$$

$$l_{rz}^{I}(\theta)=\sqrt{\frac{1}{2\pi}}\left(\frac{1}{2}-2\nu\right)\cos\frac{\theta}{2}+\left(\frac{3}{2}-2\nu\right)\cos\frac{3\theta}{2},$$

$$l_{\theta z}^{II}(\theta)=\sqrt{\frac{1}{2\pi}}\left(2\nu-\frac{3}{2}\right)\cos\frac{\theta}{2},\quad l_{rz}^{II}(\theta)=\sqrt{\frac{1}{2\pi}}\left(2\nu-\frac{1}{2}\right)\sin\frac{\theta}{2},$$

$$l_{rr}^{III}(\theta)=-\frac{4}{5}\sqrt{\frac{1}{2\pi}}\sin\frac{\theta}{2},\quad l_{zz}^{III}(\theta)=\sqrt{\frac{1}{2\pi}}\left(4+\frac{16}{5}\nu\right)\sin\frac{\theta}{2},$$

$$l_{r\theta}^{III}(\theta)=-\frac{2}{5}\sqrt{\frac{1}{2\pi}}\cos\frac{\theta}{2},$$

Functions $m_{ij}^{\alpha,11}$:

<u>mode-II</u>: (A-10)

$$m_{rr}^{II,11}(\theta)=\frac{9}{2}\sqrt{\frac{1}{2\pi}}\cos\frac{\theta}{2},\quad m_{\theta\theta}^{II,11}(\theta)=\frac{15}{2}\sqrt{\frac{1}{2\pi}}\cos\frac{\theta}{2},$$

$$m_{zz}^{II,11}(\theta)=12\nu\sqrt{\frac{1}{2\pi}}\cos\frac{\theta}{2},\quad m_{r\theta}^{II,11}(\theta)=\frac{3}{2}\sqrt{\frac{1}{2\pi}}\sin\frac{\theta}{2},$$

mode-III: (A-11)

$$m_{\theta z}^{III,11}(\theta) = \frac{3}{4}\sqrt{\frac{1}{2\pi}}\sin\frac{3\theta}{2}, \quad m_{rz}^{III,11}(\theta) = -\frac{3}{4}\sqrt{\frac{1}{2\pi}}\cos\frac{3\theta}{2},$$

Functions $m_{ij}^{\alpha,13}$:

mode-I: (A-12)

$$m_{rz}^{I,13}(\theta) = \frac{1-3\nu}{8}\sqrt{\frac{1}{2\pi}}\sin\frac{3\theta}{2}, \quad m_{\theta z}^{I,13}(\theta) = \frac{3-\nu}{8}\sqrt{\frac{1}{2\pi}}\cos\frac{3\theta}{2},$$

mode-II: (A-13)

$$m_{\theta z}^{II,13}(\theta) = \sqrt{\frac{1}{2\pi}}\left(\frac{\nu-3}{8}\sin\frac{\theta}{2} + \frac{9\nu-3}{8}\sin\frac{3\theta}{2}\right),$$

$$m_{rz}^{II,13}(\theta) = \frac{1-3\nu}{8}\sqrt{\frac{1}{2\pi}}\left(\cos\frac{\theta}{2} + \cos\frac{3\theta}{2}\right),$$

mode-III: (A-14)

$$m_{rr}^{III,13}(\theta) = 2\sqrt{\frac{1}{2\pi}}\cos\frac{\theta}{2}, \quad m_{\theta\theta}^{III,13}(\theta) = 3\sqrt{\frac{1}{2\pi}}\cos\frac{\theta}{2}$$

$$m_{zz}^{III,13}(\theta) = (4\nu-1)\sqrt{\frac{1}{2\pi}}\cos\frac{\theta}{2}, \quad m_{\theta\theta}^{III,13}(\theta) = \frac{1}{2}\sqrt{\frac{1}{2\pi}}\sin\frac{\theta}{2}$$

Functions $m_{ij}^{\alpha,33}$:

mode-I: (A-15)

$$m_{rr}^{I,33}(\theta) = \sqrt{\frac{1}{2\pi}}\left(\left(\frac{21}{80} - \frac{\nu}{5}\right)\sin\frac{\theta}{2} + \left(\frac{9}{16} - \nu\right)\sin\frac{3\theta}{2}\right),$$

$$m_{\theta\theta}^{I,33}(\theta) = \sqrt{\frac{1}{2\pi}}\left(\nu - \frac{9}{16}\right)\left(\sin\frac{\theta}{2} + \sin\frac{3\theta}{2}\right),$$

$$m_{zz}^{I,33}(\theta) = \sqrt{\frac{1}{2\pi}}\left(\left(\frac{24\nu^2}{5} + \frac{\nu}{5} - \frac{7}{2}\right)\sin\frac{\theta}{2} + \frac{1+\nu}{2}\sin\frac{3\theta}{2}\right),$$

$$m_{r\theta}^{I,33}(\theta) = \sqrt{\frac{1}{2\pi}}\left(\left(\frac{33}{80} - \frac{3\nu}{5}\right)\cos\frac{\theta}{2} + \left(\frac{7}{16} - \nu\right)\cos\frac{3\theta}{2}\right),$$

mode-II: (A-16)

$$m_{rr}^{II,33}(\theta) = \sqrt{\frac{1}{2\pi}}\left(\left(5\nu - \frac{13}{16}\right)\cos\frac{\theta}{2} + \left(\frac{9}{16} - \nu\right)\cos\frac{3\theta}{2}\right),$$

$$m_{\theta\theta}^{II,33}(\theta) = \sqrt{\frac{1}{2\pi}}\left(\left(7\nu - \frac{27}{16}\right)\cos\frac{\theta}{2} + \left(\nu - \frac{9}{16}\right)\cos\frac{3\theta}{2}\right),$$

$$m_{zz}^{II,33}(\theta) = \sqrt{\frac{1}{2\pi}}\left(\left(8\nu^2 - 5\nu + \frac{3}{2}\right)\cos\frac{\theta}{2} + \frac{1+\nu}{2}\cos\frac{3\theta}{2}\right),$$

$$m_{r\theta}^{II,33}(\theta) = \sqrt{\frac{1}{2\pi}}\left(\nu - \frac{7}{16}\right)\left(\sin\frac{\theta}{2} + \sin\frac{3\theta}{2}\right),$$

mode-III: (A-17)

$$m_{\theta z}^{III,33}(\theta) = -\frac{5}{4}\sqrt{\frac{1}{2\pi}}\left(\sin\frac{\theta}{2} + \sin\frac{3\theta}{2}\right),$$

$$m_{rz}^{III,33}(\theta) = \sqrt{\frac{1}{2\pi}}\left(\frac{7}{4}\cos\frac{\theta}{2} + \frac{5}{4}\cos\frac{3\theta}{2}\right),$$

Functions n_{ij}^{α}:

mode-I: (A-18)

$$n_{rr}^{I}(\theta) = \sqrt{\frac{1}{2\pi}}\left(\left(\nu - \frac{13}{16}\right)\cos\frac{\theta}{2} + \left(\frac{9}{16} - \nu\right)\cos\frac{3\theta}{2}\right),$$

$$n_{\theta\theta}^{I}(\theta) = \sqrt{\frac{1}{2\pi}}\left(\nu - \frac{9}{16}\right)\left(3\cos\frac{\theta}{2} + \cos\frac{3\theta}{2}\right),$$

$$n_{zz}^{I}(\theta) = \sqrt{\frac{1}{2\pi}}\left(\left(8\nu^2 - \nu - \frac{5}{2}\right)\cos\frac{\theta}{2} + \frac{1+\nu}{2}\cos\frac{3\theta}{2}\right),$$

$$n_{r\theta}^{I}(\theta) = \sqrt{\frac{1}{2\pi}}\left(\nu - \frac{7}{16}\right)\left(\sin\frac{\theta}{2} + \sin\frac{3\theta}{2}\right),$$

mode-II: (A-19)

$$n_{rr}^{II}(\theta) = \sqrt{\frac{1}{2\pi}}\left(\left(\frac{107}{80} - \frac{7\nu}{5}\right)\sin\frac{\theta}{2} + \left(\nu - \frac{9}{16}\right)\sin\frac{3\theta}{2}\right),$$

$$n_{\theta\theta}^{II}(\theta) = \sqrt{\frac{1}{2\pi}}\left(\frac{9}{16} - \nu\right)\left(\sin\frac{\theta}{2} + \sin\frac{3\theta}{2}\right),$$

$$n_{zz}^{II}(\theta) = \sqrt{\frac{1}{2\pi}}\left(\left(\frac{8\nu^2}{5} + \frac{7\nu}{5} - \frac{9}{2}\right)\sin\frac{\theta}{2} - \frac{1+\nu}{2}\sin\frac{3\theta}{2}\right),$$

$$n_{r\theta}^{II}(\theta) = \sqrt{\frac{1}{2\pi}}\left(\frac{31}{80} - \frac{\nu}{5}\right)\left(\cos\frac{\theta}{2} + \left(\nu - \frac{7}{16}\right)\cos\frac{3\theta}{2}\right),$$

mode-III: (A-20)

$$n_{\theta z}^{III}(\theta) = -\frac{5}{4}\sqrt{\frac{1}{2\pi}}\cos\frac{\theta}{2},$$

$$n_{rz}^{III}(\theta) = -\frac{7}{4}\sqrt{\frac{1}{2\pi}}\sin\frac{\theta}{2},$$

Appendix B

Expressions of the universal functions $F_{\alpha\beta}$, $G_{\alpha\beta}$ and $H_{\alpha\beta}$

The non-zero expression of the universal functions $F_{\alpha\beta}$ and $G_{\alpha\beta}$ in terms of the kinking angle ϕ are (LEBLOND 1999):

$$\begin{aligned}
F_{11} =& 1 - \frac{3\pi^2}{8} m^2 + \left(\pi^2 - \frac{5\pi^4}{128}\right) m^4 + \left(\frac{\pi^2}{9} - \frac{11\pi^4}{72} + \frac{119\pi^6}{15360}\right) m^6 \\
&+ 5.07790\, m^8 - 2.88312\, m^{10} - 0.0925\, m^{12} + 2.996\, m^{14} \\
&- 4.059\, m^{16} + 1.63\, m^{18} + 4.1\, m^{20} + O(m^{22}), \\
F_{12} =& -\frac{3\pi}{2} m + \left(\frac{10\pi}{3} + \frac{\pi^3}{16}\right) m^3 + \left(-2\pi - \frac{133\pi^3}{180} + \frac{59\pi^5}{1280}\right) m^5 \\
&+ 12.313906\, m^7 - 7.32433\, m^9 + 1.5793\, m^{11} + 4.0216\, m^{13} \\
&- 6.915\, m^{15} + 4.21\, m^{17} + 4.56\, m^{19} + O(m^{21}), \\
F_{21} =& \frac{\pi}{2} m - \left(\frac{4\pi}{3} + \frac{\pi^3}{48}\right) m^3 + \left(-\frac{2\pi}{3} + \frac{13\pi^3}{30} - \frac{59\pi^5}{3840}\right) m^5 \\
&- 6.176023\, m^7 + 4.44112\, m^9 - 1.5340\, m^{11} - 2.0700\, m^{13} \\
&+ 4.684\, m^{15} - 3.95\, m^{17} - 1.32\, m^{19} + O(m^{21}), \\
F_{22} =& 1 - \left(4 + \frac{3\pi^2}{8}\right) m^2 + \left(\frac{8}{3} + \frac{29\pi^2}{18} - \frac{5\pi^4}{128}\right) m^4 + \left(-\frac{32}{15} - \frac{4\pi^2}{9}\right. \\
&\left. + -\frac{1159\pi^4}{7200} + \frac{119\pi^6}{15360}\right) m^6 + 10.58254\, m^8 - 4.78511\, m^{10} \\
&- 1.8804\, m^{12} + 7.280\, m^{14} - 7.591\, m^{16} + 0.25\, m^{18} + 12.5\, m^{20} + O(m^{22}), \\
F_{13} =& F_{31} = F_{23} = F_{32} = 0, \\
F_{33} =& \left(\frac{1-m}{1+m}\right)^{m/2},
\end{aligned} \tag{B-1}$$

where $m = \phi/\pi$, and

$$\begin{aligned}
G_{11} =& 15.74961\, m^2 - 47.93339\, m^4 + 63.66599\, m^6 - 50.7088\, m^8 \\
&+ 26.66807\, m^{10} - 6.0205\, m^{12} - 7.314\, m^{14} + 10.947\, m^{16} \\
&- 2.85\, m^{18} - 13.7\, m^{20} + O(m^{22}), \\
G_{21} =& -5.013257\, m + 30.07954\, m^3 - 59.565733\, m^5 + 61.17444\, m^7 \\
&- 39.90249\, m^9 + 15.6222\, m^{11} + 3.0343\, m^{13} - 12.781\, m^{15} \\
&+ 9.69\, m^{17} + 6.62\, m^{19} + O(m^{21}), \\
G_{32} =& -2\, m \sqrt{\frac{2\pi}{1-m^2}} \left(\frac{1-m}{1+m}\right)^m.
\end{aligned} \tag{B-2}$$

In (LEBLOND 1999), the in-plane components of $\mathbf{H}_{\alpha\beta}(\phi)$ are given as tabulated numerical data

$\phi°$	$H_{11}(\phi)$	$H_{12}(\phi)$	$H_{21}(\phi)$	$H_{22}(\phi)$
0	0	-2.250	0.750	0
5	-0.098	-2.236	0.746	-0.189
10	-0.194	-2.196	0.731	-0.374
15	-0.288	-2.129	0.708	-0.553
20	-0.377	-2.037	0.675	-0.723
25	-0.461	-1.922	0.635	-0.879
30	-0.538	-1.786	0.587	-1.021
35	-0.608	-1.631	0.533	-1.145
40	-0.669	-1.460	0.474	-1.250
45	-0.721	-1.276	0.410	-1.334
50	-0.763	-1.082	0.344	-1.396
55	-0.796	-0.881	0.276	-1.436
60	-0.819	-0.677	0.207	-1.454
65	-0.833	-0.472	0.139	-1.450
70	-0.837	-0.270	0.072	-1.424
75	-0.832	-0.073	0.008	-1.378
80	-0.818	0.115	-0.052	-1.313

Table B-1: numerical values of the in-plane components $\mathbf{H}_{\alpha\beta}(\phi)$

The resulting functions may be obtained from curve fitting, where $H_{11}(\phi)$ and $H_{22}(\phi)$ are odd functions of ϕ and $H_{12}(\phi)$ and $H_{21}(\phi)$ even functions

$$
\begin{aligned}
H_{11} = &-1.12400\,m + 0.360546\,m^3 + 0.025559\,m^5 - 0.459497\,m^7 \\
&+ 1.27174\,m^9 - 1.86604\,m^{11} + 1.56091\,m^{13} - 0.748144\,m^{15} \\
&+ 0.191592\,m^{17} - 0.020345\,m^{19} + O(m^{21}), \\
H_{12} = &-2.24987 + 1.7846\,m^2 - 0.274494\,m^4 - 0.51285\,m^6 \\
&+ 1.60245\,m^8 - 2.57438\,m^{10} + 2.42131\,m^{12} - 1.33571\,m^{14} \\
&+ 0.405271\,m^{16} - 0.055258\,m^{18} + O(m^{20}), \\
H_{21} = &0.750252 - 0.618181\,m^2 - 0.128243\,m^4 + 1.88129\,m^6
\end{aligned}
\tag{B-3}
$$

$$
\begin{aligned}
&- 6.8318\,m^8 + 14.2247\,m^{10} - 18.0754\,m^{12} + 14.22\,m^{14} \\
&- 6.75317\,m^{16} + 1.77205\,m^{18} + O(m^{20}), \\
H_{22} = &- 2.16823\,m + 0.793333\,m^3 + 0.234458\,m^5 - 1.42031\,m^7 \\
&+ 3.15283\,m^9 - 4.07036\,m^{11} + 3.14437\,m^{13} - 1.42864\,m^{15} \\
&+ 0.351761\,m^{17} - 0.036189\,m^{19} + O(m^{21}),
\end{aligned}
$$

and the out of plane component $H_{33}(\phi)$ is given by

$$
H_{33} = \frac{1}{\cos(\pi m/2)} \left\{ \frac{3}{4} \left(\frac{1-m}{1+m} \right)^{m/2} \sin\left(\frac{\pi m}{2} \right) - \frac{2m}{\sqrt{1-m^2}} \left(\frac{1-m}{1+m} \right)^{m} \right\}. \tag{B-4}
$$

Appendix C

The fundamental integral and its partial derivatives

The solution to the fundamental integral (sections 2.2.3 and 2.2.4)

$$\mathcal{P} = \frac{1}{2}\int_{\xi}^{\infty}\left(\frac{x^2}{\alpha^2+s}+\frac{y^2}{\beta^2+s}+\frac{z^2}{s}-1\right)\frac{ds}{\sqrt{Q(s)}}, \tag{C-1}$$

is obtained by considering the result of each single term (BYRD & FRIEDMAN 1971):

$$\int_{\xi}^{\infty}\frac{x^2}{\alpha^2+s}\frac{ds}{\sqrt{Q(s)}} = \frac{2}{k_1^2\alpha^3}\left(F(\phi|k_1)-E(\phi|k_1)\right), \tag{C-2}$$

$$\int_{\xi}^{\infty}\frac{y^2}{\beta^2+s}\frac{ds}{\sqrt{Q(s)}} = \frac{2}{k_1^2k_2^2\alpha^3}\left(E(\phi|k_1)-k_2^2F(\phi|k_1)-k_1^2\frac{\sin\phi\cos\phi}{\sqrt{1-k_1^2\sin^2\phi}}\right),$$

$$\int_{\xi}^{\infty}\frac{z^2}{s}\frac{ds}{\sqrt{Q(s)}} = \frac{2}{k_2^2\alpha^3}\left(\tan\phi\sqrt{1-k_1^2\sin^2\phi}-E(\phi|k_1)\right),$$

$$\int_{\xi}^{\infty}\frac{ds}{\sqrt{Q(s)}} = \frac{2}{\alpha}F(\phi|k_1),$$

where

$$\phi = am(u_1) = \arcsin\left(\frac{\alpha}{\sqrt{\alpha^2+\xi}}\right), \tag{C-3}$$

$$k_1 = \sqrt{1-\frac{\beta^2}{\alpha^2}},$$

$$k_2 = \sqrt{1-k_1^2} = \frac{\beta}{\alpha}.$$

To evaluate the needed terms of partial derivatives of the potential functions, following derivatives should be applied

$$\frac{\partial\xi}{\partial x} = \frac{2\xi(\beta^2+\xi)\sqrt{(\alpha^2+\xi)(\alpha^2+\eta)(\alpha^2+\zeta)}}{\alpha\sqrt{\alpha^2-\beta^2}(\xi-\eta)(\xi-\zeta)}, \tag{C-4}$$

$$\frac{\partial\xi}{\partial y} = \frac{2\xi(\alpha^2+\xi)\sqrt{-(\beta^2+\xi)(\beta^2+\eta)(\beta^2+\zeta)}}{\beta\sqrt{\alpha^2-\beta^2}(\xi-\eta)(\xi-\zeta)},$$

$$\frac{\partial\xi}{\partial z} = \frac{2(\alpha^2+\xi)(\beta^2+\xi)\sqrt{\xi\eta\zeta}}{\alpha\beta(\xi-\eta)(\xi-\zeta)},$$

$$\frac{\partial \eta}{\partial x} = \frac{2\eta(\beta^2+\eta)\sqrt{(\alpha^2+\xi)(\alpha^2+\eta)(\alpha^2+\zeta)}}{\alpha\sqrt{\alpha^2-\beta^2}(\eta-\xi)(\eta-\zeta)},$$
$$\frac{\partial \eta}{\partial y} = \frac{2\eta(\alpha^2+\eta)\sqrt{-(\beta^2+\xi)(\beta^2+\eta)(\beta^2+\zeta)}}{\beta\sqrt{\alpha^2-\beta^2}(\eta-\xi)(\eta-\zeta)}, \tag{C-5}$$
$$\frac{\partial \eta}{\partial z} = \frac{2(\alpha^2+\eta)(\beta^2+\eta)\sqrt{\xi\eta\zeta}}{\alpha\beta(\eta-\xi)(\eta-\zeta)},$$

$$\frac{\partial \zeta}{\partial x} = \frac{2\zeta(\beta^2+\zeta)\sqrt{(\alpha^2+\xi)(\alpha^2+\eta)(\alpha^2+\zeta)}}{\alpha\sqrt{\alpha^2-\beta^2}(\zeta-\xi)(\zeta-\eta)},$$
$$\frac{\partial \zeta}{\partial y} = \frac{2\zeta(\alpha^2+\zeta)\sqrt{-(\beta^2+\xi)(\beta^2+\eta)(\beta^2+\zeta)}}{\beta\sqrt{\alpha^2-\beta^2}(\zeta-\xi)(\zeta-\eta)}, \tag{C-6}$$
$$\frac{\partial \zeta}{\partial z} = \frac{2\zeta(\alpha^2+\zeta)(\beta^2+\zeta)\sqrt{\xi\eta\zeta}}{\alpha\beta(\zeta-\xi)(\zeta-\eta)},$$

The pertinent terms from which stress and displacement fields (2.22), (2.23), (2.39), (2.40) result are

$$\frac{\partial \mathcal{P}}{\partial x} = x\int_{\xi}^{\infty}\frac{1}{\alpha^2+s}\frac{ds}{\sqrt{Q(s)}},$$
$$\frac{\partial \mathcal{P}}{\partial y} = y\int_{\xi}^{\infty}\frac{1}{\beta^2+s}\frac{ds}{\sqrt{Q(s)}}, \tag{C-7}$$
$$\frac{\partial \mathcal{P}}{\partial z} = z\int_{\xi}^{\infty}\frac{ds}{s\sqrt{Q(s)}},$$

$$\frac{\partial^2 \mathcal{P}}{\partial x^2} = \int_{\xi}^{\infty}\frac{1}{\alpha^2+s}\frac{ds}{\sqrt{Q(s)}} - x\frac{\partial \xi}{\partial x}\frac{1}{(\alpha^2+\xi)\sqrt{Q(\xi)}},$$
$$\frac{\partial^2 \mathcal{P}}{\partial y^2} = \int_{\xi}^{\infty}\frac{1}{\beta^2+s}\frac{ds}{\sqrt{Q(s)}} - y\frac{\partial \xi}{\partial y}\frac{1}{(\beta^2+\xi)\sqrt{Q(\xi)}}, \tag{C-8}$$
$$\frac{\partial^2 \mathcal{P}}{\partial z^2} = \int_{\xi}^{\infty}\frac{ds}{s\sqrt{Q(s)}} - z\frac{\partial \xi}{\partial z}\frac{1}{\xi\sqrt{Q(\xi)}},$$

$$\frac{\partial^2 \mathcal{P}}{\partial x\,\partial y} = -y\,\frac{\partial \xi}{\partial x}\,\frac{1}{(\beta^2+\xi)\sqrt{Q(\xi)}}, \qquad \text{(C-9)}$$

$$\frac{\partial^2 \mathcal{P}}{\partial y\,\partial z} = -z\,\frac{\partial \xi}{\partial y}\,\frac{1}{\xi\sqrt{Q(\xi)}},$$

$$\frac{\partial^2 \mathcal{P}}{\partial x\,\partial z} = -x\,\frac{\partial \xi}{\partial z}\,\frac{1}{(\alpha^2+\xi)\sqrt{Q(\xi)}},$$

where $Q(\xi) = \sqrt{\xi(\alpha^2+\xi)(\beta^2+\xi)}$.

Index

Mitteilungen aus dem Institut für Mechanik

Nr. 1 Theodor Lehmann:
Große elasto-plastische Formänderungen (Dezember 1976)

Nr. 2 Bogdan Raniecki/Klaus Thermann:
Infinitesimal Thermoplasticity and Kinematics of Finite Elastic-Plastic Deformations. Basic Concepts (Juni 1978)

Nr. 3 Wolfgang Krings:
Beitrag zur Finiten Element Methode bei linearem, viskoelastischem Stoffverhalten Stoffverhalten (Januar 1976)

Nr. 4 Burkhard Lücke:
Theoretische und experimentelle Untersuchen der zyklischen elastoplastischen Blechbiegung bei endlichen Verzerrungen (Januar 1976)

Nr. 5 Knut Schwarze:
Einfluß von Querschnittsverformungen bei dünnwandigen Stäben mit stetig gekrümmter Profilmittellinie (Februar 1976)

Nr. 6 Hubert Sommer:
Ein Beitrag zur Theorie des ebenen elastischen Verzerrungszustandes bei endlichen Formänderungen (Januar 1977)

Nr. 7 H. Stumpf/F. J. Biehl:
Die Methode der orthogonalen Projektionen und ihre Anwendungen zur Berechnung orthotroper Platten (März 1977)

Nr. 8 Albert Meyers:
Ein Beitrag zum optimalen Entwurf von schnellaufenden Zentrifugenschalen (April 1977)

Nr. 9 Berend Fischer:
Zur zyklischen, elastoplastischen Beanspruchen eines dickwandigen Zylinders bei endlichen Verzerrungen (April 1977)

Nr. 10 Wojciech Pietraszkiewicz:
Introduction to the Non-Linear Theory of Shells (Mai 1977)

Nr. 11 Wilfried Ullenboom:
Optimierung von Stäben unter nichtperiodischer dynamischer Belastung (Juni 1977)

Nr. 12 Jürgen Güldenpfennig:
Anwendung eines Modells der Vielkristallplastizität auf ein Problem gekoppelter elastoplastischer Wellen (Juli 1977)

Nr. 13 Pawel Rafalski:
Minimum Principles in Plasticity (März 1978)

Nr. 14 Peter Hilgers:
Der Einsatz eines Mikrorechners zur hybriden Optimierung und Schwingungsanalyse (Juli 1978)

Nr. 15 Hans-Albert Lauert:
Optimierung von Stäben unter dynamischer periodischer Beanspruchung bei Beachtung von Spannungsrestriktionen (August 1979)

Nr. 16 Martin Fritz:
Berechnund der Auflagerkräfte und der Muskelkräfte des Menschen bei ebenen Bewegungen aufgrund von kinematographischen Aufnahmen (Juli 1979)

Nr. 17 H. Stumpf/F. J. Biehl:
Approximations and Error Estimates in Eigenvalue Problems of Elastic Systems with Application to Eigenvibrations of Orthotropic Plates (Dezember 1979)

Nr. 18 Uwe Kohlberg:
Variational Principles and theirNumerical Application to Geometrically Nonlinear v. Karman Plates (Juli 1979)

Nr. 19 Heinz Antes:
Über Fehler und Möglichkeiten ihrer Abschätzung bei numerischen Berechnungen von Schalentragwerken (Januar 1980)

Nr. 20 Czeslaw Wozniak:
Large Deformations of Elastic and Non-Elastic Plates, Shells and Rods (März 1980)

Nr. 21 Maria K. Duszek:
Problems of Geometrically Non-Linear Theory of Plasticity (Juni 1980)

Nr. 22 Burkhard von Bredow:
Optimierung von Stäben unter stochastischer Erregung (Dezember 1980)

Nr. 23 Jürgen Preuss:
Optimaler Entwurf von Tragwerken mit Hilfe der Mehrzielmethode (Februar 1981)

Nr. 24 Ekkehard Großmann:
Kovarianzanalyse mechanischer Zufallsschwingungen bei Darstellung der mehrfachkorrelierten Erregungen durch stochastische Differentialgleichungen (Februar 1981)

Nr. 25 Dieter Weichert:
Variational Formulation and Solution of Boundary-Value Problems in the Theory of Plasticity and Application to Plate Problems (März 1981)

Nr. 26 Wojciech Pietraszkiewicz:
On Consistent Approximations in the Geometrically Non-Linear Theory of Shells (Juni 1981)

Nr. 27 Georg Zander:
Zur Bestimmung von Verzweigungslasten dünnwandiger Kreiszylinder unter kombinierter Längs- und Torsionslast (September 1981)

Nr. 28 Pawel Rafalski:
An Alternative Approach to the Elastic-Viscoplastic Initial-Boundary Value Problem (September 1981)

Nr. 29 Heinrich Oeynhausen:
Verzweigungslasten elastoplastisch deformierter, dickwandiger Kreiszylinder unter Innendruck und Axialkraft (November 1981)

Nr. 30 F.-J. Biehl:
Zweiseitige Eingrenzung von Feldgrößen beim einseitigen Kontaktproblem (Dezember 1981)

Nr. 31 Maria K. Duszek:
Foundations of the Non-Linear Plastic Shell Theory (Juni 1982)

Nr. 32 Reinhard Piltner:
Spezielle finite Elemente mit Löchern, Ecken und Rissen unter Verwendung von analytischen Teillösungen (Juli 1982)

Nr. 33 Petrisor Mazilu:
Variationsprinzipe der Thermoplastizität I. Wärmeausbreitung und Plastizität (Dezember 1982)

Nr. 34 Helmut Stumpf:
Unified Operator Description, Nonlinear Buckling and Post-Buckling Analysis of Thin Elastic Shells (Dezember 1982)

Nr. 35 Bernd Kaempf:
Ein Exremal-Variationsprinzip für die instationäre Wärmeleitung mit einer Anwendung auf thermoelastische Probleme unter Verwendung der finiten Elemente (März 1983)

Nr. 36 Alfred Kraft:
Zum methodischen Entwurf mechanischer Systeme im Hinblick auf optimales Schwingungsverhalten (Juli 1983)

Nr. 37 Petrisor Mazilu:
Variationsprinzipe der Thermoplastizität II. Gekoppelte thermmomechanische Prozesse (August 1983)

Nr. 38 Klaus-Detlef Mickley:
Punktweise Eingrenzung von Feldgrößen in der Elastomechanik und ihre numerische Realisierung mit Fundamental-Splinefuntionen (November 1983)

Nr. 39 Lutz-Peter Nolte:
Beitrag zur Herleitung und vergleichende Untersuchung geometrisch nichtlinearer Schalentheorien unter Berücksichtigung großer Rotationen (Dezember 1983)

Nr. 40 Ulrich Blix:
Zur Berechnung der Einschnürung von Zugstäben unter Berücksichtigung thermischer Einflüsse mit Hilfe der Finite-Element-Methode (Dezember 1983)

Nr. 41 Peter Becker:
Zur Berechnung von Schallfeldern mit Elemtmethoden (Februar 1984)

Nr. 42 Diemar Bouchard:
Entwicklung und Anwendung eines an die Diskrete-Fourier-Transformation angepaßten direkten Algorithmus zur Bestimmung der modalen Parameter linearer Schwingungssysteme (Februar 1984)

Nr. 43 Uwe Zdebel:
Theoretische und experimentelle Untersuchungen zu einem thero-plastischen Stoffgesetz (Dezember 1984)

Nr. 44 Jan Kubik:
Thermodiffusion Flows in a Solid with a Dominant Constituent (April 1985)

Nr. 45 Horst J. Klepp:
Über die Gleichgewichtslagen und Gleichgewichtsbereiche nichtlinearer autonomer Systeme (Juni 1985)

Nr. 46 J. Makowsky/L.-P. Nolte/H. Stumpf:
Finite In-Plane Deformations of Flexible Rods - Insight into Nonlinar Shell Problems (Juli 1985)

Nr. 47 Franz Karl Labisch:
Grundlagen einer Analyse mehrdeutiger Lösungen nichtlinearer Randwertprobleme der Elastostatik mit Hilfe von Variationsverfahren (August 1985)

Nr. 48 J. Chroscielewski/L.-P. Nolte:
Strategien zur Lösung nichtlinearer Probleme der Strukturmechanik und ihre modulare Aufbereitung im Konzept MESY (Oktober 1985)

Nr. 49 Karl-Heinz Bürger:
Gewichtsoptimierung rotationssymmetrischer Platten unter instationärer Erregung (Dezember 1985)

Nr. 50 Ulrich Schmid:
Zur Berechnung des plastischen Setzens von Schraubenfedern (Februar 1987)

Nr. 51 Jörg Frischbier:
Theorie der Stoßbelastung ortotroper Platten und ihr experimentelle Überprüfung am Beispiel einer unidirektional verstärkten CFK-Verbundplatte (März 1987)

Nr. 52 W. Tampczynski:
Strain history effect in cyclic plasticity (Juli 1987)

Nr. 53 Dieter Weichert:
Zum Problem geometrischer Nichtlinearitäten in der Plastizitätstheorie (Dezember 1987)

Nr. 54 Heinz Antes/Thomas Meise/Thomas Wiebe:
Wellenausbreitung in akustischen Medien Randelement-Prozeduren im 2-D Frequenzraum und im 3-D Zeitbereich (Januar 1988)

Nr. 55 Wojciech Pietraszkiewicz:
Geometrically non-linear theories of thin elastic shells (März 1988)

Nr. 56 Jerzy Makowski/Helmut Stumpf:
Finite strain theory of rods (April 1988)

Nr. 57 Andreas Pape:
Zur Beschreibung des transienten und stationären Verfestigungsverhaltens von Stahl mit Hilfe eines nichtlinearen Grenzflächenmodells (Mai 1988)

Nr. 58 Johannes Groß-Weege:
Zum Einspielverhalten von Flächentragwerken (Juni 1988)

Nr. 59 Peihua LIU:
Optimierung von Kreisplatten unter dynamischer nicht rotationssymmetrischer Last (Juli 1988)

Nr. 60 Reinhard Schmidt:
Die Anwendung von Zustandsbeobachtern zur Schwingungsüberwachung und Schadensfrüherkennung auf mechanische Konstruktionen (August 1988)

Nr. 61 Martin Pitzer:
Vergleich einiger FE-Formulierungen auf der Basis eines inelastischen Stoffgesetzes (Juli 1988)

Nr. 62 Jerzy Makowski/Helmut Stumpf:
Geometric structure of fully nonlinear and linearized Cosserat type shell theory (Dezember 1988)

Nr. 63 O. T. Bruhns:
Große plastische Formänderungen - Bad Honnef 1988 (Januar 1989)

Nr. 64 Khanh Chau Le/Helmut Stumpf/Dieter Weichert:
Variational principles of fracture mechanics (Juli 1989)

Nr. 65 Guido Obermüller:
Ein Beitrag zur Strukturoptimierung unter stochastischen Lasten (Juni 1989)

Nr. 66 Herbert Diehl:
Ein Materialmodell zur Berechnung von Hochgeschwindigkeitsdeformationen metallischer Werkstoffe unter besonderer Berücksichtigung der Schädigung durch Scherbänder (Juni 1989)

Nr. 67 Michael Geis:
Zur Berechnund ebener, elastodynamischer Rißprobleme mit der Randelementmethode (November 1989)

Nr. 68 Günter Renker:
Zur Identifikation nichtlinearer strukturmechanischer Systeme (November 1989)

Nr. 69 Berthold Schieck:
Große elastische Dehnungen in Schalen aus hyperelastischen inkompressiblen Materialien (November 1989)

Nr. 70 Frank Szepan:
Ein elastisch-viskoplastisches Stoffgesetz zur Beschreibung großer Formänderungen unter Berücksichtigung der thermomechanischen Kopplung (Dezember 1989)

Nr. 71 Christian Scholz:
Ein Beitrag zur Gestaltsoptimierung druckbelasteter Rotationsschalen (Dezember 1989)

Nr. 72 J. Badur/H. Stumpf:
On the influence of E. and F. Cosserat on modern continuum mechanics and field theory (Dezember 1989)

Nr. 73 Werner Fornefeld:
Zur Parameteridentifikation und Berechnung von Hochgeschwindigkeitsdeformationen metallischer Werkstoffe anhand eines Kontinuums-Damage-Modells (Januar 1990)

Nr. 74 J. Saczuk/H. Stumpf:
On statical shakedown theorems for non-linear problems (April 1990)

Nr. 75 Andreas Feldmüller:
Ein thermoplastisches Stoffgesetz isotrop geschädigter Kontinua (April 1991)

Nr. 76 Ulfert Rott:
Ein neues Konzept zur Berechnung viskoplastischer Strukturen (April 1991)

Nr. 77 Thomas Heinrich Pingel:
Beitrag zur Herleitung und numerischen Ralisierung eines mathematischen Modells der menschlichen Wirbelsäule (Juli 1991)

Nr. 78 O. T. Bruhns:
Große plastische Formänderungen - Bad Honnef 1991 (Dezember 1991)

Nr. 79 J. Makowski/J. Chroscielewski/H. Stumpf:
Computational Analysis of Shells Undergoing Large Elastic Deformation Part I:Theoretical Foundations

Nr. 80 J. Chroscielewski/J. Makowski/H. Stumpf:
Computational Analysis of Shells Undergoing Large Elastic Deformation Part II: Finite Element Implementation

Nr. 81 R. H. Frania/H. Waller:
Entwicklung und Anwendung spezieller finiter Elemente für Kerbspannungsprobleme im Maschienebau (Mai 1992)

Nr. 82 B. Bischoff-Beiermann:
Zur selbstkonsistenten Berechnung von Eigenspannungen in polykristallinem Eis unter Berücksichtigung der Monokristallanisotropie (Juli 1992)

Nr. 83 J. Pohé:
Ein Beitrag zur Stoffgesetzentwicklung für polykristallines Eis (Februar 1993)

Nr. 84 U. Kikillus:
Ein Beitrag zum zyklischen Kiechverhalten von Ck 15 (Mai 1993)

Nr. 85 T. Guo:
Untersuchung des singulären Rißspitzenfeldes bei stationärem Rißwachstum in verfestigendem Material (Juni 1993)

Nr. 86 Achim Menne:
Identifikation der dynamischen Eigenschaften von hydrodynamischen Wandlern (Januar 1994)

Nr. 87 Uwe Folchert:
Identifikation der dynamischen Eigenschaften Hydrodynamischer Kopplungen (Januar 1994)

Nr. 88 Jörg Körber:
Ein verallgemeinertes Finite-Element-Verfahren mit asymptotischer Stabilisierung angewendet auf viskoplastische Materialmodelle (April 1994)

Nr. 89 Peer Schieße:
ein Beitag zur Berechnung des Deformationsverhaltens anisotrop geschädigter Kontinua unter Berücksichtigung der thermoplastischen Kopplung (April 1994)

Nr. 90 Egbert Schopphoff:
Dreidimensionale mechanische Analyse der menschlichen Wirbelsäule (Juli 1994)

Nr. 91 Christoph Beerens:
Zur Modellierung nichtlinearer Dämpfungsphänomene in der Strukturmechanik (Juli 1994)

Nr. 92 K. C. Le/H. Stumpf:
Finte elastoplasticity with microstructure (November 1994)

Nr. 93 O. T. Bruhns:
Große plastische Formänderungen - Bad Honnef 1994 (Dezember 1994)

Nr. 94 Armin Lenzen:
Untersuchung von dynamischen Systemen mit der Singulärwertzerlegung - Erfassung von Strukturveränderungen (Dezember 1994)

Nr. 95 J. Makowski/H. Stumpf:
Mechanics of Irregular Shell Structures (Dezember 1994)

Nr. 96 J. Chroscielewski/J. Makowski/H. Stumpf:
Finte Elements for Irregular Nonlinear Shells (Dezember 1994)

Nr. 97 W. Krings/A. Lenzen/u. a.:
Festschrift zum 60. Geburtstag von Heinz Waller (Februar 1995)

Nr. 98 Ralf Podleschny:
Untersuchung zum Instabilitätsverhalten scherbeanspruchter Risse (April 1995)

Nr. 99 Bernd Westerhoff:
Eine Untersuchung zum geschwindigkeitsabhängigen Verhalten von Stahl (Juli 1995)

Nr. 100 Marc Mittelbach:
Simulation des Deformations- und Schädigungsverhaltens beim Stoßversuch mit einem Kontinuums-Damage-Modell (Dezember 1995)

Nr. 101 Ulrich Hoppe:
Über grundlegende Konzepte der nichtlinearen Kontinuumsmechanik und Schalentheorie (Mai 1996)

Nr. 102 Marcus Otto:
Erweiterung des Kaustikenverfahrens zur Analyse räumlicher Spannungskonzentrationen (Juni 1996)

Nr. 103 Horst Lanzerath:
Zur Modalanalyse unter Verwendung der Randelementemethode (Juli 1996)

Nr. 104 Andreas Wichtmann Entwicklung eines thermodynamisch konsistenten Stoffgesetzes zur Beschreibung der Reckalterung (August 1996)

Nr. 105 Bjarne Fosså Ein Beitrag zur Fließflächenmessung bei vorgedehnten Stoffen (Oktober 1996)

Nr. 106 Khanh Cha Le:
Kontinuumsmechanisches Modellieren von Medien mit veränderlicher Mikrostruktur (Dezember 1996)

Nr. 107 Holger Behrens:
Nichtlineare Modellierung und Identifikation hydrodynamischer Kupplungen mit allge- meinen diskreten Modellansätzen (Januar 1997)

Nr. 108 Johannes Moosheimer:
Gesteuerte Schwingungsdämpfung mit Elektrorheologischen Fluiden (Juli 1997)

Nr. 109 Dirk Klaus Anding:
Zur simultanen Bestimmung materialabhängiger Koeffizienten inelastischer Stoffgesetze (Oktober 1997)

Nr. 110 Stephan Weng:
Ein Evolutionsmodell zur mechanischen Analyse biologischer Strukturen (Dezember 1997)

Nr. 111 Michael Straßberger:
Aktive Schallreduktion durch digitale Zustandsregelung der Strukturschwingungen mit Hilfe piezo-keramischer Aktoren (Dezember 1997)

Nr. 112 Hans-Jörg Becker:
Simultation des Deformationsverhaltens polykristallinen Eises auf der Basis eines monokristallinen Stoffgesetzes (Dezember 1997)

Nr. 113 Thomas Nerzak:
Modellierung und Simulation der Ausbreitung adiabatischer Scherbänder in metallischen Werkstoffen bei Hochgeschwindigkeitsdeformationen (Dezember 1997)

Nr. 114 O. T. Bruhns:
Große plastische Formänderungen (März 1998)

Nr. 115 Jan Steinhausen:
Die Beschreibung der Dynamik von Antriebssträngen durch Black-Box-Modelle hydrodynamischer Kupplungen (August 1998)

Nr. 116 Thomas Pandorf:
Experimentelle und numerische Untersuchungen zur Kerbspitzenbeanspruchung bei schlagbelasteten Biegeproben (August 1998)

Nr. 117 Claus Oberste-Brandenburg:
Ein Materialmodell zur Beschreibung der Austenit-Martensit Phasentransformation unter Berücksichtigung der transformationsinduzierten Plastizität (Juni 1999)

Nr. 118 Michael Märtens:
Regelung mechanischer Strukturen mit Hilfe piezokeramischer Stapelaktoren (Dezember 1999)

Nr. 119 Dirk Kamarys:
Detektion von Systemveränderungen durch neue Identifikationsverfahren in der experimentellen Modalanalyse (Dezember 1999)

Nr. 120 Wolfgang Hiese:
Gültigkeitskriterien zur Bestimmung von Scherbruchzähigkeiten (Januar 2000)

Nr. 121 Peter Jaschke:
Mathematische Modellierung des Betriebsverhaltens hydrodynamischer Kupplungen mit hybriden Modellansätzen (Februar 2000)

Nr. 122 Stefan Müller:
Zum Einsatz von semi-aktiven Aktoren zur optimalen Schwingungsreduktion in Tragwerken (Februar 2000)

Nr. 123 Dirk Eichel:
Zur Kondensation strukturdynamischer Aufgaben mit Hilfe von Polynommatrizen (Juni 2000)

Nr. 124 Andreas Bürgel:
Bruchmechanische Kennwerte beim Wechsel im Versagensverhalten dynamisch scherbeanspruchter Risse (August 2000)

Nr. 125 Daniela Lürding:
Modellierung großer Deformationen in orthotropen, hyperelastischen Schalenstrukturen (März 2001)

Nr. 126 Thorsten Quent:
Ein mikromechanisch begründetes Modell zur Beschreibung des duktilen Verhaltens metallischer Werkstoffe bei endlichen Deformationen unter Berücksichtigung von Porenschädigung (Mai 2001)

Nr. 127 Ndzi C. Bongmba:
Ein finites anisotropes Materialmodell auf der Basis der Hencky-Dehnung und der logarithmischen Rate zur Beschreibung duktiler Schädigung (Mai 2001)

Nr. 128 Henning Schütte:
Ein finites Modell für spröde Schädigung basierend auf der Ausbreitung von Mikrorissen (August 2001)

Nr. 129 Henner Vogelsang:
Parameteridentifikation für ein selbstkonsistentes Stoffmodell unter Berücksichtigung von Phasentransformationen (Dezember 2001)

Nr. 130 Jörn Mosler:
Finite Elemente mit sprungstetigen Abbildungen des Verschiebungsfeldes für numerische Analysen lokalisierter Versagenszustände (Dezember 2002)

Nr. 131 Karin Preusch:
Hierarchische Schalenmodelle für nichtlineare Kontinua mit der p-Version der Finite-Element Methode (Mai 2003)

Nr. 132 Christoph Müller:
Thermodynamic modeling of polycrystalline shape memory alloys at finite strains (August 2003)

Nr. 133 Martin Heiderich:
Ein Beitrag zur zerstörungsfreien Schädigungsanalyse (Juni 2004)

Nr. 134 Raoul Costamagna:
Globale Materialbeziehungen für das geklüftete Gebirge (Juli 2004)

Nr. 135 Markus Böl:
Numerische Simulation von Polymernetzwerken mit Hilfe der Finite-Elemente-Methode (Januar 2005)

Nr. 136 Gregor Kotucha:
Regularisierung von Problemen der Topologieoptimierung unter Einbeziehung von Dichtegradienten (August 2005)

Nr. 137 Michael Steiner:
Deformations- und Versagensverhalten innendruckbeanspruchter Stahlrohre durch Stoßbelastung (Februar 2006)

Nr. 138 Dirk Bergmannshoff:
Das Instabilitätsverhalten zug-/scherbeanspruchter Risse bei Variation des Belastungspfades (Dezember 2006)

Nr. 139 Olaf Schilling:
über eine implizite Partikelmethode zur Simulation von Umformprozessen (Januar 2007)

Nr. 140 Jörn Mosler :
On the numerical modeling of localized material failure at finite strains by means of variational mesh adaption and cohesive elements (Mai 2007)

Nr. 141 Rainer Fechte-Heinen:
Mikromechanische Modellierung von Formgedächtnismaterialien (Juni 2007)

Nr. 142 Christian Grabe:
Experimental testing and parameter identification on the multidimensional material behavior of shape memory alloys (Juni 2007)

Nr. 143 Markus Peters:
Modellierung von Rissausbreitung unter Verwendung der p-Version der XFEM mit einer adaptiven Integrationsmethode (Juli 2007)

Nr. 144 Claus Oberste-Brandenburg:
Thermomechanical modeling of shape memory alloys at different length scales (Juli 2007)

Nr. 145 Stefan Reichling:
Das inverse Problem der quantitativen Ultraschallelastografie unter Berücksichtigung großer Deformationen (Juli 2007)

Nr. 145 Stefan Reichling:
Das inverse Problem der quantitativen Ultraschallelastografie unter Berücksichtigung großer Deformationen (Juli 2007)

Nr. 146 Kianoush Molla-Abbasi:
A Consistent Anisotropic Brittle Damage Model Based on the Concept of Growing Elliptical Cracks (Januar 2008)

Mitteilungen aus dem Institut für Mechanik
RUHR-UNIVERSITÄT BOCHUM
Nr. 146

978-3-935892-23-0